

Effect of experimental hyperglycemia on oxidative transformations of endogenous and exogenous compounds in the rat

Doctoral (Ph.D.) Dissertation



Hawsar Othman Mohammed

Doctoral School of Pharmacological and Pharmaceutical Sciences

Head of the doctoral school: **Prof. Dr. Erika Pintér**

Program Leader: **Prof. Dr. Pál Perjési**

Supervisor: **Prof. Dr. Pál Perjési**

Institute of Pharmaceutical Chemistry,
Faculty of Pharmacy, University of Pécs

Pécs, 2022

Table of Contents

1. LIST OF ABBREVIATIONS	3
2. INTRODUCTION	6
2.1. EXPERIMENTAL DIABETES AND OXIDATIVE STRESS	7
2.1.1. <i>Mechanism of action of streptozotocin</i>	9
2.2. HYPERGLYCEMIA AND OXIDATIVE STRESS	10
2.3. OXIDATIVE DAMAGE TO LIPIDS.....	12
2.4. OXIDATIVE DAMAGE TO PROTEINS	13
2.5. OXIDATIVE DAMAGE TO NUCLEIC ACIDS (DNA).....	15
2.6. NON-ENZYMATIC OXIDATIVE TRANSFORMATIONS OF EXOGENOUS COMPOUNDS	16
2.6.1. <i>Biotransformation of ibuprofen</i>	17
2.6.1.1. Pharmacokinetics and pharmacodynamics.....	18
2.6.1.2. Stereochemistry	20
3. AIMS	22
4. MATERIALS AND METHODS	23
4.1. CHEMICALS	23
4.2. ANIMALS AND EXPERIMENTAL PROCEDURE.....	23
4.3. SAMPLE PREPARATION	24
4.4. UV-VIS DETERMINATION OF PROTEIN CONTENT (BIURET ASSAY)	24
4.5. UV-VIS DETERMINATION OF PROTEIN CARBONYL CONTENT (DNPH-PROTEIN ADDUCTS).....	25
4.6. UV-VIS DETERMINATION OF DIENE CONJUGATES.....	25
4.7. UV-VIS DETERMINATION OF MALONDIALDEHYDE (MDA) (TBARS ASSAY)	26
4.8. UV-VIS DETERMINATION OF NON-PROTEIN THIOLS (NPSH).....	26
4.9. HPLC DETERMINATION OF TYROSINE ISOMERS	26
4.9.1. <i>Sample preparation</i>	26
4.10. IBUPROFEN.....	27
4.10.1. <i>Ibuprofen experiments in vitro</i>	27
4.10.1.1. Fenton test	27
4.10.1.2. Udenfriend's assay	27
4.10.2. <i>Ibuprofen experiments in vivo</i>	28
4.10.2.1. Intestinal perfusion	28
4.10.2.2. Sample preparation.....	29
4.10.3. Analysis of racemic ibuprofen samples (Items 4.10.1. and 4.10.2.)	29
4.10.3.1. HPLC-UV	29
4.10.3.2. HPLC-MS	30
4.10.4. CHIRAL ANALYSIS	30
4.10.4.1. <i>Animal experiment and intestinal perfusion procedure</i>	30
4.10.4.2. <i>Sample preparation</i>	31
4.10.4.3. <i>HPLC-UV analysis-Instrumentation</i>	31
4.10.4.4. <i>HPLC-UV analysis - Validation data</i>	31

4.10.4.4.1. Specificity	31
4.10.4.4.2. System suitability	32
4.10.4.4.3. Precision	32
4.10.4.4.4. Accuracy	34
4.10.4.4.5. Linearity.....	34
4.10.4.4.6. Determination of LOQ.....	35
4.11. STATISTICS	36
4.12. ETHICAL APPROVAL	36
5. RESULTS	37
5.1. OXIDATIVE TRANSFORMATIONS OF SELECTIVE ENDOGENOUS COMPOUNDS UNDER THE INFLUENCE OF STZ-INDUCED EXPERIMENTAL DIABETES	37
5.1.1. BLOOD GLUCOSE LEVEL	37
5.1.2. PROTEIN CONTENT	37
5.1.3. CARBONYL (PROT-DNPH) CONTENT	38
5.1.4. DETERMINATION OF DIENE CONJUGATES	39
5.1.5. TBARS DETERMINATION.....	40
5.1.6. DETERMINATION OF NON-PROTEIN THIOLS (NPSH)	41
5.1.7. DETERMINATION OF HYDROXYLATED PHENYLALANINE DERIVATIVES	42
5.2. <i>IN VITRO</i> INVESTIGATION OF NON-ENZYME CATALYZED (FENTON AND UDENFRIEND) OXIDATION OF IBUPROFEN	43
5.2.1. FENTON TEST	43
5.2.2. UDENFRIEND'S TEST	49
5.3. INVESTIGATION OF THE MAIN OXIDATIVE AND CONJUGATED METABOLITES OF IBUPROFEN IN SMALL INTESTINE PERFUSATES AND BILE OF CONTROL AND HYPERGLYCEMIC RATS	50
5.4. INVESTIGATION OF THE RATIO OF <i>R</i> (-) AND <i>S</i> (+)-IBUPROFEN IN SMALL INTESTINAL PERFUSATES AND BILE OF CONTROL AND HYPERGLYCEMIC RATS	61
6. DISCUSSION	71
7. CONCLUSION.....	80
8. PUBLICATION AND PRESENTATION	82
9. ACKNOWLEDGMENTS.....	84
10. REFERENCES.....	85

1. List of abbreviations

DM	Diabetes mellitus
STZ	Streptozotocin
OTC	Over the counter
ROS	Reactive oxygen species
RNS	Reactive nitrogen species
GLUT2	Glucose transport protein 2
DNA	Deoxyribonucleic acid
ATP	Adenosine triphosphate
NAD ⁺	Nicotinamide adenine dinucleotide
PTP 1B	Protein-tyrosine Phosphatase 1B
H ₂ O ₂	Hydrogen peroxide
NADPH	Nicotinamide adenine dinucleotide phosphate hydrogen
GAPDH	Glyceraldehyde-3-P dehydrogenase
PARP-1	Poly-ADP-ribose polymerase-1
DAG	Diacylglycerol
PKC	Protein kinase C
AGEs	Advanced glycation end-products
SOD	Superoxide dismutase
•OH	Hydroxyl radical
HNE	4-Hydroxy-2-nonenal
MDA	Malondialdehyde
TBARS	Thiobarbituric acid reactive substances
L•	Lipid radicals
LOO•	Lipid peroxy radicals
LOOH	Lipid hydroperoxide
LO•	Lipid alkoxyl radical
4-HHE	4-Hydroxy-2-hexenal
DNPH	2,4-Dinitrophenyl-hydrazine
MCO	Metal-catalyzed oxidation
O ₂ •	Superoxide radical
AAS	α-Aminoadipic semialdehyde
GS	γ-Glutamic semialdehyde

ONE	4-Oxo-2-nonenal
3-DG	3-Deoxyglucosone
MGO	Methylglyoxal
ABA	<i>p</i> -Aminobenzoic acid
8-OHdG	8-Hydroxydeoxyguanosine
8-oxo- <i>d</i> Guo	8-Oxo-deoxyguanosine
NF- <i>κ</i> B	Nuclear factor kappa B
AP-1	Activator protein 1
GSH	Reduced glutathione
UVB	Ultraviolet-B
PCR	Polymerase chain reaction
PMN	Polymorpho-nuclear leukocytes
IBP	Ibuprofen
NSAIDs	Non-steroidal anti-inflammatory drugs
IUPAC	International Union of Pure and Applied Chemistry
GIT	Gastrointestinal tract
CYP	Cytochrome P450
1-OH-IBP	1- Hydroxyibuprofen
2-OH-IBP	2- Hydroxyibuprofen
3-OH-IBP	3- Hydroxyibuprofen
HOOC-IBP	Carboxylic acid metabolite of ibuprofen
IBP-GLU	Ibuprofen-β-D-glucuronide
IBP-TAU	Ibuprofen taurate
IBP-CoA	Ibuprofen-coenzyme A thioester
UGTs	UDP-glucuronosyltransferases
COX	Cyclooxygenase
PGE ₂	Prostaglandin E ₂
TxA ₂	Thromboxane A ₂
DTNB	5,5'-Dithiobis-(2-nitrobenzoic acid) (Ellman's reagent)
CuSO ₄ •5H ₂ O	Copper(II) sulfate pentahydrate
KNaC ₄ H ₄ O ₆ •4H ₂ O	Sodium potassium tartrate tetrahydrate
KCl	Potassium chloride
TCA	Trichloroacetic acid
NaCl	Sodium chloride

EDTA	Ethylenediaminetetraacetic acid disodium
NaOH	Sodium hydroxide
CH ₃ COOH	Glacial acetic acid
TBA	Thiobarbituric acid
SDS	Sodium dodecyl sulfate
BSA	Bovine serum albumin
MeOH	Methanol
EtOH	Ethanol
EtOAc	Ethyl acetate
BHT	Butylated hydroxytoluene
NAP	Naproxen sodium
SA	Salicylic acid
HPLC	High performance liquid chromatography
LC-MS	Liquid chromatography-mass spectrometry
ACN	Acetonitrile
X-OH-IBP	Hydroxylated ibuprofen
OH-IBP-OH	Dihydroxyibuprofen
X-OH-IBP-GLU	Hydroxyibuprofen-glucuronide
(S)-IBP	<i>S</i> (+)-ibuprofen
(R)-IBP	<i>R</i> (-)-ibuprofen
T1DM	Type-1 diabetes mellitus
GSSG	Glutathione disulfide
P-gp	P-glycoprotein
OAT	Organic anion transporter
ECCS	Extended clearance classification system
MDR	Multiple drug resistance
BCRP	Breast Cancer Resistant Protein
Phe	Phenylalanine
<i>p</i> -Tyr	<i>Para</i> -tyrosine
<i>m</i> -Tyr	<i>Meta</i> -tyrosine
<i>o</i> -Tyr	<i>Ortho</i> -tyrosine
DOPA	Dihydroxy-phenylalanine
RSD	Relative standard deviation
SD	Standard deviation

2. Introduction

Diabetes mellitus (DM) is a common disease with a complex metabolic and endocrine system influencing a large proportion of the global population. The prevalence rate of diabetes keeps increasing, estimated to reach 10.2% in 2030 (1). DM is described by high blood glucose levels because of insufficient action and secretion of insulin from beta-cells of the pancreas. Hyperglycemia is considered a source of the development of diabetic complications *via* altering a variety of signaling pathways, leading to the induction of reactive oxygen species, oxidative stress, and cell death (2). A high rate of reactive oxygen species generated from the induced oxidative stress will contribute to the pathogenesis of diabetic patients (3, 4). In fact, in the absence of an appropriate response from endogenous antioxidant mechanisms, the redox imbalance causes the activation of stress-sensitive intracellular signaling pathways. The redox imbalance promotes the induction of diabetic mechanisms; cellular insulin resistance, and impaired insulin secretion or beta-cells dysfunction (3). The high dominant diabetic vascular complications are retinopathy, neuropathy, and nephropathy leading to several common health disorders and death.

In addition, besides their insulin injection and/or consumption of diabetic medications, patients are supposed to use a variety of other medicines. However, how and to what degree diabetes affects the metabolism of drugs has not been well studied. Pathophysiological changes during diabetes can affect various drugs' absorption, distribution, metabolism, and excretion. In the first comprehensive review of the field, Gwilt et al. concluded that further clinical studies are warranted to explain the variability in observed data and to understand the mechanisms behind diabetes-mediated changes (5). However, previous studies have provided inconsistent data for multiple drugs, possibly due to variations in patient characteristics or control of patients' diabetes at the time of data collection (5-8).

Therefore, research on the effect of hyperglycemia using experimental animals is of great importance in better understanding the changes in the fate of drugs in diabetic individuals. Streptozotocin (STZ) induced hyperglycemia in the rat is a frequently used animal model for such investigations [7]. There have been a series of previous investigations in the Institute of Pharmaceutical Chemistry studying the effect of experimental hyperglycemia on the pharmacokinetics of various xenobiotics [110-112]. As a continuation of these previous studies, the present work aims to investigate the change in the pharmacokinetics (metabolism and elimination) of ibuprofen, a widely used non-steroid anti-inflammatory drug. Furthermore,

chemical characterization of oxidative damage of lipids, proteins, and selected peptides (glutathione) and amino acids (phenylalanine) was to be performed under our regularly used animal model. The research also seeks information on whether oxidized ibuprofen metabolites could indicate oxidative stress in the small intestine and the liver.

2.1. Experimental diabetes and oxidative stress

Oxidative stress is an imbalance in the production of reactive oxygen species (ROS) and defenses of antioxidant systems followed by high potential harmful impacts. ROS are highly reactive chemicals that hold unpaired electrons. ROS are generated from biochemical reactions of normal cell physiology and cell defense as unneglectable byproducts that may damage tissues due to their unpaired electrons (9). Intracellular organelles, like mitochondria, peroxisomes, and endoplasmic reticulum, utilize high oxygen proportion in their regular duties, and thus they have a significant role in their endogenous source generation (10). As a result of their instability and high reactivity, they can impair the stability of adjacent molecules. This develops a spoiling chain reaction terminated with tissue damage (10). This destruction comes from excess production of both ROS and RNS compared to the shortage of antioxidant molecules, enzymatic and non-enzymatic, leading to oxidative stress and nitrosative stress. These reactive species can react with sensitive endogenous and exogenous molecules to form characteristic products. ROS target the dominant biomolecules like proteins, lipids, and nucleic acids by impairing their structural integrity to initiate and/or advocate many common human diseases (10). The toxic effects of these oxygen species increase when trace iron is present since iron can catalyze the formation of hydroxyl radicals (Fenton reaction) (Figure 1). Therefore, the importance of non-enzymatic oxidation can be particularly significant under inflammatory conditions and any other ones under which elevated ROS are formed (11, 12). The most reactive species are hydroxyl radicals that attack various biological molecules, although they have a short life span. Superoxide radicals are less reactive than hydroxyl radicals, but they have a significant role in generating hydroxyl radicals and hydrogen peroxide (9, 13).

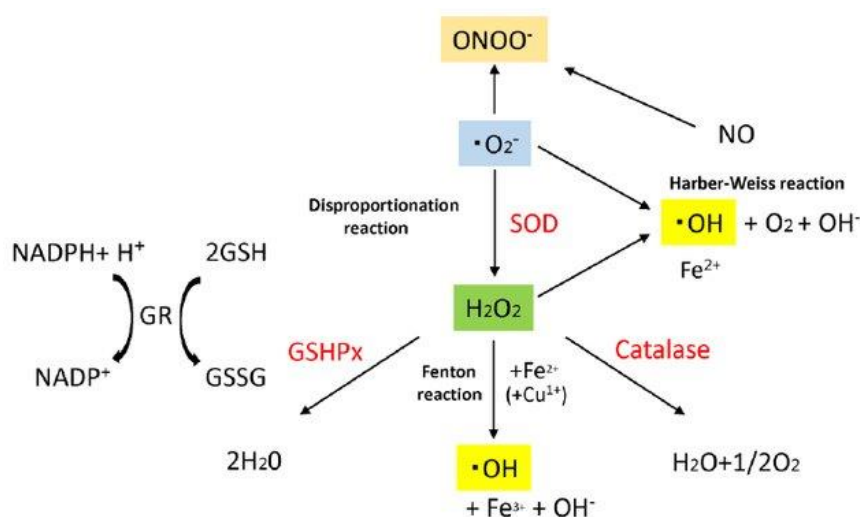


Figure 1. Generation and elimination of reactive oxygen species (ROS) with the Fenton reaction (14).

Hyperglycemia brings oxidative stress *via* generating a higher rate of reactive oxygen species contributing to the pathogenesis of diabetes from several modes of cell death causation (3, 15). Antioxidant defenses in diabetes are insufficient and not well-matched with the redox imbalance, leading to further development of oxidative stress. Hyperglycemia and oxidative stress are considered the primary sources in the pathogenesis of diabetic complications. In addition, oxidative stress plays a significant role in the onset of diabetes, cellular insulin resistance, and impairment of insulin secretion (16).

The induction of hyperglycemia is usually accountable as experimental diabetes to investigate unfavorable diabetic outcomes. Streptozotocin (STZ) and alloxan are the most utilized substances in diabetic research (17). Both agents have a similar structure and chemical properties to the glucose molecule. (As a matter of fact, streptozotocin is a glucose derivative.) Therefore, they are acceptable to cellular transport *via* the glucose transport protein (GLUT2). This transport protein is present in pancreatic beta cells, which clarifies the mechanisms of the toxicity of alloxan and STZ. Cellular toxicity comes through generating ROS but with a different means of oxidative stress (17, 18).

2.1.1. Mechanism of action of streptozotocin

Streptozotocin is a broad-spectrum antibiotic derived from the bacteria of *Streptomyces achromogenes*. STZ targets a group of membrane proteins on pancreatic β -cells (19). After cellular influx *via* GLUT2, streptozotocin (N-(methylnitrosocarbamoyl)- α -D-glucosamine) will be metabolized into a methylnitrosourea (N-nitroso-N-methylurea) and a glucose moiety. Methylnitrosourea is an alkylating agent that causes DNA alkylation or damage and then activation of poly-ADP ribosylation. As a result, poly ADP-ribosylation yields reduction of ATP and NAD^+ , then the destruction of beta-cells, and finally, the insulin-dependent type of diabetes (Figure 2). STZ is also a source of ATP dephosphorylation and boosts xanthine oxidase activity, which leads to superoxide radicals, hydrogen peroxides, and hydroxyl radicals. In the end, beta-cell damage will happen because of oxidative stress formation. Furthermore, by releasing nitric oxides, streptozotocin precludes the action of aconitase, joining the process of DNA and beta-cell damage (17, 20). While GLUT2 is present in the liver and kidney but with a lower proportion than β -cells. The liver metabolism of STZ is rapid, has a short half-life, and has fast elimination through urine. Consequently, STZ toxicity in the liver and kidney can count due to continuous hyperglycemia (21, 22).

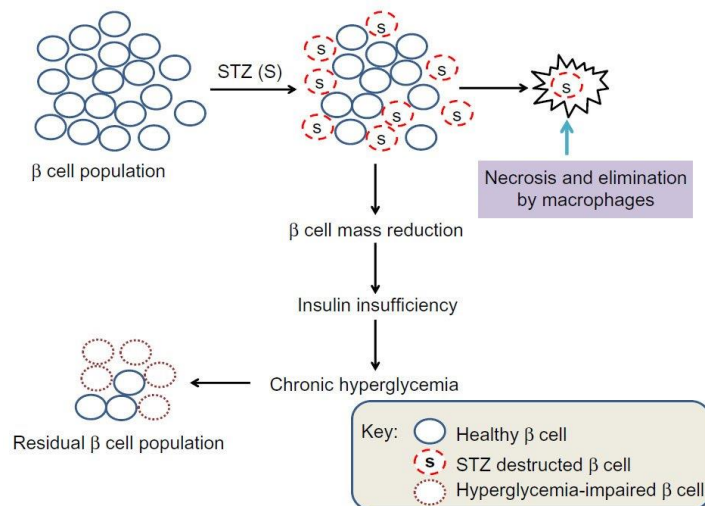


Figure 2. Partial destruction of β -cell and hyperglycemia derived from streptozotocin induction (22).

2.2. Hyperglycemia and oxidative stress

Investigations are shown the existence of a connotation between hyperglycemia and oxidative stress (4). Hyperglycemia enhances the production number of reactive oxygen species and reduces antioxidant defense activities (23). The enzymatic source of ROS formation is enzymes of the mitochondrial respiratory chain, xanthine oxidases, cyclooxygenases, lipoxygenases, peroxidases, and nitric oxide synthases (2, 14). Because the insufficient antioxidant system and not compatible with the redox imbalance leads to further development of oxidative stress. Together, hyperglycemia and oxidative stress participate in the onset of diabetes and are considered the source of the pathogenesis of diabetic complications (3, 16). Hyperglycemia upsets the ordinary mitochondria and non-mitochondrial ancestries *via* metabolic disorders to generate extra superoxide production. This step triggers many long oxidative stress pathways causing diabetic complications (4, 10). Reactive oxygen species (ROS) have a physiological role at low dosage (24) in insulin signaling *via* inhibiting one of the phosphatase action pathways, PTP 1B. This results in H_2O_2 formation from NADPH oxidase once insulin binds to the receptor, and hydrogen peroxide prevents dephosphorylation and keeps tyrosine phosphorylation (25, 26).

Several metabolic and signaling pathways are proposed to promote oxidative stress, oxidative damage, and diabetic complications in diabetes, generally correlating to the metabolism of glucose and lipids. In addition, extramitochondrial production of superoxide is central to these metabolic mechanisms and the development of disease complications. The proposed pathways are glucose oxidation, glyceraldehyde-3-P dehydrogenase (GAPDH) or (PARP) pathway, polyol pathway, hexosamine pathway, diacylglycerol (DAG) formation, and protein kinase C (PKC) activation, glyceraldehyde autooxidation, advanced glycation end-products (AGEs), and stress-sensitive signaling pathways (4, 16, 23).

As a primary suggested mechanism, glucose oxidation raises the level of reactive oxygen species. Glucose is oxidized to a reactive intermediate (enediol radical) in a transition metal-dependent reaction and converted to ketoaldehyde with superoxide emission. Superoxide is converted to hydrogen peroxide (H_2O_2) *via* the action of superoxide dismutase (SOD). H_2O_2 can be converted, in the presence of transition metals, to a highly reactive oxidative radical named hydroxyl radical ($\bullet OH$) (27, 28). Moreover, the reaction of nitric oxide with superoxide generates reactive peroxynitrite radicals (29, 30).

In the process of glycolysis, glucose is oxidized to produce energy. Glucose is converted to glucose-6-phosphate, fructose-6-phosphate, and glyceraldehyde-3-phosphate. Then this product is extra phosphorylated by GAPDH and ends up with pyruvate to enter the Krebs cycle and mitochondrial metabolism. Hyperglycemia enhances mitochondria to generate superoxide radicals disturbing the pathway by inactivating the enzyme activity of GAPDH (31, 32). Poly-ADP-ribose polymerase-1 (PARP-1), a DNA repair and apoptosis enzyme, is activated due to ROS causing DNA strand breaks. By poly-ADP-ribosylation, PARP-1 inhibits glyceraldehyde-3-phosphate dehydrogenase leading to the accumulation of glyceraldehyde 3-phosphate intracellularly (33). Two signaling pathways are activated by these high levels of glyceraldehyde-3-phosphate; namely, advanced glycation end-products (AGEs) and diacylglycerol (DAG) formation generating PKC activation (Figure 3). Further accumulation of glycolytic metabolites increases fructose 6-phosphate and activates the hexosamine pathway. At the last stage, the glucose level increases, leading to activation of the polyol pathway and NADPH consumption. All the above processes result from the inhibition of GAPDH (4).

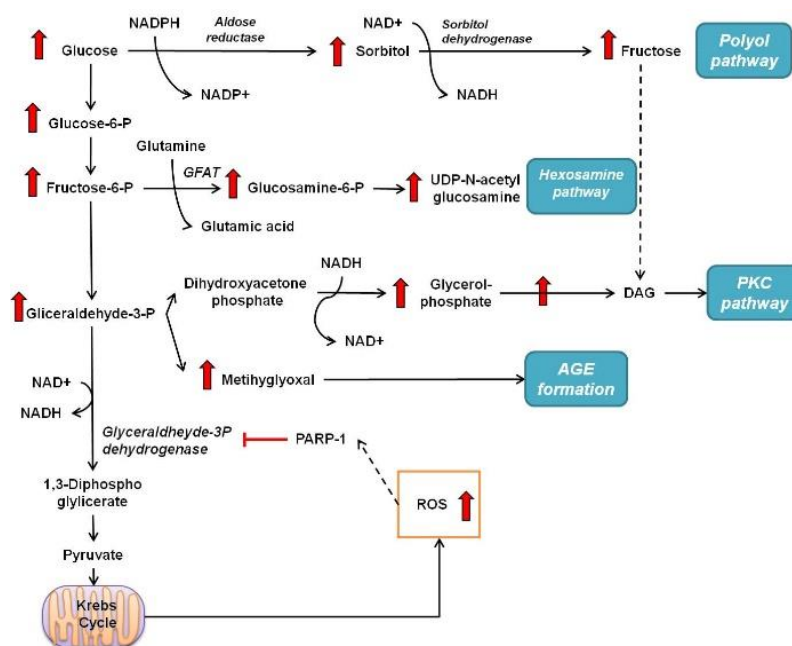


Figure 3. Oxidative stress-related pathways derived from glucose metabolism (16).

2.3. Oxidative damage to lipids

ROS promote diabetic complications due to their damaging impacts on cellular macromolecules such as lipids, proteins, and DNA (29). Consequently, oxidative stress is mediated in pathophysiological conditions like diabetes mellitus, cancer, and rheumatoid arthritis (34). It is well established that lipids of the cell membrane containing polyunsaturated fatty acids having double bonds are highly susceptible to free radical attacks (35). Lipid peroxidation is a valuable research area related to ROS and oxidative stress and is considered a biomarker of oxidative stress in experimental studies (36). 4-Hydroxy-2-nonenal (HNE) and malondialdehyde (MDA) are the two main harmful lipid peroxidation products. They are very useful biomarkers to determine the extent of the peroxidation process of the lipids, particularly the reaction of MDA with thiobarbituric acid (37). The conjugated diene products are also employed as a biomarker for assessing lipid peroxidation, which is critical in the pathophysiology of several disease conditions (38, 39).

The process of lipid peroxidation is classified into three main steps; initiation, propagation, and termination (40). As a result of the combination of hyperglycemia and oxidative stress conditions, free radicals are further distributed with the susceptibility to forming different forms of ROS; superoxide radicals, hydrogen radicals, and hydroxyl radicals. ROS, particularly hydroxyl radicals ($\bullet\text{OH}$), can abstract allylic hydrogen of the methylene group of polyunsaturated lipids to form lipid radicals ($\text{L}\bullet$). This stable radical undergoes a molecular rearrangement, resulting in conjugated diene formation. Conjugated diene is a hydrocarbon chain containing two double bonds parted with a single bond (38, 41). The formed radicals are ready to react with molecular oxygen and form lipid peroxyl radicals ($\text{LOO}\bullet$). Lipid peroxyl radicals can abstract a hydrogen atom from another polyunsaturated fatty acid to generate lipid hydroperoxide (LOOH) and a new lipid radical ($\text{L}\bullet$) (Figure 4) (40, 42). While reduced metals, like Fe^{2+} , can react with LOOH to form lipid alkoxyl radical ($\text{LO}\bullet$) (Fenton-type reaction). Lipid peroxyl radicals ($\text{LOO}\bullet$) and alkoxyl radicals ($\text{LO}\bullet$) induce a continuous chain reaction of lipid peroxidation (43, 44).

Peroxidation deteriorates cellular membrane integrity, membrane permeability and fluidity, ion transport modulations, and suppression of metabolic processes (45). It produces several low molecular weight carbonyl compounds due to the degradation of the formed lipid hydroperoxides (46). Reduced metals and vitamin C breaks down LOOH into reactive aldehyde products such as malondialdehyde (MDA), 4-hydroxy-2-nonenal (HNE), 4-hydroxy-2-hexenal

(4-HHE), and acrolein (47-50). Aldehyde byproducts are reactive and may cause several undesired health conditions, while some have a carcinogenic capability. Their measurement is challenging in biological tissue samples due to instability. Therefore, aldehyde products require derivatization techniques; for this purpose, 2,4-dinitrophenylhydrazine (DNPH) is generally used in their analysis.

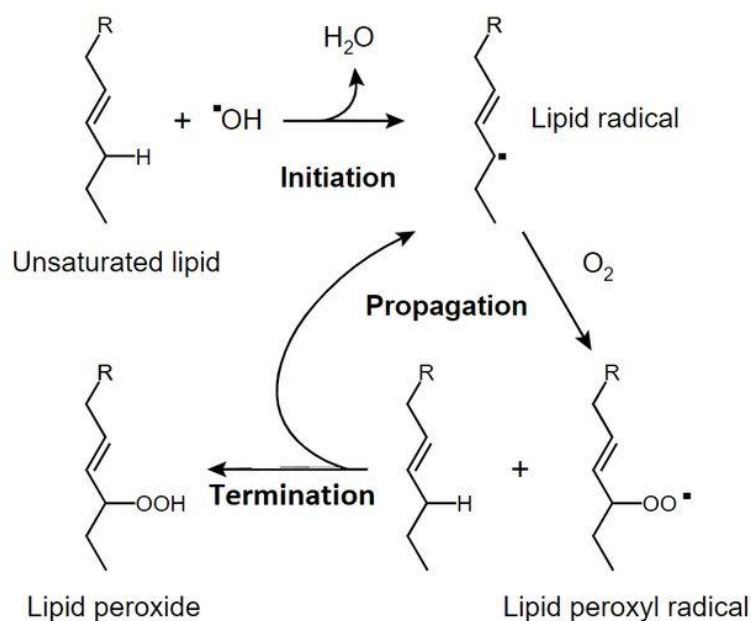


Figure 4. The mechanism of lipid peroxidation with the exhibition of its three main steps; initiation, propagation, and termination (51).

2.4. Oxidative damage to proteins

The structure and activity of proteins are susceptible to many post-translational modifications such as phosphorylation, methylation, acetylation, oxidation, etc. In addition, proteins can be modified by several reactive physiological byproducts such as free radicals like ROS, reactive aldehydes from peroxidation, and glycation. After protein biosynthesis, these structural modifications can change the biological activities of proteins. The main characteristic of oxidized proteins is the proposed amino acid side chains with a carbonyl group. The process is known as protein carbonylation. These changes are considered irreversible modifications, possibly inducing polypeptide conformational variations with a lack of biological actions. As a biomarker, the carbonyl content is commonly measured to assess the degree of protein oxidation. The deficiency of the antioxidant system against the increasing number of reactive

radicals augments the environment of oxidative stress and then turns into the oxidative alteration of proteins (52-54).

The first and significant mechanism proposed for induction of protein carbonylation and oxidative impairment, scientifically supported, is metal-catalyzed oxidation (MCO) (55, 56). In this mechanism, the oxygen molecule is reduced through an electron donor system to superoxide radicals (O_2^\bullet) and then to the accumulation of hydrogen peroxide (H_2O_2). As well as, trace metal (Fe^{3+} or Cu^{2+}) is reduced by reacting with superoxide. The reduced metal ion binds to the specific binding site on the protein. The transition metal ion *via* the Fenton reaction reacts with hydrogen peroxide (H_2O_2), followed by the generation of hydroxyl radicals ($^\bullet OH$) and oxidized metals. Oxidized protein modification will mainly occur because ($^\bullet OH$) reacts with the amino acid side chains, forming aldehydes or ketones (Figure 5). This is the reason for protein spoilage and loss of action (52). α -aminoadipic semialdehyde (AAS) and γ -glutamic semialdehyde (GGS) are carbonyl products that are dominantly deriving from lysine, arginine, and proline, respectively, as a result of protein oxidation (57, 58).

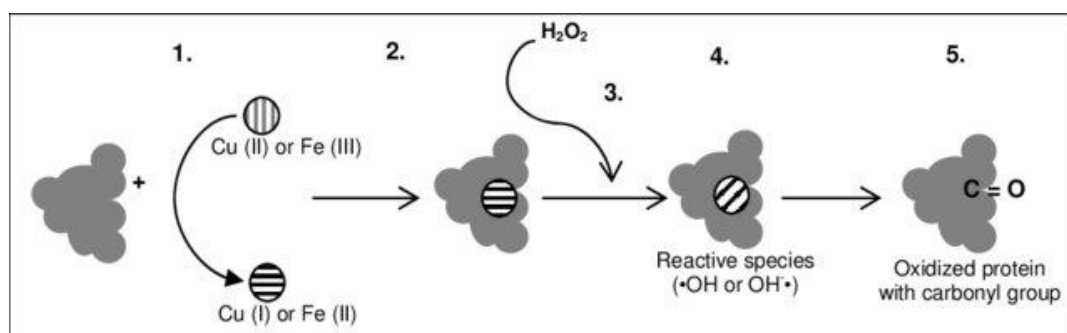


Figure 5. Protein carbonylation by the mechanism of metal-catalyzed oxidation (MCO). The mechanism steps are highlighted; reduction of trace metals (1) and their binding to the protein (2), the reaction of H_2O_2 with reduced metals (3), oxidation of metal ions with $^\bullet OH$ formation (4), $^\bullet OH$ attack and aldehydes/ketones formation (5) (59).

Protein carbonylation can occur from additional proposed mechanisms, such as lipid peroxidation and glycation reactions. Reactive aldehydes of the lipid peroxidation (like 4-hydroxy-2-nonenal (HNE), malondialdehyde (MDA), 4-oxo-2-nonenal (ONE), acrolein, and glyoxal), formed from oxidative stress, can also react with the amino acid side chains. They react with proteins *via* Schiff base formation or Michael reaction (52, 60). Glycation, through non-enzymatic reactions, may generate protein carbonylation. This proceeds by nucleophilic addition of carbonyl groups of reducing sugars to the amino acid side chains. The reaction leads

to form reversible Schiff bases and Amadori products *via* structural rearrangements. The number of this product is associated with an increase in the quantity of sugars. Under continuous oxidative stress conditions, new highly reactive compounds named α -dicarbonyls are generated from Amadori products such as 3-deoxyglucosone (3-DG), glyoxal, and methylglyoxal (MGO). Alpha-dicarbonyls products can bind to amino acid residues of proteins like lysine and arginine and alters them into irreversible adducts known as advanced glycation end products (AGEs) (61, 62). AGEs impair post-translational proteins' physiological functions besides interfering with their receptor and enzymatic activities (63). In addition, α -dicarbonyl products can able to deaminate the ϵ -amino group of lysine through a metal-catalyzed reaction and generate α -aminoadipic semialdehyde (AAS) (52, 64).

Several analytical methods are available to determine the number of carbonylated proteins, such as the derivatization method with 2,4-dinitrophenylhydrazine (DNPH), biotin hydrazide, and *p*-aminobenzoic acid (ABA), and immunochemical detection. The most commonly applied analytical approach in determining protein carbonylation is the DNPH derivatization method to assess the oxidized proteins.

2.5. Oxidative damage to nucleic acids (DNA)

Additional cellular biomolecules exposed to ROS and oxidative stress are DNA. This initiates several DNA lesions, such as oxidized bases, DNA strand breaks, and the formation of cross-links between DNA and proteins. Hydroxyl radicals are highly reactive species most commonly formed in biological Fenton-type reactions, damaging DNA (65). Position-8 of guanine is the site of the radical attack and yields 8-hydroxydeoxyguanosine (8-OHdG) excreted in the urine. Before DNA replication, 8-OHdG enhances spontaneous transversion mutations of G:C \rightarrow T:A, which can be restored *via* a base excision repair system (65). 8-Oxo-*d*Guo, as a biomarker, is measurable to determine DNA damage status by HPLC in diabetic specimens. Single-cell gel electrophoresis and Comet assay used to detect oxidized purines in DNA are alternative methods to determine DNA damage (66).

Secondary lipid peroxidation products, particularly 4-HNE and MDA, can contribute to the structural modification of nucleic acids. 4-HNE has a mutagenic and genotoxic effect. It can react with DNA bases. The 4-HNE-dG residue is considered a good marker for evaluating its genotoxic impacts and is mainly found in nuclear DNA. 4-HNE-dG induces p53 mutation,

a well-known tumor suppressor gene in human cancers (67). MDA also has a vital role in DNA damage and mutations. MDA biomarker is M1dG, which can be repaired by nucleotide excision repair. MDA-DNA adducts result in several lesions, such as point and frameshift mutations, strand breaks, and cell cycle arrest (41).

The mitochondrial genome is highly susceptible to oxidative damage. It was conducted that oxidative stress degrades mitochondrial RNAs, and there is a positive relation between GSH and mitochondrial DNA destruction. ROS degrades mtDNA's bases resulting from high levels of 8-hydroxydeoxyguanosine, which leads to mispairing and point mutations. PCR is a selected method to detect these kinds of mitochondrial mutations. (68).

2.6. Non-enzymatic oxidative transformations of exogenous compounds

Pathophysiological changes during diabetes can potentially affect the absorption, distribution, metabolism, and excretion of various exogenous compounds, among them drugs (5-8). Such changes can be the results of (1) the damaging effect of the ROS on the enzymes and transporters involved in the biotransformation of drugs and/or (2) direct reactions of the reactive species with the parent (or metabolized) drugs. Cytochrome P450, for example, is a superfamily of enzymes generally involved in the metabolism of various exogenous and endogenous compounds by oxidation and reduction reaction (69, 70). The enzyme family of P450 1, 2, and 3 metabolize 96% of xenobiotics, particularly the subfamily of P450 3A (71). Some pathophysiological conditions may change the activity of P450 isoenzymes, *via* induction or suppression, like diabetes, hypertension, and cancer (72-74). In diabetes, several factors may affect the enzyme activity of cytochrome P450, such as age, gender, diabetes duration, and diabetes control (75). In STZ-treated diabetic rats, there are various changes in the expression of P450 isoenzymes, and similarly, GSH-dependent enzymes are altered in experimental and human diabetes (76-79). Oian and Hall, for example, reported that experimental diabetes in the rat led to alterations of the elimination of *R*(-) and *S*(+)-ibuprofen and a change in the inversion rate of *R*(-) -ibuprofen (80). Furthermore, reactive oxygen species can react with sensitive endogenous and exogenous molecules to form characteristic oxidized products. Therefore, non-enzymatic (ROS-initiated) oxidation can be particularly significant at the sites of inflammations and under any other conditions accompanied by elevated ROS formations (11, 12). In this study, ibuprofen was selected to analyze its biotransformation under STZ-induced hyperglycemia in the rats.

2.6.1. Biotransformation of ibuprofen

Ibuprofen (IBP) is a white or colorless crystalline and stable compound highly soluble in organic solvents and less in water (21 mg/l) (81). IBP is one of the non-steroidal anti-inflammatory drugs (NSAIDs) and widely used over the counter (OTC) medicines, after aspirin and paracetamol. Ibuprofen belongs to the group of 2-arylpropionic acid derivatives with a molecular formula of $C_{13}H_{18}O_2$ and IUPAC name; (*RS*)-2-[4-(2-methylpropyl) phenyl] propanoic acid (Figure 6). The acid dissociation constant (pK_a) and octanol-water partition coefficient ($\log K_{ow}$) of ibuprofen are 4.91 and 3.97, respectively (82). The main structural feature of its 2-arylpropionic acid side is an sp^3 -hybridized chiral carbon atom. Although the current therapy of ibuprofen is in racemic doses, the stereoselectivity of its enantiomer forms is noticeable. The *S*(+)-enantiomer displays higher effectiveness compared to the *R*(-) form (83). IBP has three main pharmacological properties of NSAIDs: anti-inflammatory, analgesic, and antipyretic. It is generally applied to relieve minor pains and inflammation at over-the-counter doses, and used for some chronic diseases, for instance, rheumatoid arthritis, at prescription doses (84, 85).

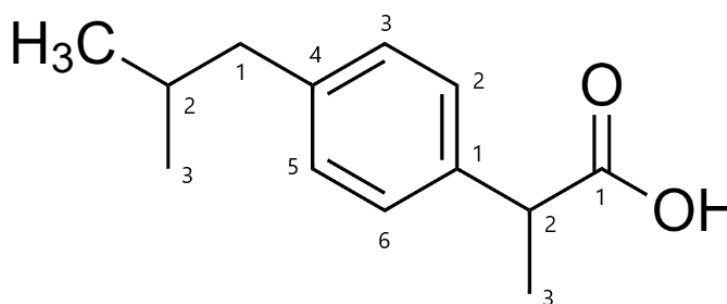


Figure 6. Chemical structure of ibuprofen or (*RS*)-2-[4-(2-methylpropyl) phenyl] propanoic acid.

2.6.1.1. Pharmacokinetics and pharmacodynamics

Oral intake of ibuprofen is the usual therapeutic route, although other administration routes, such as rectal, topical, and intravenous, are confirmed. Following oral intake, IBP has a rapid absorption (t_{\max} ; 1-2 h) depending on its formulation in the gastrointestinal tract (GIT), particularly in the small intestine. For instance, the formulated combination of granular ibuprofen and L-arginine has faster absorption and a higher plasma concentration (84). Ibuprofen is extensively exposed to combine with plasma proteins (up to 98%), making the wide range of its therapeutic concentration. As a result, IBP has a low tissue distribution volume (0.1 L/kg) and short plasma half-life ($t_{1/2}$; 1-3 h), along with the need for frequent doses to provide therapeutic effects. Besides its small volume of distribution, ibuprofen can accumulate and penetrate the central nervous system, cerebrospinal fluid, and synovial fluid leading to its analgesic and anti-inflammatory outcomes (83-85). The equal ratio of racemic dose of IBP will be shifted, a unidirectional inversion, from the *R*(-)-enantiomer toward the more active *S*(+)-enantiomer after the absorption. This inversion might occur in the GIT and systemic circulation. At the same time, it is still controversial whether the absorption dose will affect the pharmacokinetics of *R*(-) and *S*(+)-ibuprofen and whether this inversion ratio is significant or not (83, 84). In a newborn child, the half-life of IBP, compared with adults, is very long (30-45 h), maybe because of inadequate metabolic enzyme activity (cytochrome P450) and poor neonatal renal filtration. In comparison, ibuprofen pharmacokinetics in young children is similar to adults (84, 85).

The high proportion of ingested ibuprofen will undergo biotransformation, with the bit of remaining amount of the parent drug unchanged. The first metabolism step of ibuprofen is oxidation, to inactivate the molecule through CYP enzymes. In humans, the main CYP isoform responsible for the clearance of ibuprofen *via* hydroxylation is extensively CYP2C9, with the minor role of CYP2C8, CYP3A4, and CYP2C19 (84, 86-89). These enzymes catalyze aliphatic hydroxylation on primary, secondary, and tertiary carbon atoms of IBP, resulting in the formation of 1-hydroxy- (1-OH-IBP), 2-hydroxy- (2-OH-IBP), and 3-hydroxyibuprofen (3-OH-IBP). 3-OH-IBP is further oxidized to form carboxylic metabolite (HOOC-IBP) by cytosolic dehydrogenase reactions (Figure 7). 2-OH-IBP and HOOC-IBP are the most common metabolites of ibuprofen after oral intake compared to the rest oxidized metabolites and can be detected in the feces and urines (84, 88, 90). Conjugation metabolism of ibuprofen and its hydroxylated metabolites will be followed, primarily with glucuronic acid, to form acyl-glucuronides that can react with proteins. Marginally, ibuprofen will conjugate with taurine,

leading to ibuprofen taurate (IBP-TAU). Still, this conjugation needs the production of ibuprofen-coenzyme A thioester (IBP-CoA) previously (88, 91). A part of ibuprofen is directly conjugated with glucuronic acid to form ibuprofen-acyl glucuronide utilizing UDP-glucuronosyltransferases (UGTs) in phase II biotransformation. Several UGTs have a role in ibuprofen metabolisms such as UGT1A3, UGT1A9, UGT2B4, UGT2B7, UGT2B17, and UGT 1A1 (92, 93). These isozymes are also distributed in the gastrointestinal tract, primarily UGT 1A1, and they can generate ibuprofen glucuronides. However, individual UGT isozymes are not well known in the glucuronidation path of IBP oxidized metabolites in phase I metabolism. After the metabolism phase, a high proportion of IBP metabolites and IBP conjugates are excreted through urine within 24 hours (94). A small proportion of the parent IBP and conjugated metabolites are excreted *via* bile ducts (85).

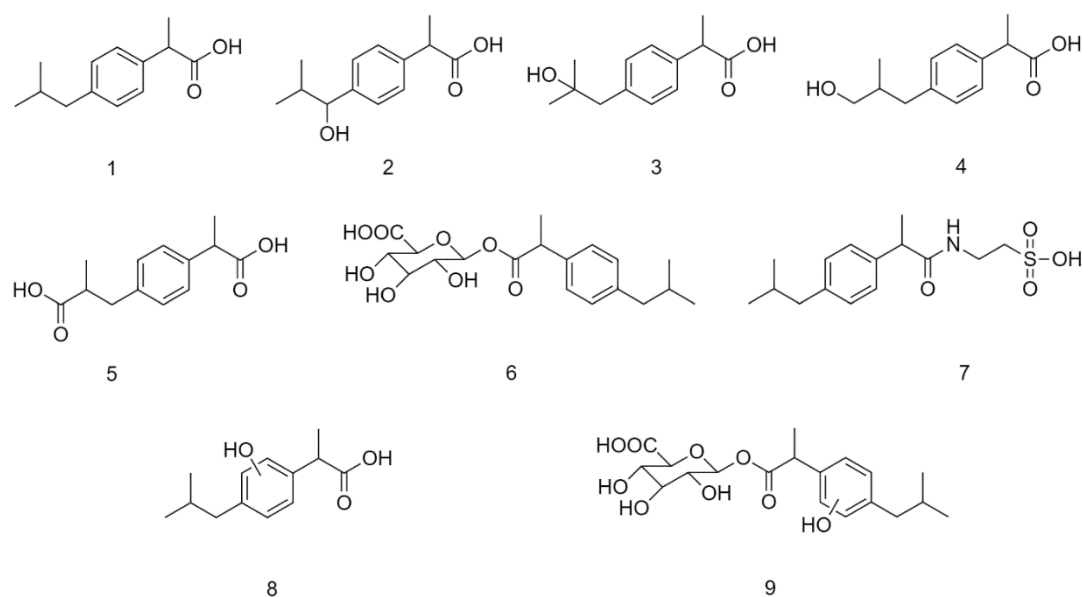


Figure 7. Structural formula of plausible metabolites of ibuprofen (IBP) (**1**): 1-hydroxyibuprofen (1-OH-IBP) (**2**), 2-hydroxyibuprofen (2-OH-IBP) (**3**), 3-hydroxyibuprofen (3-OH-IBP) (**4**), carboxyibuprofen (HOOC-IBP) (**5**), ibuprofen- β -D-glucuronide (IBP-GLU) (**6**), ibuprofen taurate (IBP-TAU) (**7**), aromatic hydroxylated ibuprofen (**8**), and glucuronide conjugate of an aromatic hydroxylated ibuprofen (**9**). (The position of the hydroxyl substitution of **8** and **9** is uncertain.)

Ibuprofen, like other NSAIDs, has a non-selective inhibition property for cyclooxygenases (COX). COX-1 is mainly in charge of producing prostanoids in normal tissue functions, while COX-2 is induced during inflammation and pain *via* the synthesis of

prostaglandin E₂ (PGE₂). IBP strongly inhibits the activity of both constituted COX-1 and inducible COX-2 (95). This leads to ceasing inflammation, pain, and platelet aggregation symptoms by preventing the formation of their precursors, such as prostaglandin E₂ and thromboxane A₂ (TxA₂) (85). As it was concluded, *S*(+)-enantiomer has a higher activity than the *R*(-)-enantiomer toward the inhibition of cyclooxygenases, especially with COX-1 (96).

2.6.1.2. Stereochemistry

Ibuprofen as one of 2-arylpropionic acid derivatives holding a tetrahedral chiral carbon. The market formulation of IBP is frequently available in racemate doses. As well studied that the *S*(+)-isomer shows more potent activity than the *R*(-)-isomer, which looks like an inactive form (83, 96, 97). For instance, Neupert et al. showed that the inhibition potency (IC₅₀) of *S*(+)-ibuprofen toward both cyclooxygenases are (2.1 μM) and (1.6 μM), respectively, and the inhibition of *R*(-)-ibuprofen toward COX-1 is (34.9 μM) and no inhibition of COX-2 (up to 250 μM) (97). In addition, the equal ratio of the prescribed racemate dose will be adjusted as the *R*(-)-enantiomer undergoes a unidirectional inversion to the *S*(+)-enantiomer (active form) (98).

The inversion mechanism will occur enzymatically, *in vivo*, by forming two structural intermediates. The initial step is the activating of *R*(-)-ibuprofen stereoselectively by a long fatty acid chain enzyme (acyl-CoA synthetase) to a reversible structure named *R*(-)-ibuprofenoyl-CoA thioester (99). The new structure can be epimerized into a reversible structure of *S*(+)-ibuprofenoyl-CoA thioester by epimerase (100). The inversion mechanism can be completed by hydrolysis of *S*(+)-ibuprofenoyl-CoA thioester to the irreversible active form of IBP (101) (Figure 8). Acyl-CoA synthetase cannot activate, *in vivo*, *S*(+)-ibuprofen *via* formulating *S*(+)-ibuprofenoyl-CoA to be inverted to the inactive form (97, 100). The enantiomer inversion may happen in the gastrointestinal tract and blood circulation (83, 84). The proportion of this configuration is not well clarified under abnormal physiological conditions such as hyperglycemia.

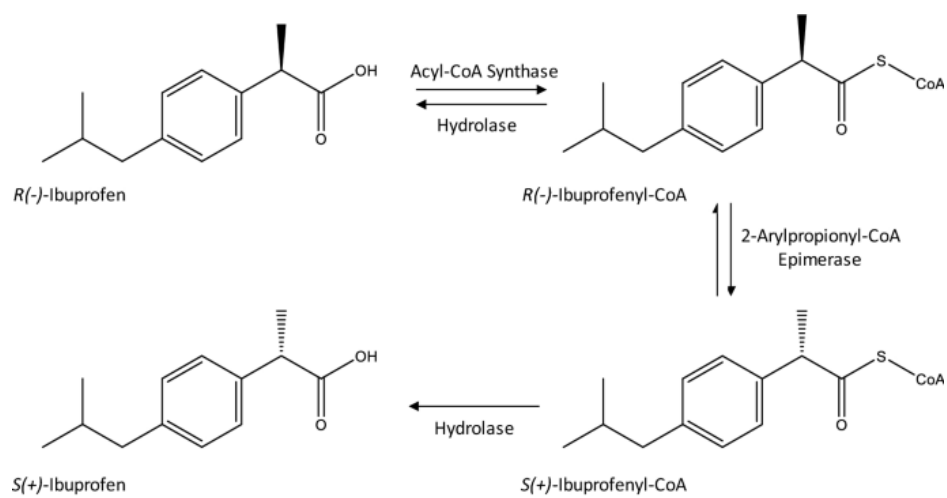


Figure 8. Proposed mechanism of *R*(-)-ibuprofen inversion in rat liver (102).

3. Aims

- To study the oxidative transformations of selective endogenous compounds – lipids, proteins, peptides (glutathione), and amino acids (phenylalanine) under the influence of STZ-induced experimental diabetes in the small intestine, the liver, and the kidney of rats.

 - *In vitro* investigation of ibuprofen oxidation to explore the main oxidative products in two (Fenton and Udenfriend) non-enzyme catalyzed reactions.

 - To study the *in vivo* oxidative transformations of ibuprofen in the small intestine and the liver under the experimental diabetes of the rat.
- (a) Investigate the main oxidative and conjugated metabolites of ibuprofen in small intestine perfusates and bile of control and hyperglycemic rats.
- (b) Investigate intestinal absorption and biliary excretion of ibuprofen and its oxidized metabolites in control and streptozotocin-induced rats.
- (c) Investigate the ratio of *R*(-) and *S*(+)-ibuprofen in small intestinal perfusates and bile of control and hyperglycemic rats.

4. Materials and Methods

4.1. Chemicals

Copper(II) sulfate pentahydrate ($\text{CuSO}_4 \cdot 5\text{H}_2\text{O}$), sodium sulfate (Na_2SO_4), sodium potassium tartrate tetrahydrate ($\text{KNaC}_4\text{H}_4\text{O}_6 \cdot 4\text{H}_2\text{O}$), potassium iodide (KI), and potassium chloride (KCl) were obtained from Reanal (Budapest, Hungary). Trichloroacetic acid (TCA), sodium hydroxide (NaOH), sodium chloride (NaCl), and ethylenediaminetetraacetic acid disodium ($\text{EDTA} \cdot \text{Na}_2$) were from Molar Chemicals (Budapest, Hungary). Guanidine hydrochloride, glacial acetic acid (CH_3COOH), and thiobarbituric acid (TBA) were purchased from M.P. Biomedicals (Illkirch, France), Scharlau (Barcelona, Spain), and AppliChem (Darmstadt, Germany), respectively. Sodium dodecyl sulfate (SDS), methanol (MeOH), ethanol (EtOH), ethyl acetate (EtOAc), and n-hexane were obtained from VWR chemicals (Debrecen, Hungary). Butylated hydroxytoluene (BHT), Trizma, 5,5'-dithiobis-(2-nitrobenzoic acid) (DTNB), racemic ibuprofen (IBP), (S)-(+)-ibuprofen, naproxen sodium (NAP), salicylic acid (SA), streptozotocin (STZ), ibuprofen- β -D-glucuronide (IBP-GLU), and carboxyibuprofen (HOOC-IBP) were from Sigma-Aldrich (Budapest, Hungary). 3-Hydroxyibuprofen (3-OH-IBP) was from HPC Standards GmbH (Cunnersdorf, Germany). 1-Hydroxyibuprofen (1-OH-IBP) and 2-hydroxyibuprofen (2-OH-IBP) were obtained from Dr. Ehrenstorfer GmbH (Augsburg, Germany). All chemicals and reagents were analytical or HPLC grade. The standard isotonic perfusion medium had the following compositions (mM): NaCl 96.4, KCl 7.0, CaCl_2 3.0, MgSO_4 1.0, sodium phosphate buffer (pH 7.4) 0.9, Tris buffer (pH 7.4) 29.5, glucose 14.0, mannitol 14.0. Blood glucose level was checked with an AccuChek blood glucose meter (Roche).

4.2. Animals and experimental procedure

Male Wistar rats (9-11 weeks old; weighing 250-300 g; TOXI-COOP, Hungary, Budapest) were separated into four groups. Group I was the control, and Group II, III, and IV were induced diabetic animals ($n=4$ each). They are subdivided into one-week (Group II), two-week (Group III), and four-week (Group IV) diabetic animals. Experimental diabetes was induced by intravenous injection of streptozotocin (STZ) (65 mg/kg bw). The experimental animals were provided standard chaw (Safe D40, Scientific Diets, Rosenberg, Germany) and water ad libitum. The chaw was withdrawn the day before the experiments (at 4 p.m.). Blood glucose levels were tested on the day of the experiments (at 8 a.m.) to confirm hyperglycemia.

The animals were anesthetized with an intraperitoneal injection of urethane (1.2 g/kg bw). The abdomen was opened by a midline incision, and the selected organs were collected. The collected samples were stored in a deep freezer (-70°C) until the analysis.

4.3. Sample preparation

Samples were taken from the freezer (-70°C) and incubated on ice for 5 minutes to become de-frozen and ready. A particular mass of the organ sample was weighted, then homogenized with the homogenizing buffer pH 7.4, in a proportion (1:3). The buffer was composed of KCl (0.154 M), Trizma (50 mM), and EDTA.Na₂ (5 mM). The matrix was completed with BHT (50 mg/ml in MeOH). The mixture was homogenized on ice by Witeg[®] homogenizer (HG-15A) for 90 seconds (50 speed rate). The homogenate was diluted with the buffer to reach the final mass/volume, in a proportion (1:4), sample preparation (homogenate 25%). The prepared samples were dispensed in Eppendorf vials and stored in a deep freezer (-70°C) until the time of experiments. Before the experiments, the homogenate was removed from the fridge and incubated (37°C) for 10 minutes in a water bath.

4.4. UV-Vis determination of protein content (Biuret assay)

To 0.1 ml of organ homogenate (25%) in a 10 mL test tube, 1.0 mL of SDS (8.1%), 0.9 ml of NaCl (0.9%), and 8.0 ml of biuret reagent (CuSO₄•5H₂O, KNaC₄H₄O₆•4H₂O, KI, and NaOH in distilled water) were added. The mixture was incubated for 10 minutes at room temperature. Then, 1.0 ml of the sample was measured by UV-spectrophotometer (Jasco[®] V-750) at 550 nm against the blank. The protein concentration of samples was determined by the equation of calibration curve of bovine serum albumin (BSA) ($y = 0.2583x + 0.1124$, $R^2 = 0.9997$). The calibration curve plot was achieved with different concentrations of BSA in the same procedure of biuret assay designed and performed before sample measurements, as shown in Table 1 (103).

Table 1. Determination of protein content by Biuret assay of different concentrations of the bovine serum albumin (BSA).

No.	BSA volume (mL)	8.1% SDS (mL)	0.9% NaCl (mL)	Biuret reagent (mL)	BSA concentration (mg/mL)
1	--	1	1	8	Blank
2	0.1	1	0.9	8	0.3
3	0.2	1	0.8	8	0.6
4	0.3	1	0.7	8	0.9
5	0.4	1	0.6	8	1.2
6	0.5	1	0.5	8	1.5

4.5. UV-Vis determination of protein carbonyl content (DNPH-protein adducts)

To 0.2 mL of organ homogenate (25%), 1.0 mL of 0.1 M phosphate buffer pH 7.2 and 0.8 mL of distilled water and 2.0 mL of 5mM 2,4-DNPH (in 2 M hydrochloric acid) were added. The mixture was incubated in the dark at room temperature for one hour by vortexing every 15 minutes. Then, 2.0 mL of 50% trichloroacetic acid was added, and the mixture was kept for another hour under the same condition. After that, the mixture was centrifuged for 15 minutes/5000 rpm. The supernatant was discarded, and the residue was washed with 1.0 mL of EtOH/EtOAc (1:1). The sample was vortexed and centrifuged for 15 minutes (5000 rpm), and the supernatant was discarded. This washing step was repeated three times, and the final residue was dissolved in 1 mL of 8 M guanidine hydrochloride. After the sample was completely dissolved, 0.1 mL of the solution was diluted in 0.9 mL of 8 M guanidine hydrochloride to be measured using a UV-spectrophotometer (Jasco® V-750). The absorbance was measured at 375 nm against 8 M guanidine hydrochloride (104, 105).

4.6. UV-Vis determination of diene conjugates

To 1.0 mL of organ homogenate (25%) in a conical flask with a ground glass joint, 20 mL of chloroform: methanol (2:1 v/v) mixture was added. The mixture was incubated for 20 minutes in a water bath (50°C) with mechanical shaking. After that, it was washed into a separatory funnel using 10 mL of chloroform: methanol (2:1 v/v) mixture and 5 mL of distilled water. The mixture was allowed to stand for 20 minutes to allow separation. Then, the bottom phase was filtered into an Erlenmeyer flask and dried over anhydrous sodium sulfate. It was filtered into a weighted round-bottomed flask and evaporated by a rotary evaporator (Heidolph Hei-VAP) at 30°C/100 rpm (20 minutes). After evaporation, the mass of the flask mass was

weighed, and the residue was dissolved in MeOH to obtain a 1 mg/mL solution. The absorbance of the obtained solution was measured by UV-spectrophotometer (VWR® U-1600PC) in a range of 400-200 nm against MeOH. After that, the solution was diluted ten times with MeOH, and the measurement was repeated (39).

4.7. UV-Vis determination of malondialdehyde (MDA) (TBARS assay)

To 0.1 ml of organ homogenate (25%), in a well-sealed ground-glass stoppered test tube, 0.2 mL of SDS (8.1%) and 1.5 ml of CH₃COOH (20%; pH 3.5) were added. After that, 1.5 ml of thiobarbituric acid (0.8%) and 0.7 ml of distilled water were pipetted into the mixture. The mixture was incubated in boiling water (95°C) for one hour to achieve the color reaction (TBARS). The sample was cooled down on the ice (5 minutes) and centrifuged (5 minutes, 3000 rpm). 1 mL of the clear supernatant was measured by UV-spectrophotometer (Jasco® V-750) at 532 nm against distilled water (106).

4.8. UV-Vis determination of non-protein thiols (NPSH)

To 1.0 ml of organ homogenate (25%), 0.25 mL of BHT (50 mg/ml in methanol) and 0.25 mL of trichloroacetic acid (25%) were added. The mixture was vortexed and then centrifuged for 5 minutes/5000 rpm. 0.1 mL of the collected supernatant was combined with 2.8 mL of Trizma buffer pH 8.9. The reaction was started after pipetting 0.1 mL of Ellman's reagent (DTNB) (0.01 M in MeOH). The sample was incubated at room temperature for 30 minutes, allowed the maximum reaction, and then measured at 412 nm against the blank (107, 108).

4.9. HPLC determination of tyrosine isomers

4.9.1. Sample preparation

To 50 mg organ sample, 400 µl of 6 N hydrochloric acid, 40 µl of 500 mM BHT in methanol, and 4 µl of 400 mM desferrioxamine solution are added. The sample was vortexed for 1 minute and then hydrolyzed at 120°C for 18 hours. Then, the sample was allowed to cool, centrifuged at 3000 rpm for 10 minutes, and filtered through a syringe filter (0.2 µm) before analysis (109).

4.9.2. HPLC-FLD measurements

HPLC-FLD analyses were performed on a Shimadzu Class 10 HPLC system equipped with an RF-10 AXL fluorescent detector (Shimadzu, Canby, OR, USA). Separation of compounds was performed on a LiChrospher 100 C18 (5 μ m) LiChroCART® 250-4 column at ambient temperature. The mobile phase consisted of 1% (m/v) sodium acetate and 1% (v/v) acetic acid in water (isocratic run). Flow rate: 1.0 ml/min. For Phe: excitation: 258 nm, emission: 305 nm. For Tyr: excitation: 275 nm, emission: 305 nm. Concentrations were determined using external calibration (110).

4.10. Ibuprofen

4.10.1. Ibuprofen experiments *in vitro*

4.10.1.1. Fenton test

The experiments were performed as described before (111). Iron (II) sulfate (100 μ L of 30 mM) solution (in pH 3.0 sulfuric acid) was mixed with 700 μ L of sulfuric acid (pH 3.0), and the mixture was vortexed for 30 seconds. Then, 100 μ L of 10 mM IBP in phosphate buffer pH 7.2 was added and vortexed. The total volume was set to 1 mL by adding 100 μ L of 10 mM hydrogen peroxide. The components were mixed in the respective order, and the reaction mixtures were placed in a 37 °C water bath. The samples were analyzed after 0, 10, 60, 80, and 120 minutes of incubation. "Blank" samples didn't contain IBP.

At the end of each incubation period, the mixtures were acidified with 20 μ L of 2 M sulfuric acid, and 50 μ L of 10 mM salicylic acid as an internal standard was added (final concentration 0.467 mM). The samples were vortex-mixed and extracted twice with 2 ml of diethyl ether. The combined ether extracts were evaporated under N₂ gas. Before HPLC and LC-MS analysis, the dry residue was reconstructed in 100 μ L of acetonitrile.

4.10.1.2. Udenfriend's assay

The assay was performed as reported earlier (112). To a test tube, 3.0 mL of distilled water, 4.0 mL of 2.5 mM IBP solution in 0.1 M phosphate buffer (pH 7.2), 1.0 mL of 10 mM ascorbic acid, 1.0 mL of 2.4 mM EDTA, and 1.0 mL of 2.0 mM Fe(NH₄)₂(SO₄)₂ solution were

added, in the listing order. The mixture was vortexed after adding each component. Then, it was incubated in a water bath at 37°C for 2 hours, with gently mechanical shaking, and 1.0 mL aliquot was taken from the mixture at 0, 10, 60, 80, and 120 min.

To the 1.0 mL aliquot, 1.0 mL of 0.4 M ice-cold perchloric acid and 100 µL of 10 mM of salicylic acid (as an internal standard) were added (final concentration of 0.476 mM). The acidic solution was cooled in icy water and extracted twice with 3.0 mL of diethyl ether. The combined ether layers were evaporated under N₂ gas. Before analysis, the dry residue was reconstructed in 100 µL of acetonitrile.

4.10.2. Ibuprofen experiments *in vivo*

4.10.2.1. Intestinal perfusion

The experiments were performed according to the protocol before (113-115). Male Wistar rats (9-11 weeks old; weighing 250-300g) were separated into two groups. Group I was the control, and Group II was diabetic animals ($n=5$ per group). Experimental diabetes was induced by streptozotocin (STZ) one week before the intestinal perfusion, as stated in section (4.2.). The animals had fasted for 18–20 h before the experiments; then anesthetized with an intraperitoneal injection of urethane (1.2 g/kg bw). The abdomen was opened by a midline incision. A jejunal loop (length of the jejunal loop about 10 cm) was “*in vivo*” isolated and cannulated at its proximal and distal ends. Body temperature was maintained at 37°C using a heat lamp.

Perfusion through the lumen of the jejunal loop with an isotonic medium containing 250 µM ibuprofen was carried out at a rate of 13 mL/min in a recirculation mode. Perfusate samples (250 µL) were collected at selected timepoints (15, 30, 45, 60, 75, and 90 minutes) from the perfusion medium flowing out from the intestinal loop. The initial volume of the perfusate was 15 ml, and its temperature was maintained at 37°C. For parallel investigation of the biliary excretion, the bile duct was cannulated with PE-10 tubing. The bile outflow was collected in 15 minute-periods into tared Eppendorf tubes placed in ice. The collected samples were stored in a deep freezer (-70°C) until analysis. Bile flow was measured gravimetrically, assuming a specific gravity of 1.0 (116).

4.10.2.2. Sample preparation

To 0.1 mL of perfusate sample or 50 μ L of bile sample, 20 μ L of 2 M sulfuric acid and 10 μ L of 10 mM salicylic acid (as an internal standard) were added. (The final concentration of the salicylic acid in the perfusate and the bile samples was 0.77 mM and 1.25 mM, respectively). Then, the samples were vortex-mixed and extracted twice with 0.5 ml of diethyl ether. After vortexing (30 sec) and centrifugation (5 min, 5000 rpm), the ether layers were separated, and the combined ether extracts were evaporated under N₂ gas. Before HPLC-UV and HPLC-MS analysis, the evaporation residue was reconstructed in 100 μ L of acetonitrile.

4.10.3. Analysis of racemic ibuprofen samples (Items 4.10.1. and 4.10.2.)

4.10.3.1. HPLC-UV

HPLC-UV analysis (Method I) of the Fenton and the Udenfriend's samples was performed on an integrated Agilent 1100 HPLC system equipped with a quaternary HPLC pump, a degasser, an autosampler, a thermostated column holder compartment, and a diode-array detector. Data were recorded and evaluated by Agilent ChemStation software (Rev.B.03.02-SR2).

HPLC-UV analysis (Method II) of the perfusate and bile extracts was performed on an integrated Jasco HPLC (LC-4000) system equipped with a quaternary HPLC pump, a degasser, an autosampler, a thermostated column holder compartment, and a PDA detector. Data were recorded and evaluated by ChromNAV Data System (Ver.2).

Method I. Separation of compounds was performed on a Teknokroma (NUCLEOSIL C18) (4.6 mm x 250 mm, 5 μ m particle size) column with a Teknokroma (ODS cartridge, 1 cm x 0.32 cm) guard column at 40°C. The mobile phase consisted of 0.02 M phosphate buffer pH 2.5 (A) and acetonitrile (B) with a flow rate of 1.5 mL/min. The analyses (detection at 220 nm) were performed using the following gradient profile: 20% B for 15 min followed by a 5 min linear gradient to 60% B, a 4 min isocratic elution followed by a 2 min linear gradient to 20% B and a 4 min equilibration. The injected volume was 10 μ L.

Method II. Separation of compounds was performed on a Zorbax SB C-18 (4.6 mm x 150 mm, 5 μ m particle size) column with a Teknokroma (ODS cartridge, 1 cm x 0.32 cm) guard column at 40°C. The mobile phase consisted of 0.02 M phosphoric acid pH 2.5 (A) and acetonitrile (B) with a flow rate of 1.6 mL/min. The analyses (detection at 220 nm) were

performed using the following gradient profile: 20% B for 5 min followed by a 0.5 min linear gradient to 30% B, a 4.5 min isocratic elution followed by a 0.1 min linear gradient to 60% B, a 4.9 min isocratic elution followed by a 0.1 min linear gradient to 20% B and a 4.9 min equilibration. The injected volume was 10 μ L.

4.10.3.2. HPLC-MS

To identify the metabolites, a Thermo Dionex UltiMate 3000 liquid chromatography (Dionex, Sunnyvale, USA) connected to a Thermo Q Exactive Focus quadrupole-Orbitrap hybrid mass spectrometer (Thermo Scientific) was used. Data acquisition and analysis were performed using the Q Exactive Focus 2.1, Xcalibur 4.2., and FreeStyle 1.8 software (Thermo Scientific). The HPLC separation was performed on an XTerra MS C18 column (150 mm x 2.1 mm, 3.5 μ m) with XTerra MS C18 precolumn (5 mm x 2.1 mm, 3.5 μ m) at 40°C. The injection volume was 5 μ L; the flow rate was 0.4 ml/min. The tray of the autosampler vials was thermostated at 25°C. A binary gradient of the eluents is as follows. Eluent: 5 mM ammonium-acetate/5 mM acetic acid in water (A) and methanol (B). Gradient: 10% B for 1 min, followed by a 9 min linear gradient to 90% B, a 2 min an isocratic elution followed by a 0.5 min linear gradient to 10% B, and a 2.5 min equilibration.

Analysis of the compounds was performed in HESI negative ionization modes with the following parameters: spray voltage 3.0 kV; probe heater temperature 300°C; capillary temperature 350°C; spray and auxiliary N₂ gas flows 20 and 5 arbitrary units, respectively; S-Lens RF level 50%; automatic gain control 1e6; resolution (at m/z 200) 70000. Data acquisition range of m/z 100-1000, in full scan mode.

4.10.4. Chiral analysis

4.10.4.1. Animal experiment and intestinal perfusion procedure

The animal experiment and intestinal perfusion were identical to the section (4.10.2.1.).

4.10.4.2. Sample preparation

Perfusate and bile samples were kept at room temperature for a short time to become defrost. The extraction technique of this experiment was the modified method by Bonato et al. (117). The sample volume (50 μ L) was placed in an Eppendorf tube, and then 10 μ L of naproxen sodium salt (250 μ M) was added as an internal standard. The mixture was acidified by 40 μ L of hydrochloric acid (2 M) and extracted with 1.5 ml (3-times 0.5 ml) of a mixture of n-hexane and ethyl acetate (8:2 v/v). The mixture was vortexed for 30 seconds and centrifuged for 5 minutes at 3500 rpm, and the transparent upper layer was collected. The combined extracts were evaporated under nitrogen at 40°C. The evaporated residue was reconstituted in 50 μ L of the mobile phase and ready for the HPLC analysis.

4.10.4.3. HPLC-UV analysis-Instrumentation

HPLC-UV analysis of the perfusate and bile samples was performed on an integrated Jasco HPLC (LC-4000) system equipped with a quaternary HPLC pump, a degasser, an autosampler, a thermostated column holder compartment, and a PDA detector. Data were recorded and evaluated by ChromNAV Data System (Ver.2).

Ibuprofen enantiomers were separated on a Kromasil 3-amyICoat RP (4.6 mm x 150 mm, 3 μ m) chiral column with a Teknokroma (ODS cartridge, 1 cm x 0.32 cm) guard column. The mobile phase consisted of methanol/water/acetic acid (70/30/0.1). The run time was 30 minutes with a 0.5 mL/min flow rate and 10 μ L injection volume. The temperature and the U.V. detector were set at 22°C and 220 nm, respectively. The analytical method is based on the Kromasil application note (118). Identification of the separated peaks was made by determination of the retention time of (*S*)-(+)-ibuprofen (Figure 41).

4.10.4.4. HPLC-UV analysis - Validation data

4.10.4.4.1. Specificity

Results were evaluated based on the chromatograms of extracts of blank perfusate and blank bile samples. The examined extracts didn't give a detectable chromatographic peak at the retention time of ((*R*)-IBP (**1**) t_R =14.5 min, (*S*)-IBP (**2**) t_R =16.72 min, and NAP (**3**) t_R =20.3 min)

of the perfused medium, and at the retention time of ((*R*)-IBP (**1**) t_R =14.4 min, (*S*)-IBP (**2**) t_R =16.61 min and NAP (**3**) t_R =20.18 min) of the bile (Figure 40).

4.10.4.4.2. System suitability

System suitability data were evaluated from chromatograms of the standard solutions of racemic IBP (100 μ M, 250 μ M) and NAP (50 μ M) in methanol. Results were obtained from five parallel injections. The evaluation was based on the relative standard deviation (RSD%). The percent RSD values are shown in Table 2.

Table 2. Data for system suitability of methanol solutions of racemic ibuprofen (*rac*-IBP) (100 μ M, 250 μ M) and naproxen sodium (NAP) as internal standard (IS) (50 μ M).

Injections (Standard Solutions)	NAP			<i>rac</i> -IBP				
	C (μ M)	t_R (min)	Area	C (μ M)	t_R (min)	R-Area	t_R (min)	S-Area
1	50	20.24	68666	100	14.48	12019	16.74	12119
2	50	20.22	68779	100	14.47	12081	16.72	12125
3	50	20.29	68783	100	14.50	12034	16.75	12156
4	50	20.30	68542	100	14.52	12034	16.79	12215
5	50	20.31	68632	100	14.53	12065	16.79	12247
Mean		20.27	68680		14.50	12047	16.76	12172
RSD%		0.17	0.13		0.16	0.19	0.17	0.41
Compounds	t_R	RRT	k'	T	NTP	R_s		
NAP	20.27	N/A	19.27	1.23	1567	N/A		
<i>R</i> -IBP	14.50	1.40	13.50	1.24	2057	1.63		
<i>S</i> -IBP	16.76	1.21	15.76	1.16	2009	1.99		
1	50	20.24	68740	250	14.47	32102	16.72	32200
2	50	20.24	68575	250	14.46	32121	16.70	32481
3	50	20.24	68552	250	14.46	32107	16.70	32272
4	50	20.24	68667	250	14.47	32096	16.71	32224
5	50	20.25	68244	250	14.48	31873	16.72	31979
Mean		20.24	68556		14.47	32060	16.71	32231
RSD%		0.03	0.25		0.03	0.29	0.04	0.50
Compounds	t_R	RRT	k'	T	NTP	R_s		
NAP	20.24	N/A	19.24	1.26	1522	N/A		
<i>R</i> -IBP	14.47	1.40	13.47	1.24	2057	1.63		
<i>S</i> -IBP	16.71	1.21	15.71	1.17	2026	1.99		

t_R : retention time, RRT: relative retention time ($RRT = t_{R(NAP)}/t_{R(rac-IBP)}$), k' : capacity factor, T: asymmetry factor, NTP: number of theoretical plates, R_s : resolution.

4.10.4.4.3. Precision

Precision was studied by investigating repeatability and intermediate precision. Repeatability was determined by measuring intra-day data of 3 parallel injections of 2 parallel dilutions of 2 independent weighings of racemic IBP ($c = 100 \mu$ M, $c = 250 \mu$ M in MeOH) and NAP ($c = 50 \mu$ M, in MeOH). Intermediate precision was determined by measuring inter-day (by injection of the samples over three consecutive days) data of 3 parallel injections of 2

dilutions of racemic IBP (C = 100 μ M, c = 250 μ M in MeOH) and NAP (c = 250 μ M, in MeOH). The evaluation was based on the relative standard deviation (RSD%) (Tables 3 and 4).

Table 3. Data for system repeatability methanol solution of racemic ibuprofen (rac-IBP) (100 μ M, 250 μ M) and naproxen sodium (NAP) as internal standard (IS) (50 μ M).

Weighting/Dilution Standard Solution	NAP		<i>rac</i> -IBP		
	C (μ M)	Area	C (μ M)	R-Area	S-Area
1/1	50	68358	250	31427	31471
1/2	50	68736	250	31612	31845
1/3	50	68381	250	31454	32084
2/1	50	68014	250	31765	32110
2/2	50	68568	250	31974	32247
2/3	50	68424	250	32123	32316
Mean		68414		31726	32012
RSD%		0.32		0.81	0.89
1/1	50	68901	100	12396	12362
1/2	50	68867	100	12124	12198
1/3	50	68882	100	12299	12442
2/1	50	68947	100	12284	12450
2/2	50	68993	100	12172	12268
2/3	50	68848	100	12288	12361
Mean		68906		12261	12347
RSD%		0.07		0.73	0.73

Table 4. Data for system intermediate precision of methanol solution of racemic ibuprofen (rac-IBP) (100 μ M, 250 μ M) and naproxen sodium (NAP) as internal standard (IS) (50 μ M).

Day	Dilution Standard Solution	NAP		<i>rac</i> -IBP		
		C (μ M)	Area	C (μ M)	R-Area	S-Area
1	1	50	68358	250	31427	31471
	2	50	68736	250	31612	31845
	3	50	68381	250	31454	32084
2	1	50	68313	250	31617	31781
	2	50	68687	250	31440	31686
	3	50	68747	250	31325	31546
3	1	50	68884	250	32130	32366
	2	50	68262	250	32055	32349
	3	50	68461	250	32052	32308
Mean			68537		31679	31937
RSD%			0.31		0.93	1.03
1	1	50	68901	100	12396	12362
	2	50	68867	100	12124	12198
	3	50	68882	100	12299	12442
2	1	50	68935	100	12355	12492
	2	50	68227	100	12065	12129
	3	50	68568	100	12207	12291
3	1	50	68905	100	12148	12246
	2	50	68859	100	12178	12315
	3	50	68714	100	12058	12375
Mean			68762		12203	12317
RSD%			0.32		0.94	0.88

4.10.4.4.4. Accuracy

Accuracy was calculated by spiking control perfusion and bile samples with the concentrations of racemic IBP (50 μ M, 100 μ M, 250 μ M) and NAP (50 μ M). After the extraction of the samples, the percentage of recoveries was calculated with the mean of the same concentrations of standard dilutions of racemic IBP (50 μ M, 100 μ M, 250 μ M) and NAP(50 μ M). The evaluation was based on the relative standard deviation (RSD%) (Table 5).

Table 5. Accuracy of NAP, *R*- and *S*-IBP determination in spiked control perfusates and spiked control bile with the same range of standard dilutions of racemic IBP (50 μ M, 100 μ M, 250 μ M) and NAP(50 μ M).

NAP			<i>rac</i> -IBP				
$C_{\text{spiked perfusate}} (\mu\text{M})$	Area	Recovery %	$C_{\text{spiked perfusate}} (\mu\text{M})$	<i>R</i> -Area	Recovery %	<i>S</i> -Area	Recovery %
50	67646	98.1	50	5299	86.5	5241	85.0
50	67599	98.0	50	5335	87.1	5299	85.9
50	67569	98.0	50	5320	86.8	5227	84.7
50	68004	98.4	100	11355	92.8	11248	90.9
50	67423	97.6	100	11151	91.1	11088	89.6
50	67536	97.7	100	11097	90.7	11006	88.9
50	56635	81.6	250	26897	85.7	26898	85.3
50	56225	81.1	250	26855	85.5	26741	84.8
50	55432	79.9	250	26361	83.9	26326	83.5
Mean		92.3			87.8		86.5
RSD%		8.76			3.23		2.81
$C_{\text{spiked bile}} (\mu\text{M})$	Area	Recovery %	$C_{\text{spiked bile}} (\mu\text{M})$	<i>R</i> -Area	Recovery %	<i>S</i> -Area	Recovery %
50	61456	89.1	50	5168	84.3	5164	83.7
50	61475	89.2	50	5127	83.7	5169	83.8
50	61466	89.2	50	5147	84.0	5166	83.8
50	60576	87.7	100	10930	89.3	11049	89.3
50	60411	87.4	100	10916	89.2	11003	88.9
50	60494	87.5	100	10923	89.3	11026	89.1
50	60968	87.9	250	28149	89.6	29544	93.7
50	61118	88.1	250	27995	89.2	28732	91.1
50	61043	88.0	250	28072	89.4	29138	92.4
Mean		88.2			87.6		88.4
RSD%		0.77			2.88		4.09

4.10.4.4.5. Linearity

Linearity was studied by analysis of standard solutions of racemic IBP of five different concentrations (250 μ M, 200 μ M, 150 μ M, 100 μ M, 50 μ M) using methanol as solvent. Each solution had a known concentration of NAP as an internal standard (50 μ M). Data were obtained from three parallel injections of each concentration. Calibration curves were generated by

plotting the theoretical concentrations against the relative peak areas (ratio of the peak areas of the enantiomers and the internal standard). Linearity was determined by least-squares regression. The regression equation for (*R*)- and (*S*)-IBP was as follows: (*R*)-IBP: $y=0.3704x-0.4497$, $R^2=0.999$; (*S*)-IBP: $y=0.3683x-0.3253$, $R^2=0.9992$) as shown in Figure 9.

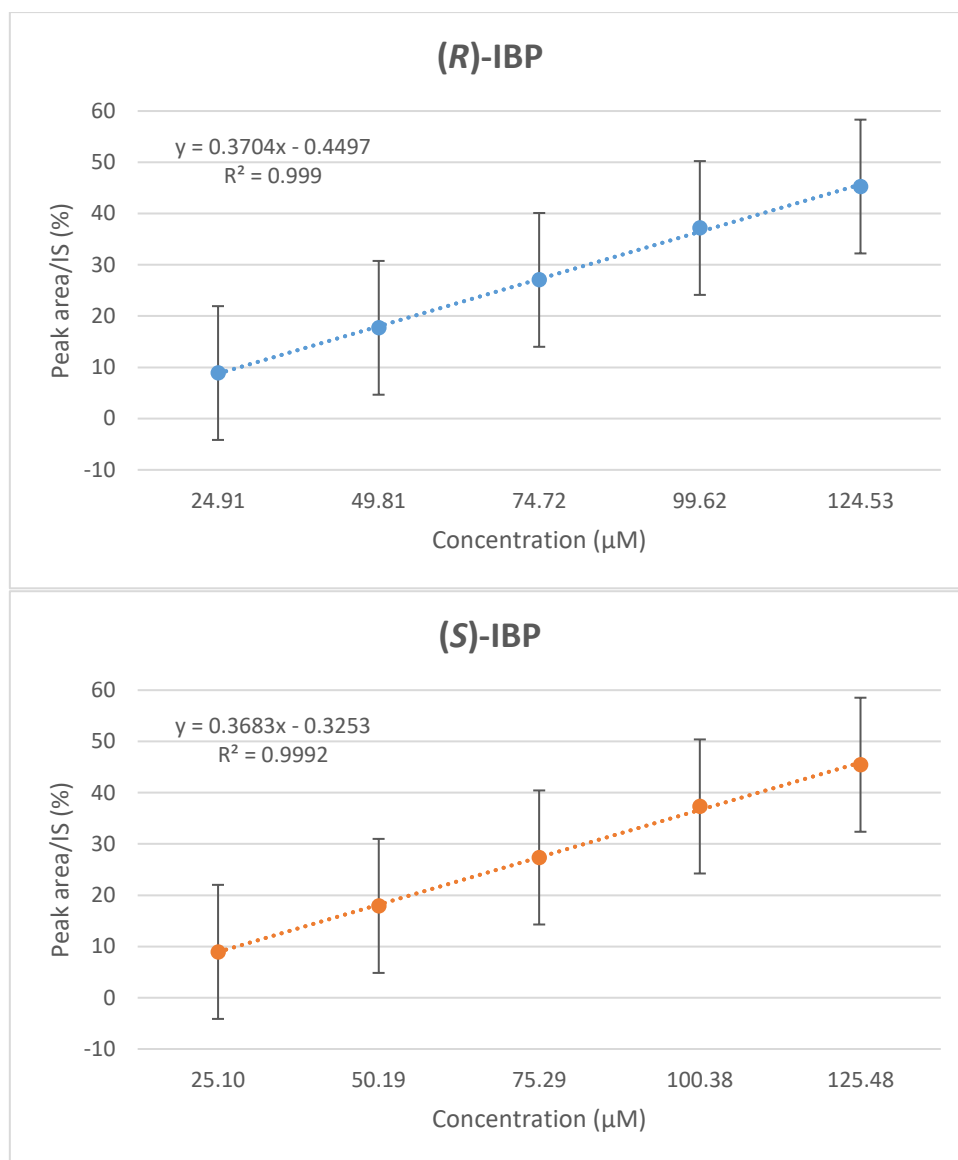


Figure 9. The HPLC-UV calibration curves of *R*-IBP (**A**) and *S*-IBP (**B**) with the linear regression trend lines, constructed by five different concentrations (250 µM, 200 µM, 150 µM, 100 µM, 50 µM) of standard racemic IBP.

4.10.4.4.6. Determination of LOQ

The limit of quantitation (LOQ) was considered the lowest concentration (50 µM) of the calibration curve constructed by using racemic ibuprofen. Regarding the exact concentration of

the two enantiomers in the investigated sample (R-IBP: 49.81%; S-IBP: 50.019% - See Table 2), the LOQ of the R-IBP and S-IBP is 24.91 μ M and 25.09 μ M, respectively.

4.11. Statistics

The protein content of homogenate samples was measured by Biuret assay according to the calibration curve of different known concentrations of BSA. TBARS (nmol/mg protein/g) and GSH (μ mol/mg protein/g) amounts represent the mean \pm SD of four animal samples in each group. The value of protein carbonyl content (μ mol/Port-DNPH/mg protein/g) and diene conjugates ($E_{1cm}^{1\%}$ /mg protein/g) are the mean \pm SD of animal groups ($n= 4$). HPLC-FLD integrated peak areas of tyrosine derivatives (nmol/mmol) represent the mean \pm SD of animal groups ($n= 2$). The difference among groups was analyzed by SPSS one-way Anova. Significant differences from the control value: * $p < 0.05$, ** $p < 0.01$, and *** $p < 0.001$.

HPLC-UV integrated peak areas (relative to the internal standard) of oxidized ibuprofen metabolites were qualitatively analyzed in the Fenton and Udenfreind experiments based on incubation time. Biliary excretion was expressed as the product of the HPLC peak areas (relative to the internal standard) and the 15-minute period of bile flows (μ L/kg/min). The values (arbitrary units) represent the mean \pm SD of five independent experiments. The difference among groups was determined by SPSS independent t-test. Significant differences from the control value: * $p < 0.05$ and ** $p < 0.01$.

For the *R-S* inversion study, the luminal disappearance of the IBP enantiomers was calculated based on their luminal concentrations and the volume of the perfusion solution. The biliary excretion was calculated on the base of the volume of bile flow in 15 minutes periods. Data show the mean \pm SD of four independent experiments. The difference among groups was determined by SPSS One-way Anova. Significant differences from the control value: * $p < 0.05$, ** $p < 0.01$, and *** $p < 0.001$.

4.12. Ethical approval

The study was designed and conducted according to European legislation (Directive 2010/63/E.U.) (119) and the Hungarian Government regulation (40/2013., II. 14.) (120) on the protection of animals used for scientific purposes. The project was approved by the Animal Welfare Committee of the University of Pécs and by the Government Office of Baranya County (license No. BAI35/51-61/2016 and license supplement (supplement No. BAI35/90-5/2019).

5. Results

5.1. Oxidative transformations of selective endogenous compounds under the influence of STZ-induced experimental diabetes

5.1.1. Blood glucose level

Diabetes was induced with a single i.v. dose of 65 mg/kg STZ (121). Hyperglycemia was confirmed after one week of the STZ-treatment (121, 122). The average blood glucose level of the control animals was 6.7 ± 1.5 mM, while that of the STZ-treated rats was 23.4 ± 2.8 mM.

5.1.2. Protein content

The protein content (mg/g wet tissue) of the liver, small intestine, and kidney were determined using the calibration curve ($y = 0.2583x + 0.1124$, $r^2 = 0.9997$) obtained by BSA (Figure 10). The results showed that the protein content of each organ was affected by the hyperglycemic conditions (Figure 11). The protein content of the small intestine in all groups is lowered, showing similar reduced values over the four-week period. In the kidney, the values were continuously lowered. The protein content of the liver showed the least reductions having the two-week STZ-treated samples the lowest values (Figure 11).

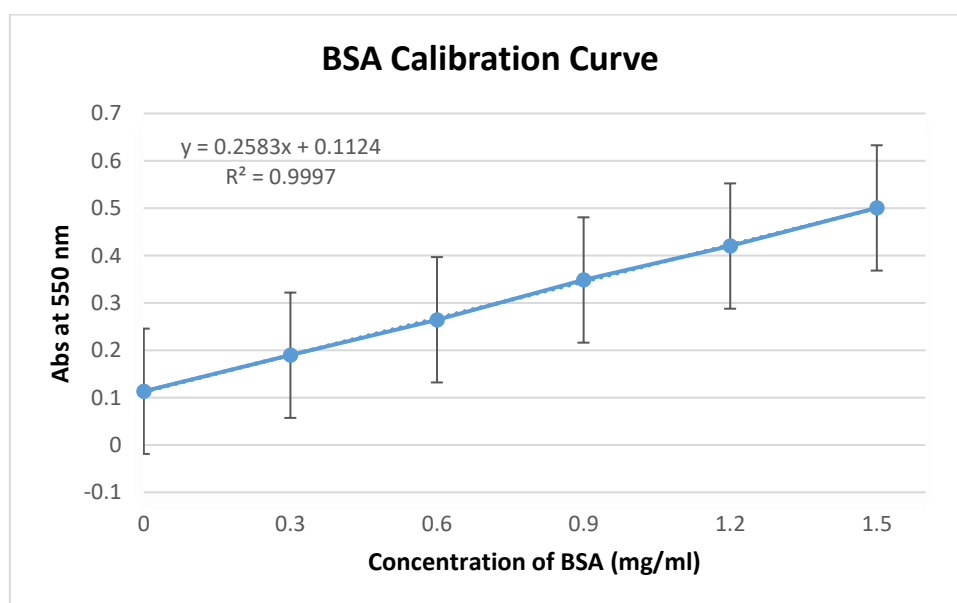


Figure 10. The calibration curve of the UV-absorbance of different concentrations of the bovine serum albumin (BSA) by Biuret assay.

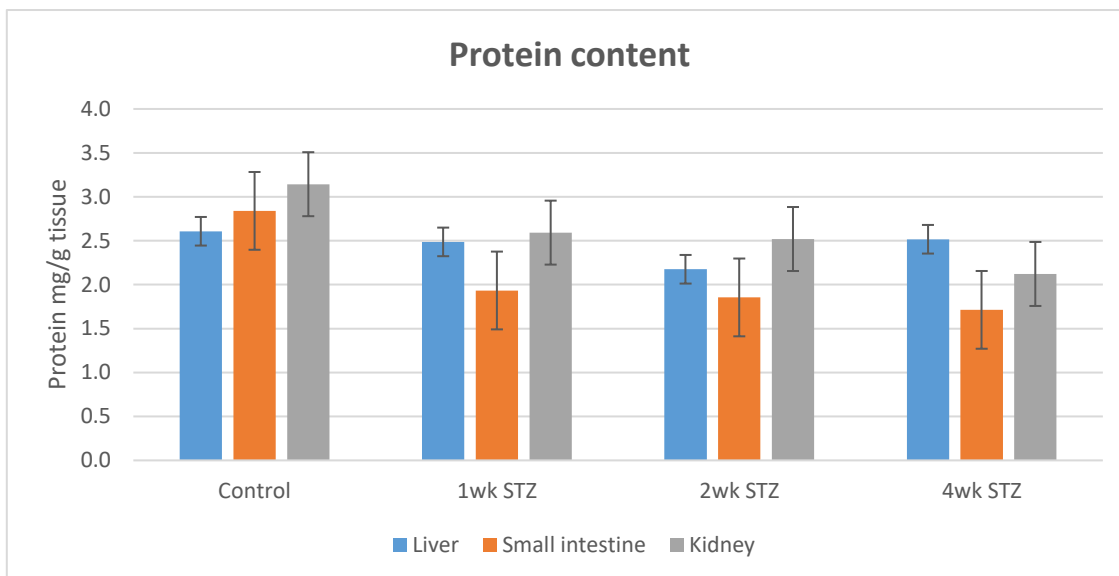


Figure 11. Comparison of the protein contents (mg protein/g wet tissue) in the control, one-week-, two-week-, and four-week-STZ treated rats.

5.1.3. Carbonyl (Prot-DNPH) content

The carbonyl content of oxidized proteins was determined after derivatization with 2,4-dinitrophenylhydrazine (DNPH). Protein-DNPH content of the STZ- treated samples showed a distinct continuous increase compared to the controls in each tissue homogenate. Each two-week STZ-treated organ level was significantly different from the control. The protein-DNPH level in the four-week STZ-treated liver samples decreased. In the kidney, the protein carbonyl content showed a moderate continuous increase over the four-weeks (Figure 12).

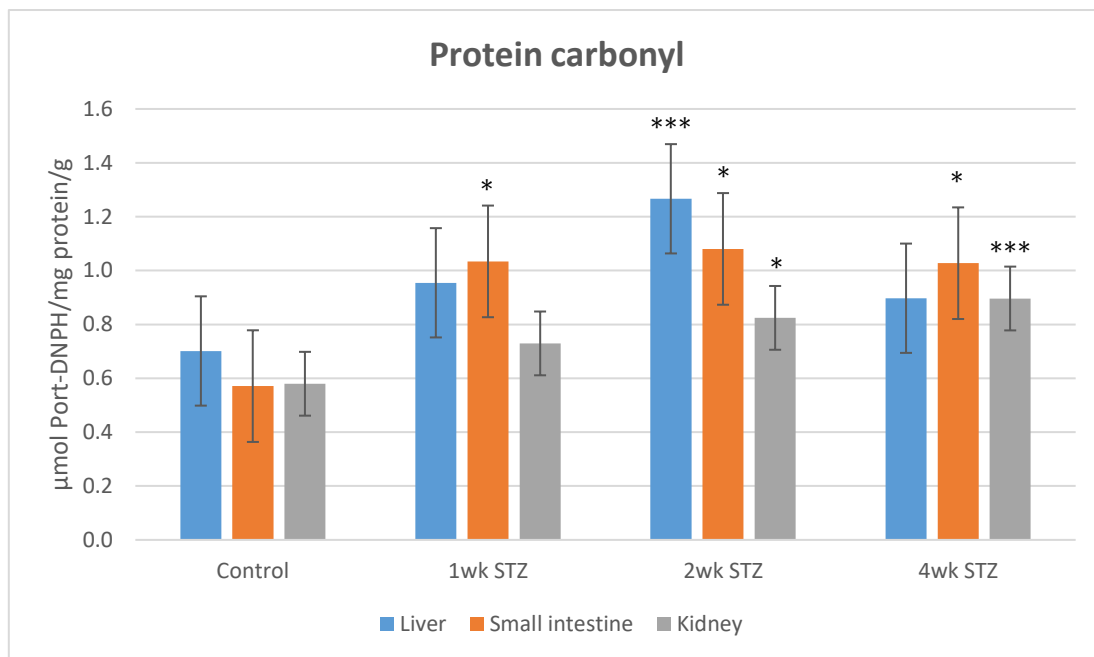


Figure 12. Comparison of the protein carbonyl content ($\mu\text{mol Prot-DNPH/mg protein/g tissue}$) in control, one-week-, two-week-, and four-week-STZ treated rats (* $p < 0.05$, ** $p < 0.01$, *** $p < 0.001$).

5.1.4. Determination of diene conjugates

In the liver, the conjugated diene level slightly increased in the hyperglycemic rats at each timepoint. In the small intestine, the conjugated diene level significantly increased at each timepoint. However, the relative increase, specifically in the two-week and four-week hyperglycemic samples, was much higher than in the liver. In the kidney, the diene level was significantly higher in the four-week STZ-treated samples. The one-week and two-week STZ treatment didn't significantly affect the conjugated diene level. The four-week samples showed a statistically higher value than the control (Figure 13).

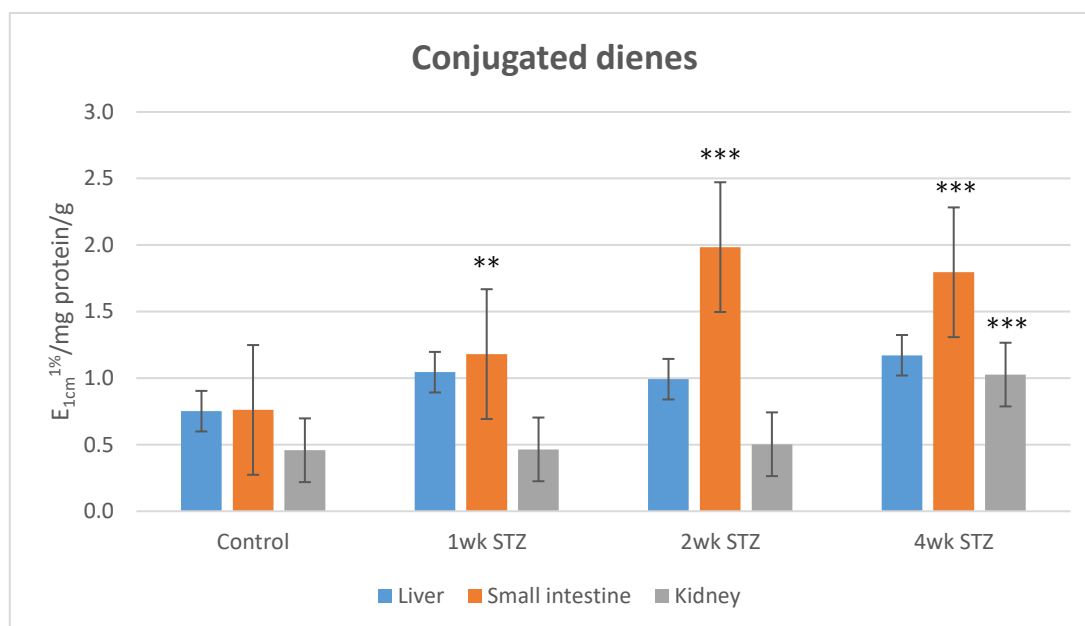


Figure 13. Comparison of the conjugated diene levels ($E_{1cm}^{1\%}/\text{mg protein/g tissue}$) in the control, one-week-, two-week-, and four-week-STZ treated rats (** $p < 0.01$, *** $p < 0.001$).

5.1.5. TBARS determination

MDA is frequently determined as an indicative endogenous metabolite resulting in lipids oxidation by reactive oxygen species (106, 123). It is a reactive carbonyl compound, readily reacting with nucleophilic sites of proteins and other cellular macromolecules. Accordingly, the MDA test-results indicate the steady-state lipid-peroxide levels, which can undergo rearrangements to form MDA under the test conditions. Our results showed a continuous slight increase in the MDA (TBARS) levels in each organ. The TBARS levels of the four-week STZ-treated small intestine and kidney samples significantly differ from the control (Figure 14).

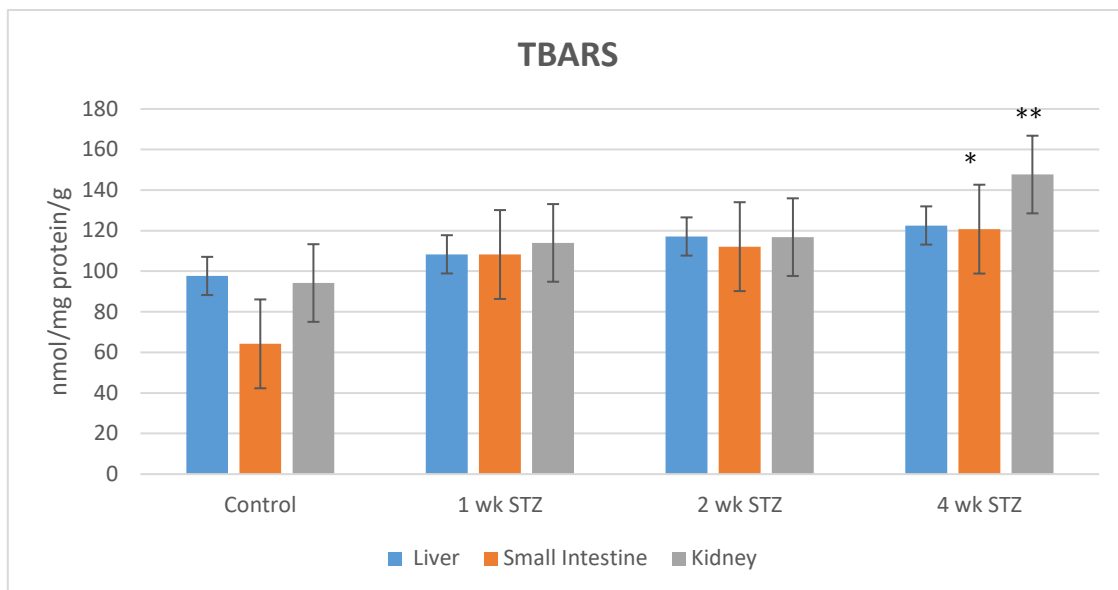


Figure 14. Comparison of the TBARS levels (nmol TBARS /mg protein/g tissue) in control, one-week-, two-week-, and four-week-STZ treated rats (* $p < 0.05$, ** $p < 0.01$).

5.1.6. Determination of non-protein thiols (NPSH)

STZ-treatment of the experimental animals decreased the NPSH levels in the liver at the one-week and four-week timepoints. In contrast, the two-week STZ liver samples had somewhat increased values compared to the control. In the kidney, the NPSH content marginally raised at each timepoint. In the small intestine, the NPSH levels in the STZ-treated samples increased at each timepoint compared to the control. The lowest values could be measured in the two-week STZ-treated samples (Figure 15).

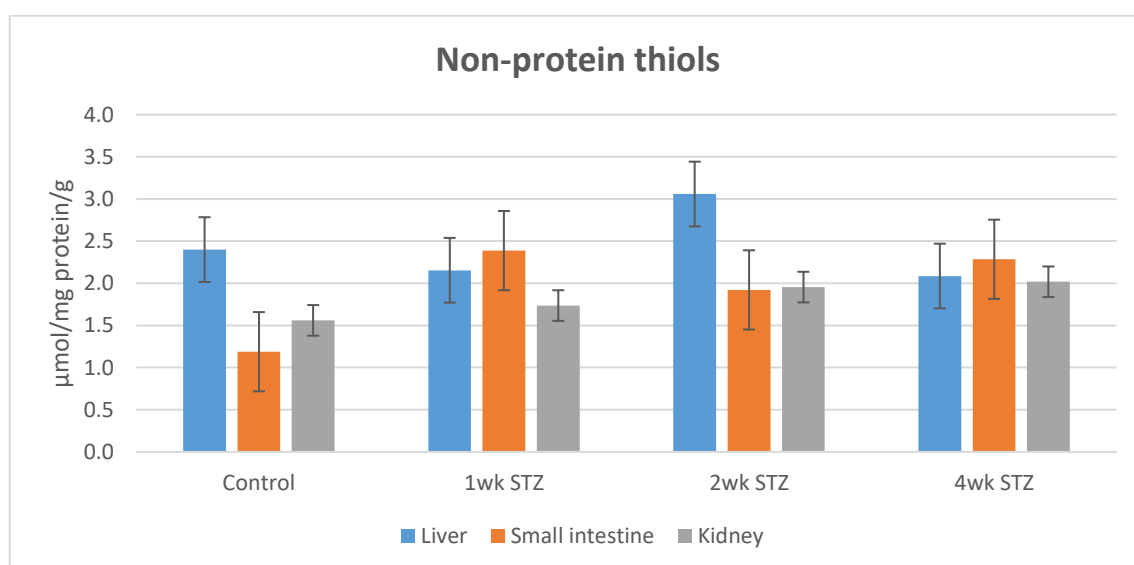


Figure 15. The NPSH quantities (μmol GSH/mg protein/g tissue) in control, one-week-, two-week-, and four-week-STZ treated rats.

5.1.7. Determination of hydroxyated phenylalanine derivatives

Phenylalanine (Phe) is an essential amino acid that is the physiological precursor of *para*-tyrosine (*p*-Tyr), dihydroxy-phenylalanine (DOPA), catecholamines, melanine, and thyroid hormones (124). Beyond these enzymatic reactions, Phe, due to the nucleophilic character of its aromatic ring, is a subject of non-enzymatic oxidation processes, i.e., the attack of ROS (125). In such reactions, all the three hydroxylated Phe isomers (*p*-Tyr, *m*-Tyr, and *o*-Tyr) are formed (126). Under our experimental conditions, the relative amount of the *m*-Tyr, and *o*-Tyr isomers, formed in non-enzyme-catalyzed hydroxylation reactions, increased at the two- and four-week timepoints in each investigated organ (Figure 16).

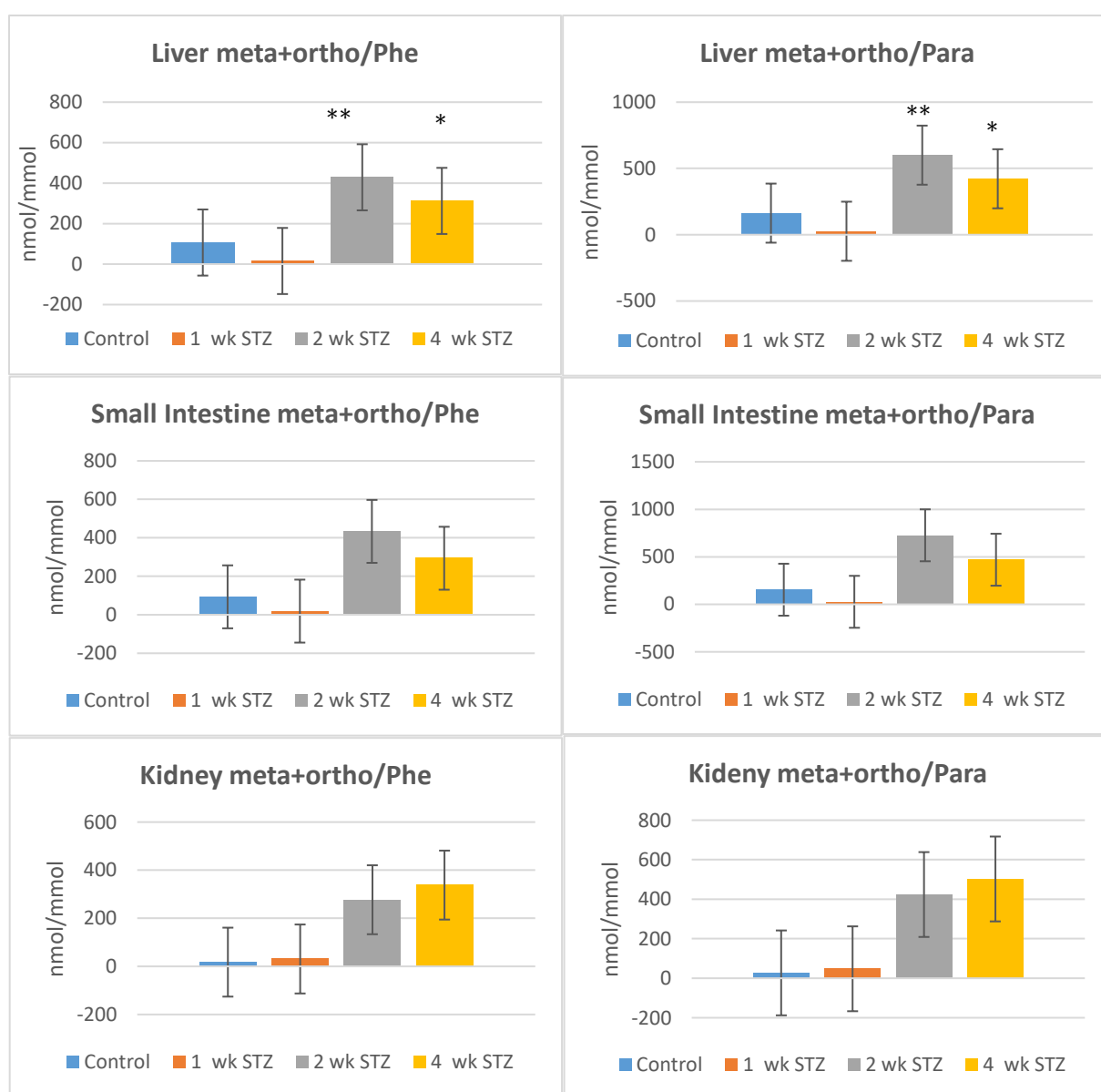


Figure 16. The relative amount of the *m*-Tyr + *o*-Tyr to Phe and *p*-Tyr (nmol/mmol) in control, one week-, two week-, and four week-STZ treated rats (* p < 0.05, ** p < 0.01).

5.2. *In vitro* investigation of non-enzyme catalyzed (Fenton and Udenfriend) oxidation of ibuprofen

5.2.1. Fenton test

Based on earlier investigation upon how the ratio of the molar concentration of the substrate (salicylic acid) to the iron (II) ion in the Fenton test affects the effectiveness of the hydroxylation reaction. The present investigations were performed using the more effective conditions, using the substrate: iron (II): hydrogen peroxide molar ratio as 1:3:1 (111).

For high-performance liquid chromatography with UV detection (HPLC-UV) analysis of the samples, a gradient method (Method I) was developed to separate the available oxidative metabolites of IBP. The available and separated oxidative metabolites of ibuprofen in this experiment are 1-hydroxyibuprofen (1-OH-IBP) (**2**), 2-hydroxyibuprofen (2-OH-IBP) (**3**), 3-hydroxyibuprofen (3-OH-IBP) (**4**), and carboxyibuprofen (HOOC-IBP) (**5**) (Figure 17).

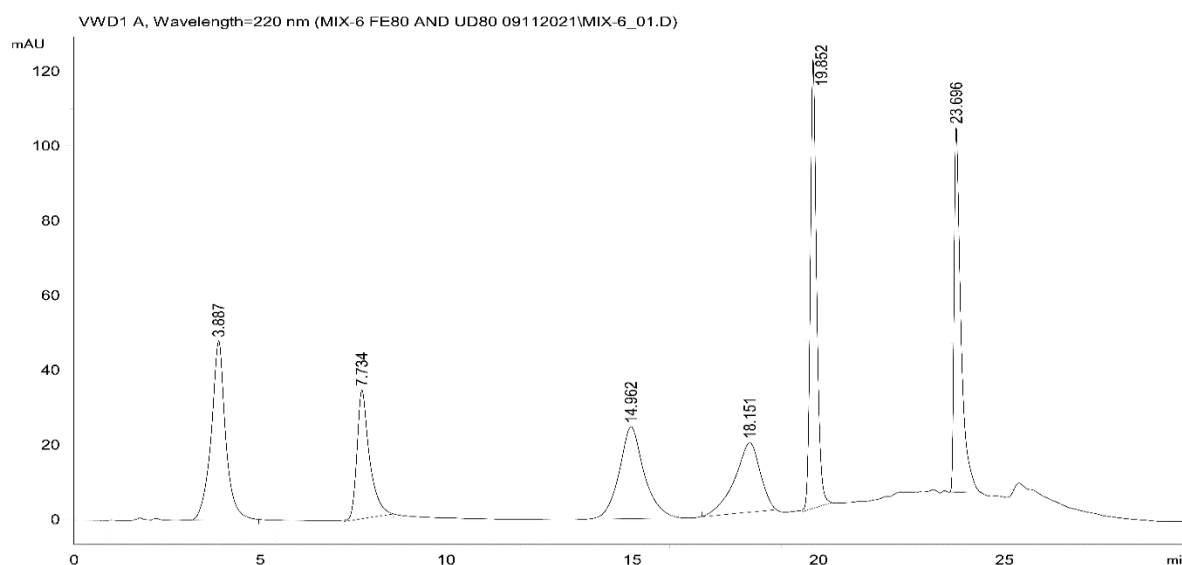


Figure 17. HPLC-UV chromatogram (Method I) of IBP and oxidative metabolites of IBP in ACN (30 $\mu\text{g mL}^{-1}$ each). The retention times (t_R) of the separated standards are as follows: 3-OH-IBP (**4**) (3.89 min), SA (internal standard) (7.73 min), 2-OH-IBP (**3**) (14.96 min), HOOC-IBP (**5**) (18.15 min), 1-OH-IBP (**2**) (19.85 min), and IBP (**1**) (23.70 min).

HPLC-UV analysis (Method I) of the Fenton extracts indicated the formation of 1-HO-IBP (**2**), 2-OH-IBP (**3**), and several other products (Figure 18). To verify the structures of **2** and **3** and identify other oxidation products, a high-performance liquid chromatographic analysis using mass spectrometric detection (HPLC-MS) of the extracts was performed. HPLC-MS investigations of the extracts confirmed the presence of **2** (m/z 221.1176), **3** (m/z 221.1176), and HOOC-IBP (**5**) (m/z 235.0969) (Figures 19-21).

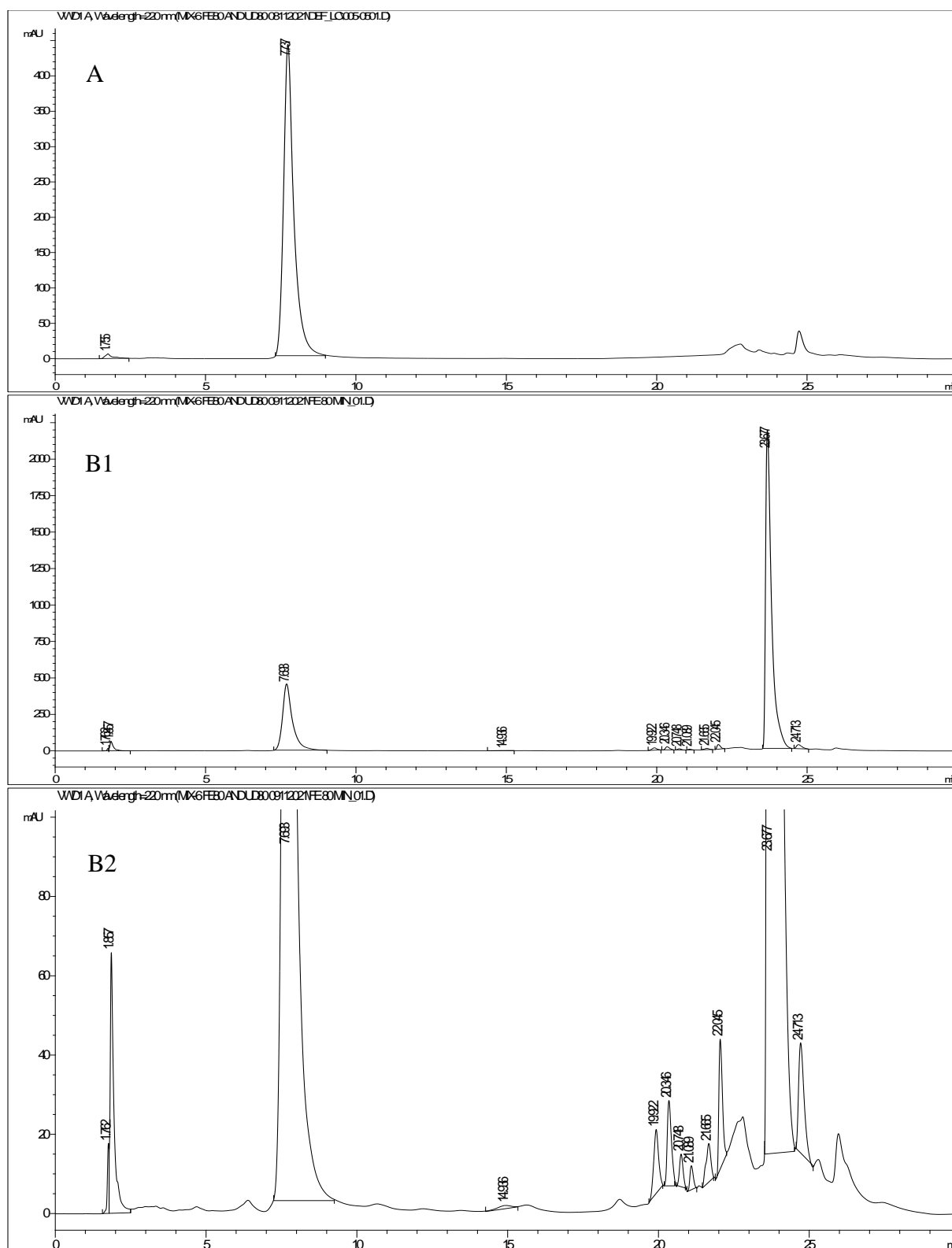


Figure 18. A. HPLC-UV chromatogram (Method I) of the blank Fenton extract. Salicylic acid (internal standard) $t_R = 7.74$ min. **B1 and B2.** HPLC-UV chromatogram (Method I) of the Fenton extract of IBP (80-minute). Salicylic acid (internal standard) $t_R = 7.69$ min, 2-hydroxyibuprofen (**3**) $t_R = 14.94$ min, 1-hydroxyibuprofen (**2**) $t_R = 19.92$ min, dihydroxyibuprofen (**10**) $t_R = 21.09$ min, aromatic-hydroxylated ibuprofen (**8**) $t_R = 22.05$ min, ibuprofen $t_R = 23.68$ min.

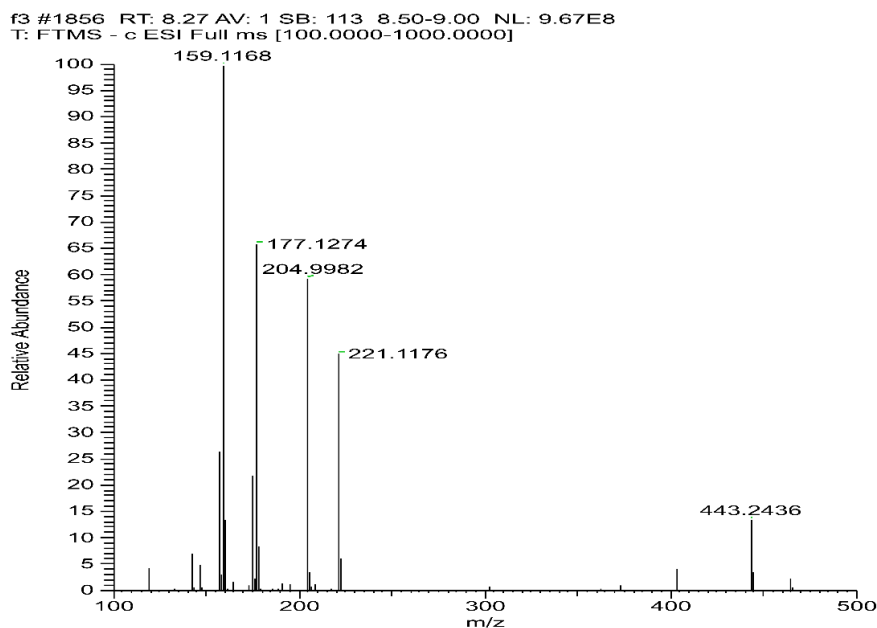


Figure 19. HPLC-MS spectrum of the 1-hydroxyibuprofen (**2**) (1-OH-IBP) standard. ($C_{13}H_{17}O_3$; Exact mass: 221.1178) Mass error: -0.90 ppm. (The m/z 204.9982 signal is a background ion.). The following ion-signals are formed in the ionization source: 443.2436: $[2M-H]^-$, 221.1176: $[M-H]^-$, m/z 204.9982: unknown; fragments m/z 177.1274: $[M-H-CO_2]^-$, m/z 159.1168: $[M-H-CO_2-H_2O]^-$.

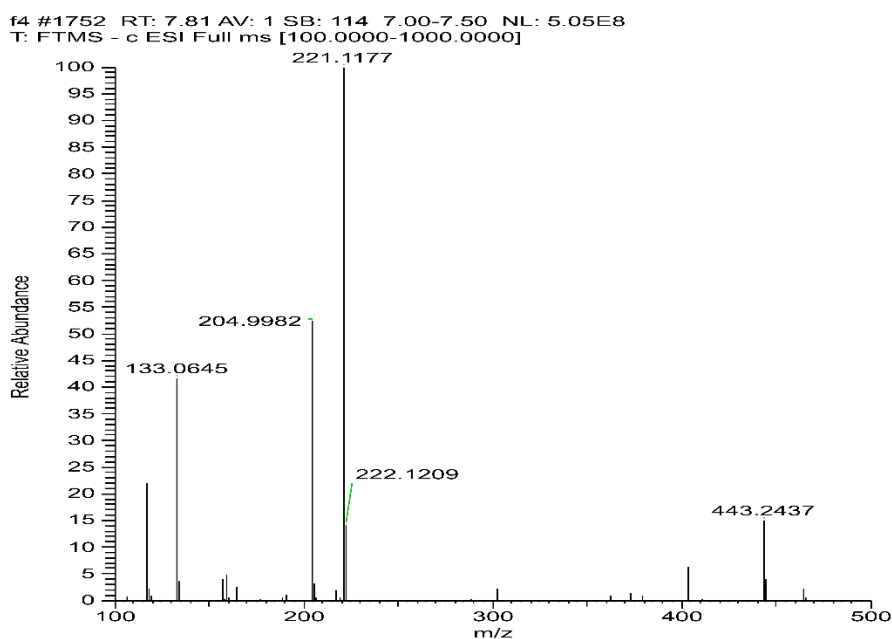


Figure 20. HPLC-MS spectrum of the 2-hydroxyibuprofen (**3**) (2-OH-IBP) standard. ($C_{13}H_{17}O_3$; Exact mass: 221.1178) Mass error: -0.45 ppm. (The m/z 204.9982 signal is a background ion.) The following ion signals are formed in the ionization source: 443.2437: $[2M-H]^-$, 221.1177: $[M-H]^-$, m/z 204.9982: unknown, m/z 133.0645: unknown.

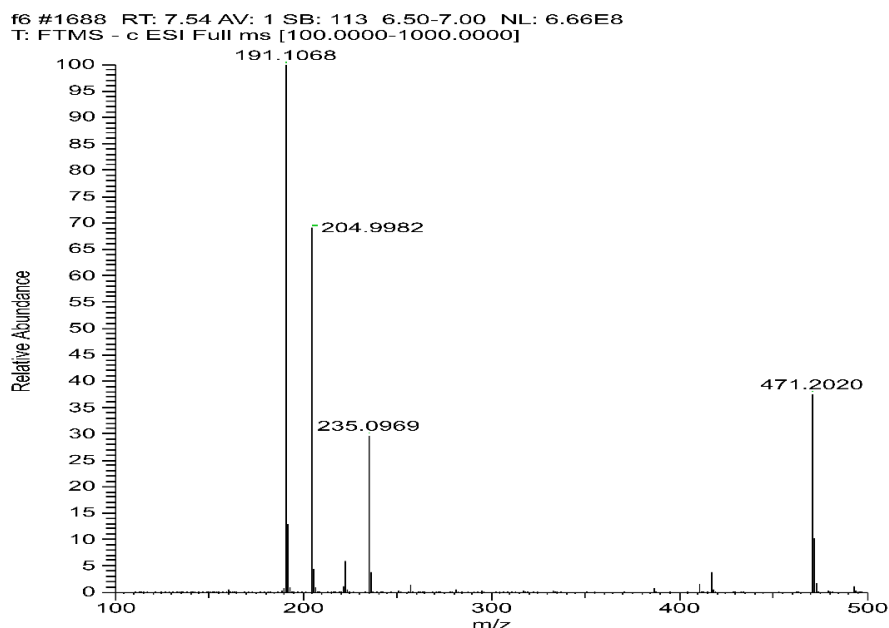


Figure 21. HPLC-MS spectrum of the carboxyibuprofen (**5**) (HOOC-IBP) standard. ($C_{13}H_{15}O_4$; Exact mass: 235.0970) Mass error: -0.43 ppm. The m/z 204.9982 signal is a background ion.) The following ion signals are formed in the ionization chamber: 471.2020: $[2M-H]^-$, 235.0969: $[M-H]^-$, m/z 204.9982: unknown, m/z 191.1068: $[M-H-CO_2]^-$.

In the mass spectra of standards **2** (Figure 19), **3** (Figure 20), and **5** (Figure 21), the peak of m/z 204.9982 systematically appears without collision of the compounds. The exact mass of ibuprofen (in negative mode) is 205.1229 amu. The m/z 204.9982 is 608 ppm smaller. Since MS measurements were performed with an instrument with high mass accuracy, the m/z 204.9982 peak was defined as unknown.

The derivative (**8**) with the highest HPLC-UV integrated peak area ($t_R=22.05$ min) couldn't be unambiguously identified (Figure 22). The formed product (X-OH-IBP) has a mass of m/z 221.1175, and its fragmentation makes no distinction between the 2'-OH-IBP and OH(Ar)-IBP structures (Figures 23.A and 23.B).

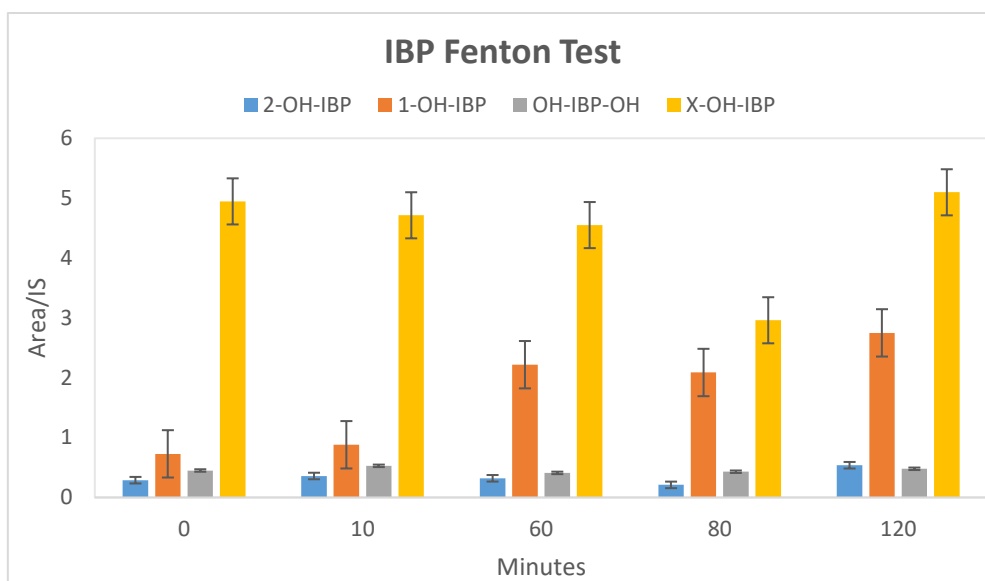


Figure 22. Change in the HPLC-UV integrated peak areas (relative to the internal standard) of the 2-OH-IBP (**3**), 1-OH-IBP (**2**), OH-IBP-OH (**10**), and the X-OH-IBP (**8**) derivatives ibuprofen(IBM)-metabolites in the diethyl ether extracts of Fenton incubation mixtures (Method I).

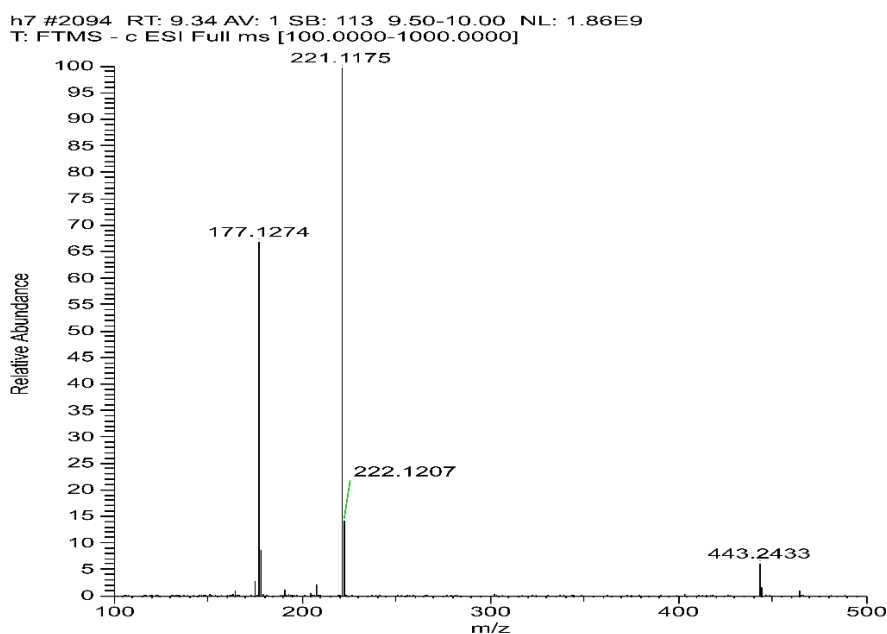


Figure 23.A. HPLC-MS spectrum of the hydroxylated ibuprofen (**8**) (X-OH-IBP) derivative. ($C_{13}H_{17}O_3$; Exact mass: 221.1178) Mass error: -1.36 ppm. The following ion signals are formed in the ionization source: 443.2433: $[2M-H]^-$, 221.1175: $[M-H]^-$, m/z 177.1274: $[M-H-CO_2]^-$.

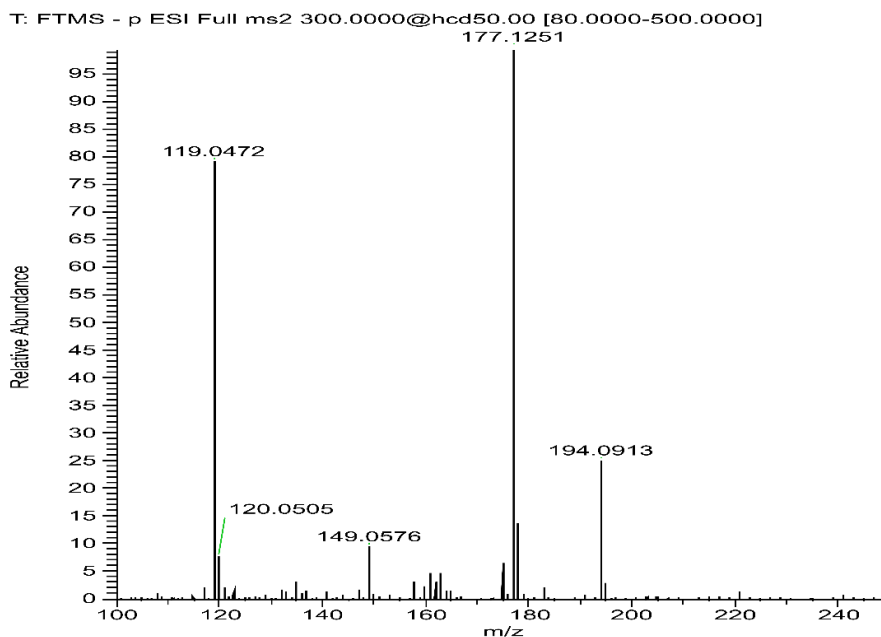


Figure 23.B. HPLC-MS fragmentation of the hydroxylated ibuprofen (**8**) (X-OH-IBP) derivative. ($C_{13}H_{17}O_3$; Exact mass: 221.1178).

Another IBP-derived HPLC-UV peak ($t_R=21.09$ min) was identified as a dihydroxyibuprofen (**10**) (OH-IBP-OH) derivative (m/z 237.1125) (Figure 24). Determination of the exact structures needs further investigation. The change in HPLC-UV integrated peak areas of **2**, **3**, **8**, and **10** (relative to that of the internal standard) as a function of incubation times is shown in Figure 22.

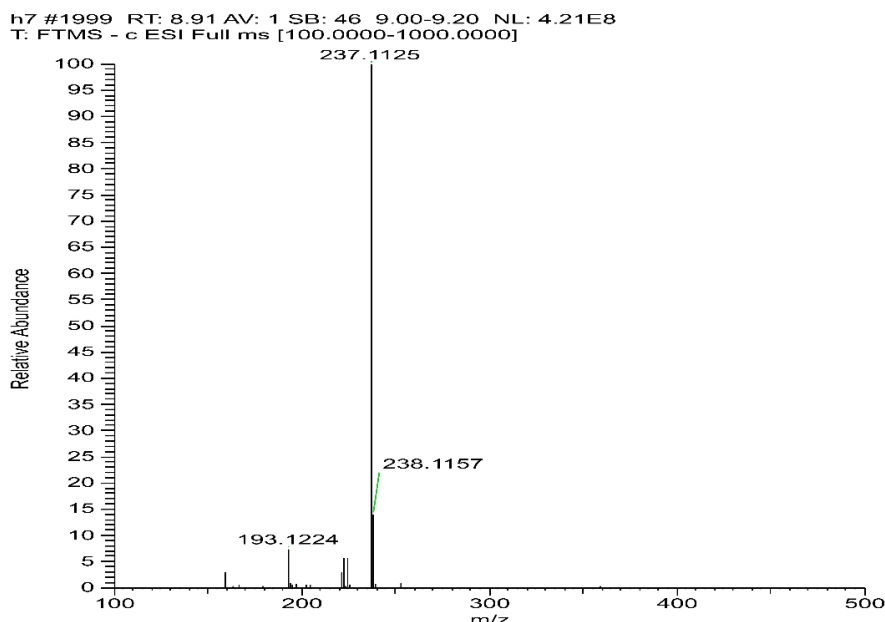


Figure 24. HPLC-MS spectrum of the dihydroxyibuprofen (**10**) (OH-IBP-OH) derivative. ($C_{13}H_{17}O_4$; Exact mass: 237.1127) Mass error: -0.84 ppm. The following fragments are formed in the ionization source: 237.1125: $[M-H]^-$, m/z 193.1224: $[M-H-CO_2]^-$.

5.2.2. Udenfriend's test

Using the *in vitro* non-enzyme-catalyzed hydroxylation test developed by Udenfriend et al. (127, 128), a similar oxidative metabolic pattern (HPLC-UV, Method I) of ibuprofen could be observed. Like the Fenton incubations, the derivatives with the t_R values of 22.03 min (**8**) and 21.07 min (**10**) were those with the highest HPLC-UV peak areas (Figure 25). 2-HO-IBP (**3**) was formed in lower amounts than in the respective Fenton-samples (Figure 26). 1-OH-IBU (**2**) couldn't be detected. HPLC-MS investigations of the samples confirmed the presence of the **2**, **3**, **5**, **8**, and **10** derivatives (Figures 19-21, 23-24).

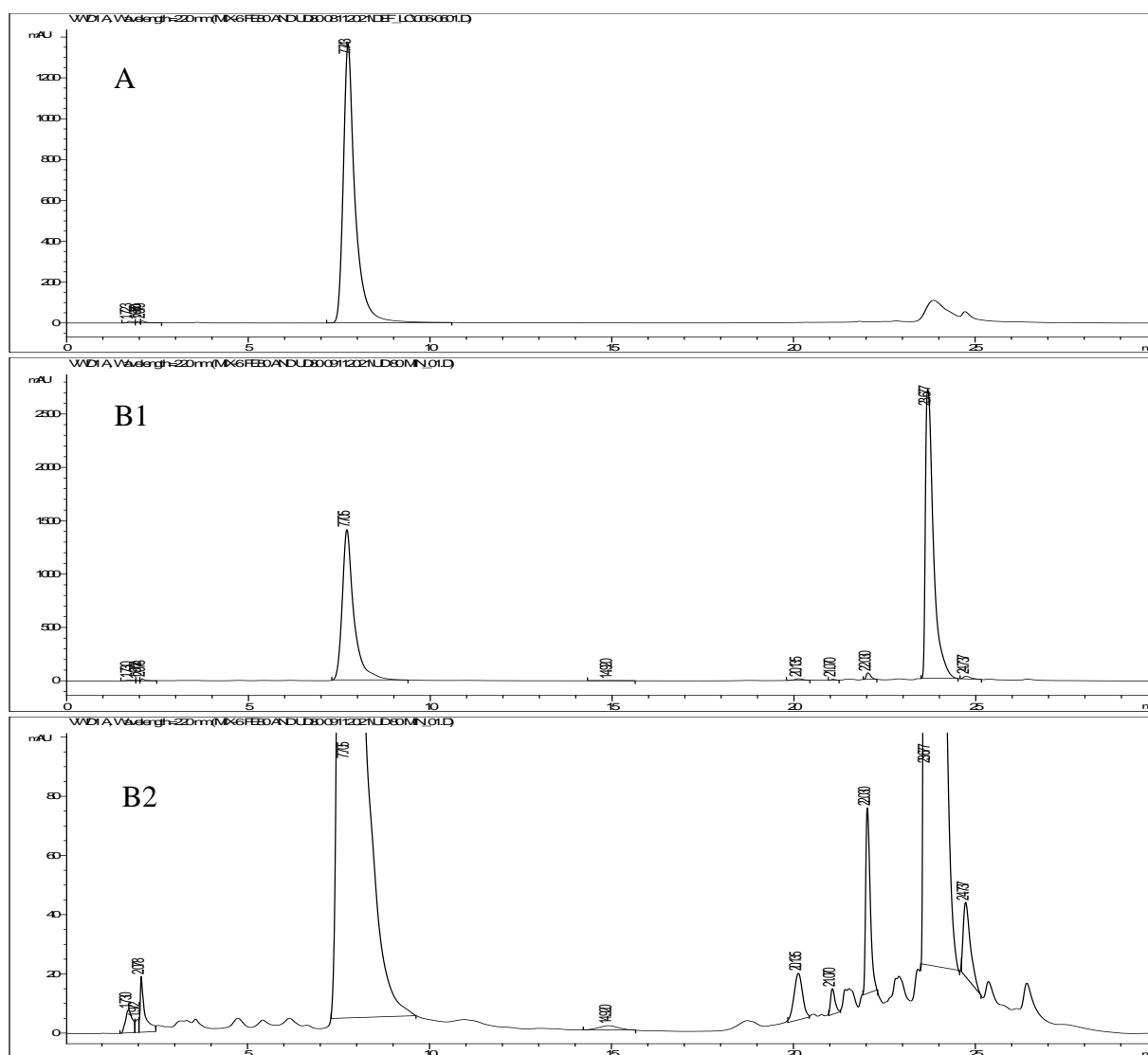


Figure 25. **A.** HPLC-UV-Vis chromatogram (Method I) of the blank Udenfriend extract. Salicylic acid (internal standard.) t_R =7.74 min. **B1** and **B2.** HPLC-UV chromatogram (Method I) of the Udenfriend extract of IBP (80-minute). Salicylic acid (internal standard) t_R =7.71 min, 2-hydroxyibuprofen (**3**) t_R =14.92 min, dihydroxyibuprofen (**10**) t_R =21.07 min, aromatic-hydroxylated ibuprofen (**8**) t_R =22.03 min, ibuprofen t_R =23.68 min.

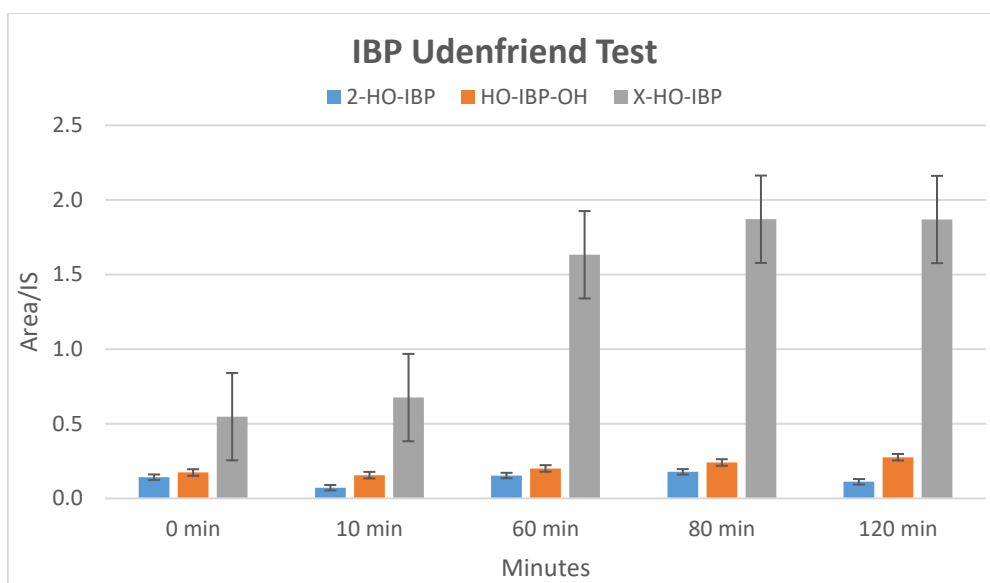


Figure 26. Change in the HPLC-UV integrated peak areas (relative to the internal standard) of the 2-OH-IBP (**3**), OH-IBP-OH (**10**), and the X-OH-IBP (**8**) derivatives in the diethyl ether extracts of the Udenfriend's incubation mixtures (Method I).

5.3. Investigation of the main oxidative and conjugated metabolites of ibuprofen in small intestine perfusates and bile of control and hyperglycemic rats

For HPLC-UV analysis of the biological samples, a gradient method was developed (Method II) to separate the oxidative metabolites and the glucuronide conjugate of IBP (Figure 27). HPLC-UV analysis of the ether extract of the intestinal perfusate samples of the control and the hyperglycemic animals did not indicate either hydroxy- or carboxyibuprofen metabolites (Figures 28-30). Contrary to our previous HPL-UV measurements (115), however, ibuprofen- β -D-glucuronide (**6**) (m/z 381.1549) could be identified by HPLC-MS in the perfusate of both the control and the STZ-treated animals (Figure 31).

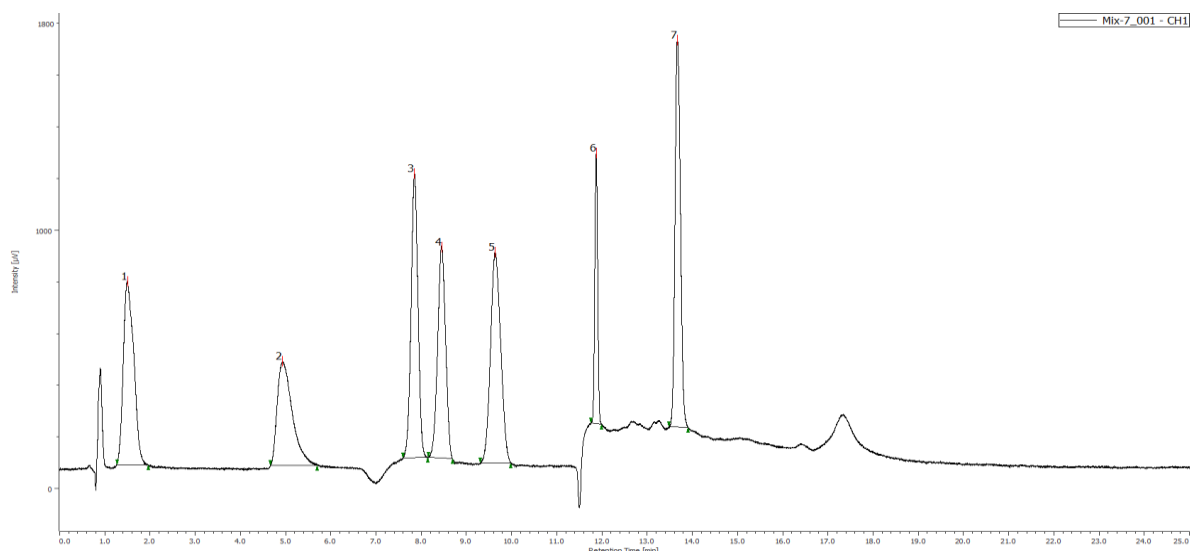


Figure 27. HPLC-UV chromatogram (Method II) of the main oxidative metabolite and the IBP-GLU standards of IBP in ACN ($30 \mu\text{g mL}^{-1}$ each). The retention times of the separated standards as follows: (1) 3-hydroxyibuprofen ($t_R=1.50$ min), (2) salicylic acid (internal standard) ($t_R=4.92$ min), (3) 2-hydroxyibuprofen ($t_R=7.85$ min), (4) carboxyibuprofen ($t_R=8.45$ min), (5) 1-hydroxyibuprofen ($t_R=9.63$ min), (6) ibuprofen- β -D-glucuronide ($t_R=11.87$ min), (7) ibuprofen ($t_R=13.67$ min). (The negative peak in the chromatogram is due to the quick change of mobile phase (solvent B) in the gradient profile)

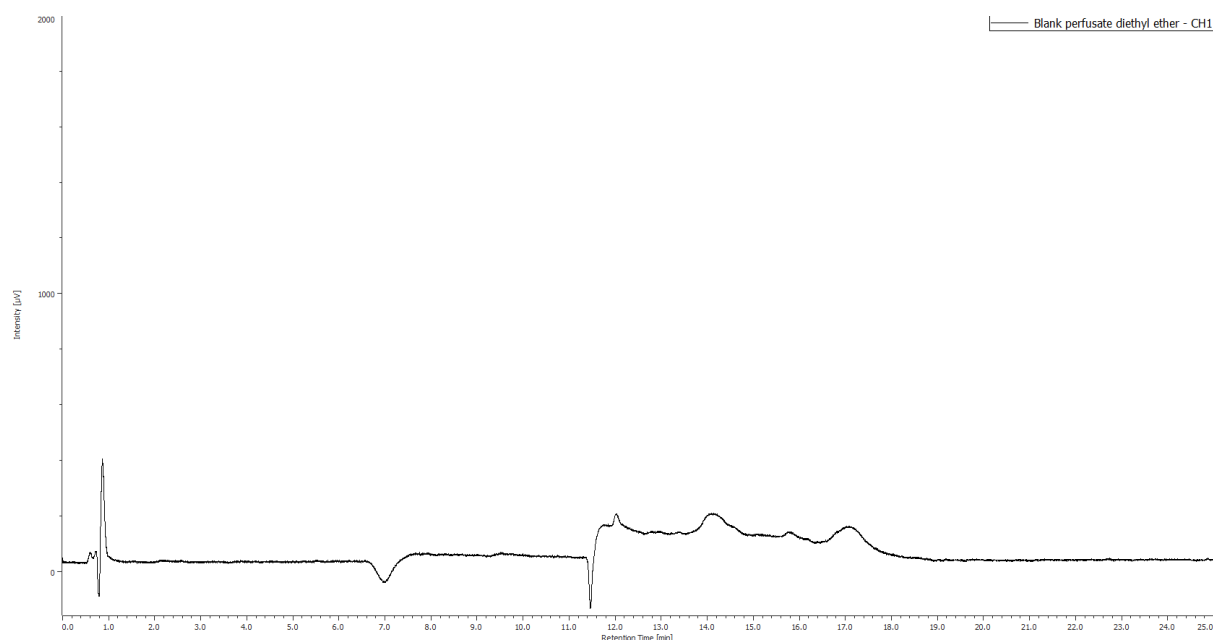


Figure 28. HPLC-UV chromatogram (Method II) of the intestinal perfusate extract of the control rats. (The negative peak in the chromatogram is due to the quick change of mobile phase (solvent B) in the gradient profile.)

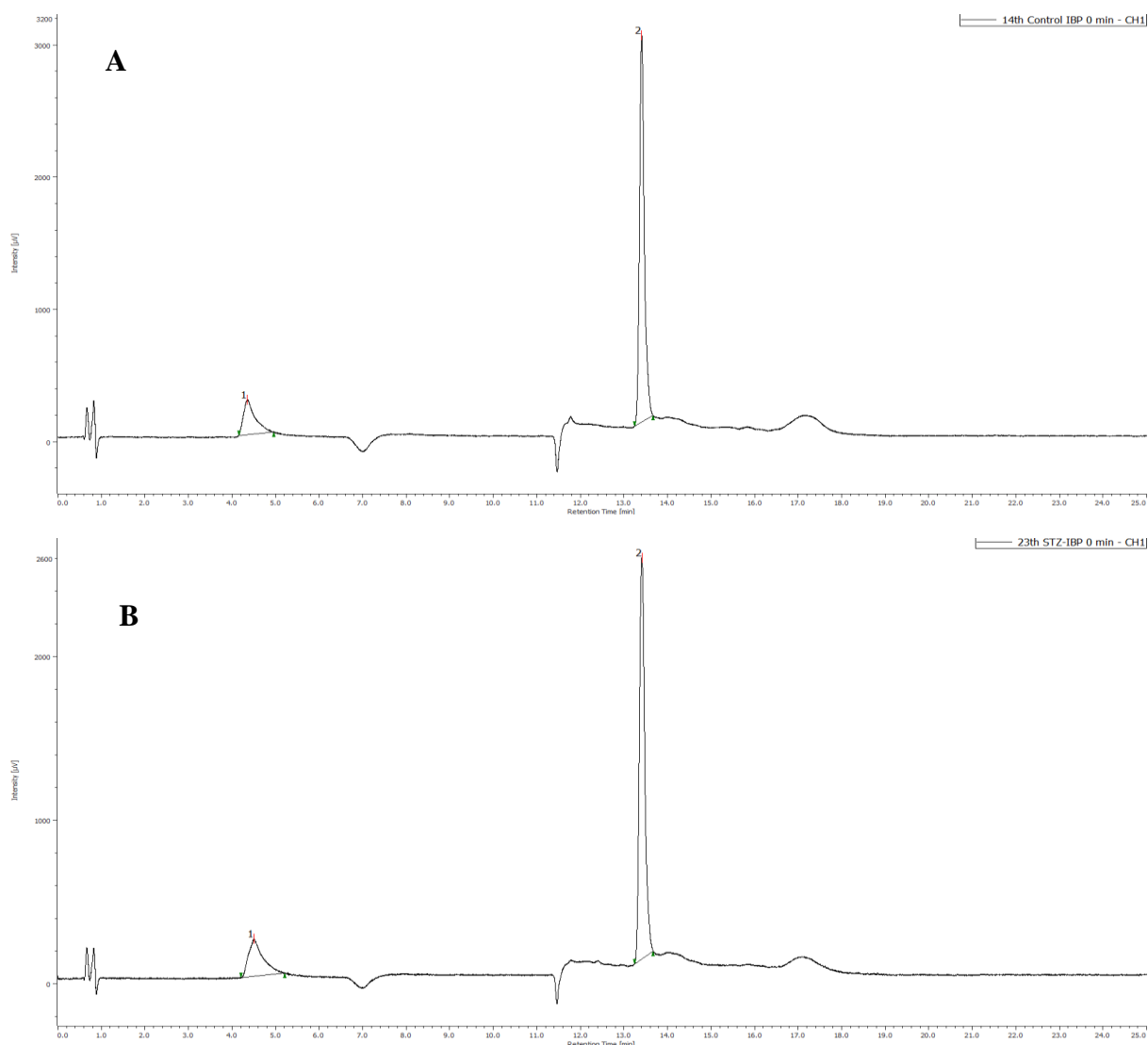


Figure 29. A. HPLC-UV chromatogram (Method II) of the intestinal perfusate extract of the control rats (0 minute). (1) Salicylic acid (internal standard) $t_R=4.35$ min, (2) ibuprofen $t_R=13.40$ min. B. HPLC-UV chromatogram of the intestinal perfusate extract of the STZ-treated rats (0 minute). (1) salicylic acid (internal standard) $t_R=4.50$ min, (2) ibuprofen $t_R=13.40$ min. (The negative peak in the chromatogram is due to the quick change of mobile phase (solvent B) in the gradient profile.)

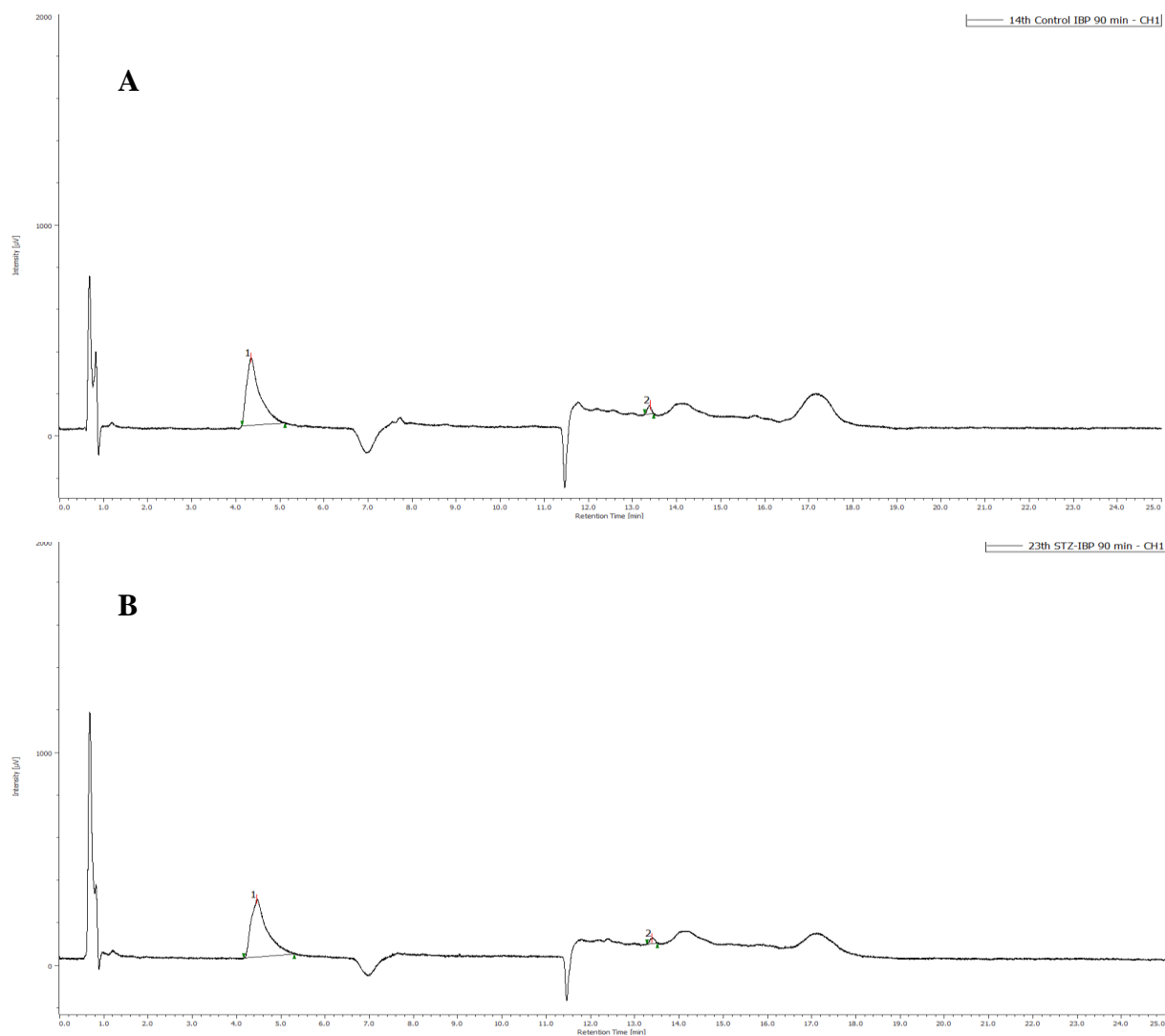


Figure 30. **A.** HPLC-UV chromatogram (Method II) of the intestinal perfusate extract of the control rats (90 minute). **(1)** Salicylic acid (internal standard) $t_R=4.34$ min, **(2)** ibuprofen $t_R=13.39$ min. **B.** HPLC-UV chromatogram (Method II) of the intestinal perfusate extract of the STZ-treated rats (90 minute). **(1)** salicylic acid (IS) t_R . 4.46 min, **(2)** ibuprofen $t_R=13.38$ min. (The negative peak in the chromatogram is due to the quick change of mobile phase (solvent B) in the gradient profile.)

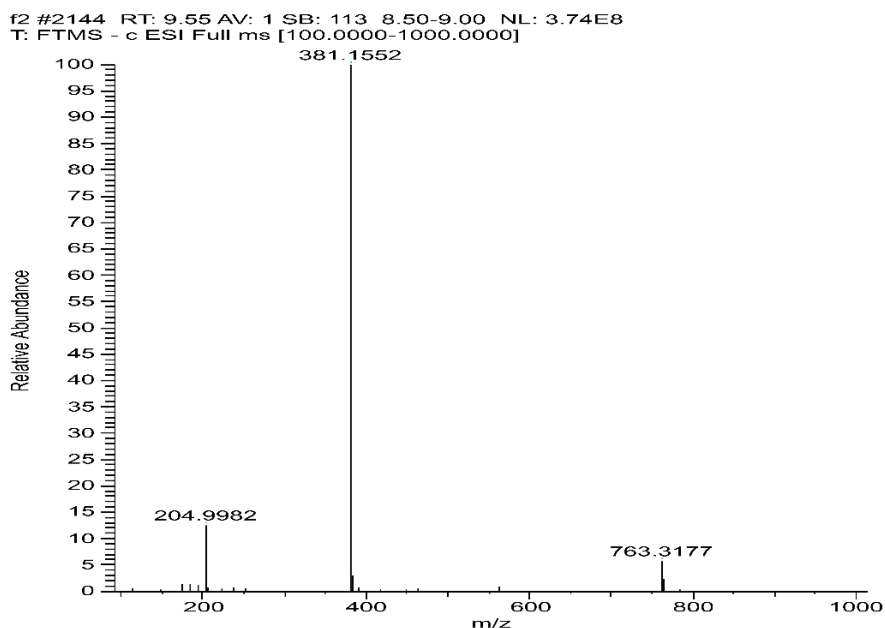


Figure 31. HPLC-MS spectrum of the ibuprofen- β -D-glucuronide (**6**) (IBP-GLU)) standard. ($C_{19}H_{25}O_8$; Exact mass: 381.1549). Mass error = 0.79 ppm. The following ion signals are formed in the ionization source: m/z 763.3177: $[2M-H]^-$, m/z 204.9982: unknown.

HPLC-UV analysis of the ether extract of bile samples showed the presence of IBP (**1**), IBP-GLU (**6**), and 2-OH-IBP (**3**). HPLC-MS analysis confirmed the presence of **1** (m/z 205.1229), **6** (m/z 381.1549), and **3** (m/z 221.1178) in both the control and the hyperglycemic samples. To keep the number of experimental animals low, the results were evaluated by comparing the integrated HPLC-UV peak areas (relative to the internal standard) of the compounds. The areas were lower in the bile samples of the STZ-treated animals at each investigated timepoint (Figure 32).

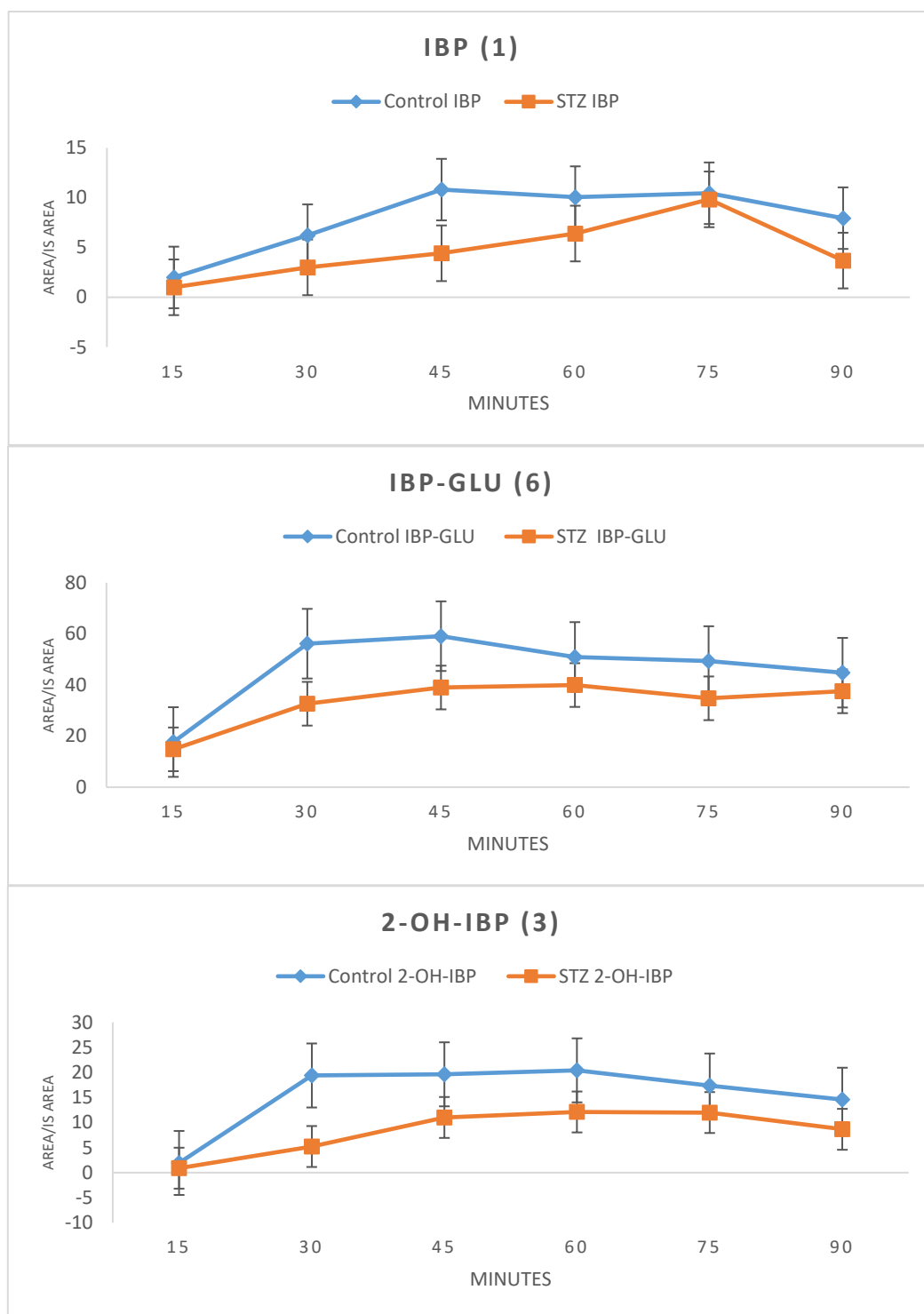


Figure 32. Change in the HPLC-UV integrated peak areas (relative to the internal standard) of ibuprofen (1) and the ibuprofen-metabolites (IBP-GLU (6) and 2-OH-IBP (3)) in the diethyl ether extract of bile of control and hyperglycemic (STZ) rats (Method II).

Considering the respective bile outflows, the relative amounts of the cumulative excretions of the IBP (**1**), IBP-GLU (**6**), and 2-HO-IBP (**3**) were calculated. The result showed depression in the biliary excretion of all three compounds in the STZ-treated animals. In earlier experiments of our research group (using the same experimental protocol), the cumulative biliary excretion of IBP was reduced by 53% (115). The present data indicated similar (58%) depression. For IBP-GLU and 2-OH-IBP, the excretion was depressed by 63% and 49%, respectively (Figure 33).

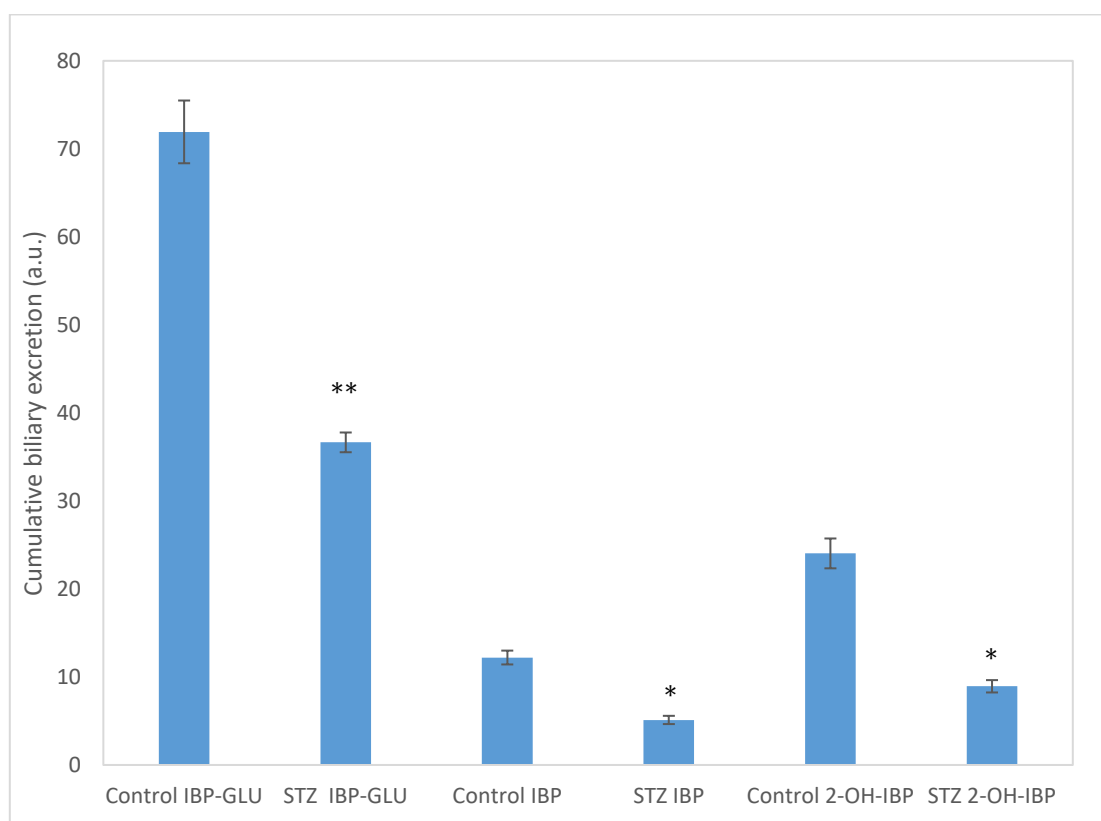


Figure 33. Cumulative biliary excretion (HPLC-UV (Method II) based integration) of IBP (**1**), IBP-GLU (**6**), and 2-OH-IBP (**3**) after the 90 min luminal perfusion of 250 μ M IBP in control and hyperglycemic (STZ-treated) rats. Each value represents the average of five independent experiments \pm standard error. Significant difference from the control value: * $p < 0.05$, ** $p < 0.01$.

Besides, several other peaks appeared in the extracts (Figures 34-36). Based on the HPLC-MS analysis of the samples, these peaks are bile acids and conjugated bile acid derivatives. Based on their high-resolution mass spectra, cholic acid (exact mass: 407.2798), glycocholic acid (exact mass: 464.3012), taurochenodeoxycholic acid (exact mass: 498.2889), and taurocholic acid (exact mass: 514.2839) were identified.

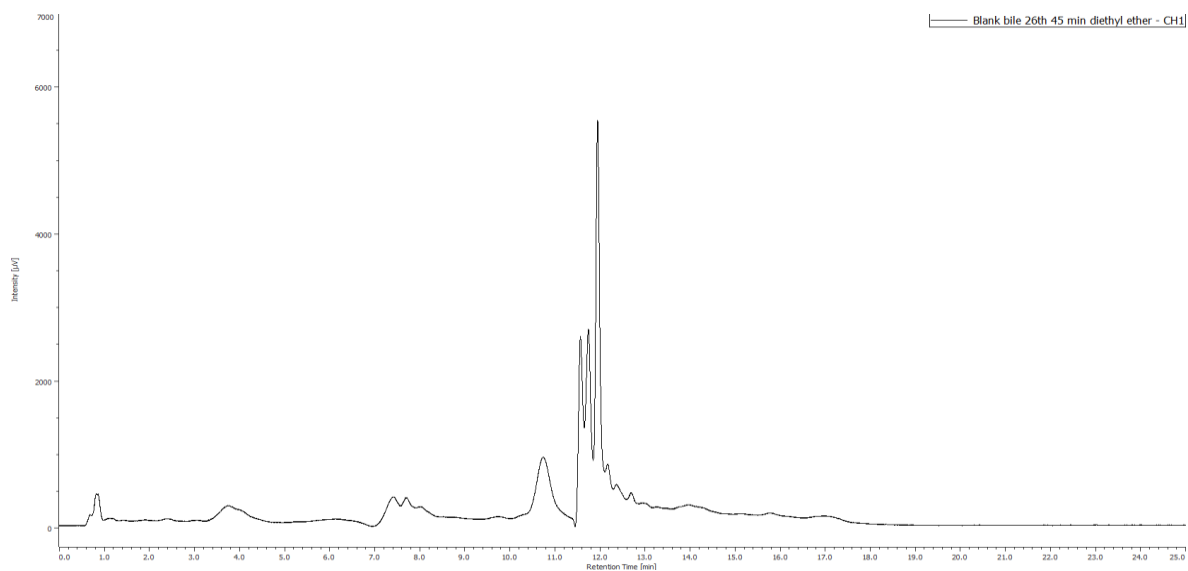


Figure 34. HPLC-UV chromatogram (Method II) of the bile extract of the control rats.

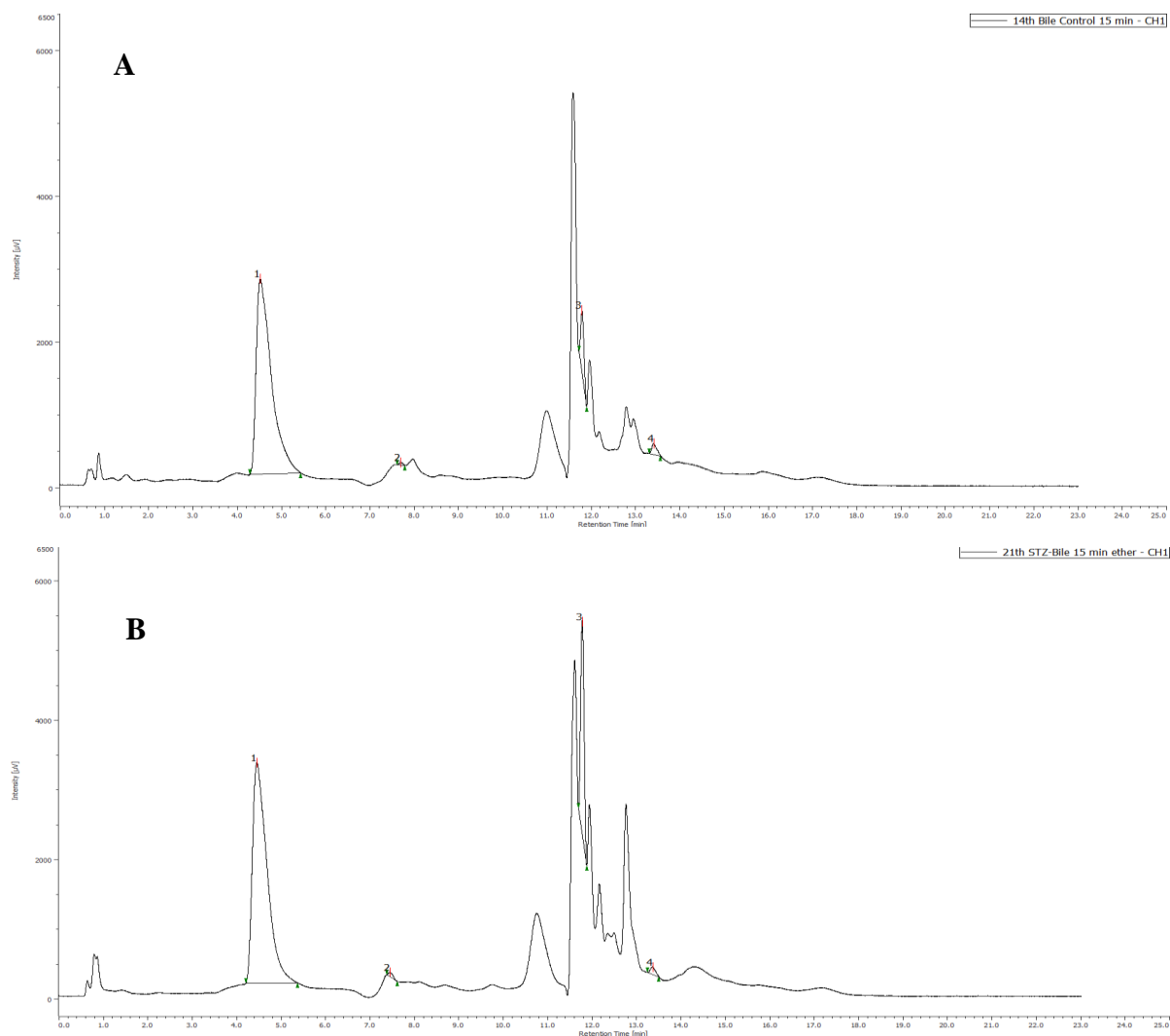


Figure 35. A. HPLC-UV chromatogram (Method II) of the bile extract of the control rats (15 min). (1) Salicylic acid (internal standard) $t_R=4.52$ min, (2) 2-hydroxyibuprofen $t_R=7.68$ min, (3) ibuprofen-glucuronide $t_R=11.78$ min, (4) ibuprofen $t_R=13.41$ min. **B.** HPLC-UV chromatogram (Method II) of the bile extract of the STZ-treated rats (15 min). (1) Salicylic acid (IS) $t_R=4.45$ min, (2) 2-hydroxyibuprofen $t_R=7.45$ min, (3) ibuprofen-glucuronide $t_R=11.77$ min, (4) ibuprofen $t_R=13.36$ min.

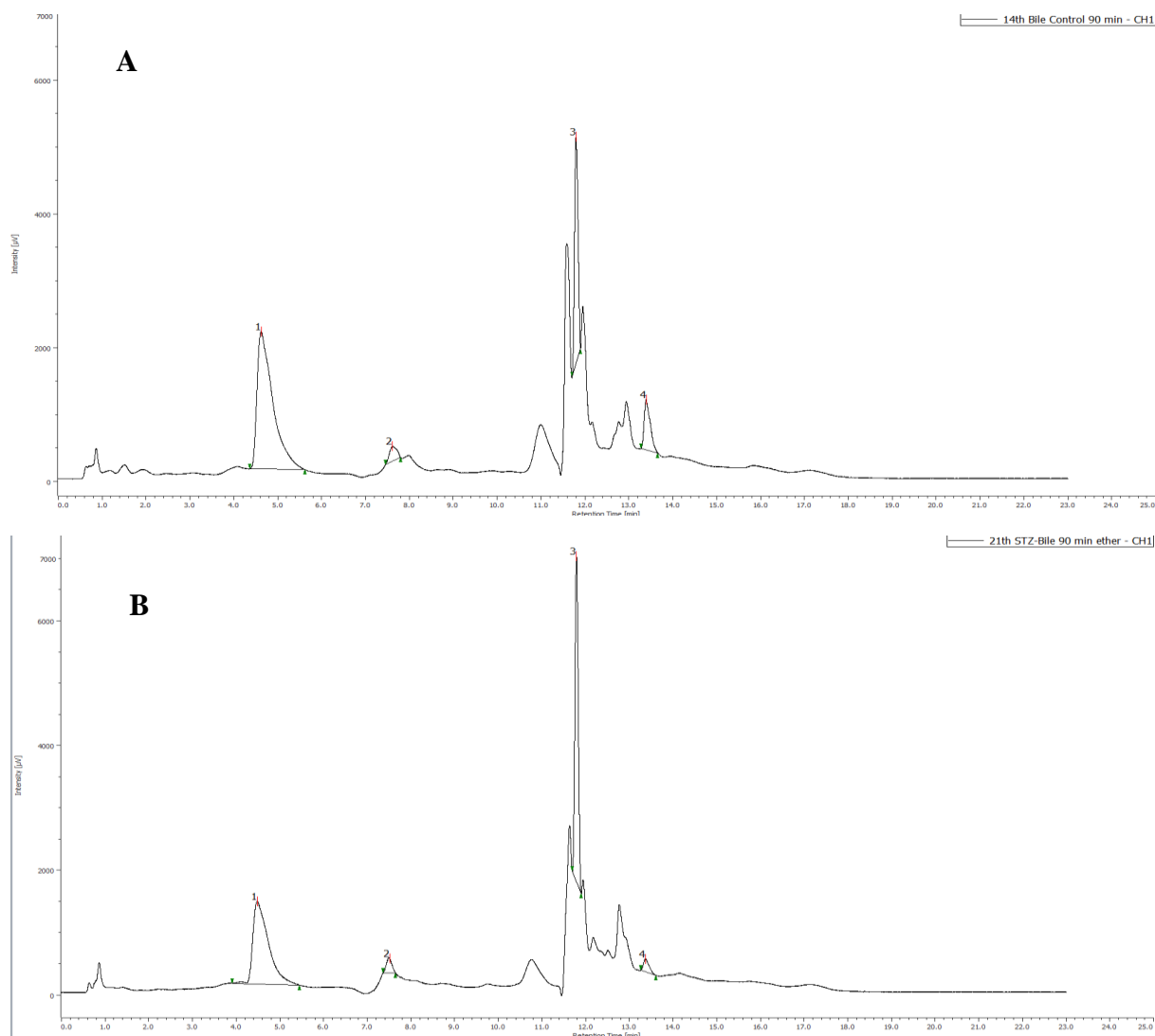


Figure 36. A. HPLC-UV chromatogram (Method II) of the bile extract of the control rats (90 min).; (1) Salicylic acid (internal standard) $t_R=4.62$ min, (2) 2-hydroxyibuprofen $t_R=7.61$ min, (3) ibuprofen-glucuronide $t_R=11.79$ min, (4) ibuprofen $t_R=13.39$ min. **B.** HPLC-UV chromatogram (Method II) of the bile extract of the STZ-treated rats (90 min). (1) Salicylic acid (IS) $t_R=4.48$ min, (2) 2-hydroxyibuprofen $t_R=7.51$ min, (3) ibuprofen-glucuronide $t_R=11.78$ min, (4) ibuprofen $t_R=13.37$ min.

Furthermore, HPLC-MS analysis of the bile samples confirmed the presence of the glucuronide conjugate of a hydroxylated ibuprofen (**9**) (m/z 397.1501) (X-HO-IBP-GLU), and the taurine conjugate of ibuprofen (**7**) (m/z 312.1274) (IBP-TAU) (see Figures 37 and 38, respectively). The cumulative biliary excretion of X-OH-IBP-GLU and IBP-TAU in control and STZ-treated rats is shown in Figures 33A and 33B. The excreted X-OH-IBP-GLU and IBP-TAU were depressed by 92% and 98%, respectively (Figure 39).

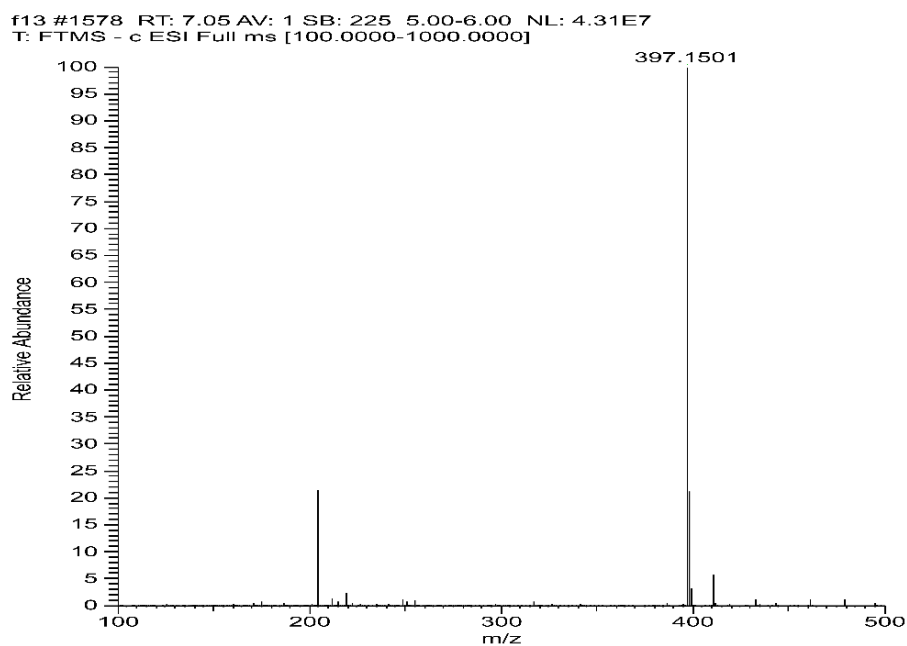


Figure 37. HPLC-MS spectrum of the hydroxyibuprofen-glucuronide (**9**) (X-OH-IBP-GLU) derivative. ($C_{19}H_{25}O_9$; Exact mass: 397.1499) Mass error: 0.50 ppm.

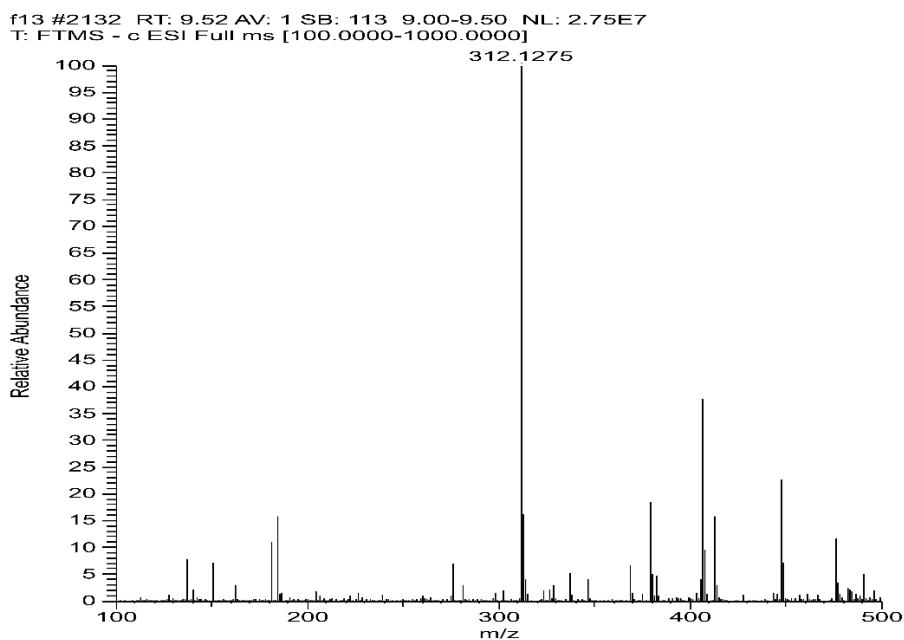


Figure 38. HPLC-MS spectrum of the ibuprofen-taurate (**7**) (IBP-TAU) derivative. ($C_{15}H_{22}NO_4S$; Exact mass: 312.1270). Mass error: 1.60 ppm. The unknown signals are from the background.

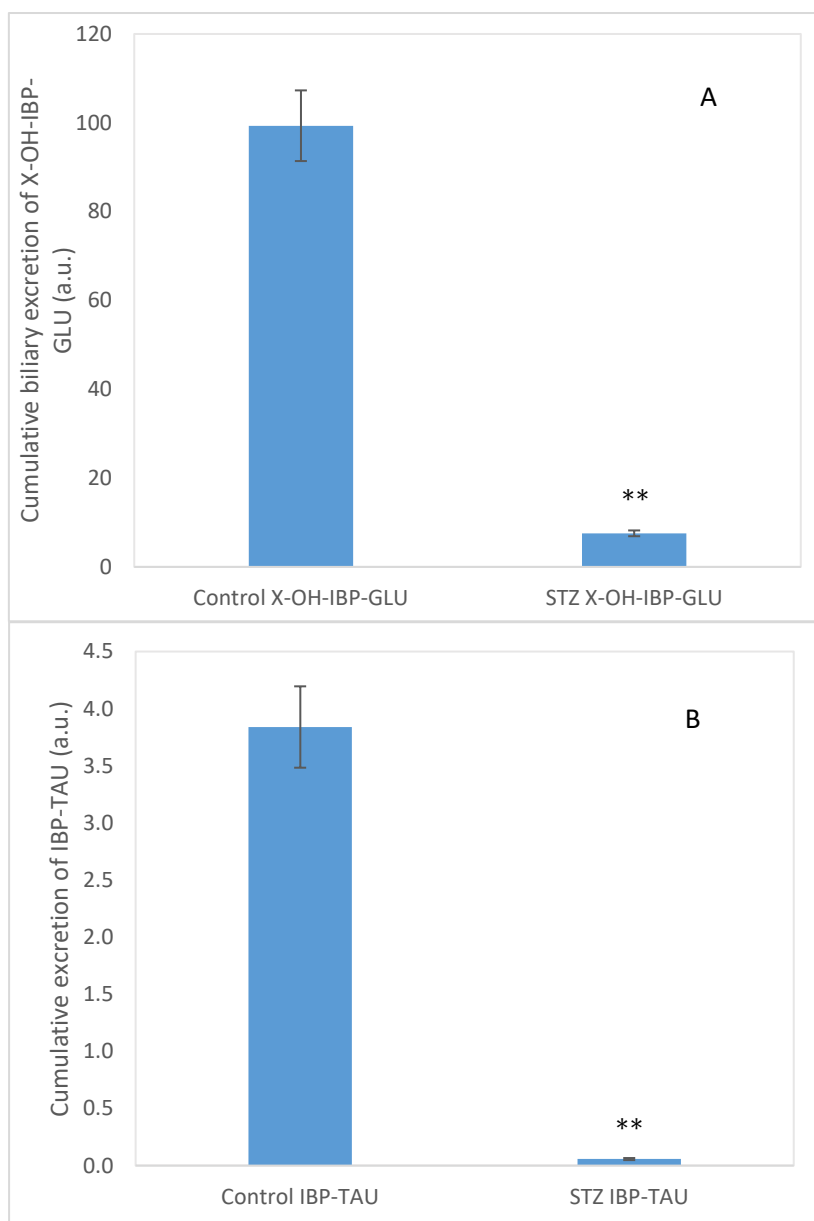


Figure 39. Cumulative biliary excretion (HPLC-MS based integration) of the (A) X-OH-IBP-GLU (9) and (B) IBP-TAU (7) after the 90 min luminal perfusion of 250 μ M IBP in control and hyperglycemic (STZ) rats. Each value represents the average of five independent experiments \pm standard error. Significant difference from the control value: ** p < 0.01.

5.4. Investigation of the ratio of *R*(-) and *S*(+)-ibuprofen in small intestinal perfusates and bile of control and hyperglycemic rats

Figure 40 shows the HPLC-UV chromatogram of the two ibuprofen enantiomers and naproxen (used as internal standard) extracted from the control perfusion medium (Figure 40A) and the control bile (Figure 40C). The blank control (buffer perfused through isolated small intestine of not treated rat) doesn't have any interfering peak (Figure 40B). The blank control

bile (biliary excretion collected from the bile duct) doesn't have any interfering peak (Figure 40D).

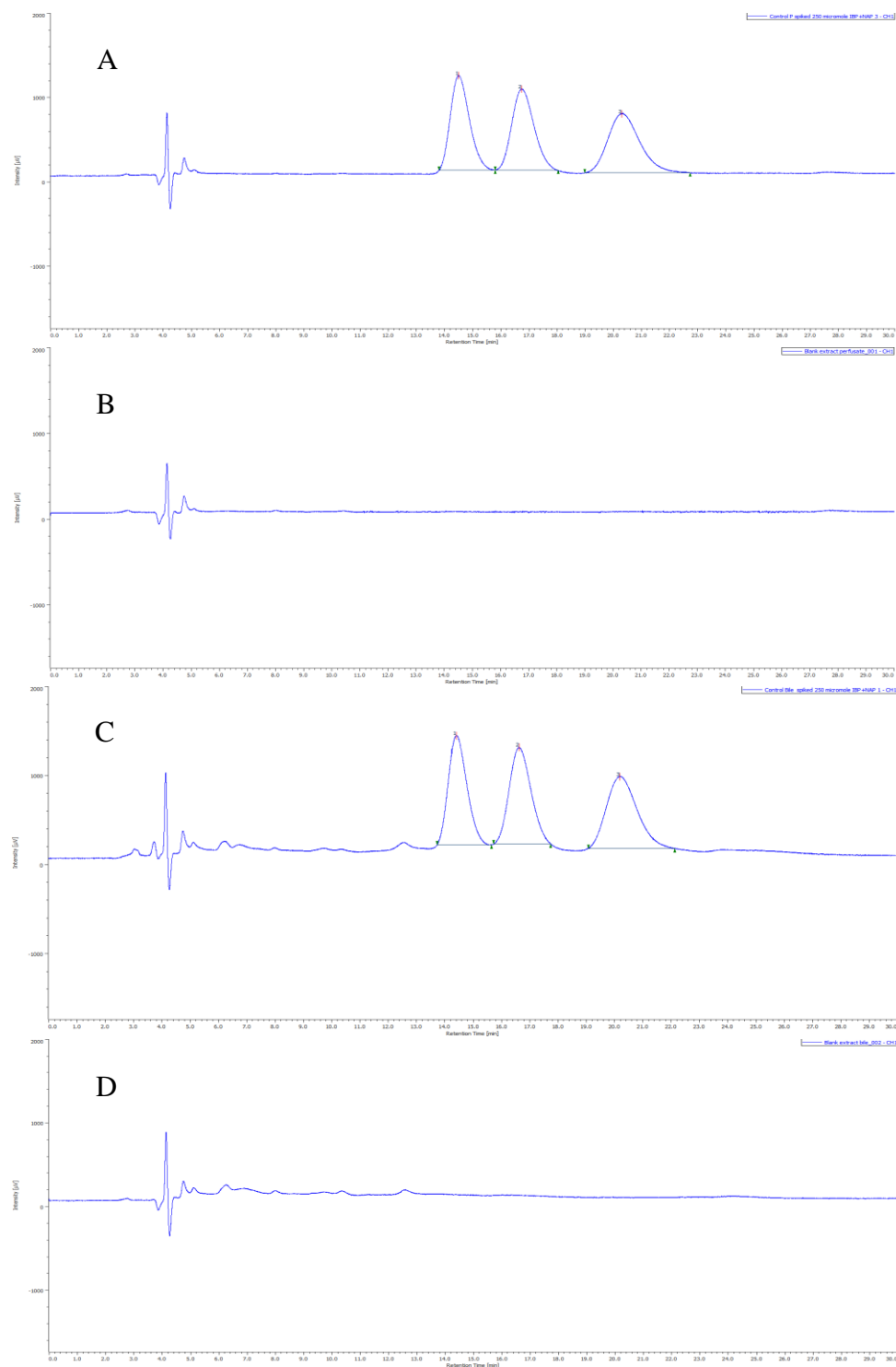


Figure 40. (A) HPLC-UV chromatogram of the two IBP enantiomers ((*R*)-IBP (**1**) t_R =14.5 min, (*S*)-IBP (**2**) t_R =16.72 min and NAP (**3**) t_R =20.3 min), extracted from the spiked control perfusion medium of non-treated animal, (B) extracted from the blank control perfused medium of non-treated animal, (C) the two IBP enantiomers ((*R*)-IBP (**1**) t_R =14.4 min, (*S*)-IBP (**2**) t_R =16.61 min and NAP (**3**) t_R =20.18 min), extracted from the spiked control bile of non-treated animal; (D) extracted from the blank control bile of non-treated animal.

According to the applied method by the chiral column brand (Kromasil application note), the two ibuprofen enantiomers were separated (118). The identification of the ibuprofen enantiomers was confirmed based on the available (*S*)-IBP standard and naproxen as the internal standard (Figure 41).

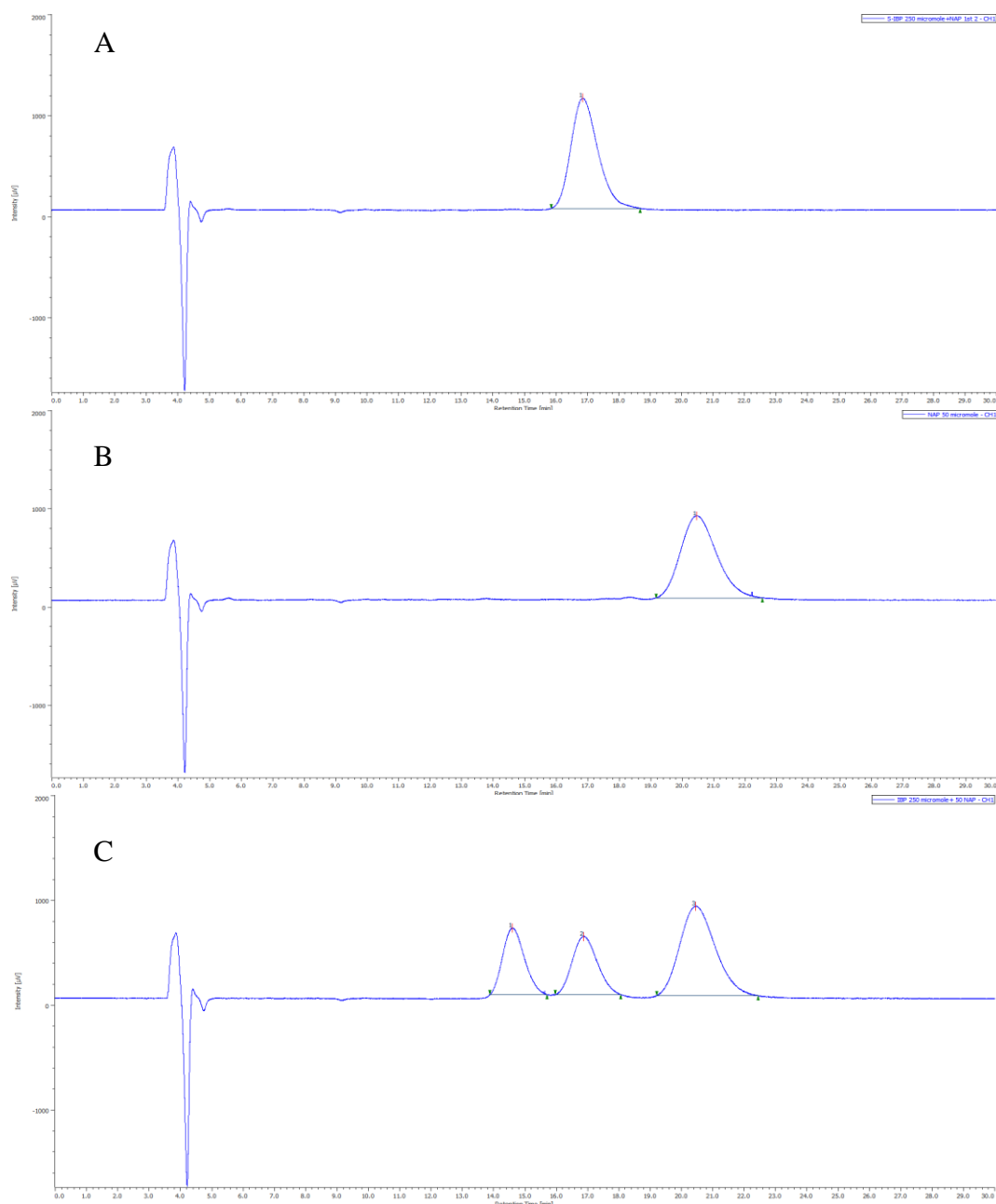


Figure 41. (A) HPLC-UV chromatogram of the (*S*)-IBP ($t_R=16.85$ min) in methanol, (B) the naproxen ($t_R=20.44$ min) in methanol, (C) the racemic IBP ((*R*)-ibuprofen (**1**) $t_R=14.59$ min, (*S*)-ibuprofen (**2**) $t_R=16.86$ min) and naproxen (**3**) ($t_R=20.43$ min) dissolved in the mobile phase.

HPLC chromatograms of the intestinal perfusates of the control and the STZ-treated (hyperglycemic) rats at the 0, 29, and 90-minute timepoints are shown in Figures 42 and 43, respectively. The cumulative peak areas of the *R*(-)- and *S*(+)-ibuprofen enantiomers are shown in Figure 44. The cumulative disappearance of both ibuprofen enantiomers was depressed in the hyperglycemic rats.

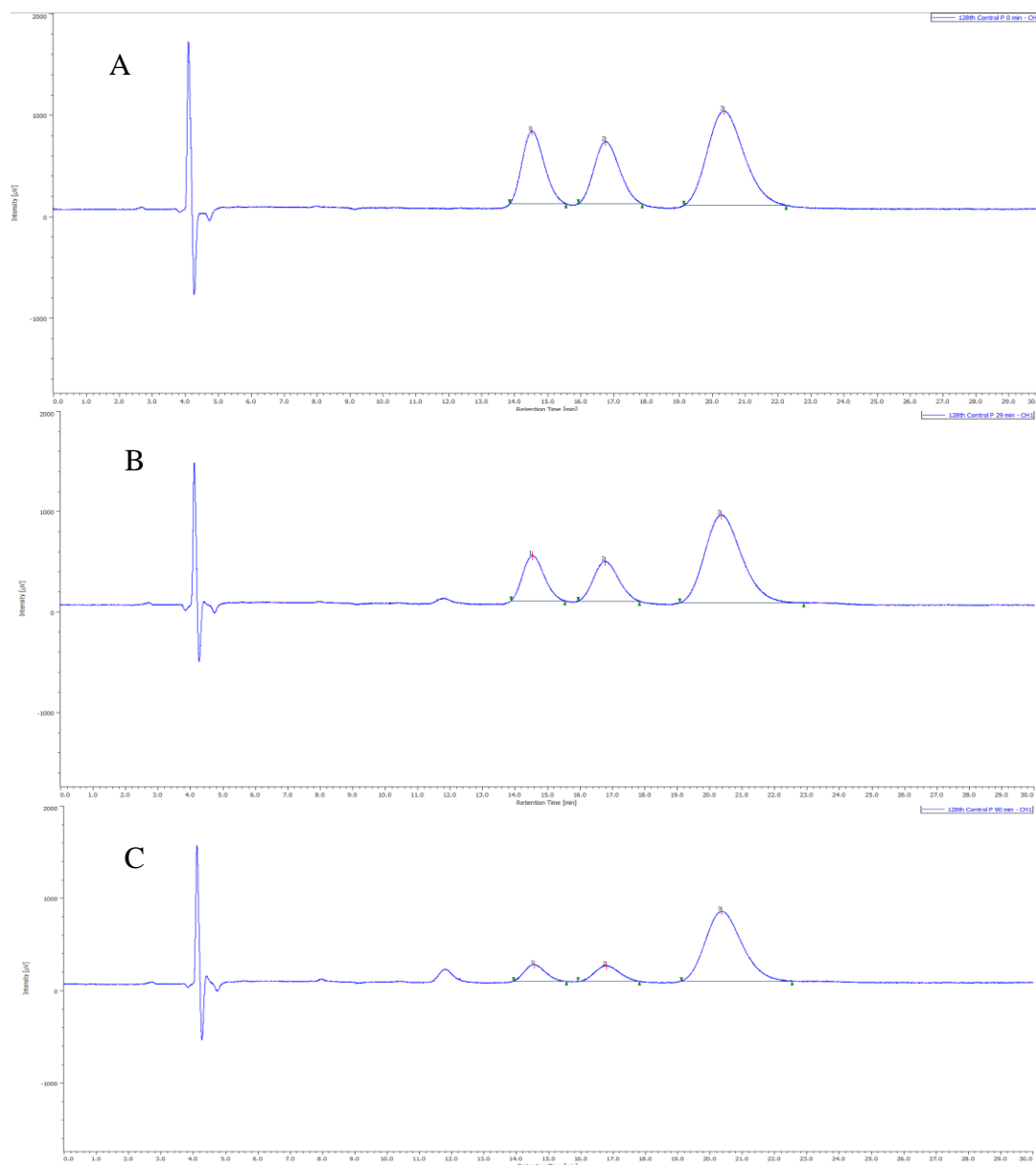


Figure 42. HPLC-UV chromatograms of extracts of intestinal perfusate of 250 μ M racemic IBP spiked with 250 μ M NAP (IS) at (A) 0 minute: (*R*)-IBP (1) (t_R =14.52 min), (*S*)-IBP (2) (t_R =16.75 min), NAP (3) (t_R =20.35 min); (B) 29-minute: (*R*)-IBP (1) (t_R =14.53 min), (*S*)-IBP (2) (t_R =16.76 min), NAP (3) (t_R =20.35 min); and (C) 90 minute: (*R*)-IBP (1) (t_R =14.54 min), (*S*)-IBP (2) (t_R =16.78 min), NAP (3) (t_R = 20.35 min) of control rats.

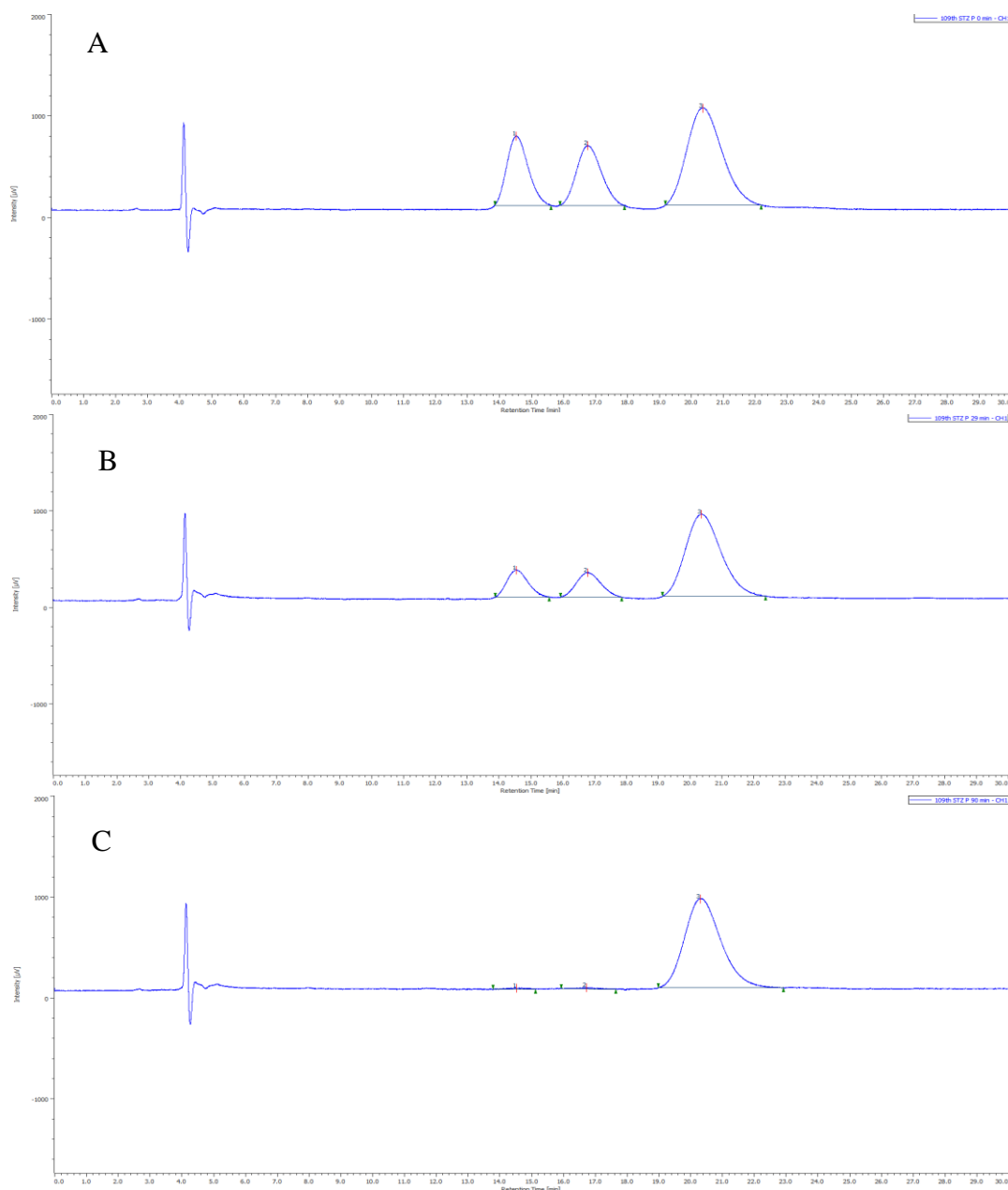


Figure 43. HPLC-UV chromatograms of extracts of intestinal perfusate of 250 μ M racemic IBP spiked with 250 μ M NAP (IS) at (A) 0 minute: (*R*)-IBP (1) (t_R =14.52 min), (*S*)-IBP (2) (t_R =16.75 min), NAP (3) (t_R = 20.35 min); (B) 29-minute: (*R*)-ibuprofen (1) (t_R =14.53 min), (*S*)-IBP (2) (t_R =16.76 min), NAP (3) (t_R =20.35 min); and (C) 90 minute: (*R*)-IBP (1) (t_R =14.51 min), (*S*)-IBP (2) (t_R =16.73 min), NAP (3) (t_R =20.31 min) of hyperglycemic rats.

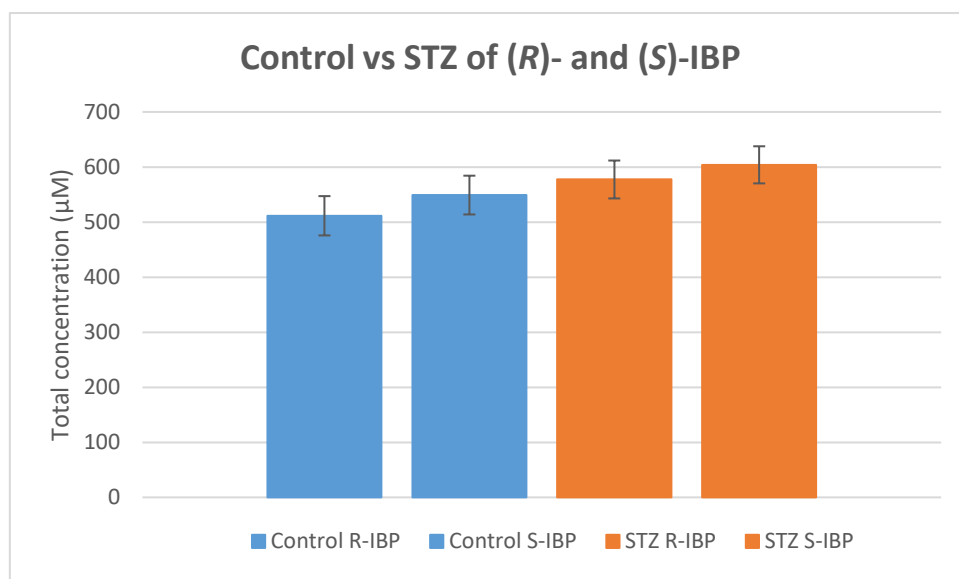


Figure 44. The total concentration of the (*R*)-IBP and (*S*)-IBP in the intestinal perfusion medium of control and hyperglycemic rats extracts ($n=4$).

Concentrations of the IBP enantiomers in the perfusions of the control and hyperglycemic rats are shown in Figure 45. The relative amount of the (*S*)-IBP enantiomer in the control animals was slightly higher from the 22 minute to the 45 minute timepoints of the experiments; however, the difference cannot be assessed statistically (Figure 45A). Such a change couldn't be observed in the samples of the hyperglycemic rats (Figure 45B).

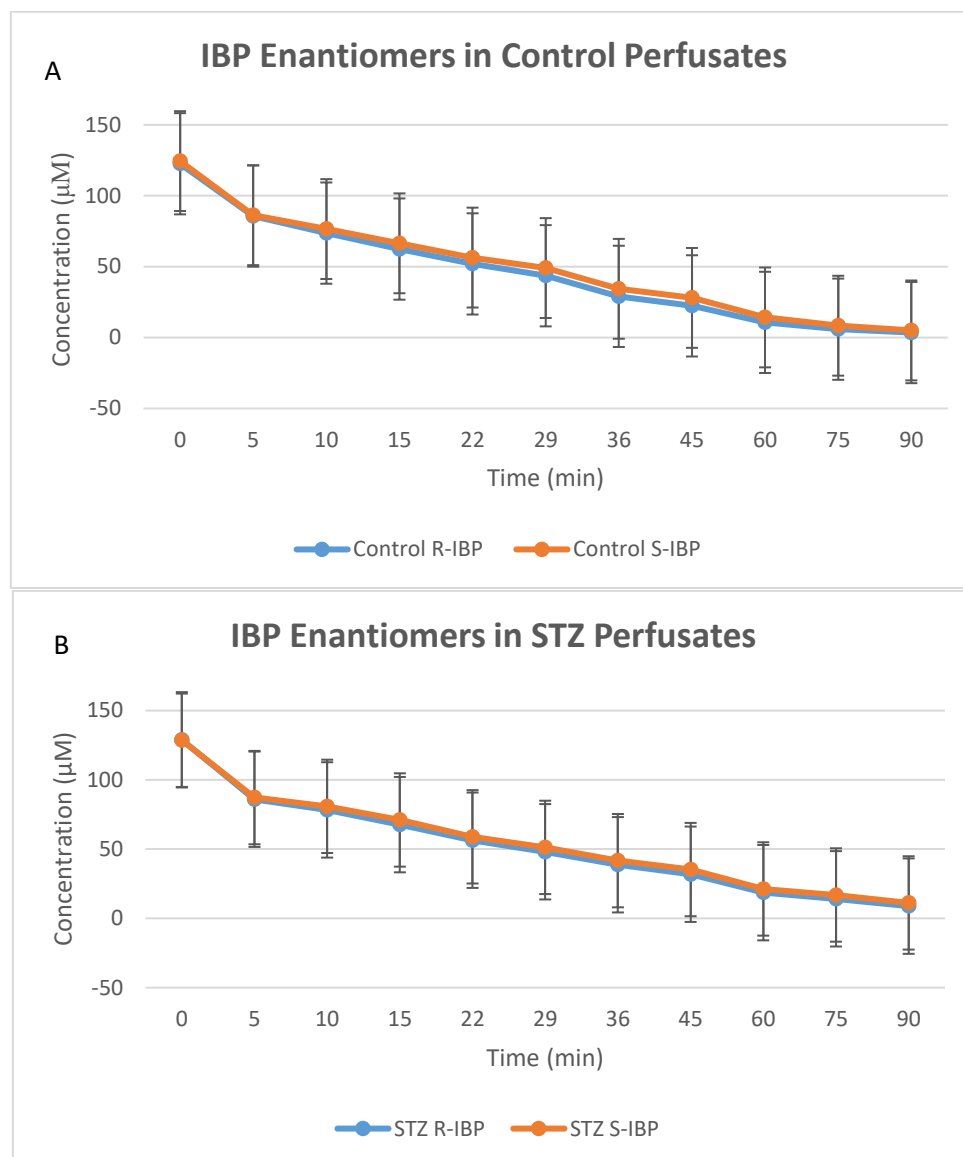


Figure 45. Concentrations of the IBP enantiomers in the extracts of the intestinal perfusates of the control (**4A**) and hyperglycemic (**4B**) rats ($n=4$).

In the bile samples collected during the intestinal perfusion of racemic IBP, only the (*S*)-IBP enantiomer could be detected. HPLC chromatograms of bile samples of control and hyperglycemic rats at the 30, 60, and 120 minute timepoints are shown in Figures 46 and 47, respectively. In the chromatograms, two unknown peaks also appeared. Based on their relative retention times (compared to the IS), none of them could be identified by the available standards (IBP, 1-, 2-, 3-OH-IBP, and IBP-GLU). The concentrations of the (*S*)-IBP enantiomer measured in the bile samples of control and hyperglycemic rats are shown in Figure 48. The biliary excretion (*S*)-IBP was statistically lower in the hyperglycemic (STZ-treated) animals.

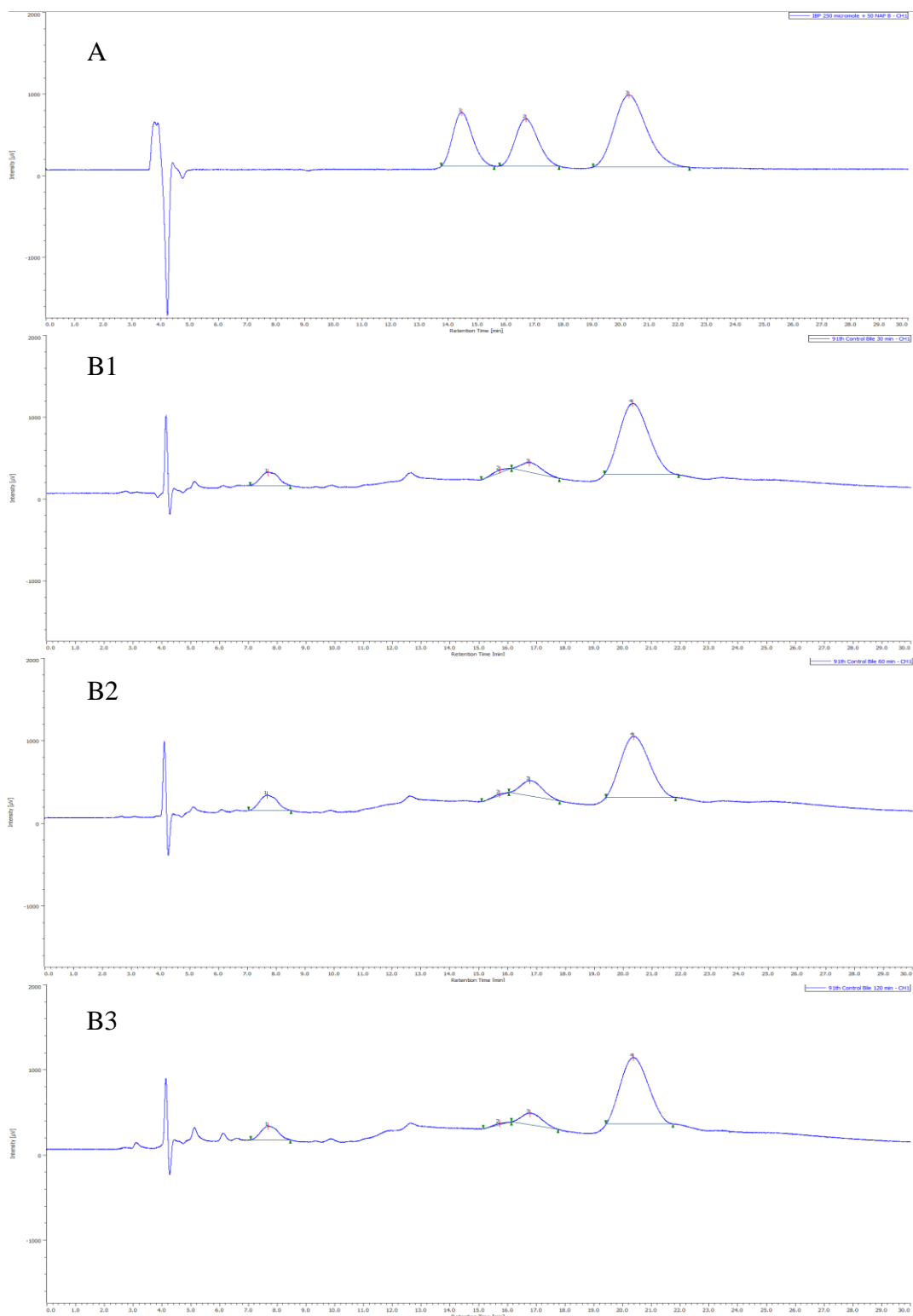


Figure 46. (A) HPLC-UV chromatogram of 250 μ M of racemic IBP ((*R*)- (1) t_R =14.45 min, (*S*)-IBP (2) t_R =16.69 min) and NAP (3) (t_R =20.26 min) in the mobile phase; HPLC-UV chromatograms of bile extract at (B1) 30 minute: unknown peak (1) (t_R =7.68 min), unknown peak (2) (t_R =15.72 min), (*S*)-IBP (3) (t_R =16.75 min), NAP (4) (t_R =20.33 min); (B2) 60 minute: unknown peak (1) (t_R = 7.68 min), unknown peak (2) (t_R =15.72 min), (*S*)-IBP (3) (t_R = 16.76 min), NAP (4) (t_R =23.35 min); and (B3) 120 minute: unknown peak (1) (t_R =7.69 min), unknown peak (2) (t_R =15.72 min), (*S*)-IBP (3) (t_R =16.76 min), NAP (4) (t_R =20.36 min) of control rats.

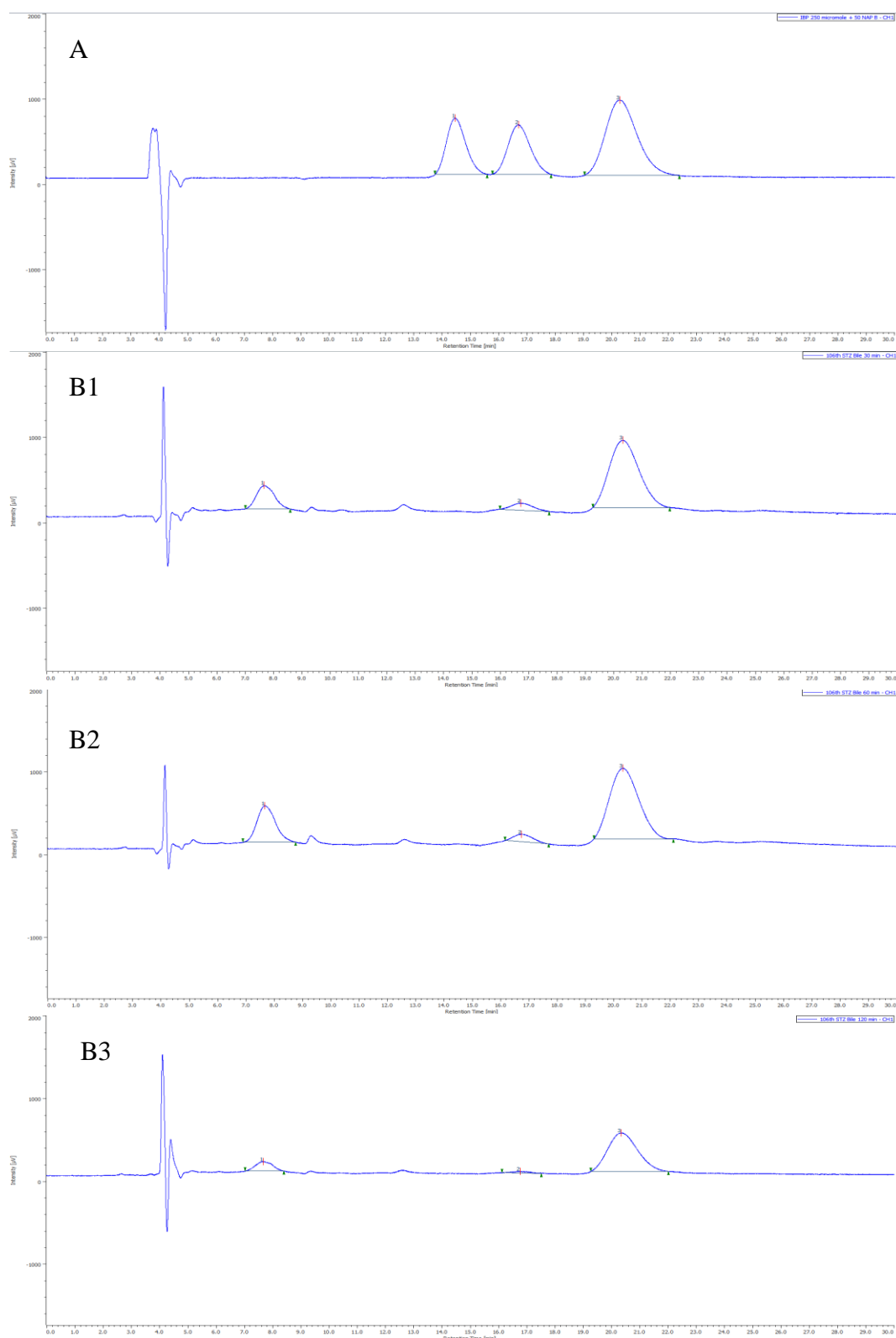


Figure 47. (A) HPLC-UV chromatogram of 250 mM of racemic IBP ((*R*)- (**1**) $t_R=14.45$ min, (*S*)-IBP (**2**) $t_R=16.69$ min) and NAP (**3**) ($t_R=20.26$ min) in the mobile phase; HPLC-UV chromatograms of excreted bile extract at (B1) 30 minute: unknown peak (**1**) ($t_R=7.68$ min), (*S*)-IBP (**2**) ($t_R=16.72$ min), NAP (**3**) ($t_R=20.3$ min); (B2) 60 minute: unknown peak (**1**) ($t_R=7.66$ min), (*S*)-IBP (**2**) ($t_R=16.73$ min), NAP (**3**) ($t_R=20.31$ min); and (B3) 120 minute: unknown peak (**1**) ($t_R=7.66$ min), (*S*)-IBP (**2**) ($t_R=16.75$ min), NAP (**3**) ($t_R=20.32$ min) of hyperglycemic rats.

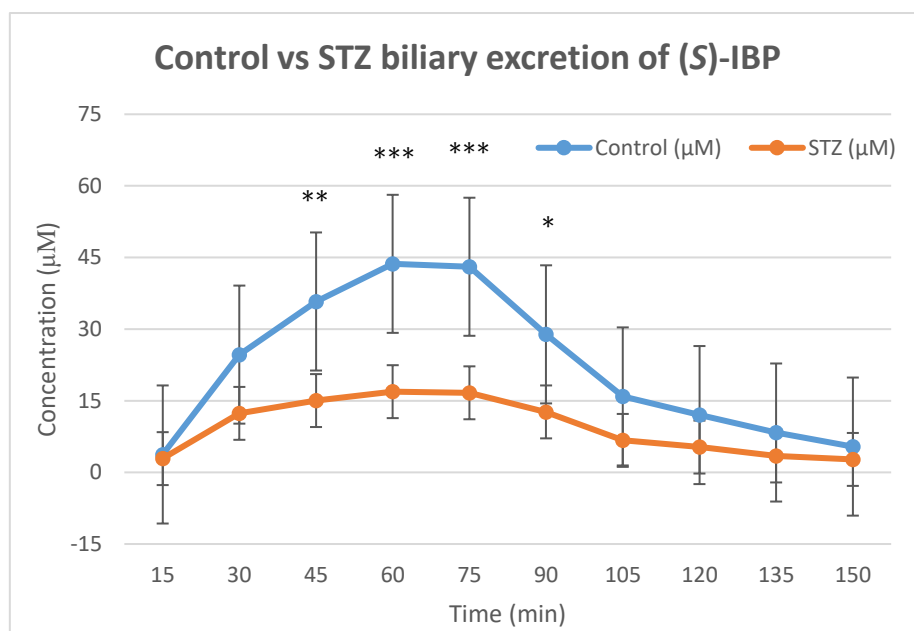


Figure 48. The concentration of (S)-IBP in the extracts of the bile samples of control and hyperglycemic animals ($n=4$). Significant differences from the control value: * $p < 0.05$, ** $p < 0.01$, and *** $p < 0.001$.

The cumulative excretion of (S)-IBP in the extracts of the bile samples of control and hyperglycemic rats is shown in Figure 49. The cumulative excretion of the IBP enantiomer was statistically lower in the hyperglycemic rats.

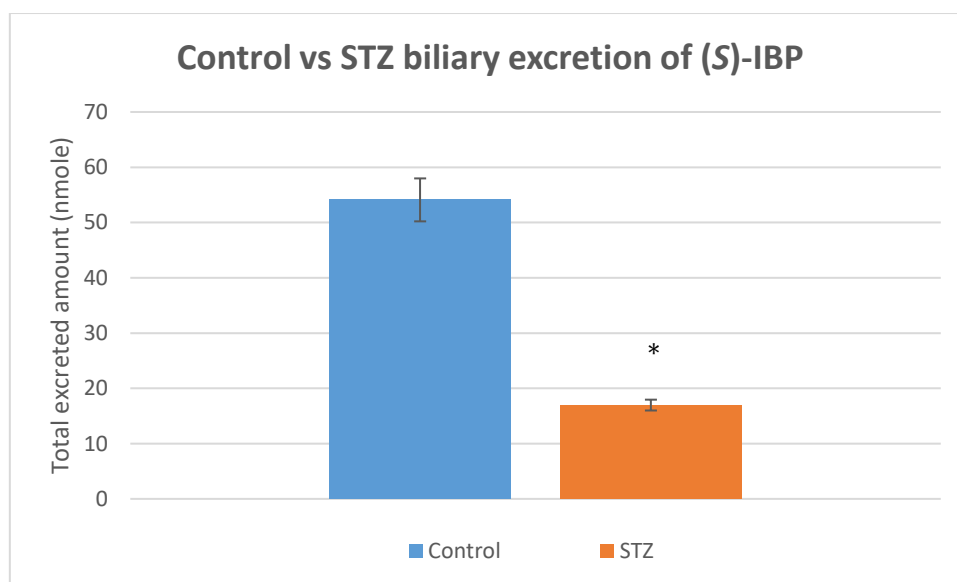


Figure 49. The cumulative excretion of (S)-IBP enantiomer in the extracts of the bile samples of control and hyperglycemic rats ($n=4$). Significant differences from the control value: * $p < 0.01$.

6. Discussion

Several investigators have studied the effect of diabetes on human whole-body protein metabolism in humans. These studies demonstrated increased protein breakdown as well as improved protein synthesis. Net protein catabolism occurs in T1DM patients during insulin deprivation because protein breakdown is more significant than protein synthesis (129). According to these previous observations, the present results showed that the protein content of the small intestine and the kidney were reduced under the hyperglycemic condition. On the contrary, no such degree of reduction in the protein content in the liver was observed (Figure 11). This latter observation can be explained by the major role of the liver in synthesizing proteins.

Proteins are one of the endogenous targets of oxidative stress. Available cysteine residues can easily form disulfide derivatives with the thiol functions of other proteins or glutathione (GSH). GSH can also be oxidized to the respective disulfide (GSSG) in reaction with various endogenous and exogenous oxidizing agents. Lysine and proline residues are the most important precursors of protein carbonylation by the oxidative formation of aldehydic derivatives (130). The most common method to analyze these latter derivatives is their reaction with 2,4-dinitrophenylhydrazine (DNPH). The resulting hydrazones (prot-DNPH) can be quantified by spectroscopic, immunological, or mass spectrometric techniques.

UV-Vis determination of carbonyl content of proteins by the DNPH method indicated increased protein oxidation at each timepoint in each organ (Figure 12). The kidney seemed the least sensitive to protein oxidation at each timepoint. Such resistance of proteins can be explained by the high turnover of the antioxidant amino acids, such as lysine, proline, and cysteinyl-glycine (131). The time dependence of the protein-content-based amount of the DNPH-reactive protein carbonyls showed some characteristic differences: 1. In the liver and the small intestine, the highest amounts could be detected at the two-weeks timepoint. The initial increase slightly dropped by the end of the fourth week. 2. In the kidney, contrary to the other two organs, the level of the oxidized protein content slightly and continuously increased. Our previous metabolic studies were performed after one week of the STZ treatment of the experimental animals (113-115, 132, 133). The data indicate a substantial increase of the protein oxidation products in the liver (35.7%) and the small intestine (80.7%) at this timepoint (Figure 12).

Peroxidative degradation of membrane lipids is another consequence of oxidative stress. It is initiated by (a) free radical species such as peroxy radicals, hydroxyl radicals, and metal-oxyl radicals derived from the iron-mediated reduction of hydrogen peroxide or (b) non-radical species such as singlet oxygen, ozone, and peroxynitrite generated by the reaction of superoxide with nitric oxide (134). The most prevalent radical species that can profoundly affect lipids are mainly hydroxyl radicals ($\bullet\text{OH}$). Radical initiators can abstract a hydrogen atom from the allylic position of polyunsaturated fatty acids. As a result, lipid hydroperoxides (LOOHs) - as primary oxidation products - are formed, and simultaneous rearrangement of the neighboring (non-conjugated) double bonds results in a conjugated diene moiety. Conjugated dienes have characteristic UV absorption around 230 nm (135).

Lipid hydroperoxides, like hydrogen-peroxide, are mild oxidative agents; however, they can be reduced to the respective alcohols (134). These primary lipid oxidation products can also undergo several decomposition pathways, resulting in - among others - an endogenous level of malondialdehyde (MDA). The endogenous MDA can be involved in enzymatic oxidation, reduction, addition, and condensation with cellular nucleophiles (47, 136, 137). One of the most frequently used methods to measure a tissue sample's lipid-derived total carbonyl content is the thiobarbituric acid (TBA) test. However, most of the MDA measured with the TBA test is formed from the more stable fatty acid hydroperoxides under the strong acid test conditions (138). Besides MDA, TBA also forms colored adducts with other compounds, including sugars, amino acids, and other aldehydic lipid oxidation products; this leads to the overestimation of MDA by the TBA test (138, 139). Thus, the results of this test are appropriately reported as thiobarbituric acid-reactive substances (TBARS) rather than MDA (140).

As Figure 13 shows - similar to the protein oxidation, it was the liver and the small intestine where the highest conjugated diene-level elevations in the STZ-treated animals were observed at the two-week timepoint. The small intestine proved to be the most sensitive organ showing a 55.3%, 160.5%, and 136.8% increase in the conjugated diene level at the one, two, and four-week timepoints, respectively. The highest elevation in the liver and kidney could be obtained in the four-week samples (Figure 13).

Comparing the increase of the conjugated dienes (Figure 13) to that of the respective TBARS levels (Figure 14) showed a relatively lower increase in the TBARS levels. At the first week timepoint, increased MDA levels could be observed in the liver and the kidney but not in the small intestine. The moderately increased levels can be explained by the effective elimination of the formed lipid hydroperoxides by catalase (in liver and kidney), and selenium-

dependent GSH-peroxidase (GPX2) (gastrointestinal system) (141), and the high reactivity of MDA with the endogenous lysine and arginine units (142). In the later timepoints, however, the oxidative stress caused by the high glucose levels can also contribute to the formation of oxidized lipids, resulting in increased MDA levels (3).

Furthermore, it is reasonable to presume that the continuous food cysteine supply (2800 mg/kg) provides enough reducing (thiol) equivalent to convert a part of the conjugated lipid-hydroperoxides to the respective alcohols (41). These latter derivatives increase the conjugated diene level but can't be converted to MDA. In agreement with this explanation, the intestinal non-protein thiol level increased in the highest ratios in the small intestine over the four-week experiment (Figure 15). Like the conjugated diene level, the highest TBARS level in the kidney could be observed at the four-week timepoint.

Non-protein thiols (NPSH) are one of the most potent cellular antioxidants. . Glutathione (GSH) is the most widespread low-molecular-weight antioxidant in the liver and kidney. The NPSH level declined after the one-week STZ treatment in the liver but not in the small intestine and the kidney (Figure 15). The reduction of NPSH levels in the liver can be associated with the high glutathione level and glutathione peroxidase (GPx) activity in this organ (143). Thus, the major portion of the decline in the hepatic NPSH level is due to the GSH-dependent detoxification of the reactive oxygen species (ROS). The initial drop in the NPSH level increased by the end of the second week through a negative feedback mechanism. After this characteristic increase, however, the hepatic GSH level dropped below the control (4th week), probably due to dysregulation of GSH synthesis by the chronic hyperglycemia (144). A similar decline was not observed either in the small intestine or the kidney. These observations can be explained by the different GSH levels and GPx activity in these two organs. The kidneys are characterized by a lower GSH concentration than the liver and the highest level of cysteine (CYS) among all body tissues (145). The kidneys' NPSH level depends highly on an adequate supply of glutathione (GSH) to maintain normal function (146). Thus, the elimination of ROS can not be effectively catalyzed by the GSH/GPx pathway in this organ.

In contrast to the liver, the intestine has extremely low GSH peroxidase activity (143). Thus, this organ has a limited capability to utilize non-protein thiols to protect against oxidative toxicity. Furthermore, the NPSH level was higher than the control over the investigation period. This observation can be explained by the continuous food methionine supply.

Phenylalanine (Phe) is an essential amino acid, which is, among others, converted to *p*-Tyr in an enzyme-catalyzed reaction. The nucleophilic aromatic ring can react with hydroxyl radicals in an addition reaction, and the primary adducts are stabilized as *o*-, *m*-, and *p*-hydroxylated phenylalanines (*o*-Tyr, *m*-Tyr, and *p*-Tyr) (147). Accordingly, *o*- and *m*-Tyr are specific, stable hydroxyl radical markers (148). As shown in Figure 16, the *o*-Tyr+*m*-Tyr/*p*-Tyr (or the *o*-Tyr+*m*-Tyr/Phe) ratios slightly decreased at the one-week timepoint of the STZ treatment. Similar to the Prot-DNPH (Figure 12) and the TBARS levels (Figure 14), the ratios substantially increased in all three organs at the two-week timepoint. A similar tendency of the three parameters could be observed at the four-week timepoint: while the values were somewhat reduced in the liver and the small intestine, they further increased in the kidney. The observations give further experimental evidence of the usefulness of the three parameters to characterize the oxidative state of the investigated organs.

Diabetic patients are at all time at risk of complications. Complications may be macrovascular (coronary heart disease, peripheral vascular disease, and stroke), microvascular (neuropathy, retinopathy, and nephropathy), and both micro- and macro-vascular (diabetic foot). It is believed that oxidative stress plays an important role in the development of these vascular complications (149). Concerning oxidative stress-induced nephropathy, the present data support this theory. The oxidized protein (Figure 12), conjugated dienes (Figure 13), TBARS level (Figure 14), and the *o*-Tyr+*m*-Tyr/*p*-Tyr ratio (Figure 16) steadily increased. On the contrary, the renal GSH didn't show a significant difference over time (Figure 16). Alterations in renal mitochondrial GSH status appear to be associated with chronic hyperglycemia, although the underlying mechanism for these changes has not been established (149). Earlier, Lash et al. reported significantly higher mitochondrial GSH contents in the kidneys of diabetic rats compared with those of control rats. On the other hand, primary cultures of renal proximal tubular cells from STZ-treated diabetic rats exhibited higher levels of reactive oxygen species and were more sensitive to oxidant-induced injury than cells from control rats (150). The authors interpreted these findings that the compensatory increases in mitochondrial GSH transport and content are insufficient to counteract the oxidative stress induced by the chronic hyperglycemic state (151).

Since the liver is the main site of enzymatic drug (xenobiotic) metabolism, the observed changes in this organ need special attention. The reduced protein (Figure 11) and GSH content (Figure 15), the increased protein oxidation (Figure 12), conjugated diene (Figure 13), and TBARS (Figure 14) levels are in accordance with the oxidative stress developing in this organ

by the end of the first week after the STZ treatment. The results are in agreement with our previous experimental findings demonstrating decreased expression of the efflux transporters Mdr1 (P-gp), Mrp2, and Bcrp in the liver of the STZ-treated (hyperglycemic) animals (115).

On the contrary, aromatic (Phe) hydroxylation was reduced at the one-week timepoint. It suggests that the lipids (152) and the proteins (153) are more vulnerable to hydroxyl radical attack than the aromatic rings. This might be the reason (at least in part) for the lack of biliary detection of hydroxylated ibuprofen metabolites formed in non-CYP-catalyzed reactions (133).

Ibuprofen (IBP) undergoes extensive Phase I and Phase II biotransformation to the main metabolites 1-OH-IBP (**2**), 2-OH-IBP (**3**), HOOC-IBP (**5**), and IBU-GLU (**6**) (84, 85, 88). In humans, the CYP2C9 isoform plays the most important role in the oxidative metabolism of IBP, mediating the 2- and 3-hydroxylations and the subsequent 3-oxidation in the liver (86, 154). Additional CYPs, particularly CYP2C8, may also play a role in these biotransformations (87, 154). The enzyme responsible for 1-OH-IBP (**2**) formation has not been identified (155, 156).

The most abundant CYP2C isoform in rats is CYP2C11, whereas the other isoforms were present at much lower levels. The human CYP2C9 and CYP2C8 proteins are orthologous to the rat CYP2C12 and CYP2C11 (157). After oral administration, IBP appeared mainly in unchanged form in the plasma of rats. In addition, two metabolites, 2-OH-IBP (**3**) and HOOC-IBP (**5**), were found in the plasma and the urine (158). Yamazoe et al. studied the effect of alloxan and STZ on the expression of hepatic CYP enzymes in rats. In most cases, the expression of the CYP proteins was either not affected or depressed (159). Later, Shimojo reviewed the effects of hyperglycemia on rat hepatic CYP expressions. According to the reviewed publications, the amount of CYP2C11 and CYP2C13 was suppressed, while CYP2C12 did not change or somewhat increased (74). Recently, Yang and Liu reviewed the effect of diabetes on the drug transporter-CYP interplays. They referred to further studies demonstrating lowered expression of hepatic CYP2C11 in diabetic rats (160). Accordingly, decreased levels of hydroxylated IBP metabolites formed in CYP-catalyzed reactions can be rationalized.

During inflammation, for example, stimulated polymorphonuclear leukocytes (PMN) and macrophages produce large amounts of superoxide ions and hydrogen peroxide (161). There are many examples of exogenous H₂O₂ initiating redox signals or stress responses. Furthermore, receptor-mediated redox signaling is widely regarded as involving endogenously

generated H_2O_2 (161, 162). On the other hand, many of the biologically damaging effects of H_2O_2 depend on transition metals such as iron and copper, which cleave the peroxide bond to generate hydroxyl radicals or activated metal complexes (163). Hydroxyl radicals are powerful electrophilic reactants that can oxidize endogenous or exogenous molecules. Therefore, the importance of non-enzymatic oxidation can be particularly significant at the sites of inflammation (164).

To model non-enzymatic oxidation, oxidation products of IBP formed under the conditions of the Fenton reaction (36) and Udenfriend's oxidation (127, 128) were investigated by HPLC-UV and HPLC-MS methods. Fenton reaction is a tool for modeling oxidative stress by forming hydroxyl radicals in a reaction of hydrogen peroxide and some transitional metals. The key features of the reaction are believed to be the reaction conditions, such as reagent concentrations, pH, and temperature (165). Earlier, these reactions were applied to study the oxidative transformation of salicylates (111, 112).

Fenton oxidation of IBP resulted in the formation of several products. Among them, 1-OH-IBP (**2**), 2-OH-IBP (**3**), and HOOC-IBP (**5**) were identified by HPLC-UV and HPLC-MS. Among these products, 1-OH-IBP (**2**) was found in the largest amount (Figure 22). Besides, a small amount of a dihydroxyibuprofen ($t_{\text{R}}=8.91$ min) (**10**) and a significant amount of a new hydroxyl-substituted derivative ($t_{\text{R}}=9.24$ min) (**8**) were found. Hydroxyl radicals have been reported to react with IBP to form 1-OH- (**2**), 2'-OH-, and OH(Ar)-IBP derivatives (166). Based on the HPLC retention time ($t_{\text{R}}=9.24$ min), the new hydroxyl-derivative could be the 2'-OH-IBP or an OH(Ar)-IBP . As shown in Figure 23B, the main fragment ion ($\text{C}_{12}\text{H}_{17}\text{O}$; m/z 177.1251) is formed by CO_2 loss of the hydroxylated IBP derivative (m/z 221.1175). The CO_2 loss occurs already in the ionization source (Figure 23A). The other main decomposition peak (m/z 119.0472) corresponds to a $\text{C}_8\text{H}_7\text{O}$ (vinyl phenol or acetophenone; exact mass: m/z 119.0497, mass error: -21.0 ppm) fragment (167). Although the m/z 149.0576 peak can be assigned as a $\text{C}_9\text{H}_9\text{O}_2$ fragment (exact mass m/z 149.0603; mass error: -18.1 ppm), the exact structure of the formed product can not be unambiguously determined. Since H-abstraction is thermodynamically more favored than $\bullet\text{O.H.}$ addition, and its reaction rate is an order of magnitude higher (168, 169), the new hydroxylated product was tentatively identified as the 2'-OH-IBP (Figure 23A and 23B). Further investigations are to be performed to prove the results of the theoretical calculations experimentally. 1,2-Dihydroxyibuprofen was reported to form in the biodegradation of IBP (170).

Udenfriend et al. described a system consisting of EDTA, ascorbic acid, molecular oxygen, and iron(II) ion, which would serve as a model of the biomimetic hydroxylation of organic substrates (127, 128). Ito et al. demonstrated that the reactive species are hydroxyl radicals (trapped by different aliphatic alcohols) in both the Fenton's and the Udenfriend's reagents (171). Udenfriend's oxidation of IBP resulted in the formation of products similar to those formed in the Fenton's incubations (Figure 26). Based on this observation, it is reasonable to presume that the reactive species are the same in both reactions. The above results indicate that *in vivo* Fentone-type (165, 172) or Udenfriend type (173) non-enzymatic hydroxylation of IBP – based on measurement of **8** and/or **9** - can be used as an early sign of oxidative stress conditions.

While analyzing the 250 μ M ibuprofen containing intestinal perfusates of control and STZ-treated hyperglycaemic rats, none of the oxidative metabolites (formed in CYP-catalyzed or non-CYP-catalyzed reactions) of IBP (**1**) could be detected by HPLC-UV or HPLC-MS. Contrary to the previous (115) (and the present) HPLC-UV measurements, IBP-GLU (**6**) conjugate could be detected and identified in the perfusates by HPLC-MS. This result indicates the formation of **6** in the rat's small intestine, which couldn't be detected by the less sensitive UV detection.

HPLC-UV analysis of the collected bile samples showed the presence of IBP (**1**), IBP-GLU (**6**), and 2-OH-IBP (**3**). HPLC-MS analysis of the bile samples of both the control and the hyperglycemic group of animals confirmed the presence of the three compounds. According to our previous results (115), excretion of both **1** and **6** into the bile decreased in experimental diabetes. Similarly, biliary excretion of **3** was also reduced in the hyperglycemic rats (Figure 33). In our earlier experiments, the biliary excretion of 4-nitrophenol and its glucuronic acid and sulfate conjugates were significantly decreased in diabetic rats (114).

Besides the above, the glucuronide conjugate of a hydroxylated IBP (**9**) and the taurine conjugate of IBP (**7**) could also be identified by HPLC-MS (Figures 36 and 37). Earlier, Shirley et al. reported on the formation of IBP-CoA and IBP-TAU (**7**) in *in vitro* incubations using rat hepatocytes (91). Like those results, HPLC-MS analysis of our bile samples indicated the presence of IBP-TAU (**7**) but not that of the glycine conjugate (IBP-GLY). To the best of our knowledge, this is the first *in vivo* observation of the excretion of IBP-TAU into the bile.

The excreted amounts of **9** and **7** were significantly lower in the STZ-treated rats' bile samples. Although the bile outflow was slightly increased in the STZ-treated animals over the studied period, a comparison of the relative amounts of the excreted **9** and **7** (based on the

HPLC-MS data) indicated reduced excretion of IBP-TAU in the STZ-treated animals (Figure 39). Depression of biliary excretion of IBP-TAU can be explained by the earlier results related to the reduced biliary excretion of IBP and IBP-GLU in hyperglycemic rats (174-176). Hasegawa et al. reported that the hepatic expression of the efflux transporter MRP2 is decreased in the STZ-treated rats (175). Similarly, expression of the efflux transporter P-gp (MDR1) was reduced in hyperglycemia (174, 176, 177). In agreement with these earlier results, our molecular biology studies on liver samples of the STZ-treated rats showed decreased expression of the efflux transporters P-gp (MDR1B), MRP2, and BCRP (115). These transporters are involved in exporting organic anions from the hepatocytes into the bile canaliculus (178). Furthermore, hyperglycemia is also associated with a decline in the levels of endogenous antioxidant taurine in several tissues (179, 180).

As shown in Figures 45A and 45B, the concentration of the two IBP enantiomers was continuously decreased in the intestinal perfusion medium over the experiments. (In the samples collected between the 105 to 150 min timepoints, IBP peaks could not be quantified.) Legen et al. demonstrated that the inwardly directed proton gradient could be a driving force for transporting monocarboxylic acid-type drugs (among them IBP) across the intestinal epithelia (181). The passive diffusion of the compound can explain the gradual decrease of concentration of the ibuprofen enantiomers in the perfusate.

Cumulative disappearance (absorption, metabolism, and excretion) of both enantiomers of IBU was lower in the hyperglycemic rats (Figure 44). The ratio of the enantiomers showed a moderate increase in the control rats; however, the change was statistically insignificant (Figure 45). Several reports have demonstrated that diabetes may decrease P-gp (MDR1) efflux transporter function and expression in the brain and intestine (176, 177, 182, 183). In addition, curcumin and ibuprofen were reported to inhibit the P-gp activity of human sarcoma MES-SA/Dx-5 cells well below their therapeutic plasma concentrations (184). P-gp effluxes drug substrates from enterocytes into the GI lumen, thus regulating the intestinal absorption of drugs. Accordingly, the observed alteration can be explained by the reduced activity of P-gp due to the experimental hyperglycemia and the accumulating ibuprofen in the endothelial cells. The progressively increasing cellular IBP level attenuates the concentration gradient, considered the most important factor in the entrance of ibuprofen (84).

In the bile samples, only the (*S*)-ibuprofen enantiomer could be detected (Figures 46 and 47). Figures 48 and 49 show that the excreted amount of (*S*)-IBP is statistically lower in the bile samples of the hyperglycemic rats. Uptake transporters are expressed highly on

the basolateral membrane of hepatocytes (185, 186). The organic anion transporters hOAT1-5 are predominantly expressed in renal proximal tubules; however, hOAT2 (Slc22a7) is also expressed in the liver (187-189). In the rat, the main site of expression of Oat2 is the sinusoidal membrane domain of the hepatocytes (190). Kimoto et al. evaluated the role of organic anion transporter 2 (OAT2)-mediated hepatic uptake in the clearance of 25 ECCS 1A drugs. The authors provided evidence for the role of OAT2-mediated hepatic uptake of most of the investigated ECCS 1A drugs, including IBP (191). Members of the organic anion transporting polypeptide (OATP) family are also important determinants of hepatic uptake of endogenous and exogenous compounds. Kindla et al. reported that only diclofenac was significantly transported by OATP1B3, whereas all other NSAIDs investigated (including IBP) were not substrates for these uptake transporters (192). Accordingly, ibuprofen is supposed to enter the hepatocytes by passive diffusion and OATP2-mediated uptake (83, 84, 191).

Schneider et al. investigated the biliary elimination of ibuprofen, indomethacin, and diclofenac in patients suffering from obstructions of the common bile duct. Whereas a very low amount (0.15%) of ibuprofen was excreted in bile as unchanged drug and active conjugates, biliary elimination of diclofenac was somewhat higher (1.09%), and that of indomethacin was substantial (above 10%) (193). Like the small intestine, the P-gp efflux transporter (Mdr1) is also expressed in the apical side of the rat hepatocytes (186). P-gp has been reported to be reduced in hyperglycemic rats (174, 176, 177). Using the present experimental protocol, we found a relatively low amount of (non-enantiomer-separated) IBP and IBP-glucuronide in the bile, which was depressed under hyperglycemic conditions. Our molecular biology studies on liver samples of the STZ-treated rats showed decreased expression of the efflux transporters P-gp (Mdr1B), Mrp2, and Bcrp (115). These transporters are involved in exporting organic anions from the hepatocytes into the bile canaliculus (178).

Biliary excretion of the parent compounds and their metabolites is crucial for the so-called enterohepatic circulation of the drugs and other xenobiotics (194). Drugs in bile are usually more concentrated than in plasma, and passive transport is considered negligible. Accordingly, biliary excretion represents an active process involving transporters embedded in the apical membrane of hepatocytes. Furthermore, the liver was the most important organ in the unidirectional conversion of (*R*)-arylpropionic acid drugs to their (*S*) enantiomer. Whether the asymmetric appearance of the IBP enantiomers is the consequence of the OAT2-mediated enantioselective hepatic uptake or the enantioselective excretion of the hepatic efflux transporters P-gp (Mdr1B), Mrp2, and Bcrp (or both) needs further molecular biology studies.

7. Conclusion

This study investigated the oxidative transformation of lipids, proteins, non-protein thiols (NPSH), and phenylalanine (Phe) in the liver, small intestine, and kidney in STZ-treated rats at the one-, two-, and four-week timepoints after the STZ-administration. The MDA, Prot-DNPH, and the *o*-Tyr + *m*-Tyr levels followed a similar pattern: the highest values were recorded after two weeks of the STZ treatment. The compensation of oxidative stress is parallel with the change in the NPSH content of the organs. Such compensation is the least effective in the kidney, where the above three parameters continuously increase over the time of investigations. Accordingly, this organ is the most vulnerable to the hyperglycemia-induced oxidative stress.

The results indicate that reactions of hydroxyl radicals (ROS) with the aromatic ring of Phe are less favored than those with sensitive amino acid/protein and lipid molecules. This observation could be one of the reasons they are only limited data on increased non-enzyme catalyzed oxidized/hydroxylated aromatic xenobiotics under the present experimental conditions. However, modulation (mostly depression) of enzyme and transporter activities (oxidative stress-induced damage of proteins/lipids) is well documented in the literature.(146, 152, 153).

The present results show that one of the main hydroxylated IBP-derivatives formed in the non-enzyme-catalyzed oxidation reactions (Fenton-test and Udenfriend's test) is a hydroxylated IBP (**8**). Since the formation of neither 2'-OH-IBP nor OH(Ar)-IBP (**8**) – the possible structures of the product - hasn't been reported in CYP-catalyzed reactions, the formation of this derivative might be used as a biomarker of oxidative stress in living organisms.

Contrary to 4-nitrophenol (114) and capsaicin (195) - both are phenolic derivatives - the glucuronide conjugate of ibuprofen could be detected only in a trace amount in the small intestinal perfusates. On the other hand, IBP (**1**), IBP-GLU (**6**), and IBP-TAU (**7**) were excreted in the bile. However, no specific non-enzymatic hydroxylation product could be detected. The results agree with the previous experimental findings demonstrating decreased expression of the organic anion transporters P-gp (MDR1), MRP2, and BCRP in the liver of the STZ-treated (hyperglycemic) animals. Such changes impact the pharmacokinetics of drugs administered in hyperglycemic individuals.

The chromatographic study using a chiral column provided experimental data on intestinal elimination and hepatic excretion of the IBP enantiomers in control and hyperglycemic experimental animals. The results demonstrated that the elimination of IBP from the small intestine is not enantioselective. Analysis of the bile showed the presence of only the pharmacologically more active (*S*)-IBP enantiomer. Since the pharmacological activity of (*S*)-IBP is one order of magnitude higher than that of the (*R*)-IBP (97), the asymmetric appearance of the enantiomers in the bile could determine the pharmacokinetics and pharmacodynamic action of the drug.

8. Publication and presentation

Number of publications related to the subject of the thesis: 4

Number of publications not related to the subject of the thesis: 3

Number of oral and poster presentations related to the subject: 3

Sum of impact factors from publications related to the topic of Ph.D. thesis: 4.927

Publications related to the topic of the Ph.D. thesis:

- Perjési, P. Perez, C. Napolitano, H. **Mohammed, HO**. 2019. Physiochemical Characterization of Glutathione (GSH). In: Perjési, P. (ed.) *Glutathione: Biosynthesis, Functions and Biological Implications*. New York: Nova Science Publisher. pp 3-53.
- **Mohammed, HO**. Almási, A. Molnár, S. Perjési, P. The intestinal and biliary metabolites of ibuprofen in the rat with experimental hyperglycemia. *Molecules*. 27 (13), 4000 (2022). doi: 10.3390/molecules27134000.
- **Mohammed, HO**. Almasi, A. Perjesi, P. Effect of experimental hyperglycemia on intestinal elimination and biliary excretion of ibuprofen enantiomers in hyperglycemic rats. (Submitted, under review).
- **Mohammed, HO**. Almási, A. Kun, Sz., Wittmann I., Perjesi, P. Study on oxidative transformations of endogenous lipids, proteins, and amino acids in hyperglycemic rats. Preference of oxidation of non-aromatic sites. (Submitted, under review).

Other publications not related to the topic of the Ph.D. thesis:

- Ali, KN, Marif, HF, Kakarash, NA, **Mohammed, HO**. Liverfluke Coprological Cross-Sectional Survey in Cattle, Sheep and Goats in Sharazur District Kurdistan-Iraq. Al-Anbar J Vet Sci. 14 (1), (2021).
- Hardi FM, Rashid ZM, **Mohammed HO**, Dyary HO. Resistance of Fasciola hepatica to triclabendazole, closantel, and rafoxanide in a sheep farm in Sharazor district, Kurdistan-Iraq. Basrah J Vet Res.18 (2), 16-26 (2019).
- Rahman HS, **Mohammed HO**, Fattah H, Othman HH, Amin KM and Abdullah R (2019). Phytochemical analysis and augmentation of pulmonary adenocarcinoma in BALB/c mice model treated with flaxseed oil. Front Pharmacol. Conference Abstract: International Conference on Drug Discovery and Translational Medicine 2018 (ICDDTM '18) “Seizing Opportunities and Addressing Challenges of Precision Medicine.” doi: 10.3389/conf.fphar.2018.63.00110. (Conference paper).

Oral and poster presentations:

- **Mohammed, HO**. Almasi, A. Molnar, S. Perjesi, P. Oxidative transformations of lipids and ibuprofen in hyperglycemic rats. XVI Congress Pharmaceuticus Hungaricus (CPH 2020) at the University of Debrecen (2020). “Poster”
- **Mohammed, HO**. Almasi, A. Molnar, S. Perjesi, P. Oxidative transformations of lipids and ibuprofen in hyperglycemic rats. 9th Medical Conference for Ph.D. Students and Experts of Clinical Sciences (MEDPE CS2019) at the University of Pecs (2019). “Poster”
- **Mohammed, HO**. Almasi, A. Molnar, S. Perjesi, P. A study of the incidence of lipid peroxidation in liver and small intestine of hyperglycemic rats by HPLC, LC-MS and UV-VIS analysis. 8th International Doctoral Conference (IDK 2019) at the University of Pecs (2019). “Oral presentation”

9. Acknowledgments

Praise be to God, who delivered me to this day to complete my Ph.D. thesis.

First and foremost, I would like to express my deepest gratitude to my supervisor Prof. Dr. Pal Perjesi, for the guidance, advice, support, and all his efforts with me throughout my study to make it successful.

I would like to thank Dr. Almasi Attila for his support and assistance, especially in the animal experiments, and I would like to thank Szilard Molnar for his advice and efforts in measuring project samples by the LC-MS device.

I would like to thank Dr. Zsuzsanna Rozmer, the head of the Institute of Pharmaceutical Chemistry, for her continued support, and special thanks to all my colleagues at the institute for their support, kindness, and friendship with me.

Thanks to the Tempus Public Foundation “Stipendium Hungaricum Scholarship program” for granting me the duration of my Ph.D. study.

Thanks to the Faculty of Pharmacy at the University of Pecs, especially the Dean, Dr. Lajos Botz, and the Vice Dean, Dr. Györgyi Horváth, for supporting me in completing my Ph.D. study.

Thanks to the Ministry of Higher Education and Scientific Research of the Kurdistan Region of Iraq and the College of Veterinary Medicine at the University of Sulaimani for their support and for giving me the opportunity to study for a Ph.D. abroad.

I cannot be grateful enough to my wife “Banw” and my daughter “Shanar” for their love, support, and standing by my side throughout my stay in Hungary. Finally, I would like to thank my parents, brothers, and sisters for their continued support of all kinds.

10. References

1. Saeedi P, Petersohn I, Salpea P, Malanda B, Karuranga S, Unwin N, et al. Global and regional diabetes prevalence estimates for 2019 and projections for 2030 and 2045: Results from the International Diabetes Federation Diabetes Atlas, 9(th) edition. *Diabetes Res Clin Pract.* 2019;157:107843. doi: 10.1016/j.diabres.2019.107843.
2. Volpe CMO, Villar-Delfino PH, Dos Anjos PMF, Nogueira-Machado JA. Cellular death, reactive oxygen species (ROS) and diabetic complications. *Cell Death Dis.* 2018;9(2):119. doi: 10.1038/s41419-017-0135-z.
3. Davi G, Falco A, Patrono C. Lipid peroxidation in diabetes mellitus. *Antioxid Redox Signal.* 2005;7(1-2):256-68. doi: 10.1089/ars.2005.7.256.
4. Giacco F, Brownlee M. Oxidative stress and diabetic complications. *Circulation research.* 2010;107(9):1058-70. doi: 10.1161/circresaha.110.223545.
5. Gwilt PR, Nahhas RR, Tracewell WG. The effects of diabetes mellitus on pharmacokinetics and pharmacodynamics in humans. *Clin Pharmacokinet.* 1991;20(6):477-90. doi: 10.2165/00003088-199120060-00004.
6. Dostalek M, Akhlaghi F, Puzanovova M. Effect of diabetes mellitus on pharmacokinetic and pharmacodynamic properties of drugs. *Clin Pharmacokinet.* 2012;51(8):481-99. doi: 10.2165/11631900-000000000-00000.
7. Michael Tran FE. Influence of diabetes mellitus on pharmacokinetics of drugs. *MOJ Bioequivalence & Bioavailability.* 2016;2(1):3-4. doi: 10.15406/mojbb.2016.02.00016.
8. Preston RA, Epstein M. Effects of diabetes on cardiovascular drug metabolism. Emerging clinical implications. *Diabetes Care.* 1999;22(6):982-8. doi: 10.2337/diacare.22.6.982.
9. Betteridge DJ. What is oxidative stress? *Metab Clin Exp.* 2000;49(2 Suppl 1):3-8. doi: 10.1016/s0026-0495(00)80077-3.
10. Phaniendra A, Jestadi DB, Periyasamy L. Free radicals: properties, sources, targets, and their implication in various diseases. *Indian J Clin Biochem.* 2015;30(1):11-26. doi: 10.1007/s12291-014-0446-0.
11. Drews G, Krippeit-Drews P, Düfer M. Oxidative stress and beta-cell dysfunction. *Pflug Arch Eur J Physiol.* 2010;460(4):703-18. doi: 10.1007/s00424-010-0862-9.
12. Tejedo J, Bernabé JC, Ramírez R, Sobrino F, Bedoya FJ. NO induces a cGMP-independent release of cytochrome c from mitochondria which precedes caspase 3 activation in insulin producing RINm5F cells. *FEBS lett.* 1999;459(2):238-43. doi: 10.1016/s0014-5793(99)01255-7.
13. Kaur H, Hippargi G, Pophali GR, Bansiwali AK. 6 - Treatment methods for removal of pharmaceuticals and personal care products from domestic wastewater. In: Prasad MNV, Vithanage M, Kapley A, editors. *Pharmaceuticals and Personal Care Products: Waste Management and Treatment Technology*: Butterworth-Heinemann; 2019. p. 129-50. URL: <https://www.sciencedirect.com/science/article/pii/B9780128161890000068>.
14. Kayama Y, Raaz U, Jagger A, Adam M, Schellinger IN, Sakamoto M, et al. Diabetic Cardiovascular Disease Induced by Oxidative Stress. *Int J Mol Sci.* 2015;16(10):25234-63. doi: 10.3390/ijms161025234.
15. Jaganjac M, Tirosh O, Cohen G, Sasson S, Zarkovic N. Reactive aldehydes--second messengers of free radicals in diabetes mellitus. *Free Radic Res.* 2013;47 Suppl 1:39-48. doi: 10.3109/10715762.2013.789136.
16. Fernández-Mejía M-LL-d-l-V-MaC. Oxidative Stress in Diabetes Mellitus and the Role Of Vitamins with Antioxidant Actions. In: Morales-González JA, editor. *Oxidative Stress and Chronic Degenerative Diseases - A Role for Antioxidants*. London: IntechOpen; 2013. URL: <https://www.intechopen.com/chapters/39159>.

17. Szkudelski T. The mechanism of alloxan and streptozotocin action in B cells of the rat pancreas. *Physiol Res.* 2001;50(6):537-46. URL: http://www.biomed.cas.cz/physiolres/pdf/50/50_537.pdf.
18. Goyal SN, Reddy NM, Patil KR, Nakhate KT, Ojha S, Patil CR, et al. Challenges and issues with streptozotocin-induced diabetes - A clinically relevant animal model to understand the diabetes pathogenesis and evaluate therapeutics. *Chem-Biol Interact.* 2016;244:49-63. doi: 10.1016/j.cbi.2015.11.032.
19. Johansson EB, Tjalve H. Studies on the tissue-disposition and fate of [14C]streptozotocin with special reference to the pancreatic islets. *Acta Endocrinol.* 1978;89(2):339-51. doi: 10.1530/acta.0.0890339.
20. Lenzen S. The mechanisms of alloxan- and streptozotocin-induced diabetes. *Diabetologia.* 2008;51(2):216-26. doi: 10.1007/s00125-007-0886-7.
21. Karunanayake EH, Hearse DJ, Mellows G. The synthesis of [14C] streptozotocin and its distribution and excretion in the rat. *The Biochemical journal.* 1974;142(3):673-83. doi: 10.1042/bj1420673.
22. Wu J, Yan LJ. Streptozotocin-induced type 1 diabetes in rodents as a model for studying mitochondrial mechanisms of diabetic β cell glucotoxicity. *Diabetes Metab Syndr Obes : Targets Ther.* 2015;8:181-8. doi: 10.2147/dmso.s82272.
23. Ahmed R. The Physiological and Biochemical Effects of Diabetes on the Balance between Oxidative Stress and Antioxidant Defense System. *J Islamic Acad Sci.* 2005;15(1):31-42. doi, <https://ssrn.com/abstract=3017953>.
24. Herb M, Glusko A, Schramm M. Reactive Oxygen Species: Not Omnipresent but Important in Many Locations. *Front Cell Dev Biol.* 2021;9:716406. doi: 10.3389/fcell.2021.716406.
25. Mahadev K, Zilbering A, Zhu L, Goldstein BJ. Insulin-stimulated hydrogen peroxide reversibly inhibits protein-tyrosine phosphatase 1b in vivo and enhances the early insulin action cascade. *J Biol Chem.* 2001;276(24):21938-42. doi: 10.1074/jbc.C100109200.
26. Pomytkin IA. H₂O₂ Signalling Pathway: A Possible Bridge between Insulin Receptor and Mitochondria. *Curr Neuropharmacol.* 2012;10(4):311-20. doi: 10.2174/157015912804143559.
27. Jiang ZY, Woollard AC, Wolff SP. Hydrogen peroxide production during experimental protein glycation. *FEBS letters.* 1990;268(1):69-71. doi: 10.1016/0014-5793(90)80974-n.
28. Wolff SP, Dean RT. Glucose autooxidation and protein modification. The potential role of 'autooxidative glycosylation' in diabetes. *Biochem J.* 1987;245(1):243-50. doi: 10.1042/bj2450243.
29. Maritim AC, Sanders RA, Watkins III JB. Diabetes, oxidative stress, and antioxidants: A review. *J Biochem Mol Toxicol.* 2003;17(1):24-38. doi: <https://doi.org/10.1002/jbt.10058>.
30. Singh PP, Mahadi F, Roy A, Sharma P. Reactive oxygen species, reactive nitrogen species and antioxidants in etiopathogenesis of diabetes mellitus type-2. *Indian J Clin Biochem.* 2009;24(4):324-42. doi: 10.1007/s12291-009-0062-6.
31. Brownlee M. Biochemistry and molecular cell biology of diabetic complications. *Nature.* 2001;414(6865):813-20. doi: 10.1038/414813a.
32. Shaw JE, Sicree RA, Zimmet PZ. Global estimates of the prevalence of diabetes for 2010 and 2030. *Diabetes Res Clin Pract.* 2010;87(1):4-14. doi: 10.1016/j.diabres.2009.10.007.
33. Brownlee M. The pathobiology of diabetic complications: a unifying mechanism. *Diabetes.* 2005;54(6):1615-25. doi: 10.2337/diabetes.54.6.1615.
34. Ighodaro OM. Molecular pathways associated with oxidative stress in diabetes mellitus. *Biomed Pharmacother.* 2018;108:656-62. doi: 10.1016/j.biopha.2018.09.058.

35. Eriksson JW. Metabolic stress in insulin's target cells leads to ROS accumulation – A hypothetical common pathway causing insulin resistance. *FEBS Lett.* 2007;581(19):3734-42. doi: <https://doi.org/10.1016/j.febslet.2007.06.044>.
36. Bloch-Damti A, Bashan N. Proposed mechanisms for the induction of insulin resistance by oxidative stress. *Antioxid Redox Signal.* 2005;7(11-12):1553-67. doi: 10.1089/ars.2005.7.1553.
37. Buse MG. Hexosamines, insulin resistance, and the complications of diabetes: current status. *Am J Physiol Endocrinol Metab.* 2006;290(1):E1-e8. doi: 10.1152/ajpendo.00329.2005.
38. Moore K, Roberts LJ, 2nd. Measurement of lipid peroxidation. *Free Radic Res.* 1998;28(6):659-71. doi: 10.3109/10715769809065821.
39. Recknagel RO, Ghoshal AK. Quantitative estimation of peroxidative degeneration of rat liver microsomal and mitochondrial lipids after carbon tetrachloride poisoning. *Exp Mol Pathol.* 1966;5(5):413-26. doi: 10.1016/0014-4800(66)90023-2.
40. Tiedge M, Lortz S, Drinkgern J, Lenzen S. Relation between antioxidant enzyme gene expression and antioxidative defense status of insulin-producing cells. *Diabetes.* 1997;46(11):1733-42. doi: 10.2337/diab.46.11.1733.
41. Ayala A, Muñoz MF, Argüelles S. Lipid peroxidation: production, metabolism, and signaling mechanisms of malondialdehyde and 4-hydroxy-2-nonenal. *Oxid Med Cell Longev.* 2014;2014:360438. doi: 10.1155/2014/360438.
42. Brownlee M. A radical explanation for glucose-induced beta cell dysfunction. *J Clin Invest.* 2003;112(12):1788-90. doi: 10.1172/jci20501.
43. Kaneto H, Matsuoka TA, Nakatani Y, Kawamori D, Matsuhisa M, Yamasaki Y. Oxidative stress and the JNK pathway in diabetes. *Curr Diabetes Rev.* 2005;1(1):65-72. doi: 10.2174/1573399052952613.
44. Rhodes CJ. Type 2 diabetes-a matter of beta-cell life and death? *Science.* 2005;307(5708):380-4. doi: 10.1126/science.1104345.
45. Kaneto H, Xu G, Song KH, Suzuma K, Bonner-Weir S, Sharma A, et al. Activation of the hexosamine pathway leads to deterioration of pancreatic beta-cell function through the induction of oxidative stress. *J Biol Chem.* 2001;276(33):31099-104. doi: 10.1074/jbc.M104115200.
46. Rizzo MA, Piston DW. Regulation of beta cell glucokinase by S-nitrosylation and association with nitric oxide synthase. *J Cell Biol.* 2003;161(2):243-8. doi: 10.1083/jcb.200301063.
47. Esterbauer H, Schaur RJ, Zollner H. Chemistry and biochemistry of 4-hydroxynonenal, malonaldehyde and related aldehydes. *Free Radic Biol Med.* 1991;11(1):81-128. doi: 10.1016/0891-5849(91)90192-6.
48. Kehrer JP, Biswal SS. The Molecular Effects of Acrolein. *Toxicol Sci.* 2000;57(1):6-15. doi: 10.1093/toxsci/57.1.6.
49. Lee SH, Oe T, Blair IA. Vitamin C-induced decomposition of lipid hydroperoxides to endogenous genotoxins. *Science.* 2001;292(5524):2083-6. doi: 10.1126/science.1059501.
50. Parola M, Bellomo G, Robino G, Barrera G, Dianzani MU. 4-Hydroxynonenal as a biological signal: molecular basis and pathophysiological implications. *Antioxid Redox Signal.* 1999;1(3):255-84. doi: 10.1089/ars.1999.1.3-255.
51. González-Minero FJ, Bravo-Díaz L, Ayala-Gómez A. *Rosmarinus officinalis* L. (Rosemary): An Ancient Plant with Uses in Personal Healthcare and Cosmetics. *Cosmetics.* 2020;7(4):77. doi: <https://www.mdpi.com/2079-9284/7/4/77>
52. Akagawa M. Protein carbonylation: molecular mechanisms, biological implications, and analytical approaches. *Free Radic Res.* 2021;55(4):307-20. doi: 10.1080/10715762.2020.1851027.

53. Stadtman ER, Levine RL. Free radical-mediated oxidation of free amino acids and amino acid residues in proteins. *Amino Acids*. 2003;25(3):207-18. doi: 10.1007/s00726-003-0011-2.
54. Wall SB, Oh JY, Diers AR, Landar A. Oxidative modification of proteins: an emerging mechanism of cell signaling. *Front Physiol*. 2012;3:369. doi: 10.3389/fphys.2012.00369.
55. Stadtman ER. Metal ion-catalyzed oxidation of proteins: biochemical mechanism and biological consequences. *Free Radic Biol Med*. 1990;9(4):315-25. doi: 10.1016/0891-5849(90)90006-5.
56. Stadtman ER. Oxidation of free amino acids and amino acid residues in proteins by radiolysis and by metal-catalyzed reactions. *Annu Rev Biochem*. 1993;62:797-821. doi: 10.1146/annurev.bi.62.070193.004053.
57. Akagawa M, Sasaki D, Ishii Y, Kurota Y, Yotsu-Yamashita M, Uchida K, et al. New method for the quantitative determination of major protein carbonyls, alpha-amino adipic and gamma-glutamic semialdehydes: investigation of the formation mechanism and chemical nature in vitro and in vivo. *Chem Res Toxicol*. 2006;19(8):1059-65. doi: 10.1021/tx060026p.
58. Requena JR, Chao CC, Levine RL, Stadtman ER. Glutamic and amino adipic semialdehydes are the main carbonyl products of metal-catalyzed oxidation of proteins. *Proc Natl Acad Sci USA*. 2001;98(1):69-74. doi: 10.1073/pnas.98.1.69.
59. Carney Almroth B. Oxidative Damage in Fish Used as Biomarkers in Field and Laboratory Studies: Göteborg University. Faculty of Science; 2008. URL: <https://gupea.ub.gu.se/handle/2077/10108>.
60. Fuentealba D, Friguet B, Silva E. Advanced Glycation Endproducts Induce Photocrosslinking and Oxidation of Bovine Lens Proteins Through Type-I Mechanism. *Photochem Photobiol*. 2009;85(1):185-94. doi: <https://doi.org/10.1111/j.1751-1097.2008.00415.x>.
61. Henning C, Glomb MA. Pathways of the Maillard reaction under physiological conditions. *Glycoconjugate journal*. 2016;33(4):499-512. doi: 10.1007/s10719-016-9694-y.
62. Vistoli G, De Maddis D, Cipak A, Zarkovic N, Carini M, Aldini G. Advanced glycoxidation and lipoxidation end products (AGEs and ALEs): an overview of their mechanisms of formation. *Free Radic Res*. 2013;47 Suppl 1:3-27. doi: 10.3109/10715762.2013.815348.
63. Chen JH, Lin X, Bu C, Zhang X. Role of advanced glycation end products in mobility and considerations in possible dietary and nutritional intervention strategies. *Nutr Metab*. 2018;15:72. doi: 10.1186/s12986-018-0306-7.
64. Akagawa M, Sasaki T, Suyama K. Oxidative deamination of lysine residue in plasma protein of diabetic rats. Novel mechanism via the Maillard reaction. *Euro J Biochem*. 2002;269(22):5451-8. doi: 10.1046/j.1432-1033.2002.03243.x.
65. Dinçer Y, Akçay T, Alademir Z, Ilkova H. Assessment of DNA base oxidation and glutathione level in patients with type 2 diabetes. *Mutat Res*. 2002;505(1-2):75-81. doi: 10.1016/s0027-5107(02)00143-4.
66. Goodarzi MT, Navidi AA, Rezaei M, Babahmadi-Rezaei H. Oxidative damage to DNA and lipids: correlation with protein glycation in patients with type 1 diabetes. *J Clin Lab Anal*. 2010;24(2):72-6. doi: <https://doi.org/10.1002/jcla.20328>.
67. Zhong H, Yin H. Role of lipid peroxidation derived 4-hydroxynonenal (4-HNE) in cancer: focusing on mitochondria. *Redox Biol*. 2015;4:193-9. doi: 10.1016/j.redox.2014.12.011.
68. Kannan K, Jain SK. Oxidative stress and apoptosis. *Pathophysiology*. 2000;7(3):153-63. doi: [https://doi.org/10.1016/S0928-4680\(00\)00053-5](https://doi.org/10.1016/S0928-4680(00)00053-5).

69. Parkinson A. An overview of current cytochrome P450 technology for assessing the safety and efficacy of new materials. *Toxicol Pathol.* 1996;24(1):48-57. doi: <https://doi.org/10.1177/019262339602400107>.
70. Raza H, Ahmed I, John A, Sharma AK. Modulation of xenobiotic metabolism and oxidative stress in chronic streptozotocin-induced diabetic rats fed with *Momordica charantia* fruit extract. *J Biochem Mol Toxicol.* 2000;14(3):131-9. doi: [https://doi.org/10.1002/\(SICI\)1099-0461\(2000\)14:3<131::AID-JBT2>3.0.CO;2-Q](https://doi.org/10.1002/(SICI)1099-0461(2000)14:3<131::AID-JBT2>3.0.CO;2-Q).
71. Guengerich FP. Cytochrome P-450 3A4: regulation and role in drug metabolism. *Annu Rev Pharmacol Toxicol.* 1999;39:1-17. doi: 10.1146/annurev.pharmtox.39.1.1.
72. Dostalek M, Court MH, Yan B, Akhlaghi F. Significantly reduced cytochrome P450 3A4 expression and activity in liver from humans with diabetes mellitus. *Br J Pharmacol.* 2011;163(5):937-47. doi: <https://doi.org/10.1111/j.1476-5381.2011.01270.x>.
73. Favreau LV, Schenkman JB. Composition changes in hepatic microsomal cytochrome P-450 during onset of streptozocin-induced diabetes and during insulin treatment. *Diabetes.* 1988;37(5):577-84. doi: 10.2337/diab.37.5.577.
74. Shimojo N. Cytochrome P450 changes in rats with streptozocin-induced diabetes. *The Int J Biochem.* 1994;26(10-11):1261-8. doi: 10.1016/0020-711x(94)90095-7.
75. Wang T, Shankar K, Ronis MJ, Mehendale HM. Mechanisms and outcomes of drug- and toxicant-induced liver toxicity in diabetes. *Crit Rev Toxicol.* 2007;37(5):413-59. doi: 10.1080/10408440701215100.
76. Hakki Kalkan I, Suher M. The relationship between the level of glutathione, impairment of glucose metabolism and complications of diabetes mellitus. *Pak J Med Sci.* 2013;29(4):938-42. doi: 10.12669/pjms.294.2859.
77. Saravanan G, Ponmurugan P. Ameliorative potential of S-allyl cysteine on oxidative stress in STZ induced diabetic rats. *Chem-Biol Interact.* 2011;189(1):100-6. doi: <https://doi.org/10.1016/j.cbi.2010.10.001>.
78. Sindhu RK, Koo JR, Sindhu KK, Ehdaie A, Farmand F, Roberts CK. Differential regulation of hepatic cytochrome P450 monooxygenases in streptozotocin-induced diabetic rats. *Free Radic Res.* 2006;40(9):921-8. doi: 10.1080/10715760600801272.
79. Volkovová K, Chorváthová V, Jurcovicová M, Koszeghyová L, Bobek P. Antioxidative state of the myocardium and kidneys in acute diabetic rats. *Physiol Res.* 1993;42(4):251-5. URL: http://www.biomed.cas.cz/physiolres/pdf/42/42_251.pdf.
80. Oian X, Hall SD. Enantioselective effects of experimental diabetes mellitus on the metabolism of ibuprofen. *J Pharmacol Exp Ther.* 1995;274(3):1192-8. URL: <https://jpet.aspetjournals.org/content/274/3/1192>.
81. Sweetman SC. *Martindale: The Complete Drug Reference, Analgesics Anti-inflammatory Drugs and Antipyretics.* 36th ed, Vol (1) p. 60. London: Pharmaceutical Press; 2009. URL: https://vnras.com/wp-content/uploads/2018/04/Martindale-The-Complete-Drug-Reference_-36th-Edition.pdf.
82. Hyland KC, Dickenson ERV, Drewes JE, Higgins CP. Sorption of ionized and neutral emerging trace organic compounds onto activated sludge from different wastewater treatment configurations. *Water Res.* 2012;46(6):1958-68. doi: <https://doi.org/10.1016/j.watres.2012.01.012>.
83. Davies NM. Clinical pharmacokinetics of ibuprofen. The first 30 years. *Clin Pharmacokinet.* 1998;34(2):101-54. doi: 10.2165/00003088-199834020-00002.
84. Mazaleuskaya LL, Theken KN, Gong L, Thorn CF, FitzGerald GA, Altman RB, et al. PharmGKB summary: ibuprofen pathways. *Pharmacogenet Genom.* 2015;25(2):96-106. doi: 10.1097/fpc.0000000000000113.
85. Rainsford KD. Ibuprofen: pharmacology, efficacy and safety. *Inflammopharmacology.* 2009;17(6):275-342. doi: 10.1007/s10787-009-0016-x.

86. Chang SY, Li W, Traeger SC, Wang B, Cui D, Zhang H, et al. Confirmation that cytochrome P450 2C8 (CYP2C8) plays a minor role in (S)-(+)- and (R)-(-)-ibuprofen hydroxylation in vitro. *Drug Metab Dispos.* 2008;36(12):2513-22. doi: 10.1124/dmd.108.022970.
87. Hamman MA, Thompson GA, Hall SD. Regioselective and stereoselective metabolism of ibuprofen by human cytochrome P450 2C. *Biochem Pharmacol.* 1997;54(1):33-41. doi: 10.1016/s0006-2952(97)00143-3.
88. Kepp DR, Sidelmann UG, Hansen SH. Isolation and characterization of major phase I and II metabolites of ibuprofen. *Pharm Res.* 1997;14(5):676-80. doi: 10.1023/a:1012125700497.
89. Tornio A, Niemi M, Neuvonen PJ, Backman JT. Stereoselective interaction between the CYP2C8 inhibitor gemfibrozil and racemic ibuprofen. *Eur J Clin Pharmacol.* 2007;63(5):463-9. doi: 10.1007/s00228-007-0273-9.
90. Markey SP. Chapter 11 - Pathways of Drug Metabolism. In: Atkinson AJ, Huang S-M, Lertora JJL, Markey SP, editors. *Principles of Clinical Pharmacology (Third Edition)*: Academic Press; 2012. p. 153-72. <https://www.sciencedirect.com/science/article/pii/B9780123854711000118>.
91. Shirley MA, Guan X, Kaiser DG, Halstead GW, Baillie TA. Taurine conjugation of ibuprofen in humans and in rat liver in vitro. Relationship to metabolic chiral inversion. *J Pharmacol Exp Ther.* 1994;269(3):1166-75. URL: <https://jpet.aspetjournals.org/content/269/3/1166.long>
92. Basu NK, Kubota S, Meselhy MR, Ciotti M, Chowdhury B, Hartori M, et al. Gastrointestinally distributed UDP-glucuronosyltransferase 1A10, which metabolizes estrogens and nonsteroidal anti-inflammatory drugs, depends upon phosphorylation. *J Biol Chem.* 2004;279(27):28320-9. doi: 10.1074/jbc.M401396200.
93. Kuehl GE, Lampe JW, Potter JD, Bigler J. Glucuronidation of nonsteroidal anti-inflammatory drugs: identifying the enzymes responsible in human liver microsomes. *Drug Metab Dispos.* 2005;33(7):1027-35. doi: 10.1124/dmd.104.002527.
94. Bushra R, Aslam N. An overview of clinical pharmacology of Ibuprofen. *Oman Med J.* 2010;25(3):155-166. doi: 10.5001/omj.2010.49.
95. Johnston SA. 88 - OSTEOARTHRITIS. In: Harari J, editor. *Small Animal Surgery Secrets (Second Edition)*. Philadelphia: Hanley & Belfus; 2004. p. 343-7. <https://www.sciencedirect.com/science/article/pii/B9781560535799500925>.
96. Boneberg EM, Zou MH, Ullrich V. Inhibition of cyclooxygenase-1 and -2 by R(-)- and S(+)-ibuprofen. *J Clin Pharmacol.* 1996;36(12 Suppl):16s-9s. URL: <https://europepmc.org/article/med/9013379>.
97. Neupert W, Brugger R, Euchenhofer C, Brune K, Geisslinger G. Effects of ibuprofen enantiomers and its coenzyme A thioesters on human prostaglandin endoperoxide synthases. *Br J Pharmacol.* 1997;122(3):487-92. doi: 10.1038/sj.bjp.0701415.
98. Geisslinger G, Schuster O, Stock KP, Loew D, Bach GL, Brune K. Pharmacokinetics of S(+)- and R(-)-ibuprofen in volunteers and first clinical experience of S(+)-ibuprofen in rheumatoid arthritis. *Eur J Clin Pharmacol.* 1990;38(5):493-7. doi: 10.1007/bf02336690.
99. Mayer JM. Ibuprofen enantiomers and lipid metabolism. *J Clin Pharmacol.* 1996;36(12 Suppl):27S-32S. URL: <http://europepmc.org/abstract/MED/9013381>.
100. Reichel C, Bang H, Brune K, Geisslinger G, Menzel S. 2-Arylpropionyl-CoA epimerase: partial peptide sequences and tissue localization. *Biochem Pharmacol.* 1995;50(11):1803-6. doi: 10.1016/0006-2952(95)02054-3.
101. Kato D, Mitsuda S, Ohta H. Microbial deracemization of alpha-substituted carboxylic acids: substrate specificity and mechanistic investigation. *J Org Chem.* 2003;68(19):7234-42. doi: 10.1021/jo034253x.

102. Petrie B, Camacho-Muñoz D. Analysis, fate and toxicity of chiral non-steroidal anti-inflammatory drugs in wastewaters and the environment: a review. *Environ Chem Lett*. 2021;19(1):43-75. doi: 10.1007/s10311-020-01065-y.
103. Dawnay AB, Hirst AD, Perry DE, Chambers RE. A critical assessment of current analytical methods for the routine assay of serum total protein and recommendations for their improvement. *Ann Clin Biochem*. 1991;28 (Pt 6):556-67. doi: 10.1177/000456329102800604.
104. Levine RL, Garland D, Oliver CN, Amici A, Climent I, Lenz AG, et al. Determination of carbonyl content in oxidatively modified proteins. *Methods Enzymol*. 1990;186:464-78. doi: 10.1016/0076-6879(90)86141-h.
105. Nakamura A, Goto S. Analysis of protein carbonyls with 2,4-dinitrophenyl hydrazine and its antibodies by immunoblot in two-dimensional gel electrophoresis. *J Biochem*. 1996;119(4):768-74. doi: 10.1093/oxfordjournals.jbchem.a021306.
106. Ohkawa H, Ohishi N, Yagi K. Assay for lipid peroxides in animal tissues by thiobarbituric acid reaction. *Anal Biochem*. 1979;95(2):351-8. doi: 10.1016/0003-2697(79)90738-3.
107. Ellman GL. Tissue sulfhydryl groups. *Arch Biochem Biophys*. 1959;82(1):70-7. doi: 10.1016/0003-9861(59)90090-6.
108. Sedlak J, Lindsay RH. Estimation of total, protein-bound, and nonprotein sulfhydryl groups in tissue with Ellman's reagent. *Anal Biochem*. 1968;25(1):192-205. doi: 10.1016/0003-2697(68)90092-4.
109. Mikolás E, Kun S, Laczy B, Molnár GA, Sélley E, Kőszegi T, et al. Incorporation of ortho- and meta-tyrosine into cellular proteins leads to erythropoietin-resistance in an erythroid cell line. *Kidney Blood Press Res*. 2013;38(2-3):217-25. doi: 10.1159/000355770.
110. Mohás-Cseh J, Molnár GA, Pap M, Laczy B, Vas T, Kertész M, et al. Incorporation of Oxidized Phenylalanine Derivatives into Insulin Signaling Relevant Proteins May Link Oxidative Stress to Signaling Conditions Underlying Chronic Insulin Resistance. *Biomedicines*. 2022;10(5):975. doi: 10.3390/biomedicines10050975.
111. Nyúl E, Kuzma M, Mayer M, Lakatos S, Almási A, Perjési P. HPLC study on Fenton-reaction initiated oxidation of salicylic acid. Biological relevance of the reaction in intestinal biotransformation of salicylic acid. *Free Radic Res*. 2018;52(9):1040-51. doi: 10.1080/10715762.2018.1517260.
112. Kuzma M, Kovács N, Sziva L, Maász G, Avar P, Perjési P. Oxidation of Hydroxy- and Dihydroxybenzoic Acids Under the Udenfriend's Conditions. An HPLC Study. *Open Med Chem J*. 2018;12:13-22. doi: 10.2174/1874104501812010013.
113. Attila Almási ÉdILNP, Noémi-Piroska Kovács, Tamás Fischer, Zoltán Markovics, Emil Fischer, Pál Perjési. Changes in hepatic metabolic enzyme activities and biliary excretion of 4-nitrophenol in streptozotocin induced diabetic rats. *Braz J Pharm Sci*. 2018;54(1):e17347. doi: 10.1590/s2175-97902018000117347.
114. Fischer E, Almási A, Bojcevs S, Fischer T, Kovács NP, Perjési P. Effect of experimental diabetes and insulin replacement on intestinal metabolism and excretion of 4-nitrophenol in rats. *Can J Physiol Pharmacol*. 2015;93(6):459-64. doi: 10.1139/cjpp-2015-0065.
115. Kovács NP, Almási A, Garai K, Kuzma M, Vancea S, Fischer E, et al. Investigation of intestinal elimination and biliary excretion of ibuprofen in hyperglycemic rats. *Can J Physiol Pharmacol*. 2019;97(11):1080-9. doi: 10.1139/cjpp-2019-0164.
116. Klaassen CD. Bile Flow and Composition During Bile Acid Depletion and Administration. *Can J Physiol Pharmacol*. 1974;52(2):334-48. doi: 10.1139/y74-045 %M 4838193.
117. Bonato PS, Del Lama MP, de Carvalho R. Enantioselective determination of ibuprofen in plasma by high-performance liquid chromatography-electrospray mass spectrometry. *J*

- Chromatogr B Analyt Technol Biomed Life Sci. 2003;796(2):413-20. doi: 10.1016/j.jchromb.2003.08.031.
118. Kromasil. Separation of ibuprofen on Kromasil AmyCoat RP: Nouryon Application Note; [cited 2022 12/06]. Available from: <https://www.kromasil.com/applications/view.php?app=c0128>.
119. UNION E. DIRECTIVE 2010/63/EU OF THE EUROPEAN PARLIAMENT AND OF THE COUNCIL: THE EUROPEAN PARLIAMENT AND THE COUNCIL OF THE EUROPEAN UNION; 2010 [Available from: <https://eur-lex.europa.eu/eli/dir/2010/63/oj>].
120. Government H. A Kormány 40/2013. (II. 14.) Korm. rendelethe az állatkísérletekről: Hungarian Government regulation; 2013 [Available from: <https://www.fao.org/faolex/results/details/en/c/LEX-FAOC124420>].
121. Wang-Fischer Y, Garyantes T. Improving the Reliability and Utility of Streptozotocin-Induced Rat Diabetic Model. J Diabetes Res. 2018;2018:8054073. doi: 10.1155/2018/8054073.
122. Bojcevic S, Rafiei A, Fischer E. Changes in the biliary excretion of exogenous organic anions by streptozotocin-induced diabetes. Acta Physiol Hung. 1996;84(3):263-4. URL: <https://pubmed.ncbi.nlm.nih.gov/9219598/>.
123. Onyango AN, Baba N. New hypotheses on the pathways of formation of malondialdehyde and isofurans. Free Radic Biol Med. 2010;49(10):1594-600. doi: 10.1016/j.freeradbiomed.2010.08.012.
124. Lerner AB. On the Metabolism of Phenylalanine and Tyrosine. J Biol Chem. 1949;181(1):281-94. doi: 10.1016/S0021-9258(18)56648-5.
125. Molnár GA, Kun S, Sélley E, Kertész M, Szélig L, Csontos C, et al. Role of Tyrosine Isomers in Acute and Chronic Diseases Leading to Oxidative Stress - A Review. Curr Med Chem. 2016;23(7):667-85. doi: 10.2174/0929867323666160119094516.
126. Pennathur S, Wagner JD, Leeuwenburgh C, Litwak KN, Heinecke JW. A hydroxyl radical-like species oxidizes cynomolgus monkey artery wall proteins in early diabetic vascular disease. J Clin Invest. 2001;107(7):853-60. doi: 10.1172/jci11194.
127. Brodie BB, Axelrod J, Shore PA, Udenfriend S. Ascorbic acid in aromatic hydroxylation. II. Products formed by reaction of substrates with ascorbic acid, ferrous ion, and oxygen. J Biol Chem. 1954;208(2):741-50. URL: [https://www.jbc.org/article/S0021-9258\(18\)65599-1/pdf](https://www.jbc.org/article/S0021-9258(18)65599-1/pdf).
128. Udenfriend S, Clark CT, Axelrod J, Brodie BB. Ascorbic acid in aromatic hydroxylation. I. A model system for aromatic hydroxylation. J Biol Chem. 1954;208(2):731-9. URL: [https://www.jbc.org/article/S0021-9258\(18\)65598-X/pdf](https://www.jbc.org/article/S0021-9258(18)65598-X/pdf).
129. Hebert SL, Nair KS. Protein and energy metabolism in type 1 diabetes. Clin Nutr. 2010;29(1):13-7. doi: 10.1016/j.clnu.2009.09.001.
130. Kehm R, Baldensperger T, Raupbach J, Höhn A. Protein oxidation - Formation mechanisms, detection and relevance as biomarkers in human diseases. Redox Biol. 2021;42:101901. doi: 10.1016/j.redox.2021.101901.
131. Garibotto G, Sofia A, Saffioti S, Bonanni A, Mannucci I, Verzola D. Amino acid and protein metabolism in the human kidney and in patients with chronic kidney disease. Clin Nutr. 2010;29(4):424-33. doi: 10.1016/j.clnu.2010.02.005.
132. Kuzma M, Nyúl E, Mayer M, Fischer E, Perjési P. HPLC analysis of in vivo intestinal absorption and oxidative metabolism of salicylic acid in the rat. Biomed Chromatogr. 2016;30(12):2044-52. doi: 10.1002/bmc.3783.
133. Mohammed HO, Almási A, Molnár S, Perjési P. The Intestinal and Biliary Metabolites of Ibuprofen in the Rat with Experimental Hyperglycemia. Molecules. 2022;27(13):4000. doi: 10.3390/molecules27134000.

134. Girotti AW. Lipid hydroperoxide generation, turnover, and effector action in biological systems. *J Lipid Res.* 1998;39(8):1529-42. doi: [https://doi.org/10.1016/S0022-2275\(20\)32182-9](https://doi.org/10.1016/S0022-2275(20)32182-9).
135. Corongiu FP, Banni S. Detection of conjugated dienes by second derivative ultraviolet spectrophotometry. *Methods Enzymol.* 1994;233:303-10. doi: 10.1016/s0076-6879(94)33033-6.
136. Shin BC, Huggins JW, Carraway KL. Effects of pH, concentration and aging on the malonaldehyde reaction with proteins. *Lipids.* 1972;7(4):229-33. doi: 10.1007/bf02533218.
137. Siu GM, Draper HH. Metabolism of malonaldehyde in vivo and in vitro. *Lipids.* 1982;17(5):349. doi: 10.1007/BF02535193.
138. Gutteridge JMC. Free-radical damage to lipids, amino acids, carbohydrates and nucleic acids determined by thiobarbituric acid reactivity. *Int J Biochem.* 1982;14(7):649-53. doi: 10.1016/0020-711X(82)90050-7.
139. Tsikas D. Assessment of lipid peroxidation by measuring malondialdehyde (MDA) and relatives in biological samples: Analytical and biological challenges. *Anal Biochem.* 2017;524:13-30. doi: 10.1016/j.ab.2016.10.021.
140. Janero DR. Malondialdehyde and thiobarbituric acid-reactivity as diagnostic indices of lipid peroxidation and peroxidative tissue injury. *Free Radic Biol Med.* 1990;9(6):515-40. doi: 10.1016/0891-5849(90)90131-2.
141. Bhattacharyya A, Chattopadhyay R, Mitra S, Crowe SE. Oxidative stress: an essential factor in the pathogenesis of gastrointestinal mucosal diseases. *Physiol Rev.* 2014;94(2):329-54. doi: 10.1152/physrev.00040.2012.
142. Slatter DA, Bolton CH, Bailey AJ. The importance of lipid-derived malondialdehyde in diabetes mellitus. *Diabetologia.* 2000;43(5):550-7. doi: 10.1007/s001250051342.
143. Lawrence RA, Burk RF. Species, Tissue and Subcellular Distribution of Non Se-Dependent Glutathione Peroxidase Activity. *J Nutr.* 1978;108(2):211-5. doi: 10.1093/jn/108.2.211.
144. Lu SC. Glutathione synthesis. *Biochim Biophys Acta - Gen Subj.* 2013;1830(5):3143-53. doi: <https://doi.org/10.1016/j.bbagen.2012.09.008>.
145. Hinchman CA, Ballatori N. Glutathione-degrading capacities of liver and kidney in different species. *Biochem Pharmacol.* 1990;40(5):1131-5. doi: [https://doi.org/10.1016/0006-2952\(90\)90503-D](https://doi.org/10.1016/0006-2952(90)90503-D).
146. Lash LH. Role of glutathione transport processes in kidney function. *Toxicol Appl Pharmacol.* 2005;204(3):329-42. doi: 10.1016/j.taap.2004.10.004.
147. Biondi R, Xia Y, Rossi R, Paolocci N, Ambrosio G, Zweier JL. Detection of Hydroxyl Radicals by d-Phenylalanine Hydroxylation: A Specific Assay for Hydroxyl Radical Generation in Biological Systems. *Anal Biochem.* 2001;290(1):138-45. doi: 10.1006/abio.2000.4958.
148. Molnár GA, Wagner Z, Markó L, T KS, Mohás M, Kocsis B, et al. Urinary ortho-tyrosine excretion in diabetes mellitus and renal failure: evidence for hydroxyl radical production. *Kidney Int.* 2005;68(5):2281-7. doi: 10.1111/j.1523-1755.2005.00687.x.
149. Asmat U, Abad K, Ismail K. Diabetes mellitus and oxidative stress-A concise review. *Saudi Pharm J.* 2016;24(5):547-53. doi: 10.1016/j.jsps.2015.03.013.
150. Lash LH. Renal membrane transport of glutathione in toxicology and disease. *Vet Pathol.* 2011;48(2):408-19. doi: 10.1177/0300985810375811.
151. Zhong Q, Terlecky SR, Lash LH. Diabetes increases susceptibility of primary cultures of rat proximal tubular cells to chemically induced injury. *Toxicol Appl Pharmacol.* 2009;241(1):1-13. doi: 10.1016/j.taap.2009.08.007.

152. Donovan A, McGrowder LA-J, Tazhmoye V, Crawford. Biochemical Evaluation of Oxidative Stress in Type 1 Diabetes. 2013. In: Type 1 Diabetes [Internet]. London, UK: IntechOpen; [23-248]. Available from: <https://www.intechopen.com/chapters/43298>.
153. Hecker M, Wagner AH. Role of protein carbonylation in diabetes. *J Inherit Metab Dis*. 2018;41(1):29-38. doi: 10.1007/s10545-017-0104-9.
154. Leemann TD, Transon C, Bonnabry P, Dayer P. A major role for cytochrome P450TB (CYP2C subfamily) in the actions of non-steroidal antiinflammatory drugs. *Drugs Exp Clin Res*. 1993;19(5):189-95. URL: <https://pubmed.ncbi.nlm.nih.gov/8174491/>.
155. Gliszczyńska A, Sánchez-López E. Dexibuprofen Therapeutic Advances: Prodrugs and Nanotechnological Formulations. *Pharmaceutics*. 2021;13(3):414. doi: 10.3390/pharmaceutics13030414.
156. Neunzig I, Göhring A, Drăgan CA, Zapp J, Peters FT, Maurer HH, et al. Production and NMR analysis of the human ibuprofen metabolite 3-hydroxyibuprofen. *J Biotechnol*. 2012;157(3):417-20. doi: 10.1016/j.jbiotec.2011.12.016.
157. Hammer H, Schmidt F, Marx-Stoelting P, Pötz O, Braeuning A. Cross-species analysis of hepatic cytochrome P450 and transport protein expression. *Arch Toxicol*. 2021;95(1):117-33. doi: 10.1007/s00204-020-02939-4.
158. Mills RF, Adams SS, Cliffe EE, Dickinson W, Nicholson JS. The metabolism of ibuprofen. *Xenobiotica*. 1973;3(9):589-98. doi: 10.3109/00498257309151547.
159. Yamazoe Y, Murayama N, Shimada M, Yamauchi K, Kato R. Cytochrome P450 in livers of diabetic rats: regulation by growth hormone and insulin. *Arch Biochem Biophys*. 1989;268(2):567-75. doi: 10.1016/0003-9861(89)90324-x.
160. Yang Y, Liu X. Imbalance of Drug Transporter-CYP450s Interplay by Diabetes and Its Clinical Significance. *Pharmaceutics*. 2020;12(4):348. doi: 10.3390/pharmaceutics12040348.
161. Richmond R, Halliwell B, Chauhan J, Darbre A. Superoxide-dependent formation of hydroxyl radicals: detection of hydroxyl radicals by the hydroxylation of aromatic compounds. *Anal Biochem*. 1981;118(2):328-35. doi: 10.1016/0003-2697(81)90590-x.
162. Forman HJ. Redox signaling: An evolution from free radicals to aging. *Free Radic Biol Med*. 2016;97:398-407. doi: 10.1016/j.freeradbiomed.2016.07.003.
163. Winterbourn CC. Toxicity of iron and hydrogen peroxide: the Fenton reaction. *Toxicol Lett*. 1995;82-83:969-74. doi: 10.1016/0378-4274(95)03532-x.
164. Silpak B, Rintu D, Ena Ray B. Role of free radicals in human inflammatory diseases. *AIMS Biophys*. 2017;4(4):596-614. doi: 10.3934/biophys.2017.4.596.
165. Prousek J. Fenton chemistry in biology and medicine. *Pure Appl Chem*. 2007;79(12):2325-38. doi: 10.1351/pac200779122325.
166. Arthur RB, Bonin JL, Ardill LP, Rourke EJ, Patterson HH, Stemmler EA. Photocatalytic degradation of ibuprofen over BiOCl nanosheets with identification of intermediates. *J Hazard Mater*. 2018;358:1-9. doi: 10.1016/j.jhazmat.2018.06.018.
167. Bajpai L, Varshney M, Seubert CN, Stevens SM, Johnson JV, Yost RA, et al. Mass spectral fragmentation of the intravenous anesthetic propofol and structurally related phenols. *J Am Soc Mass Spectrom*. 2005;16(6):814-24. doi: 10.1016/j.jasms.2005.02.009.
168. Jacobs LE, Fimmen RL, Chin YP, Mash HE, Weavers LK. Fulvic acid mediated photolysis of ibuprofen in water. *Water Res*. 2011;45(15):4449-58. doi: 10.1016/j.watres.2011.05.041.
169. Xiao R, Noerpel MR, Luk HL, Wei Z, Spinney R. Thermodynamic and kinetic study of ibuprofen with hydroxyl radical: A density functional theory approach. *Int J Quantum Chem*. 2014;114:74-83. doi: <https://doi.org/10.1002/qua.24518>.
170. Chopra S, Kumar D. Ibuprofen as an emerging organic contaminant in environment, distribution and remediation. *Heliyon*. 2020;6(6):e04087. doi: 10.1016/j.heliyon.2020.e04087.

171. Ito S, Ueno K, Mitarai A, Sasaki K. Evidence for hydroxyl radicals as an active species generated from Udenfriend's reagent. *J Chem Soc, Perkin Trans II*. 1993(2):255-9. doi: 10.1039/P29930000255.
172. Enami S, Sakamoto Y, Colussi AJ. Fenton chemistry at aqueous interfaces. *Proc Natl Acad Sci USA*. 2014;111(2):623-8. doi: 10.1073/pnas.1314885111.
173. Li M, Carlson S, Kinzer JA, Perpall HJ. HPLC and LC-MS studies of hydroxylation of phenylalanine as an assay for hydroxyl radicals generated from Udenfriend's reagent. *Biochem Biophys Res Commun*. 2003;312(2):316-22. doi: 10.1016/j.bbrc.2003.10.116.
174. Anger GJ, Magomedova L, Piquette-Miller M. Impact of acute streptozotocin-induced diabetes on ABC transporter expression in rats. *Chem Biodivers*. 2009;6(11):1943-59. doi: 10.1002/cbdv.200900053.
175. Hasegawa Y, Kishimoto S, Shibatani N, Nomura H, Ishii Y, Onishi M, et al. The pharmacokinetics of morphine and its glucuronide conjugate in a rat model of streptozotocin-induced diabetes and the expression of MRP2, MRP3 and UGT2B1 in the liver. *J Pharm Pharmacol*. 2010;62(3):310-4. doi: 10.1211/jpp.62.03.0004.
176. Nawa A, Fujita Hamabe W, Tokuyama S. Inducible nitric oxide synthase-mediated decrease of intestinal P-glycoprotein expression under streptozotocin-induced diabetic conditions. *Life Sci*. 2010;86(11-12):402-9. doi: 10.1016/j.lfs.2010.01.009.
177. Zhang LL, Lu L, Jin S, Jing XY, Yao D, Hu N, et al. Tissue-specific alterations in expression and function of P-glycoprotein in streptozotocin-induced diabetic rats. *Acta Pharmacol Sin*. 2011;32(7):956-66. doi: 10.1038/aps.2011.33.
178. Jetter A, Kullak-Ublick GA. Drugs and hepatic transporters: A review. *Pharmacol Res*. 2020;154:104234. doi: 10.1016/j.phrs.2019.04.018.
179. Baliou S, Adamaki M, Ioannou P, Pappa A, Panayiotidis MI, Spandidos DA, et al. Protective role of taurine against oxidative stress (Review). *Mol Med Rep*. 2021;24(2). doi: 10.3892/mmr.2021.12242.
180. Schaffer SW, Azuma J, Mozaffari M. Role of antioxidant activity of taurine in diabetes. *Can J Physiol Pharmacol*. 2009;87(2):91-9. doi: 10.1139/y08-110.
181. Legen I, Zakelj S, Kristl A. Polarised transport of monocarboxylic acid type drugs across rat jejunum in vitro: the effect of mucolysis and ATP-depletion. *Int J Pharm*. 2003;256(1-2):161-6. doi: 10.1016/s0378-5173(03)00073-5.
182. Drozdik M, Czekawy I, Oswald S, Drozdik A. Intestinal drug transporters in pathological states: an overview. *Pharmacol Rep*. 2020;72(5):1173-94. doi: 10.1007/s43440-020-00139-6.
183. Liu H, Xu X, Yang Z, Deng Y, Liu X, Xie L. Impaired function and expression of P-glycoprotein in blood-brain barrier of streptozotocin-induced diabetic rats. *Brain Res*. 2006;1123(1):245-52. doi: 10.1016/j.brainres.2006.09.061.
184. Angelini A, Iezzi M, Di Febbo C, Di Ilio C, Cuccurullo F, Porreca E. Reversal of P-glycoprotein-mediated multidrug resistance in human sarcoma MES-SA/Dx-5 cells by nonsteroidal anti-inflammatory drugs. *Oncol Rep*. 2008;20(4):731-5. doi: https://doi.org/10.3892/or_00000067.
185. Burckhardt G. Drug transport by Organic Anion Transporters (OATs). *Pharmacol Ther*. 2012;136(1):106-30. doi: 10.1016/j.pharmthera.2012.07.010.
186. Klaassen CD, Lu H. Xenobiotic transporters: ascribing function from gene knockout and mutation studies. *Toxicol Sci*. 2008;101(2):186-96. doi: 10.1093/toxsci/kfm214.
187. Cha SH, Sekine T, Fukushima JI, Kanai Y, Kobayashi Y, Goya T, et al. Identification and characterization of human organic anion transporter 3 expressing predominantly in the kidney. *Mol Pharmacol*. 2001;59(5):1277-86. doi: 10.1124/mol.59.5.1277.

188. Kobayashi Y, Ohshiro N, Sakai R, Ohbayashi M, Kohyama N, Yamamoto T. Transport mechanism and substrate specificity of human organic anion transporter 2 (hOat2 [SLC22A7]). *J Pharm Pharmacol*. 2005;57(5):573-8. doi: 10.1211/0022357055966.
189. Nigam SK, Bush KT, Martovetsky G, Ahn SY, Liu HC, Richard E, et al. The organic anion transporter (OAT) family: a systems biology perspective. *Physiol Rev*. 2015;95(1):83-123. doi: 10.1152/physrev.00025.2013.
190. Fork C, Bauer T, Golz S, Geerts A, Weiland J, Del Turco D, et al. OAT2 catalyses efflux of glutamate and uptake of orotic acid. *Biochem J*. 2011;436(2):305-12. doi: 10.1042/bj20101904.
191. Kimoto E, Mathialagan S, Tylaska L, Niosi M, Lin J, Carlo AA, et al. Organic Anion Transporter 2-Mediated Hepatic Uptake Contributes to the Clearance of High-Permeability-Low-Molecular-Weight Acid and Zwitterion Drugs: Evaluation Using 25 Drugs. *J Pharmacol Exp Ther*. 2018;367(2):322-34. doi: 10.1124/jpet.118.252049.
192. Kindla J, Müller F, Mieth M, Fromm MF, König J. Influence of non-steroidal anti-inflammatory drugs on organic anion transporting polypeptide (OATP) 1B1- and OATP1B3-mediated drug transport. *Drug Metab Dispos*. 2011;39(6):1047-53. doi: 10.1124/dmd.110.037622.
193. Schneider HT, Nuernberg B, Dietzel K, Brune K. Biliary elimination of non-steroidal anti-inflammatory drugs in patients. *Br J Clin Pharmacol*. 1990;29(1):127-31. doi: 10.1111/j.1365-2125.1990.tb03613.x.
194. Yang X, Gandhi YA, Duignan DB, Morris ME. Prediction of biliary excretion in rats and humans using molecular weight and quantitative structure-pharmacokinetic relationships. *AAPS J*. 2009;11(3):511-25. doi: 10.1208/s12248-009-9124-1.
195. Kuzma M, Fodor K, Maász G, Avar P, Mózsik G, Past T, et al. A validated HPLC-FLD method for analysis of intestinal absorption and metabolism of capsaicin and dihydrocapsaicin in the rat. *J Pharm Biomed Anal*. 2015;103:59-66. doi: <https://doi.org/10.1016/j.jpba.2014.10.007>.

Chapter 1

PHYSICO-CHEMICAL CHARACTERIZATION OF GLUTATHIONE (GSH)

Pál Perjési^{1,}, Caridad Noda Perez^{1,2},
Hamilton B. Napolitano³ and Hawsar O. Mohammed^{1,4}*

¹Institute of Pharmaceutical Chemistry, University of Pécs, Pécs, Hungary

²Instituto de Química, Universidade Federal de Goiás, Goiânia, Goiás, Brazil

³Ciências Exatas e Tecnológicas, Universidade Estadual de Goiás,
Anápolis, Goiás, Brazil

⁴College of Veterinary Medicine, University of Sulaimani,
Sulaymaniyah, Kurdistan Region, Iraq

ABSTRACT

Glutathione (GSH) is the most abundant intracellular thiol as well as a major cellular antioxidant. Besides its redox activity it is a powerful nucleophilic agent. Both physico-chemical properties of the compound are related to the thiol (SH) function of the cysteinyl moiety of the tripeptide. Because of its central role in maintaining the cellular homeostasis and protection against diverse (toxic) electrophilic species, it is also a component of several nutritional products. As such, knowledge of physico-chemical characteristics of the compound is essential for both pharmacopoeal characterization and molecular-level understanding of its main biological actions. The chapter summarizes the spectroscopic (IR, MS, X-ray, UV) and the relevant physico-chemical characteristics (acid-base and redox properties) that are applied in its pharmacopoeial characterization and biochemical/toxicological studies related to the compound.

* Corresponding Author E-mail: pal.perjesi@gytk.pte.hu.

Keywords: glutathione, pharmacopoeia, mass spectrometry, X-ray, IR spectroscopy, NMR spectroscopy, acid-base properties, redox properties

1. INTRODUCTION

Glutathione (GSH) is the most abundant intracellular thiol as well as a major cellular antioxidant. Besides its redox activity, it is a powerful nucleophilic agent. Both physico-chemical properties of the compound are related to the thiol (SH) function of the cysteinyl moiety of the tripeptide. Because of its central role in maintaining the cellular homeostasis and protection against diverse (toxic) electrophilic species, it is also a component of several nutritional products. As such, knowledge of physico-chemical characteristics of the compound is essential for both pharmacopoeial characterization and molecular-level understanding its main biological actions. The chapter summarizes the spectroscopic (IR, MS, X-ray, UV) and relevant physico-chemical characteristics (acid-base and redox properties) that are applied in its pharmacopoeial characterization and biochemical/toxicological studies related to the compound. Each section briefly introduces the theory of the relevant analytical technique or physico-chemical property.

2. CHEMICAL CHARACTERIZATION

2.1. Structure

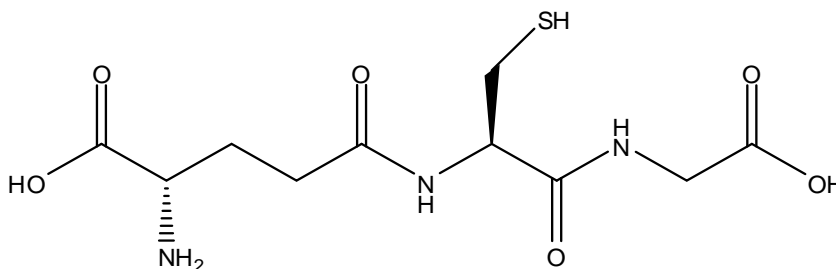


Figure 1. Structure of reduced glutathione (GSH).

Empirical formula: $C_{10}H_{17}N_3O_6S$

Molecular weight: 307.32

CAS number: 70-18-8

Melting point: 195 °C (with decomposition) [1]

Nomenclature

(2S)-2-amino-5-[[[(2R)-1-(carboxymethylamino)-1-oxo-3-sulfany]propan-2-yl]amino]-5-oxopentanoic acid,

(2S)-2-amino-4-[[[(1R)-1-[(carboxymethyl)carbamoyl]-2-sulfanylethyl]carbamoyl]butanoic acid,

γ -L-Glutamyl-L-cysteinylglycine.

Nonproprietary names

Glutathione, L-Glutathione, Reduced glutathione, Glutathione-SH, GSH

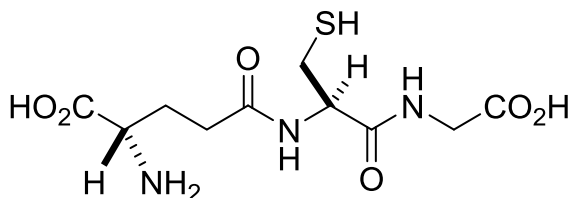
Proprietary names

Agifutol®; Atomolan®; Beamthion®; Copren®; Deltathione®; Glutamed®; Glutasan®; Glutathin®; Glutathiol®; Glutathion®; Gluthion®; Glutanil®; Glutoxil®; Ipatox®; Sethion®; Maglut®; Neuthion®; Novatox®; Ridutox®; Rition®; Scavenger®; Tad®; Tathiclon®; Tathion®; Tationil®; Thioxene®; Titition®; Triptide®

3. PHARMACOPOEIAL CHARACTERIZATION

3.1. European Pharmacopoeia Edition 9.0

The European Pharmacopoeia Edition 9.0 (Ph. Eur. 9.0) [2] lists *Glutathione* and describes its *Definition*, *Content*, *Characters*, *Identification*, *Tests*, *Assay*, *Storage*, and *Impurities* as follows.



Definition

$C_{10}H_{17}N_3O_6S$. M_r 307.3. L- γ -Glutamyl-L-cysteinylglycine. Fermentation product. CAS: 70-18-8.

Content

98.0 per cent to 101.0 per cent (dried substance).

Characters

Appearance

White or almost white, crystalline powder or colourless crystals.

Solubility

Freely soluble in water, very slightly soluble in ethanol (96 per cent) and in methylene chloride.

*Identification***A**

Specific optical rotation.

B

Infrared absorption spectrophotometry.

Comparison

Glutathione CRS.

*Tests (Selections):***Solution S**

Dissolve 5.0 g in *distilled water R* and dilute to 50 ml with the same solvent.

Appearance of solution

Solution S is clear and colourless.

Specific optical rotation.

15.5 to -17.5 (dried substance). Dissolve 1.0 g in *water R* and dilute to 25.0 ml with the same solvent.

Related substances

Capillary electrophoresis.

Prepare the solutions immediately before use.

Internal standard solution (a). Dissolve 0.100 g of *phenylalanine R* in the electrolyte solution and dilute to 50.0 ml with the same solution.

Internal standard solution (b). Dilute 10.0 ml of internal standard solution (a) to 100.0 ml with the electrolyte solution.

Test solution (a). Dissolve 0.200 g of the substance to be examined in the electrolyte solution and dilute to 10.0 ml with the same solution.

Test solution (b). Dissolve 0.200 g of the substance to be examined in internal standard solution (b) and dilute to 10.0 ml with the same solution.

Reference solution (a). Dissolve 20.0 mg of the substance to be examined in internal standard solution (a) and dilute to 10.0 ml with the same solution.

Reference solution (b). Dilute 5.0 ml of reference solution (a) to 50.0 ml with the electrolyte solution.

Reference solution (c). Dissolve 0.200 g of the substance to be examined in 5 ml of the electrolyte solution. Add 1.0 ml of internal standard solution (a), 0.5 ml of a 2 mg/ml solution of *L-cysteine R* (impurity B) in the electrolyte solution, 0.5 ml of a 2 mg/ml solution of *oxidised L-glutathione R* (impurity C) in the electrolyte solution and 0.5 ml of a 2 mg/ml solution of *L-γ-glutamyl-L-cysteine R* (impurity D) in the electrolyte solution. Dilute to 10.0 ml with the electrolyte solution.

Capillary.

-material: uncoated fused silica;

-size: length to the detector cell = 0.5 m; total length = 0.6 m; $\varnothing = 75 \mu\text{m}$.

Temperature: 25°C.

Electrolyte solution. Dissolve 1.50 g of anhydrous sodium dihydrogen phosphate R in 230 ml of water R and adjust to pH 1.80 with phosphoric acid R. Dilute to 250.0 ml with water R. Check the pH and, if necessary, adjust with phosphoric acid R or dilute sodium hydroxide solution R.

Detection: spectrophotometer at 200 nm.

Preconditioning of a new capillary: rinse the new capillary before the first injection with 0.1 M hydrochloric acid at 138 kPa for 20 min and with water R at 138 kPa for 10 min; for complete equilibration, condition the capillary with the electrolyte solution at 350 kPa for 40 min, and subsequently at a voltage of 20 kV for 60 min.

Preconditioning of the capillary: rinse the capillary with the electrolyte solution at 138 kPa for 40 min.

Between-run rinsing: rinse the capillary with water R at 138 kPa for 1 min, with 0.1 M sodium hydroxide at 138 kPa for 2 min, with water R at 138 kPa for 1 min, with 0.1 M hydrochloric acid at 138 kPa for 3 min and with the electrolyte solution at 138 kPa for 10 min.

Injection: test solutions (a) and (b), reference solutions (b) and (c) and the electrolyte solution (blank): under pressure (3.45 kPa) for 5 s.

Migration: apply a voltage of 20 kV.

Run time: 45 min.

Relative migration with reference to the internal standard (about 14 min): impurity A = about 0.77; impurity B = about 1.04; impurity E = about 1.2; impurity C = about 1.26; impurity D = about 1.3.

System suitability:

-*resolution:* minimum 1.5 between the peaks due to the internal standard and impurity B in the chromatogram obtained with reference solution (c); if necessary, increase the pH with dilute sodium hydroxide solution R;

-*peak-to-valley ratio:* minimum 2.5, where H_p =height above the baseline of the peak due to impurity D and H_v = height above the baseline of the lowest point of the curve separating this peak from the peak due to glutathione in the chromatogram obtained with reference solution (c); if necessary, lower the pH with phosphoric acid R;

-check that in the electropherogram obtained with test solution (a) there is no peak with the same migration time as the internal standard (in such case correct the area of the phenylalanine peak).

Limits: test solution (b):

-*corrected areas:* divide all the peak areas by the corresponding migration times;

-*correction factors:* for the calculation of content, multiply the ratio of time-corrected peak areas of impurity and the internal standard by the corresponding correction factor: impurity B = 3.0; impurity D = 1.4;

-*impurity C:* not more than 1.5 times the ratio of the area of the peak due to glutathione to the area of the peak due to the internal standard in the electropherogram obtained with reference solution (b) (1.5 per cent);

-*impurity D:* not more than the ratio of the area of the peak due to glutathione to the area of the peak due to the internal standard in the electropherogram obtained with reference solution (b) (1.0 per cent);

-*impurities A, B, E:* for each impurity, not more than 0.5 times the ratio of the area of the peak due to glutathione to the area of the peak due to the internal standard in the electropherogram obtained with reference solution (b) (0.5 per cent);

-*any other impurity:* for each impurity, not more than 0.2 times the ratio of the area of the peak due to glutathione to the area of the peak due to the internal standard in the electropherogram obtained with reference solution (b) (0.2 per cent);

-*total:* not more than 2.5 times the ratio of the area of the peak due to glutathione to the area of the peak due to the internal standard in the electropherogram obtained with reference solution (b) (2.5 per cent);

-*disregard limit:* 0.05 times the ratio of the area of the peak due to glutathione to the area of the peak due to the internal standard in the electropherogram obtained with reference solution (b) (0.05 per cent)

Assay

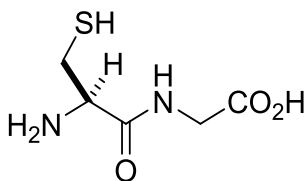
In a ground-glass-stoppered flask, dissolve 0.500 g of the substance to be examined and 2 g of *potassium iodide R* in 50 ml of *water R*. Cool the solution in iced water and add 10 ml of *hydrochloric acid R1* and 20.0 ml of 0.05 M *iodine*. Stopper the flask and allow to stand in the dark for 15 min. Titrate with 0.1 M *sodium thiosulphate* using 1 ml of *starch solution R*, added towards the end of the titration, as indicator. Carry out a blank titration. 1 ml of 0.05 M *iodine* is equivalent to 30.73 mg of $C_{10}H_{17}N_3O_6S$.

Storage

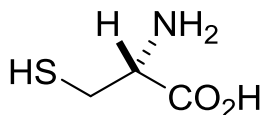
Protected from light.

Impurities

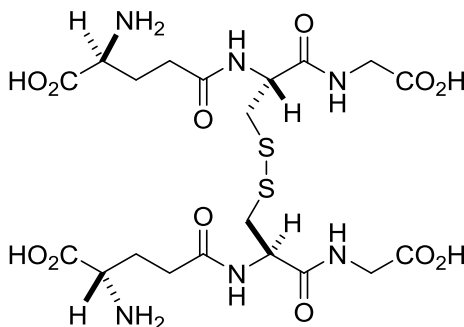
Specified impurities: A, B, C, D, E.



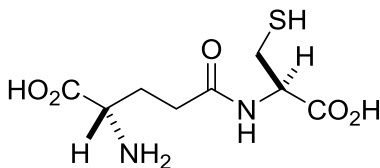
Impurity A. L-cysteinyl-glycine,



Impurity B. Cysteine,



Impurity C. Oxidized glutathione (GSSG),



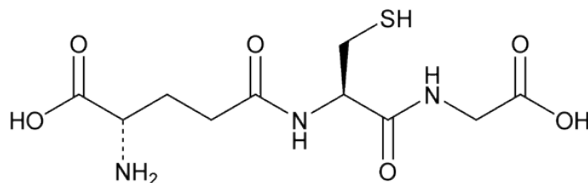
Impurity D. L-g-glutamyl-L-cysteine,

Impurity E. Impurity with unidentified structure.

3.2. The United States Pharmacopoeia – Dietary Supplement Compendium

The United States Pharmacopoeia (USP) Dietary Supplement Compendium (2015) monograph [3] includes the *name* of the ingredient or preparation; the *definition*;

packaging, storage, and labeling requirements; and the *specification*. The specification consists of a series of *tests, procedures* for the tests, and *acceptance criteria*.



$C_{10}H_{17}N_3O_6S$, 307.32

Pentanoic acid, 2-amino-5-[(R)-1-(carboxymethylamino)-3-mercapto-1-oxopropan-2-ylamino]-5-oxo, (S); N-(N-1-γ-Glutamyl-L-cysteinyl)glycine [70-18-8].

Definition

Glutathione contains NLT 98.0% and NMT 101.0% of $C_{10}H_{17}N_3O_6S$, as glutathione, calculated on the dried basis.

Identification

A

Infrared Absorption

B

Optical Rotation, Specific Rotation

Sample solution

40 mg/mL in water. Acceptance criteria: -15.5° to -17.5°, at 20°.

ASSAY

Procedure

Sample

500 mg of glutathione previously dried

Titrimetric system

Mode: Direct titration

Titrant: 0.1 N iodine VS

Endpoint detection: Visual

Blank: 50 mL of metaphosphoric acid (1 in 50)

Analysis: Dissolve the Sample in 50 mL of metaphosphoric acid (1 in 50) and titrate with the Titrant.

Calculate the percentage of glutathione ($C_{10}H_{17}N_3O_6S$) in the portion of Glutathione taken:

$$\text{Result} = [(V-B) \times N \times F \times 100]/W$$

where

V = titrant volume of the Sample (mL)

B = titrant volume of the Blank (mL)

N = titrant normality (mEq/mL)

F = equivalency factor, 307.32 mg/mEq

W = weight of the Sample (mg)

Acceptance criteria: 98.0%–101.0% on the dried basis

Impurities

Inorganic Impurities

Ammonium

Standard solution: 10 µg of ammonium from a diluted ammonium chloride solution

Sample solution: 50 mg of Glutathione

Analysis: Transfer the Sample solution and the Standard solution to separate 25-mL jars fitted with caps, and dissolve in 1 mL of water. Add 0.30 g of magnesium oxide. Close immediately after placing a piece of silver manganese paper 5-mm square, wetted with a few drops of water, under the caps. Swirl, avoiding projections of liquid, and allow to stand at 40° for 30 min.

Acceptance criteria: If the silver manganese paper shows a gray color, it is not more intense than the standard (NMT 200 ppm).

Arsenic

NMT 2 ppm

Chloride and Sulfate, Chloride: Dissolve 0.7 g with water to make 15 mL. The solution shows no more chloride than corresponds to 0.20 mL of 0.020 N hydrochloric acid (NMT 200 ppm).

Chloride and Sulfate

Sulfate: Dissolve 0.8 g in water to make 15 mL. The solution shows no more sulfate than corresponds to 0.25 mL of 0.020 N sulfuric acid (NMT 300 ppm).

Heavy Metals

Method I: NMT 10 ppm

Iron

NMT 10 ppm

Residue on Ignition

NMT 0.1%

Organic Impurities*Procedure*

Mobile phase: 6.8 g/L of potassium dihydrogen phosphate with 2.02 g/L of sodium 1-heptane sulfonate. Adjust with phosphoric acid to a pH of 3.0. Mix 970 mL of this solution with 30 mL of methanol.

System suitability solution: 0.1 mg/mL of USP l-Phenylalanine RS, 0.5 mg/mL of USP Glutathione RS, and 0.5 mg/mL of USP Ascorbic acid RS in Mobile phase

Standard solution: 0.01 mg/mL of USP Glutathione RS in Mobile phase. [Note—This solution has a concentration equivalent to 2.0% of that of the Sample solution.]

Sample solution: 50 mg of glutathione in 100 mL of Mobile phase. [Note—Allow the solution to stand for 5 min before use.]

Chromatographic system

Mode: LC

Detector: UV 210 nm

Column: 4.6-mm × 15-cm; 5-μm packing L1

Column temperature: 30°

Flow rate: Adjust so that the retention time of glutathione is about 5 min.

Injection size: 10 μL

System suitability

Sample: System suitability solution

Suitability requirements

Resolution: NLT 5.0 between the ascorbic acid and glutathione peaks; and NLT 5.0 between the glutathione and l-phenylalanine peaks

Relative standard deviation: NMT 1.5% for replicate injections

Analysis

Samples: Standard solution and Sample solution

Calculate the percentage of any impurity in the portion of Glutathione taken:

$$\text{Result} = (r_U/r_S) \times (C_S/C_U) \times 100$$

where,

 r_U = peak response of any peak from the Sample solution other than glutathione, r_S = peak response of the glutathione peak from the Standard solution, C_S = concentration of USP Glutathione RS in the Standard solution (mg/mL), C_U = concentration of Glutathione in the Sample solution (mg/mL)

Acceptance criteria

Individual impurity: NMT 1.5% for the impurity with the relative retention time of about 4.

Total impurities: NMT 2.0%.

Specific Tests

Clarity and Color of Solution

Sample solution

0.1 g/mL in water

Analysis

Using identical tubes of colorless, transparent, neutral glass with a flat base and an internal diameter of 15–25 mm, compare the liquid to be examined with water, the depth of the layer being 40 mm. Compare the colors in diffused daylight, viewing vertically against a white background.

Acceptance criteria

The solution is clear and colorless.

Loss on Drying

NMT 0.5%, 105° for 3 h

Additional Requirements

Packaging and Storage

Preserve in tight containers.

4. GAS PHASE CHARACTERIZATION

4.1. Mass Spectrometry

Mass spectrometry is a versatile, generally used analytical technique in the field of bioanalysis. It can be applied for determination of molecular weight, molecular formula (HRMS), structure (from fragmentation fingerprint), isotopic incorporation/distribution, and protein sequence (MS-MS), just to mention its most important applications [4-7].

The most important parts of the mass spectrometers are the sample *inlet*, the *ion source*, the *mass analyzer*, the *detector* and the *data analyzer* unit. The sample introduction could be direct (through a gate) or indirect (from a separation unit; e.g., GC, HPLC, SFC, CE). In the ion source the analyte particles are ionized (converted to positive or negative ions) by direct (with high speed electrons) or indirect (with neutral or charged particles; with charge transfer; or with laser photons) methods. The charged particles are separated in the mass analyzer unit. The choice of mass analyzer should be based upon the application, cost, and performance desired. There is no ideal mass analyzer that is good for all applications [8].

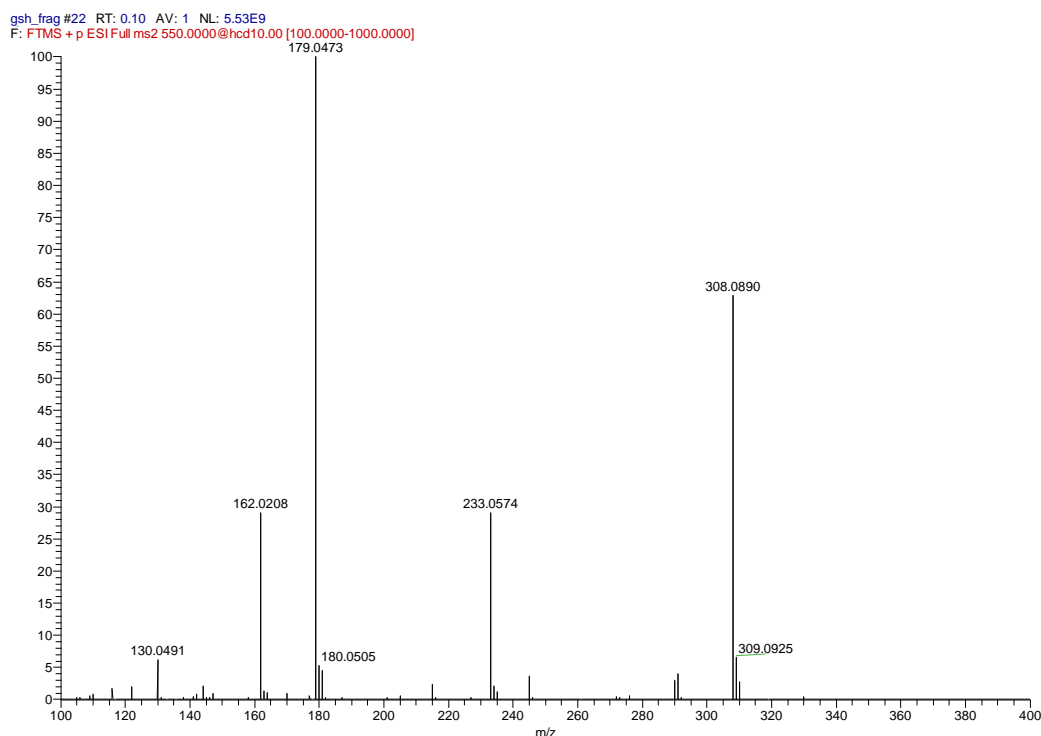


Figure 2. Positive ion mode HESI fragmentation pattern of reduced glutathione (GSH).

The commonly used mass analyzer could be a magnetic (B) or electrostatic (E) sector analyzer; a quadrupole mass filter (Q) or a time-of-flight (TOF) analyzer; an ion-trap (Penning, Paul, Kingdon traps, a quadrupole ion trap (Q) or orbitrap (OT)); or an ion-cyclotron resonance (ICR) analyzer. The mass analyzers separate the ions according to their mass-to-charge (m/z) ratio. In the detector, the signal intensity is directly proportional to the number of the ions. The most commonly used detectors are the photographic plate detectors, the Faraday Cups, and the (photo) electron multipliers [9].

The mass spectrum is presented in terms of ion abundance vs. m/z ratio (mass). If a molecule loses only one electron in the ionization process, a molecular ion is observed that gives its molecular weight – this is designated as M^+ in the spectrum. In most cases, when

a molecule loses a valence electron, bonds are broken, or the ion formed quickly fragments to lower energy ions. The masses of charged ions are recorded as fragment ions by the spectrometer (see Figure 2 and Figure 3).

Tandem mass spectrometry (MS/MS or MS²) is a technique to break down selected fragment ions (precursor ions) into fragments (product ions). The fragments then reveal aspects of the chemical structure of the precursor ion [10].

Figure 2 illustrates the positive ion mode HESI fragmentation pattern of reduced glutathione (GSH) $[M+H]^+ = 308.1$. The mass spectrometer was a Q Exactive™ Focus hybrid quadrupole-Orbitrap™ instrument (Thermo Scientific, Bremen, Germany). In the spectrum, three main intense peaks observed at m/z 233.1, 179.0 and 162.0 from the fragmentation of the $[M+H]^+$ species. The product ion at 233.1 arises by the loss of a neutral glycine residue (-75.0 Da), while the m/z 179.0 results from the loss of a glutamyl residue (-129.1 Da). The m/z 162.0 fragment ion is formed as a result of the loss of a neutral glutamate residue [11].

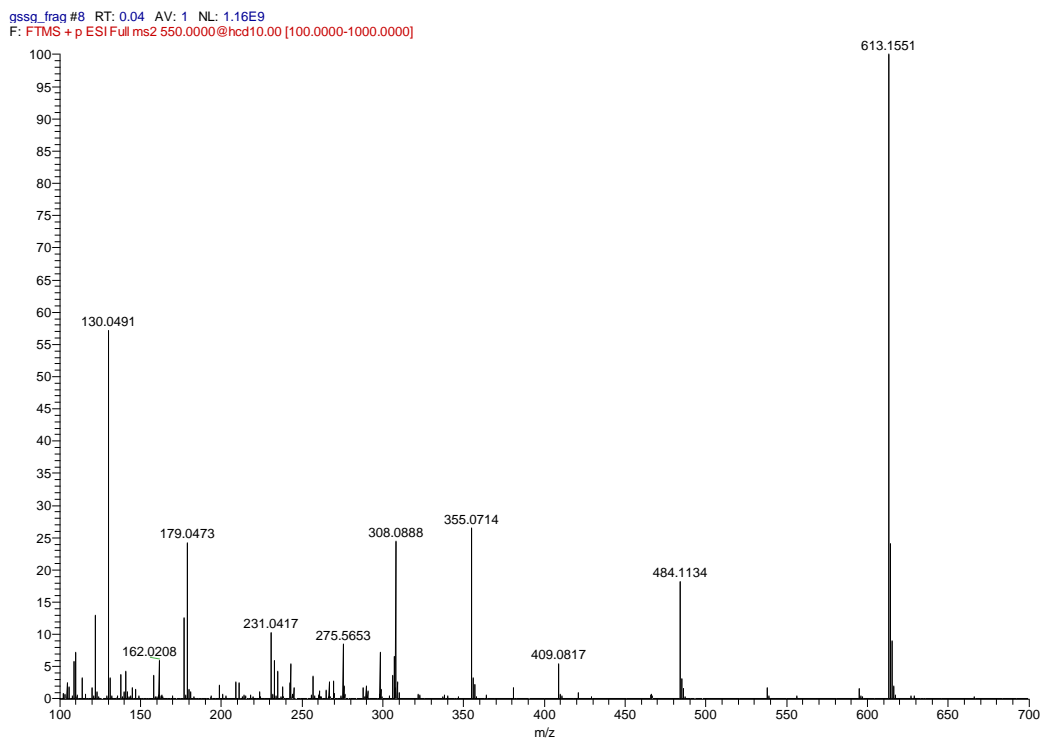


Figure 3. Positive ion mode HESI fragmentation pattern of oxidized glutathione (GSSG).

Figure 3 illustrates the positive ion mode HESI fragmentation pattern of oxidized glutathione (GSSG) $[M+H]^+ = 613.2$. In the spectrum, three main intense peaks observed at m/z 484.1, 355.1 and 308.1 from the fragmentation of the $[M+H]^+$ species. The product ion at 484.1 arises by the loss of a glutamyl residue (-129.1 Da), while the m/z 355.1 results from the loss of two glutamyl residues leaving the dipeptide Cys-Gly fragments covalently

linked *via* a disulfide bond. This result is in agreement with previous HPLC-MS investigation of GSSG. The third one, m/z 308.1, corresponds to protonated reduced glutathione (GSH) $[M+H]^+ = 308.1$. Formation of this latter fragment (and the fragments of this ion) could not be observed under the previously used ionization conditions [12].

5. SOLID STATE CHARACTERIZATION

5.1. Infrared Spectroscopy

Infrared spectroscopy is the analysis of infrared light interacting with a molecule. The main use of this technique is in organic and inorganic chemistry. It is used to determine functional groups in molecules. The infrared absorption spectra of organic small molecules are as distinctive and unique as a fingerprint [13].

Light with wavelengths from 800 nm to about 1 millimeter (1000 μm) is called infrared light. This wide band of the electromagnetic spectrum is divided into three regions; the near-, mid- and far-infrared. The higher-energy *near-IR*, approximately 12500–4000 cm^{-1} (0.8–2.5 μm wavelength), can excite overtone or harmonic vibrations. The *mid-infrared*, approximately 4000–400 cm^{-1} (2.5–25 μm), may be used to study the fundamental vibrations and associated rotational-vibrational structure. This is the region, which is most commonly used in the organic analytical practice. The *far-infrared*, approximately 400–10 cm^{-1} (25–1000 μm), has low energy and may be used for rotational spectroscopy [14].

Infrared spectroscopy exploits the fact that molecules absorb frequencies that are characteristic of their structure. These absorptions occur at resonant frequencies, i.e., the frequency of the absorbed radiation matches the vibrational frequency. The atoms in a CH_2X_2 group - commonly found in organic molecules - where X can represent any other atom, can vibrate in nine ($3N-6$) different ways. Six of these vibrations involve only the CH_2 portion: symmetric and antisymmetric stretching, scissoring, rocking, wagging and twisting. The spectra generally show the transmittance of the sample over the investigated wavenumber (cm^{-1}) range (see Figure 4 and Figure 5).

Since the observed set of absorption bands are, in essence, a display of some of the resonant vibrational frequencies of the molecule, the infrared spectrum is directly related to molecular parameters such as bond lengths and angles, bond groups (“functional groups”) and molecular symmetry. Thus, an infrared spectrum not only provides information on the identity of “unknown” compounds, but also yields definite data on its molecular structure [15].

Infrared spectra may be obtained from samples in all phases (liquid, solid and gaseous). Liquids are usually examined as a thin film sandwiched between two polished NaCl plates. If solvents are used to dissolve solids, care must be taken to avoid obscuring important spectral regions by solvent absorption. Solids may either be incorporated in a thin KBr

disk, prepared under high pressure, or mixed with a little non-volatile liquid and ground to a paste (or mull) that is smeared between salt plates.

The analytical infrared absorption spectra can be divided into four distinct regions [16]:

- 1) 4000-2800 cm^{-1} . The region of the OH, NH and CH stretching frequencies. (The OH and NH bands are more intense than the CH bands.)
- 2) 2800-2000 cm^{-1} . The region of rare functional groups (e.g., triple bonds ($\text{C}\equiv\text{N}$, $\text{C}\equiv\text{C}$), cumulated double bonds).
- 3) 2500-1500 cm^{-1} . The region of the double bonds (e.g., $\text{C}=\text{O}$, $\text{C}=\text{N}$, $\text{C}=\text{C}$ and aromatic skeletal stretching).
- 4) 1500-400 cm^{-1} . The so called “*fingerprint region*.” This region usually contains a rather complicated series of absorptions. These are mainly due to all manner of bending vibrations within the molecule. It is said so because it can be used to identify unknown or two different organic compounds by comparing the troughs in this region.

Infrared (IR) spectroscopy is a universally used instrumental method for identification of pharmacopoeial substances. The method is based on comparison of the IR spectra of the sample to be identified with the corresponding *Chemical Reference Standard* (CRS) (Ph. Eur.)/*Reference Standard* (USP RS) (USP). The IR spectrum of reduced glutathione (GSH) recorded in KBr is shown in Figure 4. The observed absorption frequencies are listed in Table 1. The spectra were recorded with an Impact 400 (Nicolet) FT-IR spectrophotometer using a KBr pellet as the background reference spectrum.

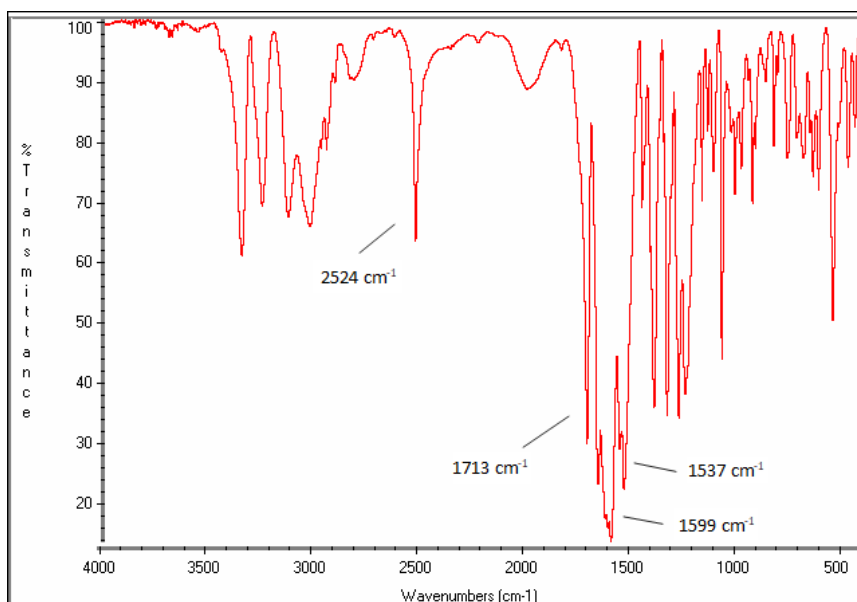


Figure 4. IR spectrum of reduced glutathione (GSH) recorded in KBr.

As it is shown, there are well separated sharp resonance peaks in the functional group region of the spectrum. Above the 3000 cm^{-1} region, several associated νOH , νNH , νNH_2 (3346 , 3249 , and 3126) and νCH (3024 cm^{-1}) bands can be seen. The band at 2524 cm^{-1} can be associated with the cysteine thiol (SH) group. The 1713 cm^{-1} band corresponds to the $\nu\text{C=O}$ band of the terminal carboxyl groups. The 1661 cm^{-1} band can be assigned as the amid I band. The bands at 1599 and 1537 cm^{-1} could be associated with the overlapping amid II ($\nu\text{C=O}$ (amide)) and δNH_3^+ resonances. The fingerprint region ($\leq 1500\text{ cm}^{-1}$) shows several unique resonances, which form an intricate pattern that can be used as a fingerprint to determine the compound.

Table 1. Characteristic IR bands of reduced (GSH) and oxidized (GSSG) glutathione

IR bands	GSH (cm^{-1})	GSSG (cm^{-1})
$\nu(\text{OH}, \text{NH})$	3346, 3249, 3126	3400-2700
$\nu(\text{CH})$	3024	3400-2700
$\nu(\text{SH})$	2524	None
$\nu(\text{C=O}, \text{carboxyl})$	1713	1736
$\nu(\text{C=O}, \text{amide I})$	1661	1655
$\nu(\text{CO}, \text{amide II}), \delta(\text{NH}_3^+)$	1599 and 1537	1524

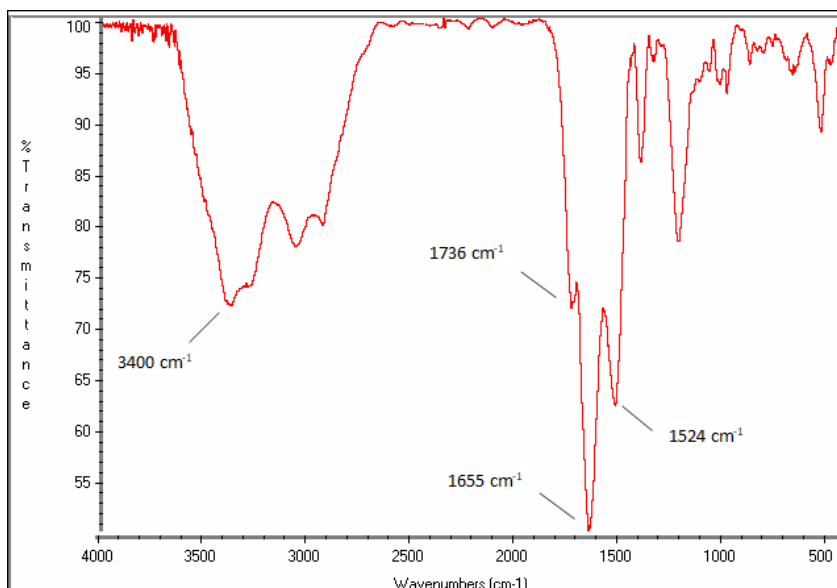


Figure 5. IR spectrum of oxidized glutathione (GSSG) recorded in KBr.

The IR spectrum of the oxidized form of glutathione shows broad, not well separated bands. In the $3400\text{-}2700\text{ cm}^{-1}$ region a broad, overlapping νOH , νNH , νNH_2 and νCH absorption can be seen. According to the modified chemical structure, no SH band appears

in the spectrum. The 1736 cm^{-1} band corresponds to the $\nu\text{C=O}$ band of the terminal carboxyl groups. The 1655 cm^{-1} band can be assigned as the amid I band. The broad band at 1524 cm^{-1} could be associated with the overlapping amid II ($\nu\text{C=O}$ (amide)) and δNH_3^+ bands. The fingerprint region ($\leq 1500\text{ cm}^{-1}$) shows much less characteristic separated bands than the spectrum of GSH.

5.2. Crystallography

5.2.1. X-Ray Diffraction

Crystallography is an experimental methodology based on X-ray diffraction by crystalline materials and studies atomic arrangement on solid state samples [17]. X-ray crystallography is essentially dependent on analysis of the diffraction patterns of one crystal by an X-ray beam. The intensities and directions of the diffracted waves on diffraction pattern are correlated to position and atomic species into the crystal. The atomic species and positions are correlated by the maximum values of the electronic density distribution on the crystal, which can be obtained through Fourier transform on diffracted X-ray function [18-20]. Because of atomic positions, information such as (1) bond distances, (2) bond angles, (3) molecular packing, (4) supramolecular arrangement and (5) charge distribution can easily be obtained. This way, once the molecular structure of a compound is obtained, its physico-chemical properties can be described [21].

Since X-rays have shorter wavelengths than those of the IR and UV radiations, they have higher energy and more penetrative power [19]. Each X-ray wave on diffraction pattern interacts with one another either constructively or destructively. The observed intensity originated from the constructive interaction of the diffracted waves and energy (1), understood as a beam of photons.

$$E = h\nu = \frac{hc}{\lambda} \quad (1)$$

where h is the Planck's constant, c is the speed of light, ν is the frequency and λ is the wavelength of the radiation.

As a consequence of monochromatic X radiation striking a crystalline material, the electrons are forced to oscillate due to the electric field that makes up the incident radiation, making it a new source of scattering in all directions. The diffraction arises from the constructive interference of these waves scattered by the various discrete atoms. William L. Bragg described the constructive conditions of the X-ray diffraction, when a wavelength comparable to atomic bond distances is scattered in a pattern dependent on atomic pattern distribution in the crystalline sample. Diffraction process in the crystal can be regarded as

if the X-rays were “reflected” by sets of parallel planes in the crystal [18-20]. Equation (2) represents Bragg’s law in a simplified way.

$$2 \times d \times \sin \theta = n \times \lambda \quad (2)$$

where d is the interplanar distance, θ is the incident angle, λ is the wavelength of the incident beam and n is the order of the diffraction.

5.2.2. Crystallographic Molecular Model

Once the X-ray radiation is diffracted by a single crystal and Bragg’s law indexes every single direction on diffraction pattern, the mathematical model used to describe this phenomenon and obtain the molecular model (structure) is based on Fourier methods. A crystallographic classical example is the calculation of an electron density map from waves diffracted by all components of the unit cell. In turn, Fourier analysis is the decomposition of an arbitrary function into its component cosine and sine harmonics [21-24]. On crystallography, the electron density functions correspond to the positions and X-ray scattering powers of the atoms, and then perform a Fourier transform on the electron density to obtain the structure factors. The measured diffraction pattern of a crystal is described by Fourier analysis and electron density distribution (structure) is described by the Fourier synthesis. The electron density function ($\rho(\mathbf{r})$) is related by equation (3)

$$\rho(\mathbf{r}) = \frac{1}{V} \sum_{\mathbf{h}} |F(\mathbf{h})| \exp[-2\pi i(\mathbf{h} \cdot \mathbf{r}) + i\varphi(\mathbf{h})] \quad (3)$$

where V is the volume of the unit cell, $F(\mathbf{h})$ is the structure factor with magnitude $|F(\mathbf{h})|$ proportional to the reflection intensity measured and \mathbf{h} indexes of each direction. The quantity $\mathbf{h} \cdot \mathbf{r}$ corresponds to the scalar product between the scattering vector in the reciprocal space \mathbf{h} and the position vector in the direct space \mathbf{r} .

The classical phase problem is evident in equation (3) since the full knowledge of electron density $\rho(\mathbf{r})$ depends on the knowledge of the phases $\varphi(\mathbf{h})$ that are lost in the measurement process. In general, the solution of the phase problem in crystallography of small molecules is obtained by the Patterson or direct methods. Once the draft of the crystallographic molecular model is first obtained [25-27], the following step is to refine this model throughout least squares procedures where the (1) accurate atomic position, (2) atomic species, (3) atomic displacement behavior, (4) solvent content, (5) chemical consistency and other important information are all assigned. In general, the programs used are SHELXL [28], SIR [29] and OLEX2 [30].

The first glutathione molecular structure, described by W. B. Wright [31], is shown in Figure 6.

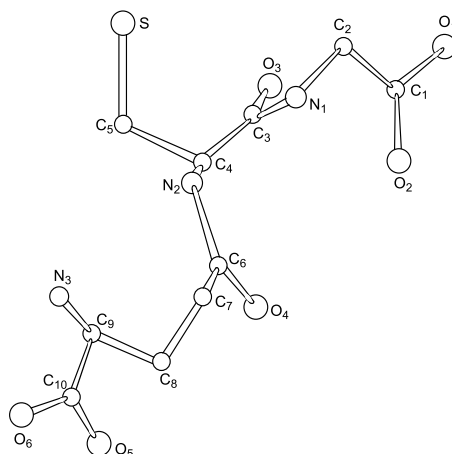


Figure 6. X-ray structure of reduced glutathione (GSH). Based on reference [31].

The X-ray analysis showed a tripeptide with a gamma peptide linkage between the carboxyl group of the glutamate side chain and the amine group of cysteine. Wright also described a molecular conformation adopting a helical configuration with almost planar structure between glycine carboxyl and amino-carboxyl groups. The glutathione crystallized in the orthorhombic space group $P2_12_12_1$ showing the carboxyl group of cysteine attached by a normal peptide linkage to glycine, and the sulphur is forming a zigzag chain [31, 32]. The molecules form a three-dimensional network of hydrogen bonds on molecular packing.

6. IN SOLUTION CHARACTERIZATION

6.1. UV-Vis Spectroscopy

UV-Vis spectroscopy is a spectroscopic method to characterize electronic structure of organic molecules. Electronic transition energies correspond to the energies of the analytical UV (200-400 nm) and the visible (400-700 nm) range photons. Absorption of visible and ultraviolet (UV) radiation is associated with excitation of electrons, in both atoms and molecules, from lower to higher energy levels. Since the energy levels of matter are quantized, only light with the precise amount of energy can cause transitions from one level to another will be absorbed.

The absorption of UV or visible radiation corresponds to the excitation of outer electrons. There are three types of electronic transitions to be considered: (a) transitions involving p, s and n electrons, (b) transitions involving charge-transfer electrons, and (c) transitions involving d and f electrons [33, 34]. In this chapter only possible transitions involving p, s, and n electrons are discussed.

The energy associated with electromagnetic radiation is defined by the following equation:

$$E = h \times \nu \quad (4)$$

where E is the energy (J), h is the Planck's constant (6.62×10^{-34} Js), and ν is the frequency (1/s).

There are a number of transitions possible involving the bonding (s and p) and nonbonding (n) electrons. The transitions generally occur from the highest occupied molecular orbital (HOMO) to the lowest unoccupied molecular orbital (LUMO) in a molecule. The larger the gap between the energy levels, the greater the energy required to promote the electron to the higher energy level; resulting in light of higher frequency, and therefore shorter wavelength, being absorbed.

Of the possible electronic transitions ($s \rightarrow s^*$, $s \rightarrow p^*$, $p \rightarrow s^*$, $n \rightarrow s^*$, $p \rightarrow p^*$ and $n \rightarrow p^*$), only the two lowest energy ones ($p \rightarrow p^*$ and $n \rightarrow p^*$) can be achieved by the energies available in the 200-700 nm region (Figure 7). Thus, only those molecules are expected to absorb in the UV-Vis region, which contains p-electrons and may also have atoms with nonbonding electrons [33, 34].

These transitions should result in very narrow absorbance bands at wavelengths highly characteristic of the difference in energy levels of the absorbing species. This is true, however, only for atoms. For molecules, vibrational and rotational energy levels are superimposed on the electronic energy levels. Because many transitions with different energies can occur, the bands are broadened (see Figures 8 and 9). The broadening is even greater in solutions owing to solvent-solute interactions [33]. Accordingly, UV-visible spectra generally show only a few broad absorbance bands. Compared with techniques such as infrared spectroscopy, which produces many narrow bands, UV-visible spectroscopy provides a limited amount of qualitative information. The method is mainly used for quantitative measurements [34, 35].

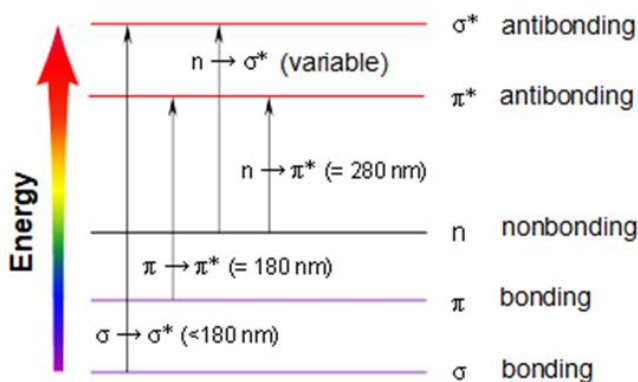


Figure 7. Possible UV-Vis electronic transitions.

The UV spectra of reduced (GSH) and oxidized (GSSG) glutathione recorded in aqueous solution are shown in Figure 8 and Figure 9. The spectra were recorded in a Jasco V-750 Spectrophotometer, using water as a solvent.

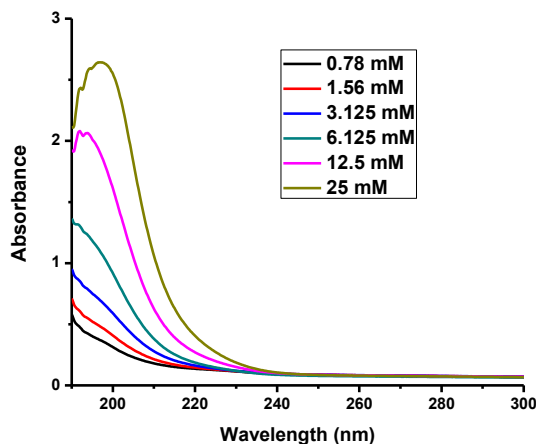


Figure 8. UV spectrum of reduced glutathione (GSH) recorded in aqueous solution.

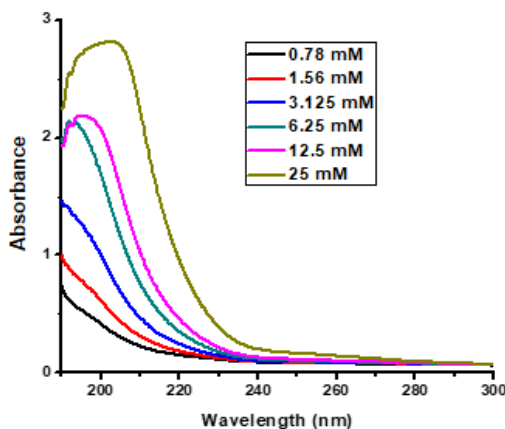


Figure 9. UV spectrum of oxidized glutathione (GSSG) recorded in aqueous solution.

Glutathione exhibits an UV absorption maximum at 197 nm. The absorption band corresponds the $n \rightarrow p^*$ electronic transitions in the carboxyl and the amide bonds. GSSG has got very similar UV spectrum with an absorption maximum of 202 nm.

6.2. NMR Spectroscopy

NMR spectroscopy is the most powerful non-destructive analytical technique available for organic structure determination in solution. The method is based on the fact that some atomic nuclei possess a nuclear spin not equal to zero. A nucleus with an odd atomic number or an odd mass number has a nuclear spin. The overall spin of the nucleus is determined by the spin quantum number S . If the numbers of both the protons and neutrons in a given nuclide are even then $S = 0$, i.e., there is no overall spin. Then, just as electrons pair up in nondegenerate atomic orbitals, so do even numbers of protons or even numbers of neutrons giving zero overall spin. When the number of protons or neutrons or both of them are uneven, however, the nucleus has an overall spin. This is because protons and neutrons will have lower energy when their spins are parallel, not anti-parallel [36, 37]. The most commonly used nuclei are summarized in Table 2.

Nuclear spins are oriented randomly in the absence of an external magnetic field but have a specific orientation in the presence of an external field, \mathbf{B} . Some nuclear spins are aligned parallel to the external field, which is the more likely, lower energy orientation; some nuclear spins are aligned antiparallel to the external field, which is the less likely, higher energy orientation.

Table 2. Characteristics of the most common NMR active nuclei

Nuclei	Unpaired protons	Unpaired neutrons	Net spin	γ (MHz/T)
^1H	1	0	1/2	42.58
^2H	1	1	1	6.54
^{13}C	0	1	1/2	10.71
^{14}N	1	1	1	3.08
^{19}F	1	0	1/2	40.08
^{23}Na	1	2	3/2	11.27
^{31}P	1	0	1/2	17.25

When nuclei that are aligned parallel with an external magnetic field are irradiated with the proper frequency (ν) of *electromagnetic radiation* (radiofrequency range), the energy is absorbed and the nuclei “spin-flips” to the higher-energy antiparallel alignment. The frequency (ν) depends on the *gyromagnetic ratio* (γ) of the particle (5).

Nuclei that undergo “spin-flips” in response to the applied radiation are said to be in resonance with the applied radiation - *nuclear magnetic resonance*. The frequency necessary for the resonance depends on the strength of the external field (\mathbf{B}) and the identity (γ) of the nuclei

$$\nu = \gamma B \quad (5)$$

where ν is the frequency of electromagnetic radiation (Hz), γ is the gyromagnetic ratio (MHz/T), and B is the magnetic field strength (T).

If the oriented nuclei are exposed to radiofrequency pulses (generated by the spectrometer console) one will be able to gain information about the magnetic and chemical environment of the studied nuclei. Nuclei are surrounded by electrons that shield them from the external field. Circulating electrons create an induced magnetic field that opposes the external magnetic field. Accordingly, each nucleus with different molecular environment has a different effective magnetic field and resonates with photons of different energy (frequency).

According to the above equation, the energy difference ($\Delta E = h\nu$) between nuclear spin states depends on the strength of the applied magnetic field (B). Consequently, the higher the magnetic field strength, the higher the resolution of two nuclei with similar ΔE value. This relationship could make it difficult to compare NMR spectra taken on spectrometers operating at different field strengths. The term *chemical shift* was developed to avoid this problem.

The chemical shift of a nucleus is the difference between the resonance frequency of the nucleus and a standard, relative to the standard. This quantity is reported in ppm and given the symbol delta (δ).

$$\delta = (\nu - \nu_{\text{REF}}) \times 10^6 / \nu_{\text{REF}}$$

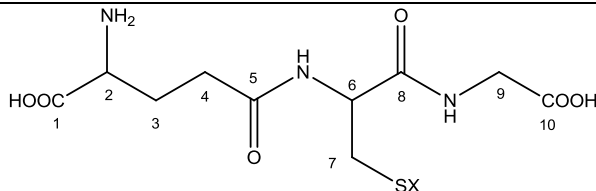
where δ is the chemical shift (ppm), ν is the resonance frequency of the nucleus (Hz), and ν_{REF} is the resonance frequency of the reference (Hz).

In ^1H NMR spectroscopy, this standard is often tetramethylsilane, $\text{Si}(\text{CH}_3)_4$, abbreviated as TMS. The chemical shift is a very precise metric of the chemical environments around a nucleus.

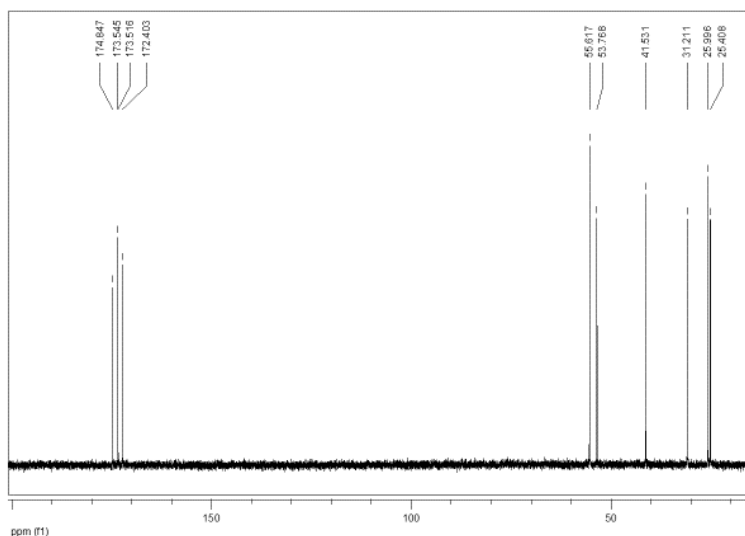
Nuclei experiencing the same chemical environment or chemical shift are called *equivalent*. Those nuclei experiencing different environments or having different chemical shifts are *nonequivalent*. Nuclei that are close to one another exert an influence on each other's effective magnetic field. This effect shows up in the NMR spectrum when the nuclei are nonequivalent. If the distance between the non-equivalent nuclei is less than or equal to three bond lengths, this effect is observable. This effect is called spin-spin coupling or *J coupling*.

The difference in ΔE of nonequivalent nuclei originated from the spin-spin coupling results in *splitting* of the NMR signal. If a ^1H signal is split by N equivalent protons, it is split into $N + 1$ peaks. (The $N+1$ rule). The value (given in Hz) of the vicinal ^1H - ^1H splitting (^3J -coupling) is related to the dihedral torsion angle of the two protons (Karplus equation) [39].

Table 3. ^1H -NMR (500 MHz) data of reduced (GSH) and oxidized (GSSG) glutathione recorded in D_2O

		
Proton (Number of protons)	GSH	GSSG
H-3 (2H)	2.17 ppm	2.15 ppm
H-4 (2H)	2.56 ppm	2.52 ppm
H-7a (1H)	2.94 ppm	2.96 ppm (9.5, 14.2 Hz)
H-7b (1H)	2.94 ppm	3.26 ppm (4.5, 14.2 Hz)
H-2 (1H)	3.83 ppm	3.81 ppm
H-9 (2H)	3.98 ppm	3.96 ppm
H-6 (1H)	4.56 ppm	4.74 ppm

The methyl proton of the glutamate moiety (H-2) gives a doublet-of-doublets at 3.83 ppm, and the methylene protons - H-3 and H-4 - give two separate multiplets at 2.17 and 2.56 ppm, respectively. The methylene (H-7) and the methyne (H-6) protons of the cysteinyl moiety forms an AA'X spin system with three doublet-of-doublets at 2.94 (H-7) and 4.56 (H-6) ppm. The methylene protons of the glycine moiety (H-9) appear a singlet at 3.98 ppm. The respective protons in the oxidized glutathione (GSSG) show similar chemical shifts and multiplicity as those of the respective protons in the reduced form (GSH).

Figure 12. ^{13}C -NMR (125 MHz) spectrum of reduced glutathione (GSH) recorded in D_2O .

The one-dimensional ^{13}C NMR spectra with broadband proton decoupling of reduced (GSH) and oxidized (GSSG) glutathione are shown in Figure 12 and Figure 13, respectively. (The spectra were recorded with a Bruker Avance III 500 (125.04 MHz for ^{13}C) spectrometer. Measurements were run at a probe temperature of 298 K in D_2O solutions.) The spectroscopic data are summarized in Table 4.

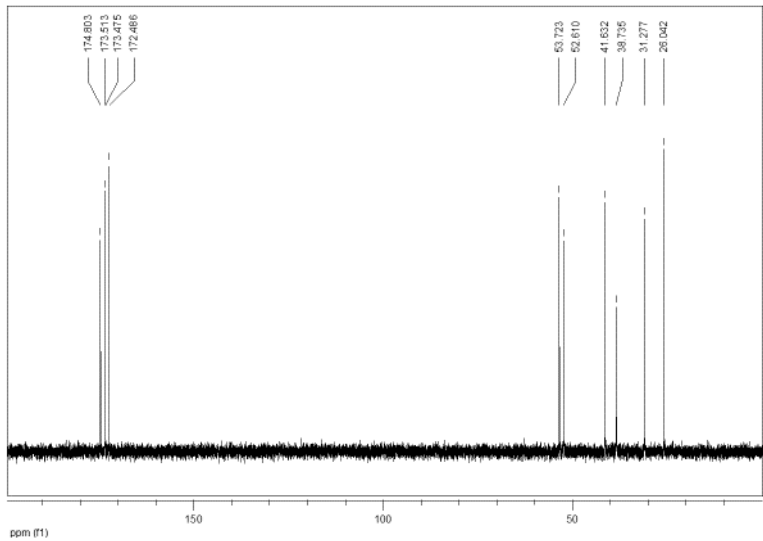


Figure 13. ^{13}C -NMR (125 MHz) spectrum of oxidized glutathione (GSSG) recorded in D_2O .

Table 4. ^{13}C -NMR (125 MHz) data of reduced (GSH) and oxidized (GSSG) glutathione recorded in D_2O

Carbon	GSH	GSSG
C-1	173.52 ppm	173.48 ppm
C-2	53.77 ppm	53.72 ppm
C-3	26.00 ppm	26.04 ppm
C-4	31.21 ppm	31.28 ppm
C-5	173.55 ppm	173.51 ppm
C-6	55.62 ppm	52.61 ppm
C-7	25.41 ppm	38.74 ppm
C-8	172.40 ppm	172.49 ppm
C-9	41.53 ppm	41.63 ppm
C-10	174.85 ppm	174.80 ppm

7. ACID-BASE PROPERTIES

7.1. Acid-Base Theories

Definition of acids and bases has been altered several times. One of the first classification of acids and bases was made by Arrhenius (1888). In Arrhenius's definitions, an *acid* is any substance that, when dissolved in water, increases concentration of the hydrogen (hydronium) ions, while a *base* is any substance that, when dissolved in water, increases concentration of the hydroxide ions [41].

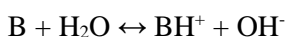
J. N. Brønsted and T. M. Lowry extended the acid-base theory of Arrhenius and emphasized the role of hydrogen ion (proton) in the acid-base reactions. According to the Brønsted and Lowry theory, an *acid* is a species that donates a proton to another species in a proton-transfer reaction. They defined a *base* as a species that accepts a proton in a proton-transfer reaction [41].

According to their theory, acids are converted into a base by releasing a proton and a base is transformed to an acid by accepting a proton. (See examples below.) An acid donates a proton only in the presence of a proton acceptor base. Accordingly, conversion of an acid to the respective base and conversion of a base to its respective acid takes place in the same reaction.

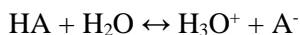
G. N. Lewis realized that the concept of acids and bases could be generalized to include reactions (e.g., reaction of acidic and basic oxides) that do not fit either the Arrhenius or the Brønsted-Lowry concepts [42]. According to this theory, a Lewis acid is a species (atom, molecule, or ion) that can form a covalent bond by accepting a pair of electrons from another species, while a Lewis base is a species (atom, molecule, or ion) that can form a covalent bond by donating an electron pair to another species.

7.2. The Importance of Acid-Basic Properties in Drugs Development

In any protonation process, one positive charge is transferred to the base. Therefore, the proton transfer affects the physico-chemical properties such as charge, solubility, polarizability, and dipole of the base (B or A⁻) [43]. Most of the present-day drug molecules are acids or bases. When they are dissolved in water, they can undergo proton transfer reactions of different degree.



and



where B is a monoprotic base, HA is a monoprotic acid

The reactions are reversible, and the composition of the equilibrium can be characterized by the pK_a value of the equilibrium (the ionization constant of the molecule). While analyzing acid-base properties of 907 drug molecules, it was found that 64% of these compounds contained an ionizable group. Within this group of ionizable compounds, 34% contained a single basic group while 20% contained a single acidic functional group [44]. Focusing on oral drugs showed that 78.6% of compounds contained an ionizable group, while 11.9% were neutral, 4.3% always ionized and the remainder (5.2%) was made up of salts, miscellaneous compounds (e.g., mixtures) and high molecular weight substance [45].

Efforts to determine the physicochemical properties that relate to long-term compound viability have been conducted in concert with gathering biology data on attributes such as cell toxicity, efflux liability, metabolic stability or inhibition, cell permeability, bioavailability, CNS permeability, protein binding, brain tissue binding, promiscuity, clearance and volumes of distribution. Among them, the charge state of the molecules turned to be one of the fundamental physico-chemical properties. Accordingly, the acid/base properties of a molecule are among the most fundamental ones for drug actions [45, 46].

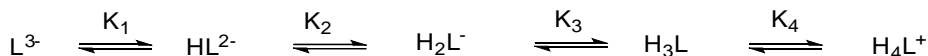
7.3. Glutathione - Acid-Basic Properties

Dissociation constants of weak acids are commonly evaluated by analyzing their titration curves. The titration curves of monoprotic acids can be analyzed conveniently on the basis of Henderson-Hasselbalch equation using different techniques e.g., potentiometry, UV/VIS spectroscopy, HPLC, NMR spectroscopy, conductometry, calorimetry, capillary zone electrophoresis, and computational methods [47]. On the other hand, the pK_a values of polyprotic acids are evaluated with great difficulty using software methods involving complex algebraic calculations and approximate formulae [48].

The acid-base chemistry of small organic molecules is usually characterized in terms of macroscopic acid dissociation/protonation constants obtained from pH-titration data. If the molecule contains two or more functional groups of comparable acidity, the pH ranges for titration of the two groups overlap and the titration can occur by two independent pathways. In such cases, the macroscopic constants are composites of the microscopic constants that describe the acid-base chemistry at the molecular level. One of the widely used methods for determining microscopic acid dissociation constants of such molecules is NMR spectroscopy [49]. Considering the number of ionizable functions of a molecule, in the case of two (e.g., morphine; phenolic OH-tertiary N) there are two macroscopic protonation constants and four microspecies with different protonation state. In the case of

three ionizable groups (e.g., thyroxine; phenolic OH-amino-carboxyl), the number of macroscopic protonation constants is 3 and the number of different microspecies is 8. These figures in the case of a compound with four ionizable groups (e.g., glutathione) are 4 and 16, respectively [50].

The acid-base properties of glutathione (GSH) have long been in the focus of scientific interest. It has three acidic (thiol, glycyl carboxyl, glutamyl carboxyl) and one basic (amino) functional groups. Accordingly, in aqueous solution glutathione can exist in five different macroscopic protonation state as follows.



where L^{3-} is the fully deprotonated glutathione, H_4L^+ is the fully protonated glutathione.

Since the HL^{2-} and the H_3L forms have 4 protonation isomers (microspecies) each, and the H_2L^- form has 6 microspecies, the molecule has got altogether 16 different protonation states (microspecies) [50].

The micro- and sub-micro protonation constants characterize the acid-base properties at the submolecular level [51]. These constants allow quantification of the proton binding capacity of submolecular basic units, when the protonation states of all other sites are defined in the molecule [52]. Group constants are special micro-constants, when the rest of the groups in the molecule are far enough apart and their protonation does not affect the basicity of the group [53]. The rotational state of the flexible parts of the molecules is defined by the sub-micro constants, when protonation occurs [54]. The correct characterization of basicity of the sites of protonation of multidentate ligands can be done using the micro and sub-micro constants. In addition, this group of constants is used to measure the concentration of different forms of protonation, of which the principal form is not always the reactive form in chemical and biological processes. [55-59]. The macroscopic protonation constants (K_1 - K_4) determined by ^1H NMR-pH titrations were as follows: $\log K_1$ 9.65; $\log K_2$ 8.78; $\log K_3$ 3.52; $\log K_4$ 2.22 [50].

The obtained values were found to be very similar to those determined in earlier works of Pirie and Pinhey [60] (9.62, 8.66, 3.53, 2.12), Li et al. [61] (9.65, 8.75, 3.59), and Martin and Edsall [62] (9.62, 8.74). The results demonstrated that the first and the second protonation constants were predominated by the overlapping protonation of the amino and the thiolate site, the amino being typically more favored. The carboxylate groups also protonated in an overlapping fashion, the glycyl carboxylate being the more basic. It is worth mentioning, that it is the protonated amino group that makes the inherently more basic glutamyl carboxylate more acidic [50].

It is important to note that the physico-chemical properties (e.g., complex formation, nucleophilic reactivity, redox properties) and biological functions of glutathione could be significantly different in different protonation states (i.e., in solutions with different pH

values) [63-66]. Furthermore, ionic strength and the nature of the ionic media also affect the acid-base characteristics of glutathione [69].

8. REDOX PROPERTIES

8.1. Redox Potentials

Redox reactions involve an electron transfer from one particle onto another. *Oxidation* means a half-reaction in which a substance (atomic, ionic or molecular) releases electron(s). In the *reduction* half-reaction electron(s) is/are accepted. Thus, oxidation and reduction are antiparallel and simultaneously occurring electron-transfer processes. In organic and biochemical reactions oxidation is frequently accompanied by gaining oxygen or losing hydrogen atoms; while reduction is manifested as losing oxygen or gaining hydrogen atoms.

Half-cell potentials of reversible redox systems can be calculated according to the *Nernst* equation, of which form referring to 25°C as follows:

$$E = E^{\circ} - \frac{RT}{nF} \ln \frac{[red]}{[ox]} \quad (6)$$

where E is the actual redox potential (V), E° is the standard redox potential (V), R is the gas constant ($8.314 \text{ J mol}^{-1} \text{ K}^{-1}$), T is the temperature (K), n is the number of transferred electrons (per particle), F is the Faraday constant (96485 C), and

$[red]$ = concentration (activity) of the reduced form of the redox system (mol/dm^3).

$[ox]$ = concentration (activity) of the oxidized form of the redox system (mol/dm^3).

The direction of flow of electrons in a spontaneous redox reaction can be determined by comparison of the electrode and/or redox potentials of the reversible redox systems (ox_1/red_1 and red_2/ox_2) of the reactions.



When $E(red_1/ox_1) > E(red_2/ox_2)$ the direction of a spontaneous redox reaction corresponds to the above generalized chemical reaction. In other words, in spontaneous redox reaction the redox system with the more positive potential oxidizes the more negative one. The redox system with the more negative potential reduces the more positive one.

Redox potentials of reversible redox systems can only be determined by measurements of potential differences. At first, the redox potentials were determined against the potential

of the *standard hydrogen electrode* (SHE) - with 1 M hydronium ion (H_3O^+) concentration (activity) and 1 atmosphere of hydrogen (H_2) gas pressure on it - of which potential was arbitrary set to be zero ($E^\circ = 0.00 \text{ V}$). The standard redox potential of the hydrogen is zero at pH 0 (1 M H_3O^+), however, for biologic systems, the biologic (apparent) half-cell redox potential (E'°) is normally expressed at pH 7 [70].

8.2. The Glutathione (GSH) and Glutathione Disulfide (GSSG) Reversible Redox System - Chemistry

Although the importance of the GSH/GSSG redox system in biological redox processes has been long recognized, there is some uncertainty as to its half-cell potential. This is because direct measurement of the GSH/GSSG redox system (and another thiol/disulfide redox systems) by standard electrochemical methods is not possible due to formation of stable metal-thiolate complexes at the electrode surfaces. Thus, the redox potentials of GSH and other thiols can only be determined indirectly by measurement of equilibrium constants for their reaction with redox systems of known redox potentials. Willis et al. reported the E'° of the GSSG/GSH half-cell potential to be -0.263 V (pH 7, 298 K, 0.1 M phosphate buffer) determined by ^1H NMR method [71].

According to the second law of thermodynamics, the criterion for spontaneous change and equilibrium in a closed system with a single chemical reaction at constant temperature and pressure is given by the reaction Gibbs energy ($\Delta_r G$). Gibbs energy is a state function, meaning that the change in Gibbs energy, when a system changes state, is independent of the path from the initial to the final state. This means that the standard reaction Gibbs energy ($\Delta_r G^\circ$) of a given reaction is the same whether it takes place in one or more steps. It follows that

$$\Delta_r G^\circ = \sum \Delta_f G^\circ \quad (8)$$

where $\Delta_r G^\circ$ is the standard reaction Gibbs energy, $\Delta_f G^\circ$ is the standard Gibbs energy of formation.

The standard reaction Gibbs energy of a reaction is related to its equilibrium constant K by

$$\Delta_r G^\circ = -RT \ln K \quad (9)$$

where $\Delta_r G^\circ$ is the standard reaction Gibbs energy, R is the gas constant, T is the temperature (K), K is the equilibrium constant.

This relation, which follows from the fact that at equilibrium $\Delta_r G=0$, enables derivation of $\Delta_r G^\circ$ from experimentally measured K . The *standard reaction Gibbs energy* of a reaction could theoretically be derived, by experimentally measuring the concentration of all reactants at equilibrium and plugging the above equation. It frequently occurs, however, that the reactants have ionizable functional groups. In such cases, if the equilibrium is set at a pH near their pK_a values, several ionic species of the reactants may be present. Different species of the same reactant have different standard Gibbs energies of formation [70].

Accordingly, using the different species of reactant concentrations in equation (9), it gives neither the standard reaction Gibbs energy nor the equilibrium constant K . Instead, it gives what is known as *standard transformed reaction Gibbs energy* ($\Delta_r G'^\circ$) and *apparent equilibrium constant* (K'). Accordingly, in a closed system with a single biochemical reaction at constant temperature and pressure, and specified pH, the criterion for spontaneous change and equilibrium is given by the transformed reaction Gibbs energy

$$\Delta_r G' \leq 0 \quad (10)$$

To date, the most comprehensive tables of estimated $\Delta_r G'^\circ$ values for biochemical compounds were compiled by Alberty [72, 73].

It is the importance of knowledge of standard transformed Gibbs energies of formation of reactants that they can be used to calculate standard apparent reduction potentials (E'°) at specified pH and ionic strength. Conversely, standard apparent reduction potentials at specified pH can be used to calculate standard transformed Gibbs energies of formation of one or two reactants in the half reaction [74]. The calculated standard apparent (biochemical) reduction potentials (E'°) of some biochemically important reversible redox systems (pH 7, T=298.15 K, ionic strength = 0.25 M) are listed in Table 5.

Table 5. Calculated standard apparent reduction potentials (pH 7, 298.15 K, 0.25 M ionic strength) of some biochemically important reversible redox systems [75]

System	E'° (V)
$O_2(aq) + 4 H^+ + 4 e^- = 2 H_2O$	+0.849
$O_2(aq) + 2 H^+ + 2 e^- = H_2O_2$	+0.357
Cytochrome c(Fe^{3+}) + e^- = Cytochrome c(Fe^{2+})	+0.212
Glutathione(ox) + $2 H^+ + 2 e^-$ = Glutathione(red)	-0.288
Thioredoxin(ox) + $2 H^+ + 2 e^-$ = Thioredoxin (red)	-0.289
$NAD^+(ox) + H^+ + 2 e^-$ = NADH(red)	-0.316
$NADP^+(ox) + H^+ + 2 e^-$ = NADPH(red)	-0.317
Cystine + $2 H^+ + 2 e^-$ = 2 Cysteine	-0.363
$2 H^+ + 2 e^- = H_2(g)$	-0.423

The pH dependent half-cell reduction potential of the GSH/GSSG reversible redox system draws attention to the reduction potentials of the variously protonated microspecies existing under different acid-base conditions. By means of determination of the species-specific protonation constants, and the conditional equilibrium constants of the pH-dependent redox equilibria, the standard redox potentials of six biogenic thiols were determined by ^1H NMR method [76]. It was found, that that even minor changes in the sites of protonation could lead to differences in redox characteristics. Furthermore, not only the protonation of the thiolate itself, its protonation fraction, and the concomitant redox behavior found to be sensitive to minor pH changes, but the protonation status of the adjacent basic moieties could also influence the redox behavior by various inductive effects on the thiolate moiety. The highest thiolate oxidizability of GSH (-383 mV) belonged to the microspecies in which all other basic sites in the molecule were in non-protonated form. The easiest reducibility of GSSG (-325 mV) was born by the microspecies of complete amino and carboxylate protonation. The correlation between the thiolate basicity and the standard redox potentials verified the previous claims that thiolate basicity and oxidizability are proportional parameters [76].

8.3. The Glutathione (GSH) and Glutathione Disulfide (GSSG) Reversible Redox System – Biological Implications

The glutathione (GSH) and glutathione disulfide (GSSG) reversible redox system



is crucially participating and having a vital role in maintaining the environment of the intracellular redox system, antioxidant defense system, and cellular signaling processes [77-82].

The intracellular concentration of GSH is quite high and ranges from approx. 0.5 to 15 mM. The concentration of GSSG is usually several orders of magnitude lower [80, 83]. The reduced form (GSH) is a key contributor to the cellular antioxidant defense system and to maintaining the intracellular redox milieu for the preservation of the thiol-disulfide redox states of proteins. In general, disruption in homeostasis of the cellular redox system will influence the normal physiology of cells such as differentiation, proliferation, cell signaling and programmed cell death [82, 84]

There are several redox couples in a cell that work together to maintain the redox environment, being the GSSG/2GSH couple the most abundant one in a cell. Within mammalian cells, glutathione exists mainly (98%) in the thiol-reduced form (GSH), whereas glutathione disulfide (GSSG) is usually less than 1% of GSH [85]. Its reduced form is largely maintained by the NADPH-dependent glutathione reductase [86]. The

average cellular concentration of glutathione and NADPH are about 5 mM, and 0.1 mM, and the half-cell reduction potential (E'_0) of GSSG/2GSH and NADP/NADPH, (pH 7.0), are reported to be -288 mV and -317 mV, respectively (Table 5).

The GSH/GSSG ratio is a critical mechanism for cell survival; in fact, it is known that it varies in association with proliferation, differentiation, and apoptosis [87]. As a result, the GSH/GSSG ratio is considering as a most common biomarker for the detection of cellular oxidative stress [84, 88, 89].

Shafer and Buettner pointed to the important feature of the cellular redox homeostasis [85]. They defined the term *cellular redox environment*, which is the summation of the products of the reduction potential and reducing capacity of the linked redox couples present in a biological fluid, organelle, cell or tissue. The *redox state* (E_{hc}) of a redox couple is defined by the half-cell reduction potential and the reducing capacity of that couple. In contrast to many other physiological redox systems, the redox state of the GSSG/GSH system not only depends on the GSH/GSSG ratio, the temperature and the pH, but also on the actual concentration of glutathione. This is in contrast with the NAD(P)⁺/NAD(P)H couples, where only the ratio of the interconvertible oxidized and reduced forms of these redox couples is enough.

Both GSH and GSSG concentrations depend on the subcellular compartment, the cell type and the organism. Accordingly, the redox potential of the GSH/GSSG system varies from tissue to tissue, from organism to organism. This relays on the proportion of GSH and GSSG, and the total concentration of glutathione, which (their actual *in vivo* concentration and ratio) is quite difficult to estimate [80, 90]. For example, taking the local pH and GSH/GSSG ratios into consideration, cytosolic $E_{pH7.0} = -289$ mV (or even lower), mitochondrial matrix $E_{pH7.0} = -296$ mV (or even lower), and human plasma $E_{pH7.4} = -118$ mV half-cell reduction potentials have been estimated [86]. Furthermore, correlation has been found between the cell cycle, the condition of the cell (stressed, apoptotic, etc.), and the GSH/GSSG ratio. For instance, in cell proliferation ($E_{hc} = \sim -240$ mV), in cell differentiation ($E_{hc} = \sim -200$ mV), and in apoptosis ($E_{hc} = \sim -170$ mV), which can be applicable for a better understanding of cellular oxidative stress [82, 91].

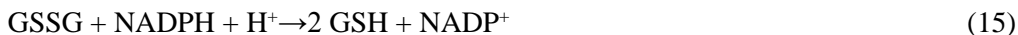
Furthermore, glutathione reversibly reacts with sulfhydryl group (SH) of thiol-containing proteins modifying them into an active or inactive form, in a process, which is known as S-glutathionylation. The aim of this alteration is for the protection of the sensitive thiol-containing proteins from irreversible oxidation. In the end, the process of S-glutathiolation (also called S-glutathionylation) affects the activity of proteins and the cellular signaling process, in both ways; regulation or deregulation [79].

In the case of an oxidative challenge, interaction of GSSG with reactive cysteine residues of proteins to form mixed disulfides can occur [92]. By means of such thiol-disulfide exchange, the oxidized form of glutathione (GSSG) can react with thiol-containing proteins to form glutathione-protein disulfides (Pr-SSG) (12) or protein disulfides (Pr-SS-Pr) (13) [90]. The GSH/GSSG redox regulation of proteins happens

under circumstances of enzymatic actions and metabolic systems to control the exchange reaction and to sustain the proportion of GSH/GSSG [80].



Oxygen, as a natural electron acceptor, is a reactive molecule altering redox states of cellular compartments. The cellular antioxidant defense system maintains reduced redox environment *via* modifying ROS to less harmless molecules [93]. Glutathione (GSH), being cosubstrate of GSH peroxidase (EC 1.11.1.9), takes part in elimination of hydrogen peroxide (H_2O_2) (14). The formed GSSG can be reduced back to GSH by the NADPH-dependent GSH reductase (EC 1.8.1.7), maintaining the physiological redox environment of the cell (15). This GSH redox cycle is the major mechanism of the maintenance of the cellular GSH homeostasis during oxidant challenge that occurs in the case of peroxide exposure [91].



8.4. Oxidation Reactions of GSH and Other Cellular Thiols

Both redox reactions and nucleophilic substitution or addition reactions of GSH are associated with the thiol chemistry of its cysteinyl moiety. They do not necessarily require enzyme catalysis to proceed and can occur in aqueous media under a wide range of conditions.

The cysteine side chain, with its high nucleophilic capacity, appears to be the principal target of reactive oxygen and nitrogen species (ROS/RNS) in cells. In the thiolate form, it can react with H_2O_2 to generate a sulfenic acid (RSOH), and this oxidized form can be considered as a central species among thiol modifications. Reaction of GSH with H_2O_2 results in formation of the respective sulfenic acid (RSOH) [94].

The heme-containing enzymes myeloperoxidase (MPO) and lactoperoxidase (LPO) use H_2O_2 to oxidize halides (Cl^- , Br^- and I^-) and thiocyanate (SCN^-) into their respective hypohalous acids (HOXs). These species are more reactive than H_2O_2 and can chemically modify cysteine and methionine residues of peptides and proteins. Thiols can react with HOCl and HOBr *via* formation of a very unstable sulfenyl halide (16, 17), which readily rearranges to sulfenic acid (RSOH) [95]. Otherwise, HOSCN generates a sulfonylthiocyanate (18), which can react with another thiol to yield a disulfide and SCN^- (19) [96]



Nitrogen monoxide (NO), one of the most important RNS, is formed in the nitric oxidesynthase(NOS)-catalyzed oxidation of guanidine moiety of L-arginine. [97]. NO such as carbon monoxide (CO) and dihydrogen sulfide (H₂S) is a small endogenous signaling molecule implicated in several biological processes. NO is a free radical with a relatively long half-life [98], which can freely diffuse across the membranes. The primary targets of NO include the soluble guanylyl cyclase, leading to production of cGMP and thus affecting its downstream targets. NO may also activate or inhibit proteins serving as a signal transducer by promoting S-nitrosylation, tyrosine nitration and binding to metal centers in proteins. The nitrosylation species are generated *via* further oxidation of NO. The main nitrosylation species is N₂O₃, of which formation can be explained by the following series of reactions (20-22).



Reaction of NO with superoxide radical (O₂^{•-}) converts the relatively unreactive NO to peroxynitrous acid (ONOOH). The pK_a value of ONOOH is 6.8 [99], thus it is in equilibrium with its deprotonated form under physiological pH. Both forms are strong oxidant and can be involved in both one- or two-electron oxidations. It can be involved in oxidation of thiols to disulfides (RSSR) and sulfenic acid (RSOH) and S-nitrosylation of thiols, involving GSH [100].

Sulfenic acids (RSOH) are directly formed *in vivo* through oxidation of thiols with hydrogen peroxide or peroxynitrous acid, or alkyl peroxides. Several enzymes form -SOH intermediates during their catalytic cycles [94]. Furthermore, RSOH can be formed by hydrolysis of sulfonyl halides [95], sulfonyl thiocyanates [101], thiosulfinates [102] and S-nitrosothiols [103]. Sulfenic acids can react with thiols to form disulfides (23) and the redox reaction represents an important biological process. The reaction allows recycling of

sulfenic acids since the formed disulfides can be reduced to thiols through the action of cellular reducing agents, such as glutathione (GSH).



Sulfenic acids can be further oxidized to sulfinic acids ($\text{R-SO}_2\text{H}$) in the presence of excess of ROS or RNS. Sulfenic acids are relatively stable species with pK_a values around 2. Thus, they can be found in deprotonated forms under physiological pH [104]. In deprotonated form, the sulfinate group ((R-SO_2^-)) can behave as a soft nucleophile [105] and can react with several electrophilic species such as alkyl halides [106] and α,β -unsaturated aldehydes [107]. Sulfinic acids can be further oxidized to sulfonic acids ($\text{R-SO}_3\text{H}$) but cannot be reduced by thiols. Sulfonic acid represents the highest S-oxidized form of cysteine and no biological pathway is known to reduce it [101].

ACKNOWLEDGMENTS

The present contribution is dedicated to the 650th anniversary of the foundation of the University of Pécs, Hungary. The authors express their special thanks to Professor Tamás Lóránd and Associate Professor Gergely Gulyás (University of Pécs, Institute of Biochemistry and Medical Chemistry) for recording and assistance in interpretation of the IR and the NMR spectra, respectively. The authors express their special thanks to Zsuzsanna Moravec for her skilled assistance in preparation of the manuscript.

REFERENCES

- [1] Alanazi, A. M.; Mostafa, G. A. E.; Al-Badr, A. A. Glutathione. In *Profiles of drug substances, excipients, and related methodologies*. Vol. 40.; Academic Press: Burlington, MA, 2015.; pp 43-158.
- [2] *European Pharmacopeia*, 9th ed.; EDQM: Strasbourg, France, 2016.
- [3] United States Pharmacopoeia, (USP 38, NF 33) *Dietary Supplement Compendium*; The United States Pharmacopoeial Convention: Rockville, MD, 2015.
- [4] Downard, K. *Mass spectrometry: A foundation course*, 1st ed.; The Royal Society of Chemistry: Cambridge, UK 2004; pp 22-66.
- [5] Skoog, D. A.; Holler, F. J.; Crouch, S. R. *Principles of instrumental analysis*, 7th ed.; Cengage Learning: Boston, MA, 2018; pp. 501-536.
- [6] Herbert, C. G.; Johnstone, R. A. W. *Mass spectrometry basics*.; CRC Press: Boca Raton, FL, 2003; pp. 275-286.

- [7] De Hoffmann, E.; Stroobant, V. *Mass spectrometry: Principles and applications*, 3rd ed.; Wiley and Sons: Chichester, UK, 2007; pp 85-174.
- [8] Brunnée, C. The ideal mass analyzer: Fact or fiction? *Int. J. Mass Spectr. Ion Proc.* 1987, 76, 125–237.
- [9] Clark, W. Mass spectrometry in the clinical laboratory: Determining the need and avoiding pitfalls. Chapter 1. pp 1-15. In *Mass spectrometry for the clinical laboratory.*; Nair, H.; Clark, W., Eds.; Academic Press: London, 2017.
- [10] Madeira, P. J. A.; Florencio, M. H. Applications of tandem mass spectrometry: From structural analysis to fundamental studies. In *Tandem mass spectrometry: Applications and principles.*; Jeevan P., Ed.; InTech: Rijeka, Croatia, 2012.; Chapter 1. pp 3-32.
- [11] Feng, S.; Zheng, X.; Wang, D.; Gong, Y.; Wang, Q.; Deng, H. Systematic analysis of reactivities and fragmentation of glutathione and its isomer GluCysGly. *J. Phys. Chem. A.* 2014, 118, 8222–8228.
- [12] Takur, S. S.; Balaram, P. Fragmentation of peptide disulfides under conditions of negative ion mass spectrometry: Studies of oxidized glutathione and contryphan. *J. Am. Mass. Spectrom.* 2008, 19, 358-366.
- [13] Skoog, D. A.; Holler, F. J.; Crouch, S. R. *Principles of instrumental analysis*, 7th ed.; Cengage Learning: Boston, MA, 2018; pp. 389-436.
- [14] Theophanides T. Introduction to infrared spectroscopy. In *Infrared spectroscopy–Materials science, engineering and technology.*; Theophile T., Ed.; InTech: Rijeka, Croatia, 2012.; Chapter 1. pp 1-11.
- [15] Günzler, H.; Gremlich, H.-U. *Infrared spectroscopy: An introduction*. Wiley-VCH: Weinheim, Germany, 2002.
- [16] Roeges, N. P. G. *A Guide to the complete interpretation of infrared spectra of organic structures*. John Wiley and Sons: New York, NY, 1994.
- [17] Clegg, W., Ed. *Crystal structure analysis: Principle and practices*, 2nd ed. IUCr-Oxford University Press: New York, NY, 2009.
- [18] Giacovazzo, C., Ed. *Fundamentals of crystallography*, 3rd ed. IUCr-Oxford University Press: New York, NY, 2011.
- [19] Glusker, J. P.; Lewis, M.; Rossi, M. *Crystal structure analysis for chemists and biologists*. Wiley-VCH: New York, NY, 1994.
- [20] Hammond, C. *The basics of crystallography and diffraction*, 4th ed. IUCr-Oxford University Press: New York, NY, 2015.
- [21] Bruno, I. J.; Cole, J. C.; Kessler, M.; Luo, J.; Motherwell, W. D. S.; Purkis, L. H.; Smith, B. R.; Taylor, R.; Cooper, R. I.; Harris, S. E.; Orpen, A. G. Retrieval of crystallographically-derived molecular geometry information. *J. Chem. Inf. Comput. Sci.* 2004, 44, 2133–2144.

- [22] Müller, P.; Irmer, R. H.; Spek, A. L.; Schneider, T. R.; Sawaya, M. R. *Crystal structure refinement: A crystallographer's guide to SHELXL*. IUCr-Oxford University Press: New York, NY, 2006.
- [23] Napolitano, H. B.; Camargo, A. J.; Mascarenhas, Y. P.; Vencato, I.; Lariucci, C. Análise da difração dos Raios X. *Revista Processos Químicos* [Analysis of X-ray diffraction. *Chemical Processes Journal*]. Goiânia. 2007, 1, 35-45.
- [24] Schwarzenbach, D. *Crystallography*. John Wiley and Sons: Chichester, UK, 1996.
- [25] Shmueli, U. *Theories and techniques of crystal structure determination*. IUCr-Oxford University Press: New York, NY, 2007.
- [26] Spek, A. L. Structure validation in chemical crystallography. *Acta Cryst.* (2009). D65, 148-155.
- [27] Stout, G. H.; Jensen, L. H.; *X-Ray structure determination - A practical guide*, 2nd ed. Wiley-Interscience, New York, NY, 1989.
- [28] Sheldrick, G. M. *The SHELX-97 Tutorial*. 1997.
- [29] Burla, M. C.; Calandro, R.; Carrozzini, B.; Cascarano, G. L.; Cuocci, C.; Giacovazzo, C.; Mallamo, M.; Mazzone, A.; Polidori, G. Crystal structure determination and refinement via SIR2014. *J. Appl. Crystallogr.* 2015, 48, 306–309.
- [30] Dolomanov, O. V.; Bourhis, L. J.; Gildea, R. J.; Howard, J. A. K.; Puschmann, H. OLEX2: A complete structure solution, refinement and analysis program. *J. Appl. Crystallogr.* 2009, 42, 339–341.
- [31] Wright, W. B. The crystal structure of glutathione. *Acta Cryst.* 1958, 11, 632-642.
- [32] Moggach, S. A.; Lennie, A. R.; Morrison, C. A.; Richardson, P.; Stefanowicz, F. A.; Warren, J. E. Pressure induced phase transitions in the tripeptide glutathione to 5.24 GPa: The crystal structure of glutathione-II at 2.94 GPa and glutathione-III at 3.70 GPa. *Cryst. Eng. Commun.* 9, 2010.
- [33] Owen, T. *Fundamentals of UV-visible spectroscopy. A primer*. Hewlett-Packard Co., Germany, 1996.
- [34] Clark, B.J.; Frost, T.; Russell, M.A.; Eds. *UV Spectroscopy. Techniques, instrumentation and data handling.*; Chapman and Hall: London, UK, 1993.
- [35] Skoog, D. A.; Holler, F. J.; Crouch, S. R. *Principles of instrumental analysis*, 7th ed.; Cengage Learning: Boston, MA, 2018; pp. 303-360.
- [36] High Resolution NMR. *Theory and Chemical Applications*. 3rd Edition. D. Becker, Editor. Academic Press, San Diego, CA, 2000.
- [37] Günther, H. *NMR spectroscopy: basic principles, concepts and applications in chemistry*, 3rd ed.; Wiley-VCH: Weinheim, Germany, 2013.
- [38] Hoffman, R. E.; Standardization of chemical shifts of TMS and solvent signals in NMR solvents. *Magn. Reson. Chem.* 2006, 44, 606-616.
- [39] Karplus, M. Vicinal proton coupling in nuclear magnetic resonance. *J. Am. Chem. Soc.* 1963, 85, 2870–2871.

- [40] Sohár, P. *Nuclear magnetic resonance spectroscopy I-III*. CRC Press: Boca Raton, FL, 1983.
- [41] Ebbing, D. D.; Gammon, S. D. *General chemistry*. Houghton Mifflin: Boston, MA, 2009.; pp 624-651.
- [42] Atkins, P. W.; Overton, T. L.; Rourke, J.; Weller, M. T.; Armstrong, F. A. Shriver and Atkins' *Inorganic Chemistry*, 5th ed.; Oxford University Press: Oxford, UK, 2010.; pp 111-146.
- [43] Rajak, S. K.; Islam N.; Ghosh, D. C. Modeling of the chemico-physical process of protonation of molecules entailing some quantum chemical descriptors. *J. Quant. Inform. Sci.* 2011, 1, 87–95.
- [44] Manallack, D. T. The acid-base profile of a contemporary set of drugs: Implications for drug discovery. *SAR QSAR Environ. Res.* 2009, 7-8, 611-655.
- [45] Manallack, D. T.; Prankerd, R. J.; Yuriev, E.; Oprea, T. I.; Chalmers, D. K. The significance of acid/base properties in drug discovery. *Chem. Soc. Rev.* 2013, 42, 485–496.
- [46] Charifson, P. S.; Walters, W. P. Acidic and basic drugs in medicinal chemistry: A perspective. *J. Med. Chem.*, 2014, 57, 9701–9717.
- [47] Pathare, B.; Tambe, V.; Patil, V. A review on various analytical methods used in determination of dissociation constant. *Intl. J. Pharm. Pharm. Sci.* 2014, 6, 26-34.
- [48] Khan, A. S. A. A simple method for analysis of titration curves of polyprotic acids. *Nucleus*. 2014, 51, 448-454.
- [49] Sayer, T. L.; Rabenstein, D. L. Nuclear magnetic resonance studies of the acid-base chemistry of amino acids and peptides. 111. Determination of the microscopic and macroscopic acid dissociation constants of α,ω -diaminocarboxylic acids. *Can. J. Chem.* 1976, 54, 3392-3400.
- [50] Mirzahassemi, A.; Somlyay, M.; Noszál, B. The comprehensive acid–base characterization of glutathione. *Chem. Phys. Lett.* 2015, 622: 50–56.
- [51] Mazák, K.; Noszál, B. Advances in microspeciation of drugs and biomolecules: Species-specific concentrations, acid-base properties and related parameters. *J. Pharm. Biomed. Anal.* 2016, 130, 390-403.
- [52] Bjerrum, N. Dissociation constants of polybasic acids and their application to the calculation of molecular dimensions. *Z. Phys. Chem.* 1923, 106, 219–242.
- [53] Noszál, B. Group constant: A measure of submolecular basicity. *J. Phys. Chem.* 1986, 90, 4104-4110.
- [54] Fujiwara, S.; Ishizuka, H.; Fudano, S. NMR study of amino acids and their derivatives. Dissociation constant of each rotational isomer of amino acids. *Chem. Lett.* 1974, 1281-1284.
- [55] Noszál, B.; Scheller-Krattiger, V.; Martin, R. B. A unified view of carbon bound hydrogen exchange of H(2) in imidazoles and H(8) in purine nucleosides and their metal ion complexes. *J. Am. Chem. Soc.* 1982. 104, 1078–1081.

- [56] Noszál, B.; Rabenstein, D. L. Nitrogen-protonation microequilibria and C(2)-deprotonation microkinetics of histidine, histamine, and related compounds. *J. Phys. Chem.* 1991, 95, 4761–4765.
- [57] Szakács, Z.; Noszál, B. Determination of dissociation constants of folic acid, methotrexate, and other photolabile pteridines by pressure-assisted capillary electrophoresis. *Electrophoresis*. 2006, 27, 3399–3409.
- [58] Orgován, G.; Tihanyi, K.; Noszál, B. NMR analysis, protonation equilibria and decomposition kinetics of tolperisone- *J. Pharm. Biomed. Anal.* 2009, 50, 718–723.
- [59] Tóth, G.; Baska, F.; Schretner, A.; Rácz, Á.; Noszál, B. Site-specific basicities regulate molecular recognition in receptor binding: In silico docking of thyroid hormones. *Eur. Biophys. J.* 2013, 42, 721–730.
- [60] Pirie, N. W.; Pinhey, K. G. The titration curve of glutathione. *J. Biol. Chem.* 1929, 84, 321–333.
- [61] Li, N. C.; Gawron, O.; Bascuas, G. Stability of zinc complexes with glutathione and oxidized glutathione. *J. Am. Chem. Soc.* 1954, 76, 225–229.
- [62] Martin, R. B.; Edsall, J. T. Glutathione: ionization in basic solutions and molecular rearrangement in strongly acid solution. *Bull. Soc. Chim. Biol.* 1958, 40, 1763–1771.
- [63] Noszál, B.; Szakács, Z. Microscopic protonation equilibria of oxidized glutathione. *J. Phys. Chem. B.* 2003, 107, 5074–5080.
- [64] Dorcák, V.; Krężel, A. Correlation of acid–base chemistry of phytochelatin PC2 with its coordination properties towards the toxic metal ion Cd(II). *Dalton Trans.* 2003, 11, 2253–2259.
- [65] Wang, X.; Li, K.; Yang, X. D.; Wang, L. L.; Shen, R. F. Complexation of Al(III) with reduced glutathione in acidic aqueous solutions. *J. Inorg. Biochem.* 2009, 103, 657–666.
- [66] Mah, V.; Jalilehvand, F. Mercury(II) complex formation with glutathione in alkaline aqueous solution. *J. Biol. Inorg. Chem.* 2008, 13, 541–553.
- [67] Madej, E.; Wardman, P. The oxidizing power of the glutathione thiyl radical as measured by its electrode potential at physiological pH. *Arch. Biochem. Biophys.* 2007, 462, 94–102.
- [68] Gough, J. D.; Lees, W. J. Effects of redox buffer properties on the folding of a disulfide-containing protein: Dependence upon pH, thiol pK_a , and thiol concentration. *J. Biotechnol.* 2005, 115, 279–290.
- [69] Cigala, R. M.; Crea, F.; De Stefano, C.; Lando, G.; Milea, D.; Sammartano, S. Modeling the acid–base properties of glutathione in different ionic media, with particular reference to natural waters and biological fluids. *Amino Acids*. 2012, 43, 629–648.
- [70] Atkins, P.; De Paula, J. Atkins' *Physical Chemistry*, 9th ed.; Oxford University Press: Oxford, UK, 2010.; pp 156–245.

- [71] Willis, K. K.; Weaver, K. H.; Rabenstein, D. L. Oxidation/reduction potential of glutathione. *J. Org. Chem.* 1993, 58, 4144-4146.
- [72] Alberty, R. A. *Thermodynamics of biochemical reactions*; Wiley-Interscience: Hoboken, NJ, 2003.
- [73] Alberty, R. A. *Biochemical thermodynamics: Applications of Mathematica.*; Wiley-Interscience: Hoboken, NJ, 2006.
- [74] Alberty, R. A. Calculation of standard transformed formation properties of biochemical reactants and standard apparent reduction potentials of half reactions. *Arch. Biochem. Biophys.* 1998, 358, 25-39.
- [75] Alberty, R. A. Standard apparent reduction potentials of biochemical half reactions and thermodynamic data on the species involved. *Biophys. Chem.* 2004, 111, 115-122.
- [76] Mirzahassemi, A.; Noszál, B. Species-specific standard redox potential of thiol-disulfide systems: A key parameter to develop agents against oxidative stress. *Sci. Rep.* 2016, 6, 37596.
- [77] Meng, D.; Zhang, P.; Zhang, L; Wang, H.; Ho, C.-T.; Li, S.; Shahidi, F.; Zhao, H. Detection of cellular redox reactions and antioxidant activity assays. *J. Funct. Foods.* 2017, 37, 467-479.
- [78] Fraternale, A.; Paoletti, M. F.; Casabianca, A.; Nencioni, L.; Garaci, E.; Palamara, A. T.; Magnani, M. GSH and analogs in antiviral therapy. *Mol. Asp. Med.* 2009, 30, 99-110.
- [79] Lu, S. C. Glutathione synthesis. *Biochim. Biophys. Acta.* 2013, 1830, 3143-3153.
- [80] Kojer, K.; Bien, M.; Gangel, H.; Morgan, B.; Dick, T. P, Riemer, J. Glutathione redox potential in the mitochondrial intermembrane space is linked to the cytosol and impacts the Mia40 redox state. *EMBO J.* 2012, 31, 3169-82.
- [81] Dalton, T. P.; Chen, Y.; Schneider S. N.; Nebert, D. W.; Shertzer, H. G. Genetically altered mice to evaluate glutathione homeostasis in health and disease. *Free Rad. Biol. Med.* 2004, 37, 1511-1526.
- [82] Jones, D. P. Redox potential of GSH/GSSG couple: Assay and biological significance; In *Methods in Enzymology*, Vol. 348; Sies H.; Lester Packer, L. Eds.; Academic Press: San Diego CA, 2002; pp 93-112.
- [83] Kalinina, E. V.; Chernov, N. N.; Novichkova, M. D. Role of glutathione, glutathione transferase, and glutaredoxin in regulation of redox-dependent processes. *Biochemistry (Moscow)* 2014, 79, 1562-1583.
- [84] Giustarini, D.; Colombo, G.; Garavaglia, M. L.; Astori, E.; Portinaro, N. M.; Reggiani F.; Badalamenti, S.; Aloisi, A. M.; Santucci, A.; Rossi, R.; Milzani, A.; Dalle-Donne, I. Assessment of glutathione/glutathione disulphide ratio and S-glutathionylated proteins in human blood, solid tissues, and cultured cells. *Free Rad. Biol. Med.* 2017, 112, 360-375.

- [85] Schafer, F. Q.; Garry R. Buettner, G. R. Redox Environment of the cell as viewed through the redox state of the glutathione disulfide/glutathione couple. *Free Rad. Biol. Med.* 2001, 30, 1191–1212.
- [86] Deponte M. Glutathione catalysis and the reaction mechanisms of glutathione-dependent enzymes. *Biochim. Biophys. Acta.* 2013, 1830, 3217–3266.
- [87] Moran, L. K.; Gutteridge, J. M. C.; Quinlan, G. J. Thiols in cellular redox signalling and control. *Curr. Med. Chem.* 2001, 8, 763 – 772.
- [88] Owen, J. B.; Butterfield, D. A. Measurement of oxidized/reduced glutathione ratio. *Methods Mol. Biol.* 2010, 648, 269–277.
- [89] Colombo, G.; Dalle-Donne, I.; Giustarini D.; Gagliano, N.; Portinaro, N.; Colombo, R.; Rossi, R.; Milzani, A. cellular redox potential and hemoglobin S-glutathionylation in human and rat erythrocytes: A comparative study. *Blood Cells Mol. Dis.* 2010, 44, 133–39.
- [90] López-Mirabal, H. R.; Winther, J. R. Redox characteristics of the eukaryotic cytosol. *Biochim. Biophys. Acta – Mol. Cell Res.* 2008, 783, 629–640.
- [91] Aw, T. Y. Cellular redox: A modulator of intestinal epithelial cell proliferation. *Physiology* 2003, 18, 201–204.
- [92] Dalle-Donne, I.; Rossi, R., Giustarini, D., Colombo, R.; Milzani, A. S-glutathionylation in protein redox regulation. *Free Rad. Biol. Med.* 2007, 43, 883–898.
- [93] Aon, M. A., Cortassa, S.; Maack, C.; O'Rourke, B. Sequential opening of mitochondrial ion channels as a function of glutathione redox thiol status. *J. Biol. Chem.* 2007, 282, 21889–21900.
- [94] Lim, J. C.; You, Z.; Kim, G.; Levine, R. L. Methionine sulfoxide reductase A is a stereospecific methionine oxidase. *Proc. Natl. Acad. Sci. USA*, 2011, 108, 10472–10477.
- [95] Nagy, P., Ashby, M. T. Reactive sulfur species: Kinetics and mechanisms of the oxidation of cysteine by hypohalous acid to give cysteine sulfenic acid. *J. Am. Chem. Soc.* 2007, 129, 14082–14091.
- [96] Ashby, M. T.; Aneetha, H. Reactive sulfur species: Aqueous chemistry of sulfenyl thiocyanates. *J. Am. Chem. Soc.* 2004, 126, 10216–10217.
- [97] Alderton, W. K.; Cooper, C. E.; Knowles, R. G. Nitric oxide synthases: structure, function and inhibition. *Biochem. J.* 2001, 357, 593–615.
- [98] Pacher, P.; Beckman, J. S.; Liaudet, L. Nitric oxide and peroxynitrite in health and disease. *Physiol. Rev.* 2007, 87, 315–424.
- [99] Kissner, R.; Nauser, T.; Bugnon, P.; Lye, P. G.; Koppenol, W. H. Formation and properties of peroxynitrite as studied by laser flash photolysis, high-pressure stopped-flow technique, and pulse radiolysis. *Chem. Res. Toxicol.* 1997, 10, 1285–1292.

- [100] Van der Vliet, A.; Hristova, M.; Cross, C. E.; Eiserich, J. P.; Goldkorn, T. Peroxynitrite induces covalent dimerization of epidermal growth factor receptors in A431 epidermoid carcinoma cells. *J. Biol. Chem.* 1998, 273, 31860-31866.
- [101] Lo Conte, M.; Carroll, K. S. The chemistry of thiol oxidation and detection. In *Oxidative stress and redox regulation*; Jakob, U.; Reichmann, D., Eds.; Springer: Dordrecht, 2013; pp 1-42.
- [102] Nagy, P.; Ashby, M. T. Reactive sulfur species: Kinetics and mechanisms of the oxidation of cysteine by hypohalous acid to give cysteine sulfenic acid. *J. Am. Chem. Soc.* 2007, 129, 14082-14091.
- [103] Percival, M. D.; Ouellet, M.; Campagnolo, C.; Claveau, D.; Li, C. Inhibition of cathepsin K by nitric oxide donors: evidence for the formation of mixed disulfides and a sulfenic acid. *Biochemistry.* 1999, 38, 13574-13583.
- [104] Burkhard, R. K.; Sellers, D. E.; DeCou, F.; Lambert, J. L. The pKa's of aromatic sulfinic acids. *J. Org. Chem.* 1959, 24, 767-769.
- [105] Reddie, K. G.; Carroll, K. S. Expanding the functional diversity of proteins: through cysteine oxidation. *Curr. Opin. Chem. Biol.* 2008, 12, 746-754.
- [106] Cremlyn, R. J. *An Introduction to Organosulfur Chemistry*. John Wiley and Sons: Chichester, UK, 1996.; pp 41-62.
- [107] Ogata, Y.; Sawaki, Y.; Isono, M. Kinetics of the addition of substituted benzenesulfinic acids to *p*-benzoquinone. *Tetrahedron.* 1970, 26, 731-736.

BIOGRAPHICAL SKETCHES

Pál Perjési

Affiliation

Institute of Pharmaceutical Chemistry, University of Pécs, Pécs, Hungary

Education

1979: Pharmacy, MS, Albert Szent-Györgyi University, Szeged, Hungary;

1983: Pharmacy, University Doctor (DrUniv), Albert Szent-Györgyi University, Szeged, Hungary;

1994: Chemistry: Candidate of Sciences (CSc), Hungarian Academy of Sciences, Budapest, Hungary;

1996: Chemistry: PhD, Albert Szent-Györgyi University, Szeged, Hungary;

2000: Chemistry: Habilitation, University of Pécs, Medical School, Pécs, Hungary

Article

The Intestinal and Biliary Metabolites of Ibuprofen in the Rat with Experimental Hyperglycemia

Hawsar Othman Mohammed ^{1,2} , Attila Almási ¹, Szilárd Molnár ¹  and Pál Perjési ^{1,*} 

¹ Institute of Pharmaceutical Chemistry, Faculty of Pharmacy, University of Pécs, H-7624 Pécs, Hungary; hawsar.mohamed@univsul.edu.iq (H.O.M.); attila.almasi@aok.pte.hu (A.A.); molnar.szilard@freemail.hu (S.M.)

² College of Veterinary Medicine, University of Sulaimani, Sulaymaniyah 46001, Iraq

* Correspondence: pal.perjesi@gytk.pte.hu

Abstract: Hyperglycemia is reported to be associated with oxidative stress. It can result in changes in the activities of drug-metabolizing enzymes and membrane-integrated transporters, which can modify the fate of drugs and other xenobiotics; furthermore, it can result in the formation of non-enzyme catalyzed oxidative metabolites. The present work aimed to investigate how experimental hyperglycemia affects the intestinal and biliary appearance of the oxidative and Phase II metabolites of ibuprofen in rats. In vivo studies were performed by luminal perfusion of 250 μ M racemic ibuprofen solution in control and streptozotocin-treated (hyperglycemic) rats. Analysis of the collected intestinal perfusate and bile samples was performed by HPLC-UV and HPLC-MS. No oxidative metabolites could be detected in the perfusate samples. The biliary appearance of ibuprofen, 2-hydroxyibuprofen, ibuprofen glucuronide, hydroxylated ibuprofen glucuronide, and ibuprofen taurate was depressed in the hyperglycemic animals. However, no specific non-enzymatic (hydroxyl radical initiated) hydroxylation product could be detected. Instead, the depression of biliary excretion of ibuprofen and ibuprofen metabolites turned out to be the indicative marker of hyperglycemia. The observed changes impact the pharmacokinetics of drugs administered in hyperglycemic individuals.

Keywords: ibuprofen; streptozotocin; hyperglycemia; intestinal metabolism; hepatic metabolism; HPLC-MS



Citation: Mohammed, H.O.; Almási, A.; Molnár, S.; Perjési, P. The Intestinal and Biliary Metabolites of Ibuprofen in the Rat with Experimental Hyperglycemia. *Molecules* **2022**, *27*, 4000. <https://doi.org/10.3390/molecules27134000>

Academic Editors: Satomi Onoue, Dorota Danielak and Katarzyna Kosicka-Noworzyń

Received: 5 June 2022
Accepted: 20 June 2022
Published: 22 June 2022

Publisher's Note: MDPI stays neutral with regard to jurisdictional claims in published maps and institutional affiliations.



Copyright: © 2022 by the authors. Licensee MDPI, Basel, Switzerland. This article is an open access article distributed under the terms and conditions of the Creative Commons Attribution (CC BY) license (<https://creativecommons.org/licenses/by/4.0/>).

1. Introduction

Ibuprofen (IBP) (1) is a non-steroidal anti-inflammatory drug (NSAID) belonging to the group of 2-arylpropionic acids (Figure 1). It is an alkylbenzene with a carboxylic acid functional group [1]. The molecule, carrying a center of symmetry, is used in therapy in racemic form. It is most commonly used by oral administration. Absorption is mediated mainly from the small intestine; however, the role of the stomach is not negligible either. After absorption, the (*R*)-enantiomer of the racemic mixture undergoes unidirectional (*R*)-(S) transformation in the liver resulting in formation of the pharmacologically more active enantiomer [2].

Over 70% of ibuprofen is metabolized and excreted in the urine. The major route of metabolism of the parent compound is oxidative conversion catalyzed by CYP enzymes, resulting in the formation of hydroxyl-substituted ibuprofen metabolites, 1-hydroxy-(1-OH-IBP) (2), 2-hydroxy-(2-OH-IBP) (3), and 3-hydroxyibuprofen (3-OH-IBP) (4). The latter is oxidized to the corresponding 3-carboxy derivative (HOOC-IBP) (5) in the cytosol (Figure 1). Both IBP and its oxidized metabolites were reported to form glucuronic acid conjugates (6) excreted in the feces or the urine [1–3].

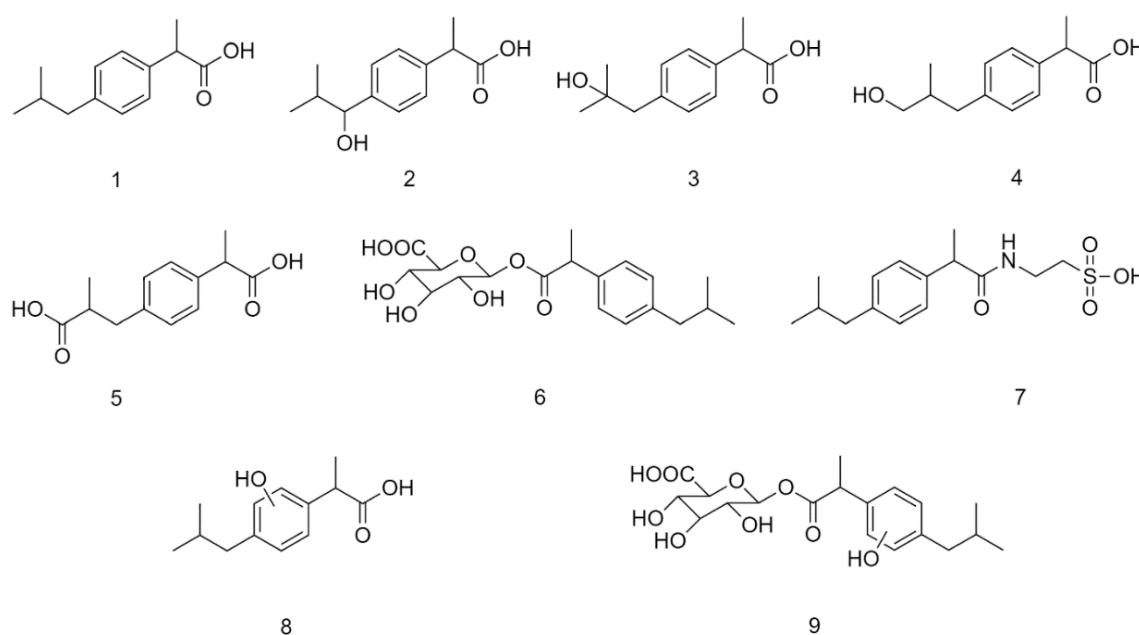


Figure 1. Structural formula of plausible metabolites of ibuprofen (IBP) (1): 1-hydroxyibuprofen (1-OH-IBP) (2), 2-hydroxyibuprofen (2-OH-IBP) (3), 3-hydroxyibuprofen (3-OH-IBP) (4), carboxy-ibuprofen (HOOC-IBP) (5), ibuprofen- β -D-glucuronide (IBP-GLU) (6), ibuprofen taurate (IBP-TAU) (7), hydroxylated ibuprofen (8), and glucuronide conjugate of a hydroxylated ibuprofen (9). (The position of the hydroxyl substitution of 8 and 9 is uncertain).

Reactive oxygen species (ROS) can be found in the background of most inflammatory (e.g., rheumatoid arthritis) and neurodegenerative diseases (e.g., Alzheimer's disease, Parkinson's disease) and in the pathomechanism of cardiovascular diseases and metabolic disorders (e.g., diabetes) [4–7]. They are capable of oxidizing endogenous and exogenous molecules in non-specific non-enzyme-catalyzed reactions. For example, while diabetic individuals were treated with acetylsalicylic acid, a significant increase in the plasma level of salicylate metabolites (e.g., 2,3-dihydroxybenzoic acid) produced exclusively by a non-enzyme-catalyzed hydroxylation reaction has been observed [4].

Diabetes mellitus is a complex endocrine metabolic disorder that affects a large proportion of the world's population. It is a well-known risk factor for cardiovascular disease and atherosclerotic complications, especially coronary heart disease. Hyperglycemia is a leading factor in diabetic complications, inducing tissue damage through different pathways [7]. These biochemical pathways generate reactive oxygen species (ROS), increasing oxidative stress [7,8]. One of the major sources of ROS formation in diabetic patients is the vascular type (Nox) NADPH oxidases [9]. Nox enzymes are, however, not the only source of ROS under hyperglycemic conditions; mitochondria and uncoupling of endothelial NO synthase also contribute to oxidative stress [10].

Strong research evidence has been accumulated to indicate that disease–drug interactions can profoundly affect the response to medication [11]. Changes in the amount and function of enzymes and transporters may alter the pharmacokinetics of the compounds [11–13]. Earlier, we investigated how the activity of the synthesizing and hydrolytic enzymes involved in glucuronide and sulfate conjugation were affected in streptozotocin (STZ)-treated rats. Activity of the UDP-glucuronyltransferase was significantly decreased in the liver of the STZ-treated rats. On the other hand, activity of the sulfotransferase and the respective hydrolytic enzymes did not change significantly [14]. According to these observations, we found the biliary excretion of ibuprofen glucuronide (IBP-GLU) in the STZ-treated (hyperglycemic) experimental animals statistically lower than in the controls [15].

As a continuation of these earlier studies, in our present experiment, biliary excretion of the oxidative and Phase II metabolites of IBP was investigated in the control and the STZ-treated rats. By application of the previously used *in vivo* protocol [14–16], we investigated how hyperglycemic conditions affect the intestinal and biliary appearance of the oxidative and Phase II metabolites of IBP. The biliary oxidative profiles were compared with those of two *in vitro* tests (Fenton and Udenfriend tests), in which reactive oxygen species (hydroxyl radicals) are supposed to react with IBP in non-enzyme-catalyzed reactions [17].

2. Results

2.1. Blood Glucose Level

Diabetes was induced with a single *iv* dose of 65 mg/kg STZ [18]. Hyperglycemia was confirmed after one week of the STZ-treatment [19]. The average blood glucose level of the control animals was 6.7 ± 1.5 mM, while that of the STZ-treated rats was 23.4 ± 2.8 mM.

2.2. Fenton Tests

Earlier, we investigated how the ratio of the molar concentration of the substrate (salicylic acid) to the iron(II) ion in the Fenton test affects the effectiveness of the hydroxylation reaction. The present investigations were performed using the more effective conditions, using the substrate: iron(II): hydrogen peroxide molar ratio as 1:3:1 [20].

For analysis of the samples, a high-performance liquid chromatographic gradient method (Method I) with UV detection (HPLC-UV) was developed to separate the available oxidative metabolites of IBP (Figure 2).

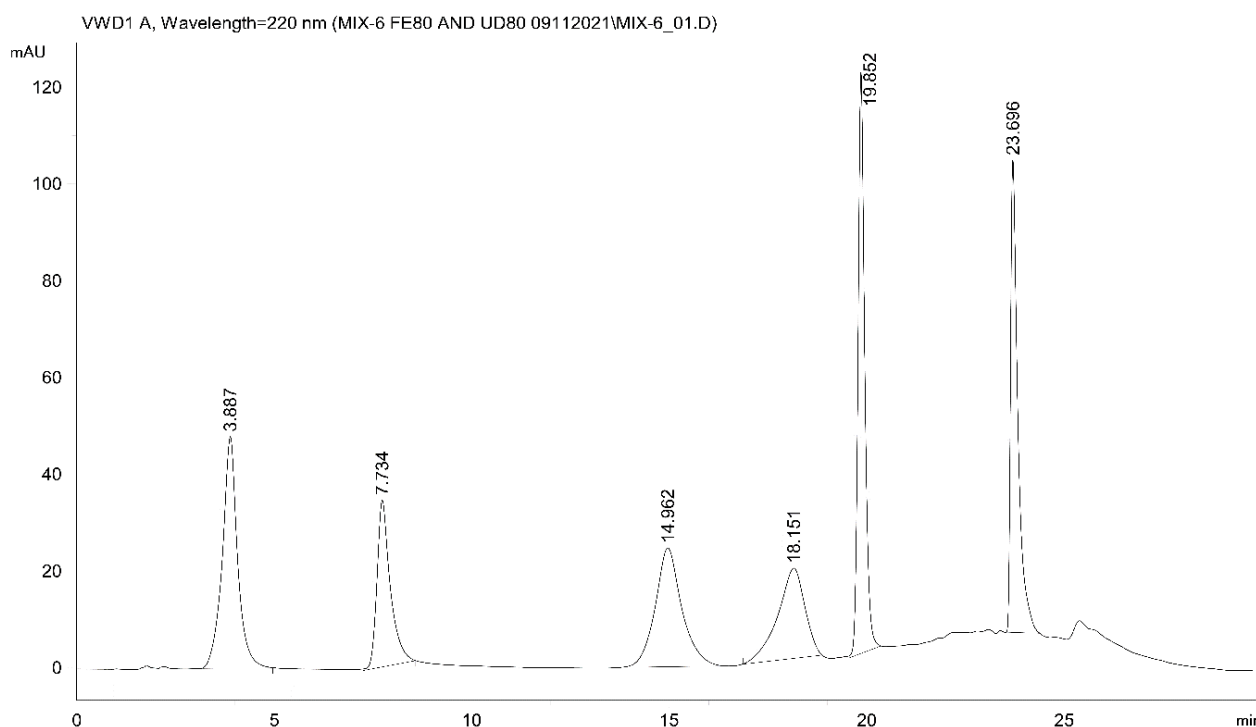


Figure 2. HPLC-UV chromatogram (Method I) of IBP and oxidative metabolites of IBP in ACN ($30 \mu\text{g mL}^{-1}$ each). The retention times (t_R) of the separated standards are as follows: 3-OH-IBP (4) (3.89 min), SA (internal standard) (7.73 min), 2-OH-IBP (3) (14.96 min), HOOC-IBP (5) (18.15 min), 1-OH-IBP (2) (19.85 min), and IBP (1) (23.70 min).

HPLC-UV analysis (Method I) of the Fenton extracts indicated the formation of 1-OH-IBP (**2**), 2-OH-IBP (**3**), and several other products (Figures S1 and S2). To verify the structures of **2** and **3** and to identify other oxidation products, a high-performance liquid chromatographic analysis using mass spectrometric detection (HPLC-MS) of the extracts was performed. HPLC-MS investigations confirmed the presence of **2** (m/z 221.1178), **3** (m/z 221.1178), and HOOC-IBP (**5**) (m/z 235.0969) (Figures S3–S5). The derivative (**8**) with the highest HPLC-UV integrated peak area (t_R = 22.05 min) could not be unambiguously identified (Figure 1). The formed product (X-HO-IBP) has an exact mass of m/z 221.1175 and its fragmentation makes no distinction between the 2'-OH-IBP and OH(Ar)-IBP structures (Figure S6A,B). Another IBP-derived HPLC-UV peak (t_R = 21.09 min) was identified as a dihydroxy ibuprofen (**10**) (OH-IBP-OH) derivative (m/z 237.1125) (Figure S7). Determination of the exact structures needs further investigation. The change in HPLC-UV integrated peak areas of **2**, **3**, **8**, and **10** (relative to that of the internal standard) as a function of incubation times is shown in Figure S8.

2.3. Udenfriend's Test Results

Using the *in vitro* non-enzyme-catalyzed hydroxylation test developed by Udenfriend et al., [21,22], a similar oxidative metabolic pattern of IBP could be observed. Similar to the Fenton incubations, the derivatives with the t_R values of 22.03 min (**8**) and 21.07 min (**10**) were those with the highest HPLC-UV peak areas (Figures S9 and S10). 2-HO-IBP (**3**) was formed in lower amounts than in the respective Fenton samples (Figure S11). 1-OH-IBU (**2**) could not be detected. HPLC-MS investigations of the samples confirmed the presence of the **2**, **3**, **5**, **8**, and **9** derivatives.

2.4. Analysis of Intestinal Perfusate and Bile Samples

For HPLC-UV analysis of the biological samples, a modified method was developed (Method II) to separate the oxidative metabolites and the glucuronide conjugate of IBP (Figure S12). HPLC-UV analysis of the ether extract of the intestinal perfusate samples of the control and the hyperglycemic animals did not indicate either hydroxy- or carboxy-ibuprofen metabolites (Figures S13–S15). However, contrary to our previous HPLC-UV measurements [15], IBP-GLU (**6**) (m/z 381.1552) could be identified by HPLC-MS in the perfusate of both the control and the STZ-treated animals (Figure S16).

HPLC-UV analysis of the ether extract of bile samples showed the presence of IBP (**1**), IBP-GLU (**6**), and 2-OH-IBP (**3**). HPLC-MS analysis confirmed the presence of **1** (m/z 205.1229), **6** (m/z 381.1549), and **3** (m/z 221.1178) in both the control and the hyperglycemic samples. To keep the number of experimental animals low, the results were evaluated by comparing the integrated HPLC-UV peak areas (relative to the internal standard) of the compounds. The areas were lower in the bile samples of the STZ-treated animals at each investigated timepoint (Figure 3).

Considering the respective bile outflows, the relative amounts of the cumulative excretions of **1**, **6**, and **3** were calculated. The result showed a depression in biliary excretion of all the three compounds in the STZ-treated animals. In our earlier experiments (using the same experimental protocol), the cumulative biliary excretion of IBP was reduced by 53% [15]. The present data indicated similar (58%) depression. For IBP-GLU and 2-OH-IBP, the excretion was depressed by 63% and 49%, respectively (Figure 4). Additionally, several other peaks appeared in the extracts (Figures S17–S19). Based on the HPLC-MS analysis of the samples, these peaks are bile acids and conjugated bile acid derivatives. Based on their high-resolution mass spectra, cholic acid (exact mass: 407.2798), glycocholic acid (exact mass: 464.3012), taurochenodeoxycholic acid (exact mass: 498.2889), and taurocholic acid (exact mass: 514.2839) was identified.

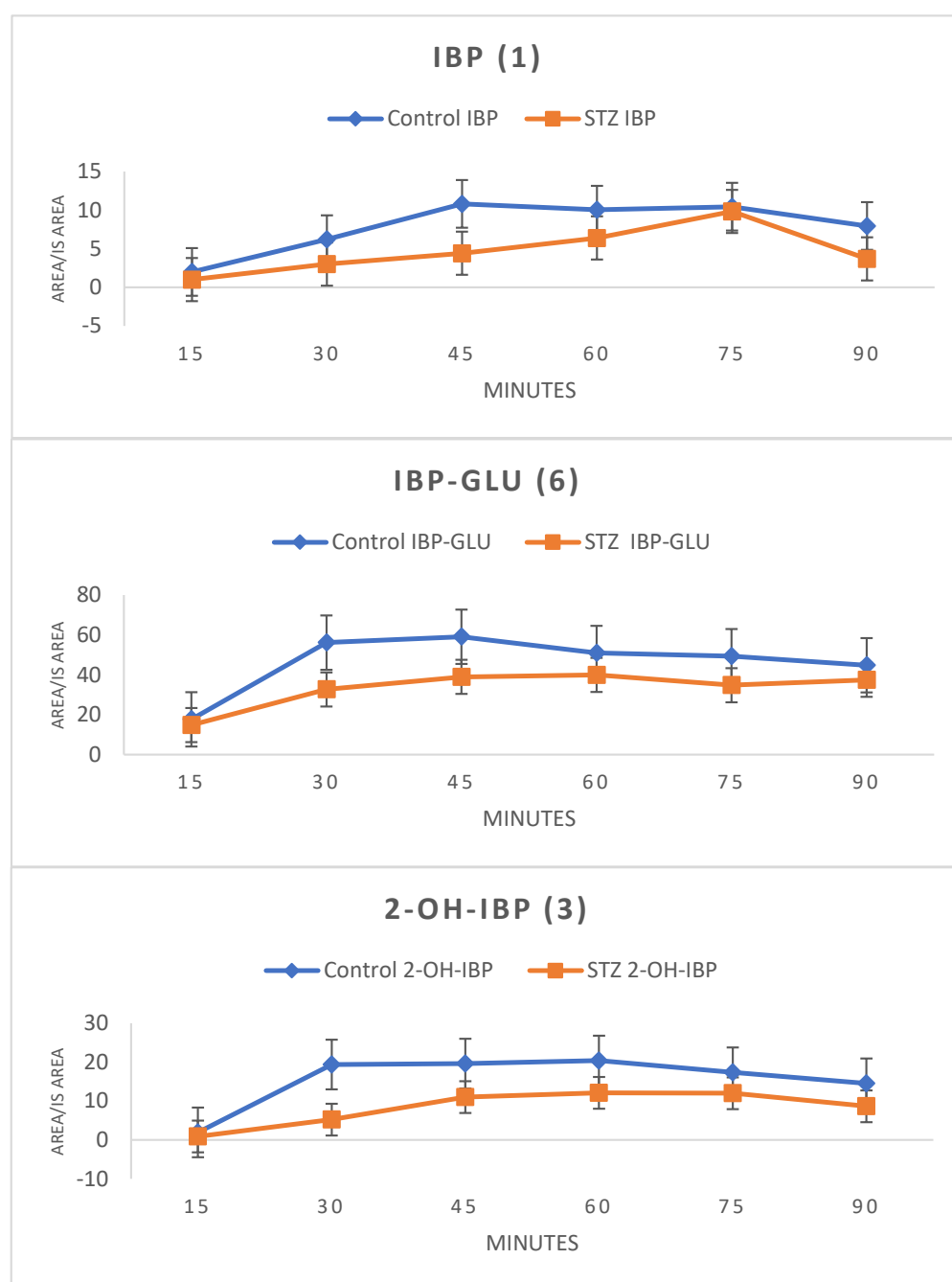


Figure 3. Change in the HPLC-UV integrated peak areas (relative to the internal standard) of ibuprofen (1) and the ibuprofen metabolites (IBP-GLU (6) and 2-OH-IBP (3)) in the diethyl ether extract of bile of control and hyperglycemic (STZ) rats (Method II).

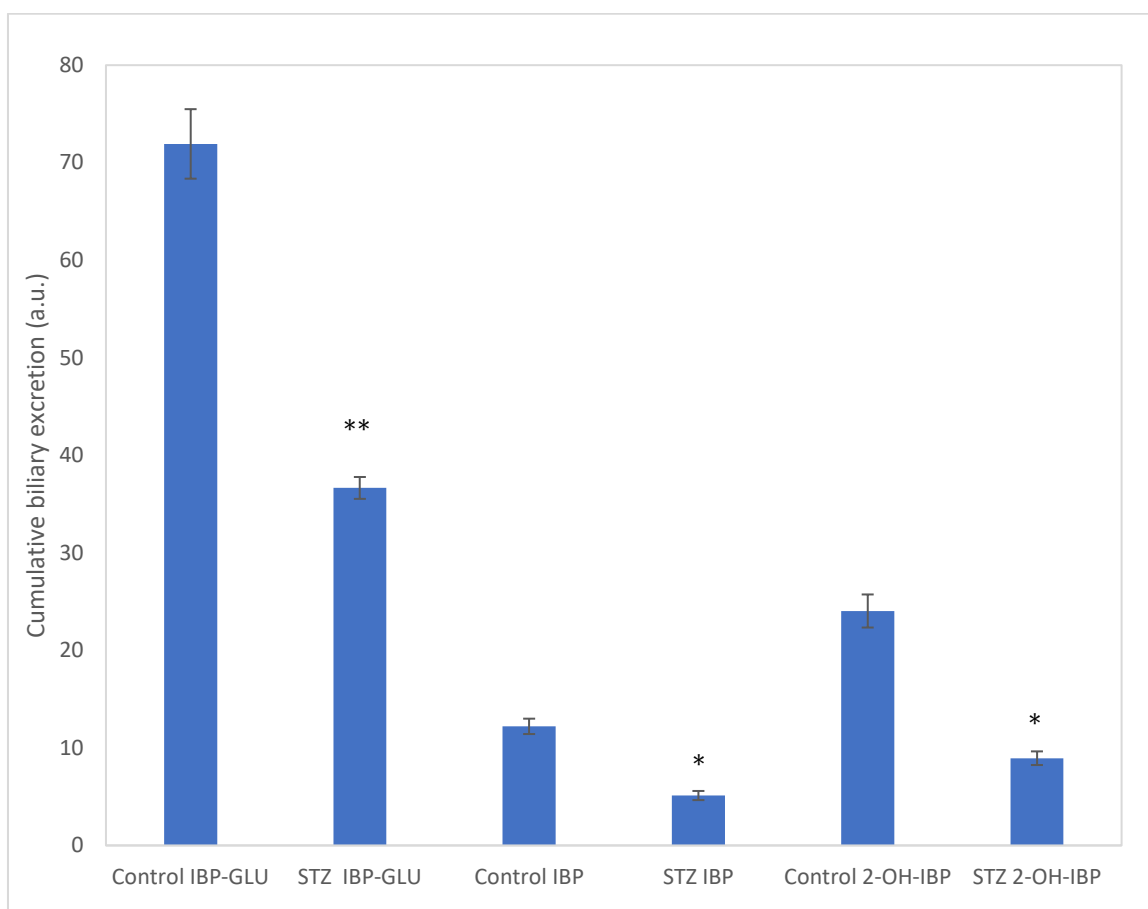


Figure 4. Cumulative biliary excretion (HPLC-UV (Method II) based integration) of IBP (1), IBP-GLU (6), and 2-OH-IBP (3) after the 90-min luminal perfusion of 250 μ M IBP in control and hyperglycemic (STZ-treated) rats. Each value represents the average of five independent experiments \pm standard error. Significant difference from the control value: * $p < 0.05$, ** $p < 0.01$.

Furthermore, an HPLC-MS analysis of the bile samples confirmed the presence of the glucuronide conjugate of a hydroxylated ibuprofen (9) (exact mass: 397.1501) (X-OH-IBP-GLU) and the taurine conjugate of ibuprofen (7) (exact mass: 312.1275) (IBP-TAU) (see Figures S20 and S21, respectively). The cumulative biliary excretion of X-OH-IBP-GLU and IBP-TAU in the control and the STZ-treated rats are shown in Figure 5A,B. The excreted X-OH-IBP-GLU and IBP-TAU were depressed by 92% and 98%, respectively.

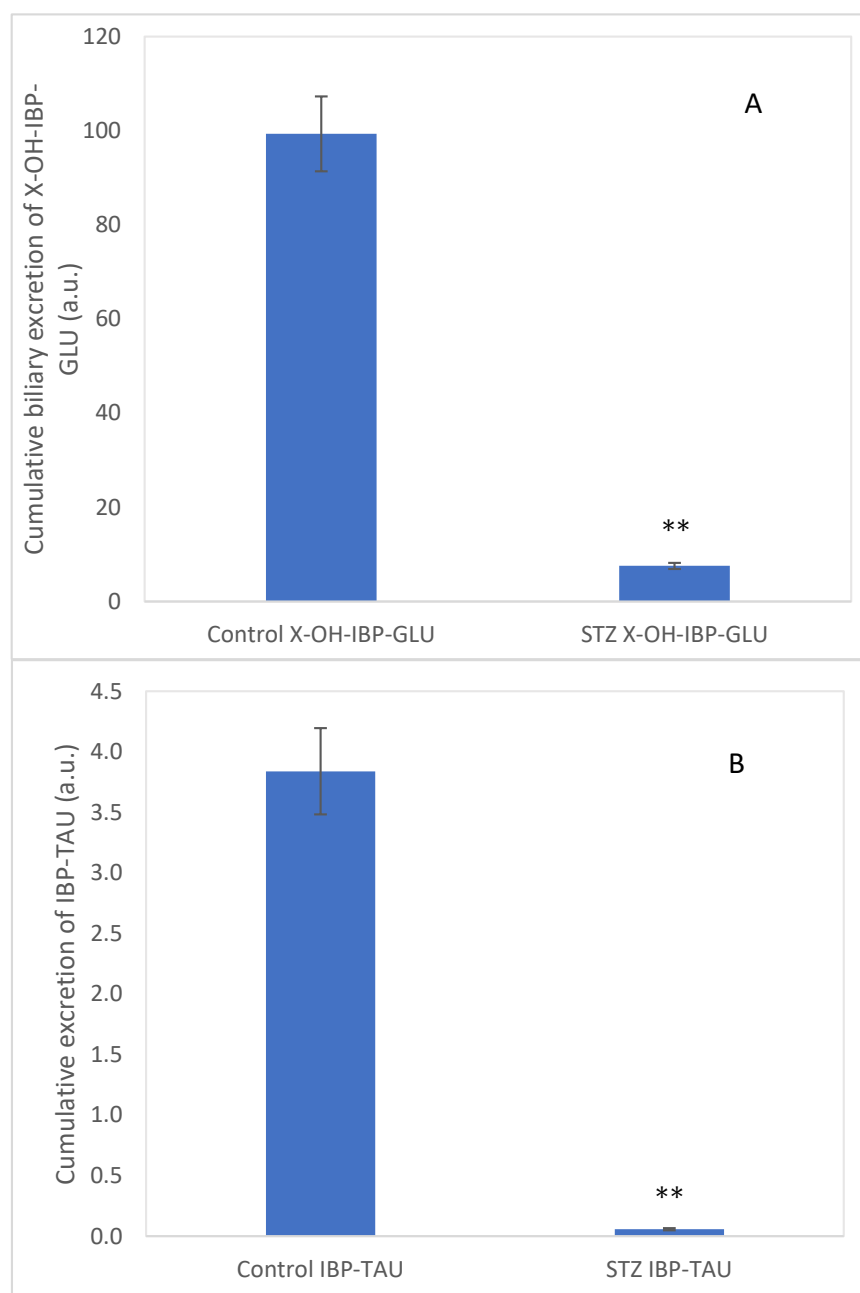


Figure 5. Cumulative biliary excretion (HPLC-MS based integration) of the (A) X-OH-IBP-GLU (9) and (B) IBP-TAU (7) after the 90-min luminal perfusion of 250 μ M IBP in control and hyperglycemic (STZ) rats. Each value represents the average of five independent experiments \pm standard error. Significant difference from the control value: ** $p < 0.01$.

3. Discussion

Ibuprofen (IBP) undergoes extensive Phase I and Phase II biotransformation to the main metabolites 1-OH-IBP (2), 2-OH-IBP (3), HOOC-IBP (5), and IBU-GLU (6) [1–3]. In humans, the CYP2C9 isoform plays the most important role in the oxidative metabolism of IBP, mediating the 2- and 3-hydroxylations and the subsequent 3-oxidation in the liver [23,24]. Additional CYPs, particularly CYP2C8, may also play a role in these biotransformations [24,25]. The enzyme responsible for the 1-OH-IBP (2) formation has not been identified [26,27].

In rats, the most abundant CYP2C isoform is CYP2C11, whereas the other isoforms were present at much lower levels. The human CYP2C9 and CYP2C8 proteins are ortholo-

gous to the rat CYP2C12 and CYP2C11 [28]. After oral administration, IBP appeared mainly in an unchanged form in the plasma of rats. In addition, two metabolites, 2-OH-IBP (3) and HOOC-IBP (5), were found in the plasma and the urine [29]. Yamazoe et al., studied the effect of alloxan and STZ on the expression of hepatic CYP enzymes in rats. In most cases, the expression of the CYP proteins was either not affected or depressed [30]. Later, Shimojo reviewed the effects of hyperglycemia on rat hepatic CYP expressions. According to the reviewed publications, the amount of CYP2C11 and CYP2C13 was suppressed, while CYP2C12 did not change or somewhat increased [31]. Recently, Yang and Liu reviewed the effect of diabetes on the drug transporter–CYP interplays. They referred to further studies that demonstrate a lowered expression of hepatic CYP2C11 in diabetic rats [13]. Accordingly, decreased levels of hydroxylated IBP metabolites formed in CYP-catalyzed reactions can be rationalized.

During inflammation, for example, stimulated polymorphonuclear leukocytes (PMN) and macrophages produce large amounts of superoxide ions and hydrogen peroxide [32]. There are many examples of exogenous H_2O_2 initiating redox signals or stress responses. Furthermore, receptor-mediated redox signaling is widely regarded as involving endogenously generated H_2O_2 [32,33]. On the other hand, many of the biologically damaging effects of H_2O_2 depend on transition metals such as iron and copper, which cleave the peroxide bond to generate hydroxyl radicals or activated metal complexes [34]. Hydroxyl radicals are powerful electrophilic reactants that can oxidize endogenous or exogenous molecules. Therefore, the importance of non-enzymatic oxidation can be particularly significant at the sites of inflammation [35].

To model non-enzymatic oxidation, oxidation products of IBP formed under the conditions of the Fenton reaction [36] and Udenfriend's oxidation [21,22] were investigated by HPLC-UV and HPLC-MS methods. The Fenton reaction is a tool for modeling oxidative stress by forming hydroxyl radicals in a reaction of hydrogen peroxide and some transitional metals. The key features of the reaction are believed to be the reaction conditions, such as reagent concentrations, pH, and temperature [37]. Earlier, we applied the reactions to study the oxidative transformation of salicylates [20,38].

The Fenton oxidation of IBP resulted in the formation of several products. Among them, 1-OH-IBP (2), 2-OH-IBP (3), and HOOC-IBP (5) were identified by HPLC-UV and HPLC-MS. Among these products, 1-OH-IBP (2) was found in the largest amount (Figure 1). Additionally, a small amount of a dihydroxyibuprofen ($t_R = 8.91$ min) (10) and a significant amount of a new hydroxyl-substituted derivative ($t_R = 9.24$ min) (8) were found. Hydroxyl radicals have been reported to react with IBP to form 1-OH-(2), 2'-OH-, and OH(Ar)-IBP derivatives [39]. Based on the HPLC retention time ($t_R = 9.24$ min), the new hydroxyl derivative could be the 2'-OH-IBP or an OH(Ar)-IBP. As shown in Figure S6B, the main fragment ion ($C_{12}H_{17}O$; m/z 177.1251) is formed by the CO_2 loss of the hydroxylated IBP derivative (m/z 221.1175). The CO_2 loss occurs already in the ionization source (Figure S6A). The other main decomposition peak (m/z 119.0472) corresponds to a C_8H_7O (vinyl phenol or acetophenone; exact mass: m/z 119.0497, mass error: -21.0 ppm) fragment [40]. Although the m/z 149.0576 peak can be assigned as a $C_9H_9O_2$ fragment (exact mass m/z 149.0603; mass error: -18.1 ppm), the exact structure of the formed product cannot be unambiguously determined. Since H-abstraction is thermodynamically more favored than the OH addition and its reaction rate is an order of magnitude higher [41,42], the new hydroxylated product was tentatively identified as the 2'-OH-IBP (Figure S6A,B). Further investigations are to be performed to experimentally prove the results of the theoretical calculations. 1,2-Dihydroxyibuprofen was reported to form in the biodegradation of IBP [43].

Udenfriend et al., described a system consisting of EDTA, ascorbic acid, molecular oxygen, and iron(II) ion, which would serve as a model of the biomimetic hydroxylation of organic substrates [21,22]. Ito et al., demonstrated that the reactive species are hydroxyl radicals (trapped by different aliphatic alcohols) in both the Fenton and the Udenfriend reagents [44]. Udenfriend's oxidation of IBP resulted in the formation of products similar to those formed in the Fenton incubations (Figure 4). Based on this observation, it is

reasonable to presume that the reactive species are the same in both reactions. The above results indicate that *in vivo* Fenton-type [37,45] or Udenfriend-type [46] non-enzymatic hydroxylation of IBP—based on measurement of **8** and/or **9**—can be used as an early sign of oxidative stress conditions.

While analyzing the 250 μ M ibuprofen containing intestinal perfusates of control and STZ-treated hyperglycemic rats, none of the oxidative metabolites (formed in CYP-catalyzed or non-CYP-catalyzed reactions) of IBP (**1**) could be detected by HPLC-UV or HPLC-MS. Contrary to the previous [15] (and the present) HPLC-UV measurements, IBP-GLU (**6**) conjugate could be detected and identified in the perfusates by HPLC-MS. This result indicates the formation of **6** in the rats' small intestine, which could not be detected by the less sensitive UV detection.

HPLC-UV analysis of the collected bile samples showed the presence of IBP (**1**), IBP-GLU (**6**), and 2-OH-IBP (**3**). HPLC-MS analysis of the bile samples of both the control and the hyperglycemic group of animals confirmed the presence of the three compounds. According to our previous results [15], excretion of both **1** and **6** into the bile decreased in experimental diabetes; similarly, biliary excretion of **3** was also reduced in the hyperglycemic rats (Figure 4). In our earlier experiments, the biliary excretion of 4-nitrophenol and its glucuronic acid and sulfate conjugates were significantly decreased in diabetic rats [16].

In addition to the above, the glucuronide conjugate of a hydroxylated IBP (**9**) and the taurine conjugate of IBP (**7**) could also be identified by means of HPLC-MS (Figures S20 and S21). Earlier, Shirley et al., reported on the formation of IBP-CoA and IBP-TAU (**7**) in *in vitro* incubations using rat hepatocytes [47]. Similar to those results, the HPLC-MS analysis of our bile samples indicated the presence of IBP-TAU (**7**) but not of the glycine conjugate (IBP-GLY). To the best of our knowledge, this is the first *in vivo* observation of the excretion of IBP-TAU into the bile.

The excreted amounts of **9** and **7** were significantly lower in the STZ-treated rats' bile samples. Although the bile outflow was slightly increased in the STZ-treated animals over the studied period, a comparison of the relative amounts of the excreted **9** and **7** (based on the HPLC-MS data) indicated reduced excretion of IBP-TAU in the STZ-treated animals (Figure 5). Depression of biliary excretion of IBP-TAU can be explained by the earlier results related to the reduced biliary excretion of IBP and IBP-GLU in hyperglycemic rats [48–50]. Hasegawa et al., [46] reported that the hepatic expression of the efflux transporter MRP2 is decreased in the STZ-treated rats. Similarly, expression of the efflux transporter P-gp (MDR1) was reduced in hyperglycemia [49–51]. In agreement with these earlier results, our molecular biology studies on liver samples of the STZ-treated rats showed decreased expression of the efflux transporters P-gp (MDR1B), MRP2, and BCRP [15]. These transporters are involved in exporting organic anions from the hepatocytes into the bile canaliculus [52]. Furthermore, hyperglycemia is also associated with a decline in the levels of the endogenous antioxidant taurine in several tissues [53,54].

4. Materials and Methods

4.1. Chemicals

1-Hydroxyibuprofen (1-OH-IBP) and 2-hydroxyibuprofen (2-OH-IBP) were obtained from Dr. Ehrenstorfer GmbH (Augsburg, Germany). Ibuprofen (IBP), salicylic acid (SA), streptozotocin (STZ), ibuprofen- β -D-glucuronide (IBP-GLU), and carboxyibuprofen (HOOC-IBP) were purchased from Sigma-Aldrich (Budapest, Hungary). 3-Hydroxyibuprofen (3-OH-IBP) was from HPC Standards GmbH (Cunnersdorf, Germany). All chemicals and reagents were analytical or HPLC grade. The standard isotonic perfusion medium had the following compositions (mM): NaCl 96.4, KCl 7.0, CaCl₂ 3.0, MgSO₄ 1.0, sodium phosphate buffer (pH 7.4) 0.9, tris buffer (pH 7.4) 29.5, glucose 14.0, mannitol 14.0. Blood glucose level was checked with an AccuChek blood glucose meter (Roche).

4.2. Fenton Test

The experiments were performed as described before [20]. Iron(II) sulfate (100 μ L of 30 mM) solution (in pH 3.0 sulfuric acid) was mixed with 700 μ L of sulfuric acid (pH 3.0) and the mixture was vortexed for 30 s. Then, 100 μ L of 10 mM IBP in phosphate buffer pH 7.2 was added and vortexed. The total volume was set to 1 mL by adding 100 μ L of 10 mM hydrogen peroxide. The components were mixed in the respective order and the reaction mixtures were placed in a 37 °C water bath. The samples were analyzed after 0, 10, 60, 80, and 120 min of incubation. “Blank” samples did not contain IBP.

At the end of each incubation period, the mixtures were acidified with 20 μ L of 2 M sulfuric acid and 50 μ L of 10 mM salicylic acid as an internal standard was added (final concentration 0.467 mM). The samples were vortex mixed and extracted twice with 2 mL of diethyl ether. The combined ether extracts were evaporated under N₂ gas. Before HPLC and LC-MS analysis, the dry residue was reconstructed in 100 μ L of acetonitrile.

4.3. Udenfriend's Assay

The assay was performed as reported earlier [38]. To a test tube, 3.0 mL of distilled water, 4.0 mL of 2.5 mM IBP solution in 0.1 M phosphate buffer (pH 7.2), 1.0 mL of 10 mM ascorbic acid, 1.0 mL of 2.4 mM Na₂EDTA, and 1.0 mL of 2.0 mM Fe(NH₄)₂(SO₄)₂ solution were added, in the order of listing. The mixture was vortexed after adding each component. Then, it was incubated in a water bath at 37 °C for 2 h with gentle mechanical shaking, and 1.0 mL aliquot was taken from the mixture at 0, 10, 60, 80, and 120 min.

To the 1.0 mL aliquot, 1.0 mL of 0.4 M ice-cold perchloric acid and 100 μ L of 10 mM of salicylic acid (as an internal standard) were added (final concentration of 0.476 mM). The acidic solution was cooled in icy water and extracted twice with 3.0 mL of diethyl ether. The combined ether layers were evaporated under N₂ gas. Before analysis, the dry residue was reconstructed in 100 μ L of acetonitrile.

4.4. Animals and Experimental Procedure

The experiments were performed following the protocol before [14–16]. Male Wistar rats (9–11 weeks old, weighing 250–300 g; TOXI-COOP, Hungary, Budapest) were separated into two groups: Group I (control) and Group II (diabetic) animals ($n = 5$ per group). Experimental diabetes was induced by a 65 mg/kg bw intravenous injection of streptozotocin (STZ) one week before the intestinal perfusion. Blood glucose levels were tested before the STZ-treatment and before starting the experiments. The experimental animals were provided standard chaw and water ad libitum.

The animals had fasted for 18–20 h before the experiments, then anesthetized with an intraperitoneal injection of urethane (1.2 g/kg bw). The abdomen was opened by a midline incision. A jejunal loop (length of the jejunal loop about 10 cm) was “in vivo” isolated and cannulated at its proximal and distal ends. Body temperature was maintained at 37 °C using a heat lamp.

Perfusion through the lumen of the jejunal loop with an isotonic medium containing 250 μ M ibuprofen was carried out at a rate of 13 mL/min in a recirculation mode. Perfusate samples (250 μ L) were collected at selected timepoints (15, 30, 45, 60, 75, and 90 min) from the perfusion medium flowing out from the intestinal loop. The initial volume of the perfusate was 15 mL and its temperature was maintained at 37 °C.

For parallel investigation of the biliary excretion, the bile duct was cannulated with PE-10 tubing. The bile outflow was collected in 15-min periods into tared Eppendorf tubes placed in ice. The collected samples were stored in a deep freezer (−70 °C) until analysis. Bile flow was measured gravimetrically, assuming a specific gravity of 1.0 [55]. Biliary excretion was expressed as the product of the HPLC peak areas (relative to the internal standard) and the 15-min periods of bile flows (μ L/kg/min). The values (arbitrary units) represent the mean \pm S.E. of five independent experiments.

4.5. Sample Preparation

To 0.1 mL of perfusate sample or 50 μ L of bile sample, 20 μ L of 2 M sulfuric acid and 10 μ L of 10 mM salicylic acid (as an internal standard) were added. (The final concentration of SA in the perfusate and the bile samples was 0.77 mM and 1.25 mM, respectively.) Then, the samples were vortex mixed and extracted twice with 0.5 mL of diethyl ether. After vortexing (30 s) and centrifugation (5 min, 5000 rpm), the ether layers were separated and the combined ether extracts were evaporated under N_2 gas. Before HPLC-UV and HPLC-MS analysis, the evaporation residue was reconstructed in 100 μ L of acetonitrile.

4.6. Sample Analysis

4.6.1. HPLC-UV

HPLC-UV analyses (Method I) of the Fenton and the Udenfriend samples were performed on an integrated Agilent 1100 HPLC system equipped with a quaternary HPLC pump, a degasser, an autosampler, a thermostated column compartment, and a diode-array detector. Data were recorded and evaluated by Agilent ChemStation software (Rev.B.03.02-SR2). HPLC-UV analysis (Method II) of the perfusate and bile extracts was performed on an integrated Jasco HPLC (LC-4000) system equipped with a PDA detector and a quaternary HPLC pump, a degasser, an autosampler, a thermostated column compartment, and a PDA detector. Data were recorded and evaluated by ChromNAV Data System (Ver.2).

Method I. Separation of compounds was performed on a Teknokroma (NUCLEOSIL C18) (4.6 mm \times 250 mm, 5 μ m particle size) column with a Teknokroma (ODS cartridge, 1 cm \times 0.32 cm) guard column at 40 $^{\circ}$ C. The mobile phase consisted of 0.02 M phosphate buffer pH 2.5 (A) and acetonitrile (B) with a flow rate of 1.5 mL/min. The analyses (detection at 220 nm) were performed using the following gradient profile: 20% B for 15 min followed by a 5 min linear gradient to 60% B, a 4 min isocratic elution followed by a 2 min linear gradient to 20% B, and a 4 min equilibration. The injected volume was 10 μ L.

Method II. Separation of compounds was performed on a Zorbax SB C-18 (4.6 mm \times 150 mm, 5 μ m particle size) column with a Teknokroma (ODS cartridge, 1 cm \times 0.32 cm) guard column at 40 $^{\circ}$ C. The mobile phase consisted of 0.02 M phosphoric acid pH 2.5 (A) and acetonitrile (B) with a flow rate of 1.6 mL/min. The analyses (detection at 220 nm) were performed using the following gradient profile: 20% B for 5 min followed by a 0.5 min linear gradient to 30% B, a 4.5 min isocratic elution followed by a 0.1 min linear gradient to 60% B, a 4.9 min isocratic elution followed by a 0.1 min linear gradient to 20% B, and a 4.9 min equilibration. The injected volume was 10 μ L.

4.6.2. HPLC-HESI-MS

To identify the metabolites, a Thermo Dionex UltiMate 3000 liquid chromatograph (Dionex, Sunnyvale, CA, USA) connected to a Thermo Q Exactive Focus quadrupole-Orbitrap hybrid mass spectrometer (Thermo Fisher Scientific, Waltham, MA, USA) was used. Data acquisition and analysis were performed using the Q Exactive Focus 2.1, Xcalibur 4.2., and FreeStyle 1.8 software (Thermo Fisher Scientific, Waltham, MA, USA).

The HPLC separation was performed on an XTerra MS C18 column (150 mm \times 2.1 mm, 3.5 μ m) with XTerra MS C18 precolumn (5 mm \times 2.1 mm, 3.5 μ m) at 40 $^{\circ}$ C. The injection volume was 5 μ L and the flow rate was 0.4 mL/min. The tray of the autosampler vials was thermostated at 25 $^{\circ}$ C. A binary gradient of the eluents is as follows.

Eluent: 5 mM ammonium-acetate/5 mM acetic acid in water (A) and methanol (B). Gradient: 10% B for 1 min, followed by a 9 min linear gradient to 90% B, a 2 min isocratic elution followed by a 0.5 min linear gradient to 10% B, and a 2.5 min equilibration.

Analysis of the compounds was performed in HESI negative ionization modes with the following parameters: spray voltage 3.0 kV; probe heater temperature 300 $^{\circ}$ C; capillary temperature 350 $^{\circ}$ C; spray and auxiliary N_2 gas flows 20 and 5 arbitrary units, respectively; S-Lens RF level 50%; automatic gain control 1×10^6 ; resolution (at 200 m/z) 70,000; data acquisition range m/z 100–1000, in full scan mode.

4.7. Statistical Analysis

HPLC-UV integrated peak areas (relative to the internal standard) of oxidized ibuprofen metabolites were qualitatively analyzed in the Fenton and Udenfriend experiments based on incubation time. Biliary excretion was expressed as the product of the HPLC peak areas (relative to the internal standard) and the 15-min period of bile flows ($\mu\text{L}/\text{kg}/\text{min}$). The values (arbitrary units) represent the mean \pm S.E. of five independent experiments. The difference among groups was determined by an SPSS independent t-test. Significant differences from the control value: * $p < 0.05$ and ** $p < 0.01$.

4.8. Ethical Approval

The study was designed and conducted according to European legislation (Directive 2010/63/E.U.) [56] and Hungarian Government regulation (40/2013, II. 14.) [57] on the protection of animals used for scientific purposes. The project was approved by the Animal Welfare Committee of the University of Pécs and by the Government Office of Baranya County (license No. BAI35/51-61/2016 and license supplement (supplement No. BAI35/90-5/2019)).

5. Conclusions

The present results show that one of the main hydroxylated IBP derivatives formed in the non-enzyme-catalyzed oxidation reactions (Fenton and Udenfriend tests) is a hydroxylated IBP derivative (8). Since the formation of neither 2'-OH-IBP nor OH(Ar)-IBP (8)—the possible structures of the product—has not been reported in CYP-catalyzed reactions, formation of this derivative might be used as a biomarker of oxidative stress in living organisms.

Contrary to 4-nitrophenol [16] and capsaicin [58]—both are phenolic derivatives—the glucuronide conjugate of ibuprofen could be detected only in a trace amount in the small intestinal perfusates. On the other hand, IBP (1), IBP-GLU (6), and IBP-TAU (7) were excreted by the liver. However, no specific non-enzymatic hydroxylation product could be detected.

The results are in agreement with the previous experimental findings demonstrating decreased expression of the organic anion transporters P-gp (MDR1), MRP2, and BCRP in the liver of the STZ-treated (hyperglycemic) animals. Such changes impact the pharmacokinetics of drugs administered in hyperglycemic individuals.

Supplementary Materials: The following supporting information can be downloaded at: <https://www.mdpi.com/article/10.3390/molecules27134000/s1>.

Author Contributions: Conceptualization, P.P.; investigation, H.O.M., A.A. and S.M.; methodology, H.O.M., A.A. and S.M.; writing—original draft, P.P. and H.O.M.; writing—review and editing, P.P. and H.O.M.; funding acquisition, P.P. All authors have read and agreed to the published version of the manuscript.

Funding: This study was supported by the European Union, co-financed by the European Social Fund (EFOP-3.6.1.-16-2016-00004).

Institutional Review Board Statement: The study was designed and conducted according to European legislation (Directive 2010/63/E.U.) [56] and Hungarian Government regulation (40/2013, II. 14.) [57] on the protection of animals used for scientific purposes. The project was approved by the Animal Welfare Committee of the University of Pécs and by the Government Office of Baranya County (license No. BAI35/51-61/2016 and license supplement (supplement No. BAI35/90-5/2019)).

Informed Consent Statement: Not applicable.

Data Availability Statement: Primary research data are stored in the Institute of Pharmaceutical Chemistry, University of Pécs, Pécs, Hungary.

Conflicts of Interest: The authors declare no conflict of interest.

Sample Availability: Samples of the compounds are not available from the authors.

References

1. Mazaleuskaya, L.L.; Theken, K.N.; Gong, L.; Thorn, C.F.; FitzGerald, G.A.; Altman, R.B.; Klein, T.E. PharmGKB summary: Ibuprofen pathways. *Pharmacogenet. Genom.* **2015**, *25*, 96–106. [\[CrossRef\]](#)
2. Rainsford, K.D. Ibuprofen: Pharmacology, efficacy and safety. *Inflammopharmacology* **2009**, *17*, 275–342. [\[CrossRef\]](#) [\[PubMed\]](#)
3. Keep, D.R.; Sidemann, U.G.; Hansen, S.H. Isolation and characterization of major phase I and II metabolites of ibuprofen. *Pharm. Res.* **1997**, *14*, 676–680. [\[CrossRef\]](#) [\[PubMed\]](#)
4. Essman, W.B.; Wollman, S.B. Free radicals, central nervous system processes and brain functions. In *Oxygen Radicals: Systemic Events and Disease Processes*; Das, D.K., Essman, W.B., Eds.; Karger: Basel, Switzerland, 1990; pp. 172–192. [\[CrossRef\]](#)
5. Ghiselli, A.; Laurenti, O.; De Mattia, G.; Maiani, G.; Ferro-Luzzi, A. Salicylate hydroxylation as an early marker of in vivo oxidative stress in diabetic patients. *Free Radic. Biol. Med.* **1992**, *13*, 621–626. [\[CrossRef\]](#)
6. Sies, H. *Antioxidants in Disease Mechanisms and Therapy. Advances in Pharmacology*, 1st ed.; Academic Press: San Diego, CA, USA, 1996; Volume 38.
7. Chatterjee, S. Chapter Two—Oxidative Stress, Inflammation, and Disease. In *Oxidative Stress and Biomaterials*; Dziubla, T., Butterfield, D.A., Eds.; Academic Press: Amsterdam, The Netherlands, 2016; pp. 35–58. [\[CrossRef\]](#)
8. Asmat, U.; Abad, K.; Ismail, K. Diabetes mellitus and oxidative stress—A concise review. *Saudi Pharm. J.* **2016**, *24*, 547–553. [\[CrossRef\]](#)
9. Brandes, R.P.; Weissmann, N.; Schröder, K. NADPH oxidases in cardiovascular disease. *Free Radic. Biol. Med.* **2010**, *49*, 687–706. [\[CrossRef\]](#) [\[PubMed\]](#)
10. Brandes, R.P.; Weissmann, N.; Schröder, K. Nox family NADPH oxidases: Molecular mechanisms of activation. *Free Radic. Biol. Med.* **2014**, *76*, 208–226. [\[CrossRef\]](#)
11. Dostalek, M.; Sam, W.J.; Paryani, K.R.; Macwan, J.S.; Gohh, R.Y.; Akhlaghi, F. Diabetes mellitus reduces the clearance of atorvastatin lactone. *Clin. Pharmacokinet.* **2012**, *51*, 591–606. [\[CrossRef\]](#)
12. Li, Y.; Meng, Q.; Yang, M.; Liu, D.; Hou, X.; Tang, L.; Wang, X.; Lyu, Y.; Chen, X.; Liu, K.; et al. Current trends in drug metabolism and pharmacokinetics. *Acta Pharm. Sin. B.* **2019**, *9*, 1113–1144. [\[CrossRef\]](#)
13. Yang, Y.; Liu, X. Imbalance of drug transporter-CYPs interplay by diabetes and its clinical significance. *Pharmaceutics* **2020**, *12*, 348. [\[CrossRef\]](#)
14. Almási, A.; Pinto, É.I.L.N.; Kovács, N.P.; Fischer, T.; Markovics, Z.; Fischer, E.; Perjési, P. Changes in hepatic metabolic enzyme activities and biliary excretion of 4-nitrophenol in streptozotocin-induced diabetic rats. *Braz. J. Pharm. Sci.* **2018**, *54*, e17347. [\[CrossRef\]](#)
15. Kovács, N.P.; Almási, A.; Garai, K.; Kuzma, M.; Vancea, S.; Fischer, E.; Perjési, P. Investigation of intestinal elimination and biliary excretion of ibuprofen in hyperglycemic rats. *Can. J. Physiol. Pharmacol.* **2019**, *97*, 1080–1089. [\[CrossRef\]](#)
16. Fischer, E.; Almási, A.; Bojcssev, S.; Fischer, T.; Kovács, N.P.; Perjési, P. Effect of experimental diabetes and insulin replacement on intestinal metabolism and excretion of 4-nitrophenol in rats. *Can. J. Physiol. Pharmacol.* **2015**, *93*, 459–464. [\[CrossRef\]](#)
17. Illés, E.; Takács, E.; Dombi, A.; Gajda-Schranz, K.; Rácz, G.; Gonter, K.; Wojnárovits, L. Hydroxyl radical induced degradation of ibuprofen. *Sci. Total Environ.* **2013**, *447*, 286–292. [\[CrossRef\]](#)
18. Wang-Fischer, Y.; Garyantes, T. Improving the reliability and utility of streptozotocin-induced rat diabetic model. *J. Diabetes Res.* **2018**, *2018*, 8054073. [\[CrossRef\]](#) [\[PubMed\]](#)
19. Bojcssev, S.; Rafiei, A.; Fischer, E. Changes in the biliary excretion of exogenous organic anions by streptozotocin-induced diabetes. *Acta Physiol. Hung.* **1996**, *84*, 263–264.
20. Nyúl, E.; Kuzma, M.; Mayer, M.; Lakatos, S.; Almási, A.; Perjési, P. HPLC study on Fenton-reaction initiated oxidation of salicylic acid. Biological relevance of the reaction in intestinal biotransformation of salicylic acid. *Free Radic. Res.* **2018**, *52*, 1040–1051. [\[CrossRef\]](#) [\[PubMed\]](#)
21. Udenfriend, S.; Clark, C.T.; Axelrod, J.; Brodie, B.B. Ascorbic acid in aromatic hydroxylation. I. A model system for aromatic hydroxylation. *J. Biol. Chem.* **1954**, *208*, 731–740. [\[CrossRef\]](#)
22. Brodie, B.B.; Axelrod, J.; Shore, P.A.; Udenfriend, S. Ascorbic acid in aromatic hydroxylation. II. Products formed by reaction of substrates with ascorbic acid, ferrous ion, and oxygen. *J. Biol. Chem.* **1954**, *208*, 741–750. [\[CrossRef\]](#)
23. Leemann, T.D.; Transon, C.; Bonnabry, P.; Dayer, P. A major role for cytochrome P450TB (CYP2C subfamily) in the actions of non-steroidal anti-inflammatory drugs. *Drugs Exp. Clin. Res.* **1993**, *19*, 189–195. [\[PubMed\]](#)
24. Chang, S.Y.; Li, W.; Traeger, S.C.; Wang, B.; Cui, D.; Zhang, H.; Wen, B.; Rodrigues, A.D. Confirmation that cytochrome P450 2C8 (CYP2C8) plays a minor role in (S)-(+)- and (R)-(–)-ibuprofen hydroxylation in vitro. *Drug Metab. Dispos.* **2008**, *36*, 2513–2522. [\[CrossRef\]](#) [\[PubMed\]](#)
25. Hamman, M.A.; Thompson, G.A.; Hall, S.D. Regioselective and stereoselective metabolism of ibuprofen by human cytochrome P450 2C. *Biochem. Pharmacol.* **1997**, *54*, 33–41. [\[CrossRef\]](#)
26. Neunzig, I.; Göhring, A.; Dragan, C.A.; Zapp, J.; Peters, F.T.; Maurer, H.H.; Bureik, M. Production and NMR analysis of the human ibuprofen metabolite 3-hydroxyibuprofen. *J. Biotechnol.* **2012**, *157*, 417–420. [\[CrossRef\]](#) [\[PubMed\]](#)
27. Gliszczynska, A.; Sánchez-López, E. Dexibuprofen therapeutic advances: Prodrugs and nanotechnological formulations. *Pharmaceutics* **2021**, *13*, 414. [\[CrossRef\]](#) [\[PubMed\]](#)
28. Hammer, H.; Schmidt, F.; Marx-Stoelting, P.; Pötz, O.; Braeuning, A. Cross-species analysis of hepatic cytochrome P450 and transport protein expression. *Arch. Toxicol.* **2021**, *95*, 117–133. [\[CrossRef\]](#) [\[PubMed\]](#)

29. Mills, R.F.; Adams, S.S.; Cliffe, E.E.; Dickinson, W.; Nicholson, J.S. The metabolism of ibuprofen. *Xenobiotica* **1973**, *3*, 589–598. [CrossRef] [PubMed]
30. Yamazoe, Y.; Murayama, N.; Shimada, M.; Yamauchi, K.; Kato, R. Cytochrome P450 in livers of diabetic rats: Regulation by growth hormone and insulin. *Arch. Biochem. Biophys.* **1989**, *268*, 567–575. [CrossRef]
31. Shimojo, N. Cytochrome P450 changes in rats with streptozocin-induced diabetes. *Int. J. Biochem.* **1994**, *26*, 1261–1268. [CrossRef]
32. Richmond, R.; Halliwell, B.; Chauhan, J.; Darbre, A. Superoxide-dependent formation of hydroxyl radicals: Detection of hydroxyl radicals by the hydroxylation of aromatic compounds. *Anal. Biochem.* **1981**, *118*, 328–335. [CrossRef]
33. Forman, H.J. Redox signaling: An evolution from free radicals to aging. *Free Radic. Biol. Med.* **2016**, *97*, 398–407. [CrossRef]
34. Winterbourn, C.C. Toxicity of iron and hydrogen peroxide: The Fenton reaction. *Toxicol. Lett.* **1995**, *82–83*, 969–974. [CrossRef]
35. Biswas, S.; Das, R.; Banerjee, E.R. Role of free radicals in human inflammatory diseases. *AIMS Biophys.* **2017**, *4*, 596–614. [CrossRef]
36. Neyens, E.; Baeyens, J. A review of classic Fenton's peroxidation as an advanced oxidation technique. *J. Hazard. Mater.* **2003**, *98*, 33–50. [CrossRef]
37. Prousek, J. Fenton chemistry in biology and medicine. *Pure Appl. Chem.* **2007**, *79*, 2325–2338. [CrossRef]
38. Kuzma, M.; Kovács, N.; Sziva, L.; Maász, G.; Avar, P.; Perjési, P. Oxidation of hydroxy- and dihydroxybenzoic acids under the Udenfriend's conditions. An HPLC study. *Open Med. Chem. J.* **2018**, *12*, 13–22. [CrossRef] [PubMed]
39. Arthur, R.B.; Bonin, J.L.; Ardill, L.P.; Rourk, E.J.; Patterson, H.H.; Stemmler, E.A. Photocatalytic degradation of ibuprofen over BiOCl nanosheets with identification of intermediates. *J. Hazard. Mat.* **2018**, *358*, 1–9. [CrossRef] [PubMed]
40. Bajpai, L.; Varshney, M.; Seubert, C.N.; Stevens, S.M.; Johnson, J.V.; Richard, A.; Yost, R.A.; Dennis, D.M. Mass spectral fragmentation of the intravenous anesthetic propofol and structurally related phenols. *J. Am. Soc. Mass Spectrom.* **2005**, *16*, 814–824. [CrossRef] [PubMed]
41. Jacobs, L.E.; Fimmen, R.L.; Chin, Y.P.; Mash, H.E.; Weavers, L.K. Fulvic acid mediated photolysis of ibuprofen in water. *Water Res.* **2011**, *45*, 4449–4458. [CrossRef] [PubMed]
42. Xiao, R.; Noerpel, M.; Luk, H.L.; Wei, Z.; Spinney, R. Thermodynamic and kinetic study of ibuprofen with hydroxyl radical: A density functional theory approach. *Int. J. Quant. Chem.* **2014**, *114*, 74–83. [CrossRef]
43. Chopra, S.; Kumar, D. Ibuprofen as an emerging organic contaminant in environment, distribution and remediation. *Heliyon* **2020**, *6*, e04087. [CrossRef] [PubMed]
44. Ito, S.; Ueno, K.; Mitarai, A.; Sasaki, K. Evidence for hydroxyl radicals as an active species generated from Udenfriend's reagent. *J. Chem. Soc. Perkin Trans.* **1993**, 255–259. [CrossRef]
45. Enamia, S.; Sakamoto, Y.; Colussie, A.J. Fenton chemistry at aqueous interfaces. *Proc. Natl. Acad. Sci. USA* **2014**, *111*, 623–628. [CrossRef] [PubMed]
46. Li, M.; Carlson, S.; Kinzer, J.A.; Perpall, H.J. HPLC and LC-MS studies of hydroxylation of phenylalanine as an assay for hydroxyl radicals generated from Udenfriend's reagent. *Biochem. Biophys. Res. Commun.* **2003**, *312*, 316–322. [CrossRef] [PubMed]
47. Shirley, M.A.; Guan, X.; Kaiser, D.G.; Halstead, G.W.; Baillie, T.A. Taurine conjugation of ibuprofen in humans and in rat liver in vitro. Relationship to metabolic chiral inversion. *J. Pharmacol. Exp. Ther.* **1994**, *269*, 1166–1175. [CrossRef] [PubMed]
48. Hasegawa, Y.; Kishimoto, S.; Shibatani, N.; Nomura, H.; Ishii, Y.; Onishi, M.; Inotsume, N.; Takeuchi, Y.; Fukushima, S. The pharmacokinetics of morphine and its glucuronide conjugate in a rat model of streptozotocin-induced diabetes and the expression of MRP2, MRP3 and UGT2B1 in the liver. *J. Pharm. Pharmacol.* **2010**, *62*, 310–314. [CrossRef] [PubMed]
49. Anger, G.J.; Magomedova, L.; Piquette-Miller, M. Impact of acute streptozotocin-induced diabetes on ABC transporter expression in rats. *Chem. Biodiv.* **2009**, *6*, 1943–1959. [CrossRef]
50. Nawa, A.; Hamabe, W.F.; Tokuyama, S. Inducible nitric oxide synthase-mediated decrease of intestinal P-glycoprotein expression under streptozotocin-induced diabetic conditions. *Life Sci.* **2010**, *86*, 402–409. [CrossRef] [PubMed]
51. Zhang, L.L.; Lu, L.; Jin, S.; Jing, X.Y.; Yao, D.; Hu, N.; Liu, L.; Duan, R.; Liu, X.D.; Wang, G.J.; et al. Tissue-specific alterations in expression and function of P-glycoprotein in streptozotocin-induced diabetic rats. *Acta Pharmacol. Sin.* **2011**, *32*, 956–966. [CrossRef] [PubMed]
52. Jetter, A.; Kullak-Ublick, G.A. Drugs and hepatic transporters: A review. *Pharmacol. Res.* **2020**, *154*, 104234. [CrossRef]
53. Schaffer, S.W.; Azuma, J.; Mozaffari, M. Role of antioxidant activity of taurine in diabetes. *Can. J. Physiol. Pharmacol.* **2009**, *87*, 91–99. [CrossRef]
54. Baliou, S.; Adamaki, M.; Ioannou, P.; Pappa, A.; Panayiotidis, M.I.; Spandidos, D.A.; Christodoulou, I.; Kyriakopoulos, A.M.; Zoumpourlis, V. Protective role of taurine against oxidative stress (Review). *Mol. Med. Rep.* **2021**, *24*, 605. [CrossRef] [PubMed]
55. Klaassen, C.D. Bile flow and composition during bile acid depletion and administration. *Can. J. Physiol. Pharmacol.* **1974**, *52*, 334–348. [CrossRef] [PubMed]
56. European Legislation (Directive 2010/63/E.U.). ELI. Available online: <https://eur-lex.europa.eu/eli/dir/2010/63/oj> (accessed on 4 June 2022).
57. Hungarian Government Regulation (40/2013., II. 14). Available online: <https://www.fao.org/faolex/results/details/en/c/LEX-FAOC124420> (accessed on 4 June 2022).
58. Kuzma, M.; Fodor, K.; Maász, G.; Avar, P.; Mózsik, G.; Past, T.; Fischer, E.; Perjési, P. A validated HPLC-FLD method for analysis of intestinal absorption and metabolism of capsaicin and dihydrocapsaicin in the rat. *J. Pharm. Biomed. Anal.* **2015**, *103*, 59–66. [CrossRef] [PubMed]



Effect of experimental hyperglycemia on intestinal elimination and biliary excretion of ibuprofen enantiomers in hyperglycemic rats

Journal:	<i>Biopharmaceutics & Drug Disposition</i>
Manuscript ID	BDD-22-0094
Wiley - Manuscript type:	Original Article
Date Submitted by the Author:	28-Aug-2022
Complete List of Authors:	Mohamed, Hawsar; University of Pécs, Institute of Pharmaceutical Chemistry Almási, Attila; University of Pécs, Institute of Pharmaceutical Chemistry Perjesi, Pal; University of Pécs, Institute of Pharmaceutical Chemistry
Keywords:	Streptozotocin, Hyperglycemia, (S)-Ibuprofen
Abstract:	<p>Diabetic complications are mostly due to hyperglycemia. Hyperglycemia is reported to be associated with oxidative stress. It can result in changes in the activities of drug-metabolizing enzymes and membrane-integrated transporters, which can modify the fate of drugs and other xenobiotics. An in vivo intestinal perfusion model was used to investigate how experimental hyperglycemia affects intestinal elimination and biliary excretion of ibuprofen enantiomers in the rat. Experimental diabetes was induced by intravenous (i.v.) administration of streptozotocin. The intestinal perfusion medium contained 250 μM (\pm)-ibuprofen. A validated isocratic chiral HPLC method with UV detection was developed to determine the amount of the two enantiomers in the intestinal perfusate and the bile. The results indicated that experimental diabetes doesn't cause a statistically significant decrease in the disappearance of ibuprofen enantiomers from the small intestine. Analysis of the bile samples detected only the (S)-IBP enantiomer. Excretion of the ibuprofen enantiomer to the bile decreased in experimental diabetes. The observed changes impact the pharmacokinetics of drugs administered in hyperglycemic individuals.</p>

SCHOLARONE™
Manuscripts

Effect of experimental hyperglycemia on intestinal elimination and biliary excretion of ibuprofen enantiomers in hyperglycemic rats

Mohammed Othman Hawsar^{1,2}, Attila Almási¹, Pál Perjési^{1*}

¹Institute of Pharmaceutical Chemistry, Faculty of Pharmacy, University of Pécs, Pécs, Hungary

²College of Veterinary Medicine, University of Sulaimani, Sulaymaniyah, Kurdistan Region, Iraq

***Corresponding Author**

Pál Perjési, PhD

ORCID: <https://orcid.org/0000-0002-1057-9664>

Institute of Pharmaceutical Chemistry

University of Pécs

H-7624 Pécs

HUNGARY

E-mail: pal.perjesi@gytk.pte.hu

E-mail addresses

Mohammed Othman Hawsar: hawsar.mohamed@univsul.edu.iq

Attila Almási: Attila.almasi@aok.pte.hu

Author contributions

Conceptualization (P.P.), Investigation (H.O.M., A.A.), Methodology (P.P., H.O.M., A.A.), Writing – original draft (P.P. and H.O.M.), Writing – review, and editing (P.P. and H.O.M.), Funding acquisition (P.P.). All authors have read and agreed to the published version of the manuscript.

Data availability

Primary research data are stored in the Institute of Pharmaceutical Chemistry, University of Pécs, Pécs, Hungary.

Funding statement

This study was supported by the European Union and co-financed by the European Social Fund (EFOP-3.6.1.-16-2016-00004).

Conflict of interest statement

None of the authors declared a conflict of interest.

Ethics approval statement

The study was designed and conducted according to the European legislation (Directive 2010/63/E.U.) [14] and the Hungarian Government regulation (40/2013., II. 14.) [15] on the protection of animals used for scientific purposes. The project was approved by the Animal Welfare Committee of the University of Pécs and by the Government Office of Baranya County (license No. BAI35/51-61/2016 and license supplement (supplement No. BAI35/90-5/2019).

1
2
3
4
5
6
7
8
9
10
11
12
13
14
15
16
17
18
19
20
21
22
23
24
25
26
27
28
29
30
31
32
33
34
35
36
37
38
39
40
41
42
43
44
45
46
47
48
49
50
51
52
53
54
55
56
57
58
59
60

Abstract

Diabetic complications are mostly due to hyperglycemia. Hyperglycemia is reported to be associated with oxidative stress. It can result in changes in the activities of drug-metabolizing enzymes and membrane-integrated transporters, which can modify the fate of drugs and other xenobiotics. An *in vivo* intestinal perfusion model was used to investigate how experimental hyperglycemia affects intestinal elimination and biliary excretion of ibuprofen enantiomers in the rat. Experimental diabetes was induced by intravenous (i.v.) administration of streptozotocin. The intestinal perfusion medium contained 250 µM (±)-ibuprofen. A validated isocratic chiral HPLC method with UV detection was developed to determine the amount of the two enantiomers in the intestinal perfusate and the bile. The results indicated that experimental diabetes doesn't cause a statistically significant decrease in the disappearance of ibuprofen enantiomers from the small intestine. Analysis of the bile samples detected only the (S)-IBP enantiomer. Excretion of the ibuprofen enantiomer to the bile decreased in experimental diabetes. The observed changes impact the pharmacokinetics of drugs administered in hyperglycemic individuals.

Keywords Streptozotocin, Hyperglycaemia, (S)-Ibuprofen, Biliary excretion

Abbreviations

72	STZ	Streptozotocin
73	HPLC	High performance liquid chromatography
74	UV	Ultraviolet
75	NSAID	Non-steroidal anti-inflammatory drug
76	IBP	Ibuprofen
77	NAP	Naproxen sodium salt
78	IS	Internal standard
79	MeOH	Methanol
80	SD	Standard Deviation
81	RSD	Relative Standard Deviation
82	MDR1/P-gp	Multidrug resistance protein 1/P-glycoprotein
83	OAT	Organic anion transporters
84	OATP	Organic anion transporting polypeptide
85	MRP2	Multidrug resistance-associated protein 2
86	BCRP	Breast cancer resistance protein
87	PDA	Photodiode array

1. Introduction

Ibuprofen (IBP) (**1**) is a non-steroidal anti-inflammatory drug (NSAID) belonging to the group of 2-arylpropionic acids (Figure 1) [1]. The molecule carrying a center of symmetry is used in therapy in racemic form, exploiting its three main pharmacological effects (anti-inflammatory, analgesic, and antipyretic). It is most commonly used in therapy by oral administration. After oral absorption, about 40–60% of the *R*(-)-form of ibuprofen is metabolically converted to the *S*(-) form [2,3] in the intestinal tract and liver [4,5]. Over 70% of the ibuprofen dose is metabolized and excreted in the urine. The major route of metabolism is CYP-catalyzed oxidative transformations resulting in the formation of hydroxyl-substituted ibuprofen metabolites. Ibuprofen and its oxidized metabolites were reported to form glucuronide conjugates excreted in the feces or the urine [6,7].

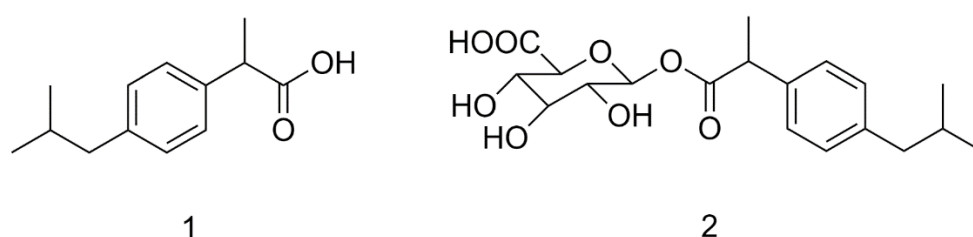


Figure 1. Structure of ibuprofen (**1**) and ibuprofen β -D-glucuronide (**2**).

Earlier, we investigated the elimination of racemic ibuprofen from the small intestine in hyperglycemic rats by HPLC-UV. In parallel, by cannulation of the bile duct, we investigated the excretion of the parent compound and its glucuronide conjugate into the bile. Unconjugated ibuprofen (**1**) and ibuprofen- β -D-glucuronide (**2**) were detected in the bile; however, no ibuprofen-glucuronide could be detected in the intestinal perfusate. Excretion of both ibuprofen and ibuprofen- β -D-glucuronide into the bile was decreased in experimental diabetes [8].

Continuing the above investigations, we report on HPLV-UV analysis of ibuprofen enantiomers in the intestinal perfusate and bile of the hyperglycemic rats. The work aimed to get data if experimental hyperglycemia can modify the enantiomeric composition of the racemic ibuprofen in the small intestinal perfusate and the bile in our previously applied *ex vivo* model.

2. Materials and Methods

2.1. Chemicals

Racemic ibuprofen (IBP), (*S*)-(+)-ibuprofen, salicylic acid, streptozotocin (STZ), and naproxen sodium (NAP) were purchased from Sigma-Aldrich (Budapest, Hungary). All chemicals and reagents were analytical or HPLC grade. The standard isotonic perfusion medium had the following compositions (mM): NaCl 96.4, KCl 7.0, CaCl_2 3.0, MgSO_4 1.0, sodium phosphate buffer (pH 7.4) 0.9, Tris buffer (pH 7.4) 29.5, glucose 14.0, mannitol 14.0. Blood glucose level was checked with an AccuChek blood glucose meter (Roche).

2.2. Animals

Male Wistar rats (9–11 weeks old, weighing 250–300 g) were separated into two groups. Group I was the control, and Group II was diabetic animals (n=4 each). Experimental diabetes was induced by a 65 mg/kg bw intravenous injection of streptozotocin (STZ) one week before the intestinal perfusion. Blood glucose levels were tested before the STZ treatment and starting the experiments. The average blood glucose level of the control animals was 6.7 ± 1.5 mM, while that of the STZ-treated rats was 23.4 ± 2.8 mM.

2.3. Intestinal perfusion procedure

The experiments were performed according to the protocol before [8-10]. The animals fasted for 18–20 h before the experiments; and then were anesthetized with an intraperitoneal injection of urethane (1.2 g/kg bw, i.p.). The abdomen was opened by a midline incision. A jejunal loop (length of the jejunal loop about 10 cm) was "in vivo" isolated and cannulated at its proximal and distal ends. Body temperature was maintained at 37 °C using a heat lamp.

Perfusion through the lumen of the jejunal loop with an isotonic medium containing 250 µM racemic ibuprofen was carried out at a rate of 13 ml/min in a recirculation mode. Perfusate samples (250 µl) were collected at selected timepoints from the perfusion medium from the intestinal loop for 150 minutes. The initial volume of the perfusate was 15 ml, and its temperature was maintained at 37 °C.

For parallel investigation of the biliary excretion, the bile duct was cannulated with PE-10 tubing. The bile outflow was collected in 15 minute-periods into tared Eppendorf tubes placed in ice. The collected samples were stored in a deep freezer until analysis. Bile flow was measured gravimetrically, assuming a specific gravity of 1.0 [11].

2.4. Sample preparation

Perfusate and bile samples were kept at room temperature for a short time to become defrost. The extraction technique applies the validated method published by Bonato et al. [12]. The sample volume (50 µl) was placed in an Eppendorf tube, and then 10 µl of NAP solution (250 µM) was added as an internal standard (IS). The mixture was acidified by 40 µl of hydrochloric acid (2 M) and extracted with 1.5 ml (3-times 0.5 ml) of a mixture of n-hexane and ethyl acetate (8:2 v/v). The mixture was vortexed for 30 seconds, centrifuged for 5 minutes at 3500 rpm, and the transparent upper layer separated. The combined organic extracts were evaporated under nitrogen at 40 °C. The residue was reconstituted in 50 µl of the mobile phase.

2.5. Instrumentation and chromatographic conditions

HPLC-UV analysis of the perfusate and bile samples extracts was performed on an integrated Jasco HPLC (LC-4000) system equipped with a PDA detector, a quaternary HPLC pump, a degasser, an autosampler, a thermostated column compartment, and a PDA detector. Data were recorded and evaluated by ChromNAV Data System (Ver.2). Ibuprofen enantiomers were separated on a Kromasil 3-amyloCoat RP (4.6 mm x 150 mm, 3 µm) chiral column with a Teknokroma (ODS cartridge, 1 cm x 0.32 cm) guard column. The mobile phase consisted of methanol/water/acetic acid (70:30:0.1 v/v). The run time was 30 minutes with a 0.5 ml/min flow rate and 10 µl injection volume. The temperature and the UV detector were set at 22 °C and 220 nm, respectively. The analytical method is based on the Kromasil application note [13]. Identification of the separated peaks was made by determination

of the retention time of (S)-(+)-ibuprofen and NAP salt as an internal standard (Figure 1S).

2.6. Validation data of HPLC analyses

2.6.1. Specificity

Results were evaluated based on the chromatograms of extracts of blank perfusate and blank bile samples. The examined extracts didn't give a detectable chromatographic peak at the retention time of ((R)-IBP (1) t_R =14.5 min, (S)-IBP (2) t_R =16.72 min, and NAP (3) t_R =20.3 min) of the perfused medium; and at the retention time of ((R)-IBP (1) t_R =14.4 min, (S)-IBP (2) t_R =16.61 min and NAP (3) t_R =20.18 min) of the bile (Figure 2).

2.6.2. System suitability

System suitability data were evaluated from chromatograms of the standard solutions of racemic IBP (100 μ M, 250 μ M) and NAP (50 μ M) in methanol. Results were obtained from five parallel injections. The evaluation was based on the relative standard deviation (RSD%). The percent RSD values are shown in Table 1S.

2.6.3. Precision

Precision was studied by investigating repeatability and intermediate precision. Repeatability was determined by measuring intra-day data of 3 parallel injections of 2 parallel dilutions of 2 independent weighings of racemic IBP (c = 100 μ M, c = 250 μ M in MeOH) and NAP (c = 50 μ M, in MeOH). Intermediate precision was determined by measuring inter-day (by injection of the samples over three consecutive days) data of 3 parallel injections of 2 dilutions of racemic IBP (c = 100 μ M, c = 250 μ M in MeOH), and NAP (c = 250 μ M, in MeOH). The evaluation was based on the relative standard deviation (RSD%) (Tables 2S and 3S).

2.6.3. Accuracy

Accuracy was calculated by spiking control perfusion and bile samples with the concentrations of racemic IBP (50 μ M, 100 μ M, 250 μ M) and NAP (50 μ M). After the extraction of the samples, the percentage of recoveries was calculated with the mean of the same concentrations of standard dilutions of racemic IBP (50 μ M, 100 μ M, 250 μ M) and NAP (50 μ M). The evaluation was based on the relative standard deviation (RSD%) (Tables 4S).

2.6.4. Linearity

Linearity was studied by analysis of standard solutions of racemic IBP of five different concentrations (250 μ M, 200 μ M, 150 μ M, 100 μ M, 50 μ M) using methanol as solvent. Each solution had a known concentration of NAP as an internal standard (50 μ M). Data were obtained from three parallel injections of each concentration. Calibration curves were generated by plotting the theoretical concentrations against the relative peak areas (ratio of the peak areas of the enantiomers and the internal standard). Linearity was determined by least-squares regression. The regression equation for (R)- and (S)-IBP was as follows: (R)-IBP: $y = 0.3360x + 0.2408$, $R^2 = 0.9993$; (S)-IBP: $y = 0.1676x + 0.2110$, $R^2 = 0.9994$) as shown in Figure 2S.

2.6.4. Determination of LOQ

The limit of quantitation (LOQ) was considered the lowest concentration (50 μ M) of the calibration curve contracted by using racemic ibuprofen. Taking into consideration the exact concentration of the two enantiomers in the investigated

sample ((*R*)-IBP: 49.81%; (*S*)-IBP: 50.019% - See Table 1S), the LOQ of the (*R*)-IBP and (*S*)-IBP are 24.91 μ M and 25.09 μ M, respectively.

2.7. Calculations and statistics

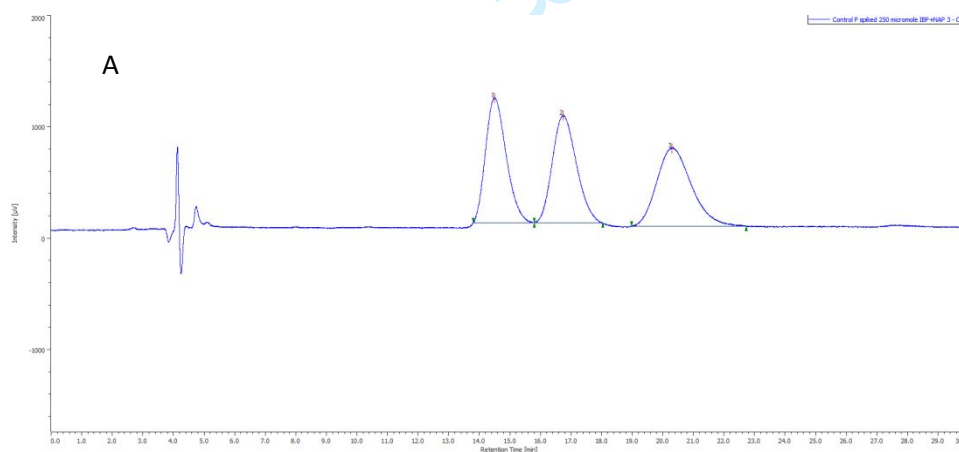
The luminal disappearance of the IBP enantiomers was calculated based on their luminal concentrations and the volume of the perfusion solution. The biliary excretion was calculated on the base of the volume of bile flow in 15 minutes periods. Data show the mean \pm SD of four independent experiments. The difference among groups was determined by SPSS One-way Anova. Significant differences from the control value: * $p < 0.05$, ** $p < 0.01$, and *** $p < 0.001$.

2.8. Ethical approval

The study was designed and conducted according to the European legislation (Directive 2010/63/E.U.) [14] and the Hungarian Government regulation (40/2013., II. 14.) [15] on the protection of animals used for scientific purposes. The project was approved by the Animal Welfare Committee of the University of Pécs and by the Government Office of Baranya County (license No. BAI35/51-61/2016 and license supplement (supplement No. BAI35/90-5/2019).

3. Results

Figure 2A shows the HPLC-UV chromatogram of the two ibuprofen enantiomers and naproxen (used as internal standard) extracted from the control perfusion medium and the control bile. The blank control (buffer perfused through isolated small intestine of not treated rat) doesn't have any interfering peak (Figure 2B). The blank control bile (biliary excretion collected from the bile duct) doesn't have any interfering peak (Figure 2D).



1
2
3
4
5
6
7
8
9
10
11
12
13
14
15
16 245
17 246
18
19
20
21
22
23
24
25
26
27
28
29
30
31 247
32
33
34
35
36
37
38
39
40
41
42
43
44
45 248
46 249
47 250
48 251
49 252
50 253
51 254
52 255
53
54 256
55 257
56 258
57 259
58 260
59 261
60

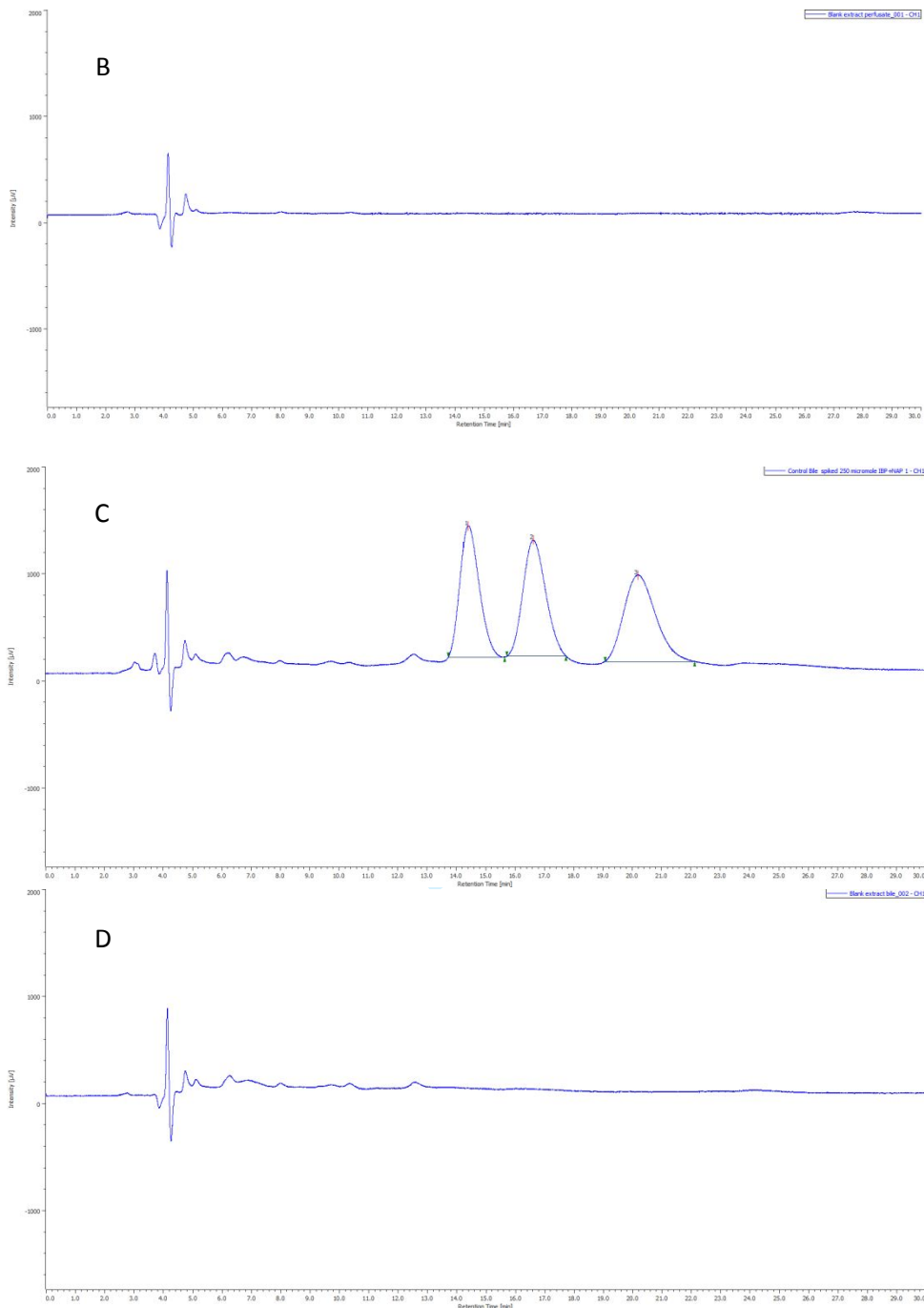


Figure 2. (A) HPLC-UV chromatogram of the two IBP enantiomers ((*R*)-IBP (**1**) t_R =14.5 min, (*S*)-IBP (**2**) t_R =16.72 min and NAP (**3**) t_R =20.3 min), extracted from the spiked control perfusion medium of non-treated animal, (B) the blank control perfused medium, (C) the two IBP enantiomers ((*R*)-IBP (**1**) t_R =14.4 min, (*S*)-IBP (**2**) t_R =16.61 min and NAP (**3**) t_R =20.18 min), extracted from the spiked control bile of non-treated animal; (D) the blank control bile.

HPLC chromatograms of the intestinal perfusates of the control and the STZ-treated (hyperglycemic) rats at the 0, 29, and 90-minute timepoints are shown in Figures 3S and 4S, respectively. Changes in concentrations of the IBP enantiomers in the perfusions of the control and hyperglycemic rats are shown in Figure 3. The relative amount of the (*S*)-IBP enantiomer in the control animals was slightly higher from the

22- to the 45-minute timepoints of the experiments; however, the difference cannot be assessed statistically (Figure 3A). Such a change couldn't be observed in the samples of the hyperglycemic rats (Figure 3B).

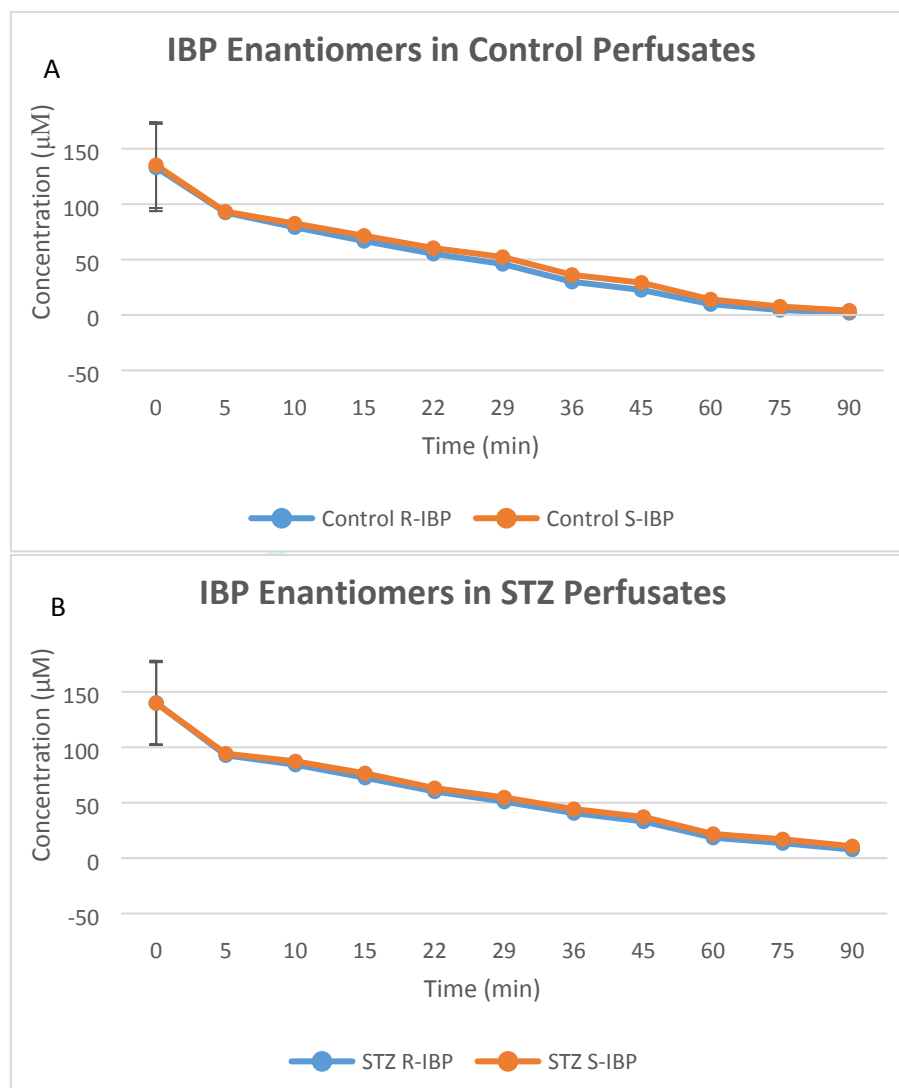


Figure 3. The concentrations of the IBP enantiomers in the extracts of the intestinal perfusates of the control (3A) and hyperglycemic (3B) rats (n=4).

In the bile samples collected during the intestinal perfusion of racemic IBP, only the (S)-IBP enantiomer could be detected. HPLC chromatograms of bile samples of control and hyperglycemic rats at the 30, 60, and 120-minute timepoints are shown in Figures 5S and 6S, respectively. In the chromatograms, two unknown peaks also appeared. Based on their relative retention times (compared to the IS), none of them could be identified by the available standards (IBP, 1-, 2-, 3-OH-IBP, and IBP-GLU). The concentrations of the (S)-IBP enantiomer measured in the bile samples of control and hyperglycemic rats are shown in Figure 4. The biliary excretion (S)-IBP was statistically lower in the hyperglycemic (STZ-treated) animals.

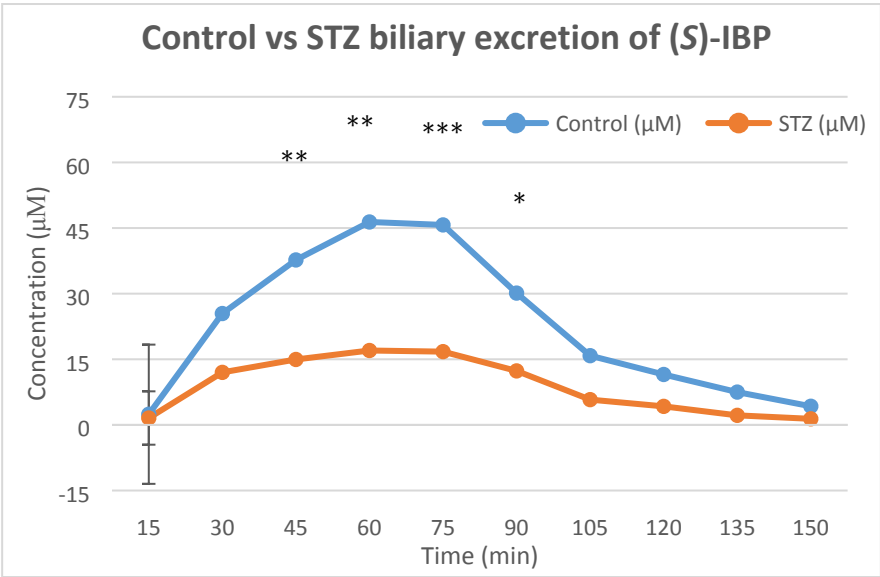


Figure 4. The concentration of (S)-IBP in the extracts of the bile samples of control and hyperglycemic animals (n=4). Significant differences from the control value: * p < 0.05, ** p < 0.01, and *** p < 0.001.

The cumulative excretion of (S)-IBP in the extracts of the bile samples of control and hyperglycemic rats is shown in Figure 5. The cumulative excretion of the IBP enantiomer was statistically lower in the hyperglycemic rats.

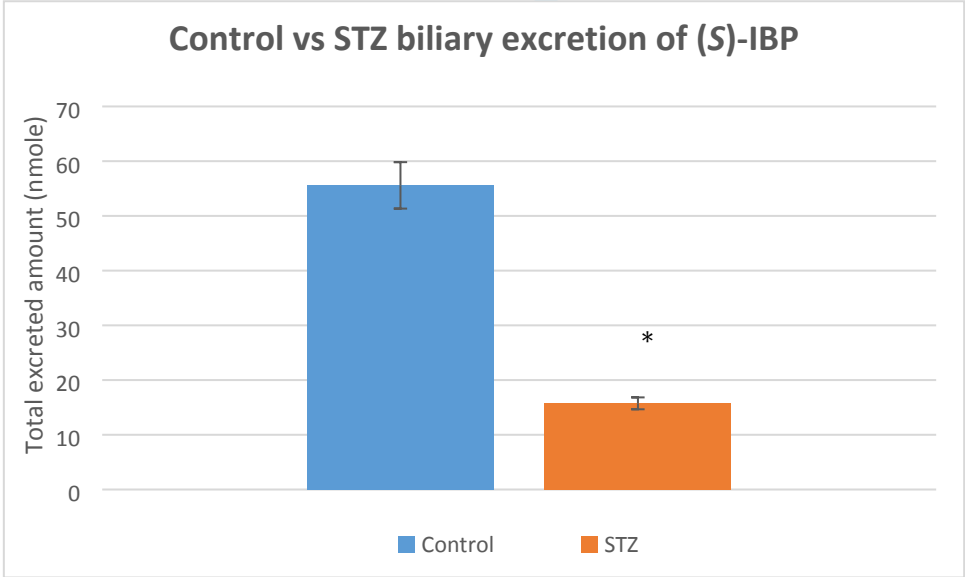


Figure 5. The cumulative excretion of (S)-IBP enantiomer in the extracts of the bile samples of control and hyperglycemic rats (n=4). Significant differences from the control value: * p < 0.01.

4. Results and discussion

As shown in Figures 3A and 3B, the concentration of the two IBP enantiomers was continuously decreased in the intestinal perfusion medium over the experiments.

(In the samples collected between the 105-150 min timepoints, IBP peaks could not be quantified. Legen et al. demonstrated that the inwardly directed proton gradient could be a driving force for transporting monocarboxylic acid-type drugs (among them IBP) across the intestinal epithelia [16]. The passive diffusion of the compound can explain the gradual decrease of concentration of the ibuprofen enantiomers in the perfusate.

Cumulative disappearance (absorption, metabolism, and excretion) of both enantiomers of IBU was lower in the hyperglycemic rats (Figures 3A and 3B). The ratio of the enantiomers showed a moderate increase in the control rats; however, the change was statistically insignificant (Figures 4A and 4B). Several reports have demonstrated that diabetes may decrease P-gp (MDR1) efflux transporter function and expression in the brain and intestine [17-20]. In addition, curcumin and ibuprofen were reported to inhibit the P-gp activity of human sarcoma MES-SA/Dx-5 cells well below their therapeutic plasma concentrations [21]. P-gp effluxes drug substrates from enterocytes into the GI lumen, thus regulating the intestinal absorption of drugs. Accordingly, the observed alteration can be explained by the reduced activity of P-gp due to the experimental hyperglycemia and the accumulating ibuprofen in the endothelial cells. The progressively increasing cellular IBP level attenuates the concentration gradient, considered the most important factor in the entrance of ibuprofen [1].

In the bile samples, only the (S)-ibuprofen enantiomer could be detected (Figures 5S and 6S). Figures 6 and 7 show that the excreted amount of (S)-IBP is statistically lower in the bile samples of the hyperglycemic rats. Uptake transporters are expressed highly on the basolateral membrane of hepatocytes [22, 23]. The organic anion transporters hOAT1-5 are predominantly expressed in renal proximal tubules; however, hOAT2 (Slc22a7) is also expressed in the liver [24-26]. In the rat, the main site of expression of Oat2 is the sinusoidal membrane domain of the hepatocytes [27]. Kimoto et al. evaluated the role of organic anion transporter 2 (OAT2)-mediated hepatic uptake in the clearance of 25 ECCS 1A drugs. The authors provided evidence for the role of OAT2-mediated hepatic uptake of most of the investigated ECCS 1A drugs, including IBP [28]. Members of the organic anion transporting polypeptide (OATP) family are also important determinants of hepatic uptake of endogenous and exogenous compounds. Kindla et al. reported that only diclofenac was significantly transported by OATP1B3, whereas all other NSAIDs investigated (including IBP) were not substrates for these uptake transporters [29]. Accordingly, ibuprofen is supposed to enter the hepatocytes by passive diffusion and OATP2-mediated uptake [1, 28, 30].

Schneider et al. investigated the biliary elimination of ibuprofen, indomethacin, and diclofenac in patients suffering from obstructions of the common bile duct. Whereas a very low amount (0.15%) of ibuprofen was excreted in bile as unchanged drug and active conjugates, biliary elimination of diclofenac was somewhat higher (1.09%), and that of indomethacin was substantial (above 10%) [31]. Like the small intestine, the P-gp efflux transporter (Mdr1) is also expressed in the apical side of the rat hepatocytes [22]. P-gp has been reported to be reduced in hyperglycemic rats [18, 32, 33]. Using the present experimental protocol, we found a relatively low amount of (non-enantiomer-separated) IBP and IBP-glucuronide in the bile, which was depressed

under hyperglycemic conditions. Our molecular biology studies on liver samples of the STZ-treated rats showed decreased expression of the efflux transporters P-gp (Mdr1B), Mrp2, and Bcrp [8]. These transporters are involved in exporting organic anions from the hepatocytes into the bile canaliculus [34].

Biliary excretion of the parent compounds and their metabolites is crucial for the so-called enterohepatic circulation of the drugs and other xenobiotics [35]. Drugs in bile are usually more concentrated than in plasma, and passive transport is considered negligible. Accordingly, biliary excretion represents an active process involving transporters embedded in the apical membrane of hepatocytes. Furthermore, the liver was the most important organ in the unidirectional conversion of (*R*)-arylpropionic acid drugs to their (*S*) enantiomer. Whether the asymmetric appearance of the IBP enantiomers is the consequence of the OAT2-mediated enantioselective hepatic uptake or the enantioselective excretion of the hepatic efflux transporters P-gp (Mdr1B), Mrp2, and Bcrp (or both) needs further molecular biology studies.

5. Conclusions

This study provided experimental data on intestinal elimination and hepatic excretion of the IBP enantiomers in control and hyperglycemic experimental animals. The results demonstrated that the elimination of IBP from the small intestine is not enantioselective. Analysis of the bile showed the presence of only the pharmacologically more active (*S*)-IBP enantiomer. Since the pharmacological activity of (*S*)-IBP is one order of magnitude higher than that of the (*R*)-IBP [36], the asymmetric appearance of the enantiomers in the bile could determine the pharmacokinetics and pharmacodynamic action of the drug.

6. Supplementary Materials

Figure captions

Figure 1S. (A) HPLC-UV chromatogram of the (*S*)-IBP ($t_R=16.85$ min) in methanol, (B) the naproxen ($t_R=20.44$ min) in methanol, (C) the racemic IBP ((*R*)-ibuprofen (1) $t_R=14.59$ min, (*S*)-ibuprofen (2) $t_R=16.86$ min) and naproxen (3) ($t_R=20.43$ min) dissolved in the mobile phase.

Figure 2S. The HPLC-UV calibration curves of *R*-IBP (A) and *S*-IBP (B) with the linear regression trend lines, constructed by five different concentrations (250 μ M, 200 μ M, 150 μ M, 100 μ M, 50 μ M) of standard racemic IBP.

Figure 3S. HPLC-UV chromatograms of extracts of intestinal perfusate of 250 μ M racemic IBP spiked with 250 μ M NAP (IS) at (A) 0-minute: (*R*)-IBP (1) ($t_R=14.52$ min), (*S*)-IBP (2) ($t_R=16.75$ min), NAP (3) ($t_R=20.35$ min); (B) 29-minute: (*R*)-IBP (1) ($t_R=14.53$ min), (*S*)-IBP (2) ($t_R=16.76$ min), NAP (3) ($t_R=20.35$ min); and (C) 90-minute: (*R*)-IBP (1) ($t_R=14.54$ min), (*S*)-IBP (2) ($t_R=16.78$ min), NAP (3) ($t_R=20.35$ min) of control rats.

Figure 4S. HPLC-UV chromatograms of extracts of intestinal perfusate of 250 μ M racemic IBP spiked with 250 μ M NAP (IS) at (A) 0-minute: (*R*)-IBP (1) ($t_R=14.52$ min),

(S)-IBP (**2**) (t_R =16.75 min), NAP (**3**) (t_R = 20.35 min); (**B**) 29-minute: (*R*)-ibuprofen (**1**) (t_R =14.53 min), (S)-IBP (**2**) (t_R =16.76 min), NAP (**3**) (t_R =20.35 min); and (**C**) 90-minute: (*R*)-IBP (**1**) (t_R =14.51 min), (S)-IBP (**2**) (t_R =16.73 min), NAP (**3**) (t_R =20.31 min) of hyperglycemic rats.

Figure 5S. (A) HPLC-UV chromatogram of 250 μ M of racemic IBP ((*R*)- (**1**) t_R =14.45 min, (S)-IBP (**2**) t_R =16.69 min) and NAP (**3**) (t_R =20.26 min) in the mobile phase; HPLC-UV chromatograms of bile extract at (**B1**) 30-minute: unknown peak (**1**) (t_R =7.68 min), unknown peak (**2**) (t_R =15.72 min), (S)-IBP (**3**) (t_R =16.75 min), NAP (**4**) (t_R =20.33 min); (**B2**) 60-minute: unknown peak (**1**) (t_R = 7.68 min), unknown peak (**2**) (t_R =15.72 min), (S)-IBP (**3**) (t_R = 16.76 min), NAP (**4**) (t_R =23.35 min); and (**B3**) 120-minute: unknown peak (**1**) (t_R =7.69 min), unknown peak (**2**) (t_R =15.72 min), (S)-IBP (**3**) (t_R =16.76 min), NAP (**4**) (t_R =20.36 min) of control rats.

Figure 6S. (A) HPLC-UV chromatogram of 250 mM of racemic IBP ((*R*)- (**1**) t_R =14.45 min, (S)-IBP (**2**) t_R =16.69 min) and NAP (**3**) (t_R =20.26 min) in the mobile phase; HPLC-UV chromatograms of excreted bile extract at (**B1**) 30-minute: unknown peak (**1**) (t_R =7.68 min), (S)-IBP (**2**) (t_R =16.72 min), NAP (**3**) (t_R =20.3 min); (**B2**) 60-minute: unknown peak (**1**) (t_R =7.66 min), (S)-IBP (**2**) (t_R =16.73 min), NAP (**3**) (t_R =20.31 min); and (**B3**) 120-minute: unknown peak (**1**) (t_R =7.66 min), (S)-IBP (**2**) (t_R =16.75 min), NAP (**3**) (t_R =20.32 min) of hyperglycemic rats.

408

Table captions

Table 1S. Data for system suitability of methanol solutions of racemic ibuprofen (*rac*-IBP) (100 μ M, 250 μ M) and naproxen sodium (NAP) as internal standard (IS) (50 μ M).

Table 2S. Data for system repeatability methanol solution of racemic ibuprofen (*rac*-IBP) (100 μ M, 250 μ M) and naproxen sodium (NAP) as internal standard (IS) (50 μ M).

Table 3S. Data for system intermediate precision of methanol solution of racemic ibuprofen (*rac*-IBP) (100 μ M, 250 μ M) and naproxen sodium (NAP) as internal standard (IS) (50 μ M).

Table 4S. Accuracy of NAP, (*R*)- and (S)-IBP determination in spiked control perfusates and spiked control bile with the same range of standard dilutions of racemic IBP (50 μ M, 100 μ M, 250 μ M) and NAP(50 μ M).

420

10. References

- [1] Mazaleuskaya LL, Theken KN, Gong L, Thorn CF, FitzGerald GA, Altman RB, Klein TE. PharmGKB summary: Ibuprofen pathways. *Pharmacogenet Genomics*. 2015; 25:96-106. DOI: 10.1097/FPC.000000000000113
- [2] Rudy AC, Knight PM, Brater DC, Hall SD. Stereoselective metabolism of ibuprofen in humans: administration of R-, S- and racemic ibuprofen. *J Pharmacol Exp Ther*. 1991; 259:1133–1139. PMID: 1762067. Erratum in: *J Pharmacol Exp Ther*. 1992;260:1456.
- [3] Brocks D, Jamali F The pharmacokinetics of ibuprofen in humans and animals. In: Rainsford KD (ed) *Ibuprofen. A critical bibliographic review*. Taylor & Francis, London, 1999, pp 89–142.
- [4] Jeffrey P, Tucker GT, Bye A, Crewe HK, Wright PA The site of inversion of R(-)-ibuprofen: studies using rat in situ isolated perfused intestine/liver preparations. *J Pharm Pharmacol*. 1991; 43:715–720. DOI: 10.1111/j.2042-7158.1991.tb03464.x
- [5] Jamali F, Mehvar R, Russell AS, Sattari S, Yakimets WW, Koo J. Human pharmacokinetics of ibuprofen enantiomers following different doses and formulations: intestinal chiral inversion. *J Pharm Sci*. 1992; 81:221–225. <https://doi.org/10.1002/jps.2600810306>
- [6] Keep DR, Sidelmann UG, Hansen SH. Isolation and characterization of major phase I and II metabolites of ibuprofen. *Pharm Res*. 1997; 14:676-680. <https://doi.org/10.1023/A:1012125700497>
- [7] Rainsford KD. Ibuprofen: pharmacology, efficacy and safety. *Inflammopharmacol*. 2009; 17:275–342. DOI: 10.1007/s10787-009-0016-x
- [8] Kovács NP, Almási A, Garai K, Kuzma M, Vancea S, Fischer E, Perjési P. Investigation of intestinal elimination and biliary excretion of ibuprofen in hyperglycemic rats. *Can J Physiol Pharmacol* 2019; 97:1080-1089. doi: 10.1139/cjpp-2019-0164.
- [9] Fischer E, Almási A, Bojcsev S, Fischer T, Kovács NP, Perjési P. Effect of experimental diabetes and insulin replacement on intestinal metabolism and excretion of 4-nitrophenol in rats. *Can J Physiol Pharmacol*. 2015; 93:459–464. doi: 10.1139/cjpp-2015-0065.
- [10] Almási A, Perjési P, Fischer E. The relative importance of the small intestine and the liver in Phase II metabolic transformations and elimination of p-nitrophenol administered in different doses in the rat. *Sci Pharm*. 2020; 88:512020. <https://doi.org/10.3390/scipharm88040051>
- [11] Klaassen CD. Bile flow and bile composition during bile acid depletion and administration. *Can J Physiol Pharmacol* 1973; 52:334–348. <https://doi.org/10.1139/y74-045>.
- [12] Bonato PS, Del Lama MPFM, de Carvalho R. Enantioselective determination of ibuprofen in plasma by high-performance liquid chromatography–electrospray mass spectrometry. *J Chrom B*. 2003; 796:413–420. DOI: 10.1016/j.jchromb.2003.08.031
- [13] Kromasil Application Note. <https://www.kromasil.com/applications/view.php?app=c0128>
- [14] European legislation (Directive 2010/63/E.U.). ELI: <https://eur-lex.europa.eu/eli/dir/2010/63/oj>
- [15] Hungarian Government regulation (40/2013., II. 14.) <https://www.fao.org/faolex/results/details/en/c/LEX-FAOC124420>

- [16] Legen I, Zakelj S, Kristl A. Polarised transport of monocarboxylic acid type drugs across rat jejunum in vitro: the effect of mucolysis and ATP-depletion. *Int J Pharm.* 2003; 256:161–166. DOI: 10.1016/s0378-5173(03)00073-5
- [17] Liu H, Xu X, Yang Z, Deng Y, Liu X, Xie L. Impaired function and expression of P-glycoprotein in blood-brain barrier of streptozotocin-induced diabetic rats. *Brain Res* 2006; 1123:245–252. <https://doi.org/10.1016/j.brainres.2006.09.061>
- [18] Nawa A, Fujita (Hamabe) W, Tokuyama S. Inducible nitric oxide synthase-mediated decrease of intestinal P-glycoprotein expression under streptozotocin-induced diabetic conditions. *Life Sci* 2010; 86:402–409. <https://doi.org/10.1016/j.lfs.2010.01.009>
- [19] Zhang L, Lu L, Jin S., Jing Xj-y, Yao D, Hu N, Liu L, Ru Duan R, Liu X-d, Wang G-j, Xie L Tissue-specific alterations in expression and function of P-glycoprotein in streptozotocin-induced diabetic rats. *Acta Pharmacol Sin.* 2011; 32:956–966. DOI: <https://doi.org/10.1038/aps.2011.33>
- [20] Drozdziak M, Czekawy I, Oswald S, Drozdziak A, Intestinal drug transporters in pathological states: an overview. *Pharmacol. Reports.* 2020; 72:1173–1194. <https://doi.org/10.1007/s43440-020-00139-6>
- [21] Angelini A, Lezzi M, di Febbo C, di Ilio C, Cuccurullo F, Porreca E. Reversal of P-glycoprotein-mediated multidrug resistance in human sarcoma MES-SA/Dx-5 cells by nonsteroidal anti-inflammatory drugs. *Oncol Reports.* 2008; 20:731-735. https://doi.org/10.3892/or_00000067
- [22] Klaassen CD, Lu H. (2008). Xenobiotic transporters: Ascribin DOI: 10.1124/pr.109.002014g function from gene knockout and mutation studies. *Toxicol Sci.* 2008; 101:186–196.
- [23] Burckhardt G. Drug transport by Organic Anion Transporters (OATs). *Pharmacol Ther.* 2012; 136:106–130. DOI: 10.1016/j.pharmthera.2012.07.010
- [24] Cha SH, Sekine T, Fukushima JI, Kanai Y, Kobayashi Y, Goya T, Endou H. Identification and characterization of human organic anion transporter 3 expressing predominantly in the kidney. *Mol Pharmacol.* 2001; 59:1277-1286. DOI: 10.1124/mol.59.5.1277
- [25] Kobayashi Y, Ohshiro N, Sakai R, Ohbayashi M, Kohyama N, Yamamoto T. Transport mechanism and substrate specificity of human organic anion transporter 2 (hOat2 [SLC22A7]). *J Pharm Pharmacol,* 2005; 57:573–578. <https://doi.org/10.1211/0022357055966>
- [26] Nigam SK, Bush KT, Martovetsky G, Ahn S-Y, Liu HC, Richard E, et al.. The organic anion transporter (OAT) family: A systems biology perspective. *Physiol Rev.* 2015; 95:83–123. DOI: 10.1152/physrev.00025.2013
- [27] Fork C, Bauer T, Golz S, Geerts A, Weiland J, Del Turco D, et al. OAT2 catalyses efflux of glutamate and uptake of orotic acid. *Biochem J.* 2011; 436:305-312. doi:10.1042/BJ20101904
- [28] Kimoto E, Mathialagan S, Tylaska L, Niosi M, Lin J, Carlo AA, et al. Organic anion transporter 2-mediated hepatic uptake contributes to the clearance of high-permeability-low-molecular-weight acid and zwitterion drugs: Evaluation using 25 drugs. *J Pharmacol Exp Ther.* 2018; 367:322–334. DOI: 10.1124/jpet.118.252049
- [29] Kindla J, Müller F, Mieth M, Fromm MF, König J. Influence of non-steroidal anti-inflammatory drugs on organic anion transporting polypeptide (OATP) 1B1- and

- 514 OATP1B3-mediated drug transport. *Drug Metabol Disp.* 2011; 39:1047–1053. DOI:
515 10.1124/dmd.110.037622
- 516 [30] Davies NM (1998) Clinical pharmacokinetics of ibuprofen. The first 30 years. *Clin*
517 *Pharmacokinet.* 1998; 34:101-154. DOI: 10.2165/00003088-199834020-00002
- 518 [31] Schneider HT, Nuernberg B, Dietzel K, Brune K. Biliary elimination of non-steroidal
519 anti-inflammatory drugs in patients. *Br J Clin Pharmac.* 1990; 29:127-131. doi:
520 10.1111/j.1365-2125.1990.tb03613.x
- 521 [32] Anger GJ, Magomedova L, Piquette-Miller M. Impact of acute streptozotocin-
522 induced diabetes on ABC transporter expression in rats. *Chem Biodivers.* 2009;
523 6:1943-1959.
- 524 [33] Zhang L, Lu L, Jin S, Jing XJ, Yao D, Hu N, et al. Tissue-specific alterations in
525 expression and function of P-glycoprotein in streptozotocin-induced diabetic rats. *Acta*
526 *Pharmacol Sin.* 2011; 32:956-966. <https://doi.org/10.1038/aps.2011.33>
- 527 [34] Jetter A.; Kullak-Ublick G.A. Drugs and hepatic transporters: A review. *Pharmacol.*
528 *Res.* 2020; 154:104234. <https://doi.org/10.1016/j.phrs.2019.04.018>
- 529 [35] Yang X, Gandhi YA, Duignan DB, Morris ME. Prediction of biliary excretion in rats
530 and humans using molecular weight and quantitative structure–pharmacokinetic
531 relationships. *AAPS J.* 2009; 11:511-525. DOI: 10.1208/s12248-009-9124-1
- 532 [36] Neupert W, Brugger R, Euchenhofer C, Brune K, Geisslinger G.. Effects of
533 ibuprofen enantiomers and its coenzyme A thioesters on human prostaglandin
534 endoperoxide synthases. *Br J Pharmacol.* 1997; 122:487-492.
535 <https://doi.org/10.1038/sj.bjp.0701415>
- 536
- 537

Figure captions

Figure 1. Structure of ibuprofen (**1**) and ibuprofen β -D-glucuronide (**2**).

Figure 2. (A) HPLC-UV chromatogram of the two IBP enantiomers ((*R*)-IBP (**1**) t_R =14.5 min, (*S*)-IBP (**2**) t_R =16.72 min and NAP (**3**) t_R =20.3 min), extracted from the spiked control perfusion medium of non-treated animal, (B) the blank control perfused medium, (C) the two IBP enantiomers ((*R*)-IBP (**1**) t_R =14.4 min, (*S*)-IBP (**2**) t_R =16.61 min and NAP (**3**) t_R =20.18 min), extracted from the spiked control bile of non-treated animal; (D) the blank control bile.

Figure 3. The concentrations of the IBP enantiomers in the extracts of the intestinal perfusates of the control (**3A**) and hyperglycemic (**3B**) rats (n=4).

Figure 4. The concentration of (*S*)-IBP in the extracts of the bile samples of control and hyperglycemic animals (n=4). Significant differences from the control value: * $p < 0.05$, ** $p < 0.01$, and *** $p < 0.001$.

Figure 5. The cumulative excretion of (*S*)-IBP enantiomer in the extracts of the bile samples of control and hyperglycemic rats (n=4) Significant differences from the control value: * $p < 0.01$.

Effect of experimental hyperglycemia on intestinal elimination and biliary excretion of ibuprofen enantiomers in hyperglycemic rats

Supplementary Material

Mohammed Othman Hawsar^{1,2}, Attila Almási¹, Pál Perjési^{1*}

¹Institute of Pharmaceutical Chemistry, Faculty of Pharmacy, University of Pécs, Pécs, Hungary

²College of Veterinary Medicine, University of Sulaimani, Sulaymaniyah, Kurdistan Region, Iraq

*Corresponding Author

Pál Perjési, PhD

ORCID: <https://orcid.org/0000-0002-1057-9664>

Institute of Pharmaceutical Chemistry

University of Pécs

H-7624 Pécs

HUNGARY

E-mail: pal.perjesi@gytk.pte.hu

Figure 1S. (A) HPLC-UV chromatogram of the (S)-IBP ($t_R=16.85$ min) in methanol, (B) the naproxen ($t_R=20.44$ min) in methanol, (C) the racemic IBP ((*R*)-ibuprofen (1) $t_R=14.59$ min, (*S*)-ibuprofen (2) $t_R=16.86$ min) and naproxen (3) ($t_R=20.43$ min) dissolved in the mobile phase.

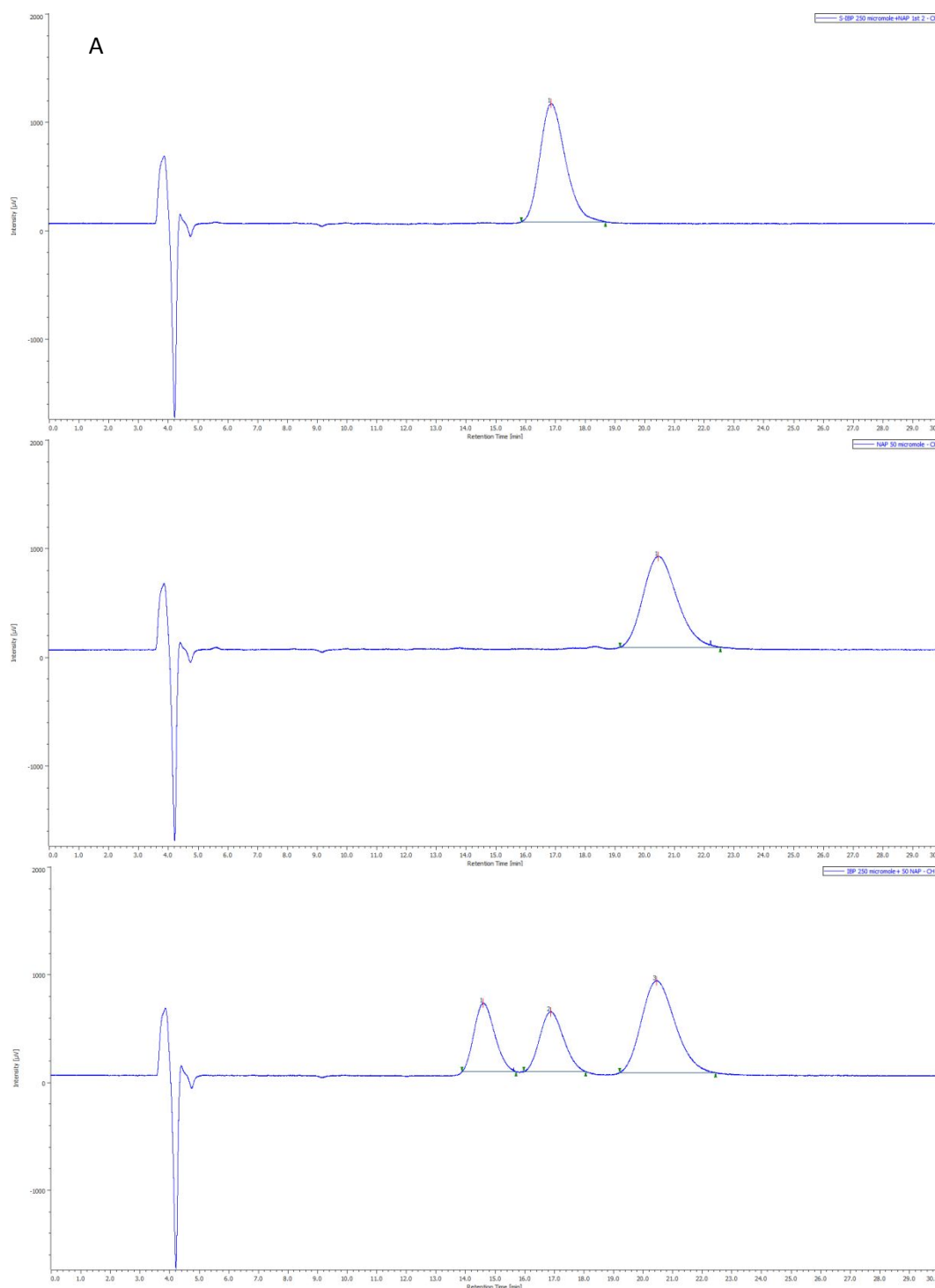


Figure 2S. The HPLC-UV calibration curves of *R*-IBP (**A**) and *S*-IBP (**B**) with the linear regression trend lines, constructed by five different concentrations (250 μ M, 200 μ M, 150 μ M, 100 μ M, 50 μ M) of standard racemic IBP.

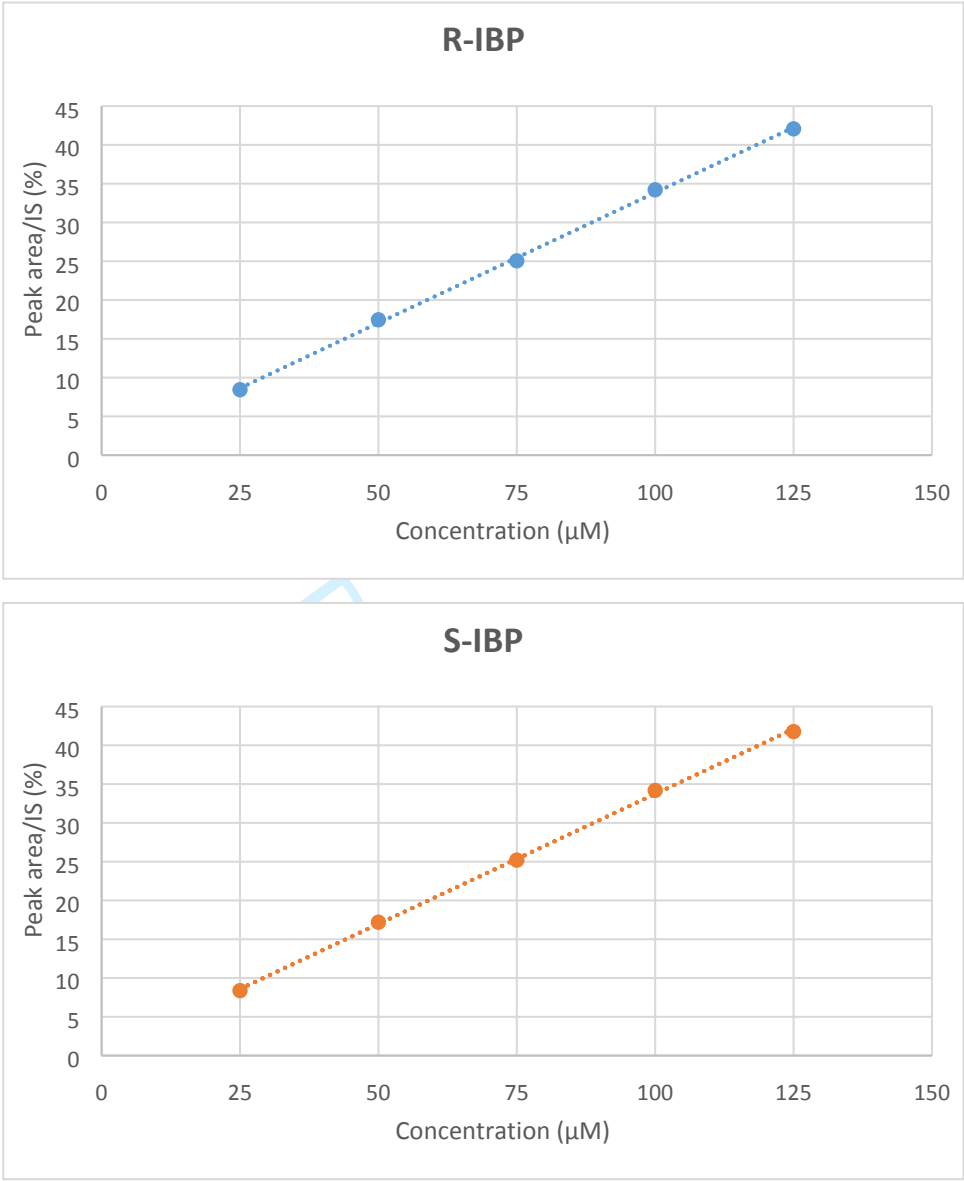


Figure 3S. HPLC-UV chromatograms of extracts of intestinal perfusate of 250 μ M racemic IBP spiked with 250 μ M NAP (IS) at (A) 0-minute: (*R*)-IBP (1) (t_R =14.52 min), (*S*)-IBP (2) (t_R =16.75 min), NAP (3) (t_R =20.35 min); (B) 29-minute: (*R*)-IBP (1) (t_R =14.53 min), (*S*)-IBP (2) (t_R =16.76 min), NAP (3) (t_R =20.35 min); and (C) 90-minute: (*R*)-IBP (1) (t_R =14.54 min), (*S*)-IBP (2) (t_R =16.78 min), NAP (3) (t_R = 20.35 min) of control rats.

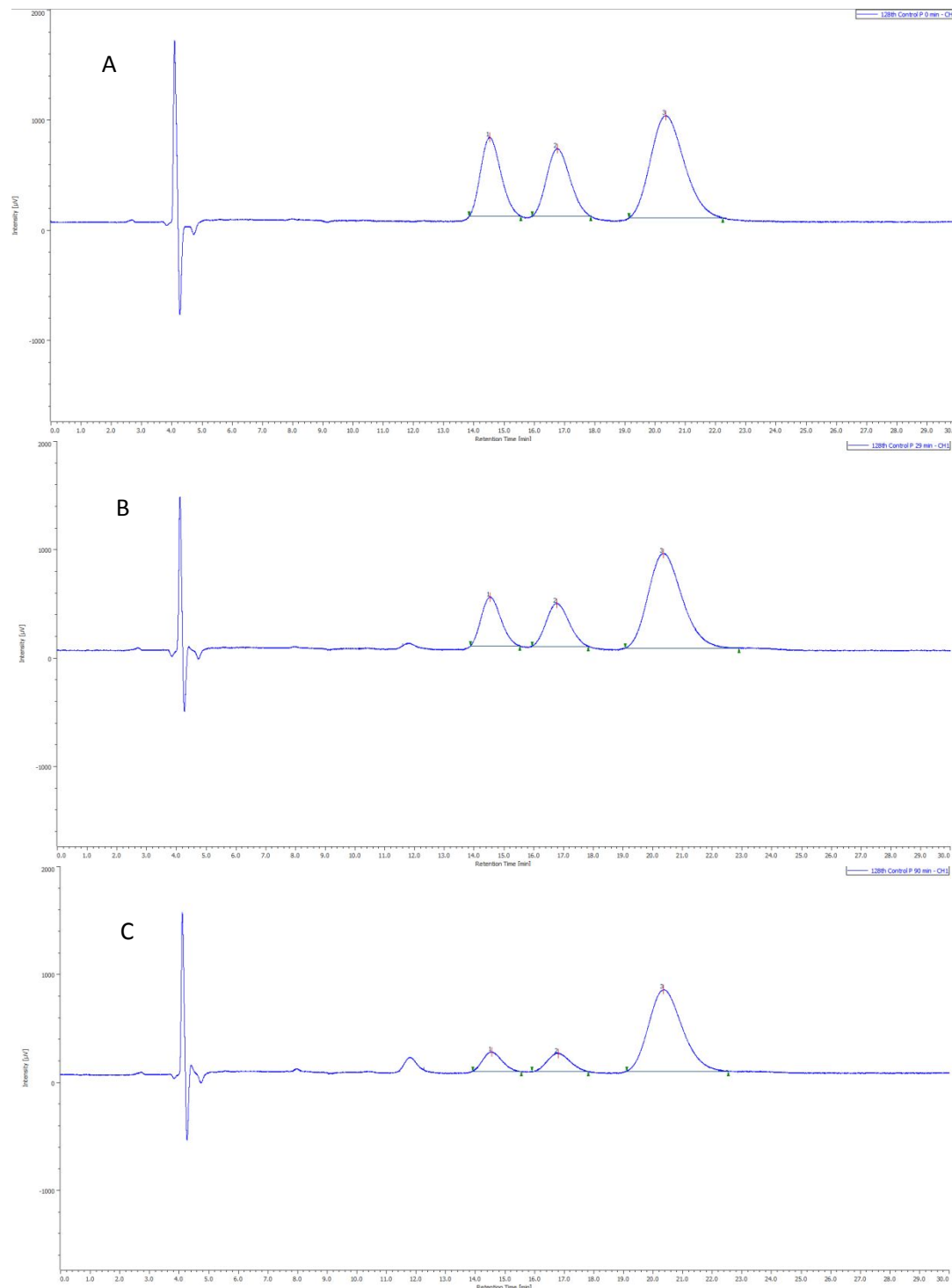


Figure 4S. HPLC-UV chromatograms of extracts of intestinal perfusate of 250 μ M racemic IBP spiked with 250 μ M NAP (IS) at **(A)** 0-minute: (*R*)-IBP (**1**) (t_R =14.52 min), (*S*)-IBP (**2**) (t_R =16.75 min), NAP (**3**) (t_R = 20.35 min); **(B)** 29-minute: (*R*)-ibuprofen (**1**) (t_R =14.53 min), (*S*)-IBP (**2**) (t_R =16.76 min), NAP (**3**) (t_R =20.35 min); and **(C)** 90-minute: (*R*)-IBP (**1**) (t_R =14.51 min), (*S*)-IBP (**2**) (t_R =16.73 min), NAP (**3**) (t_R =20.31 min) of hyperglycemic rats.

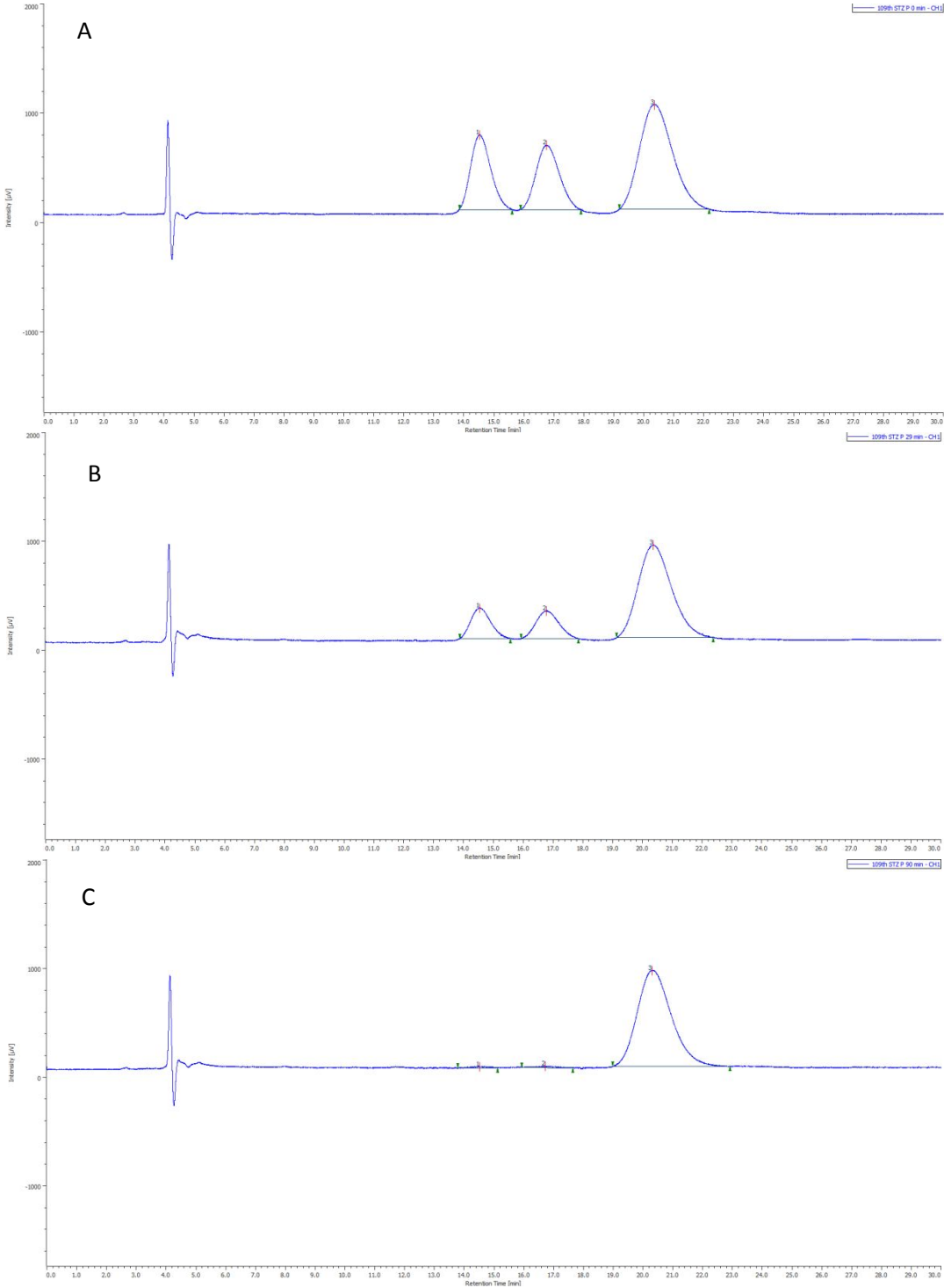
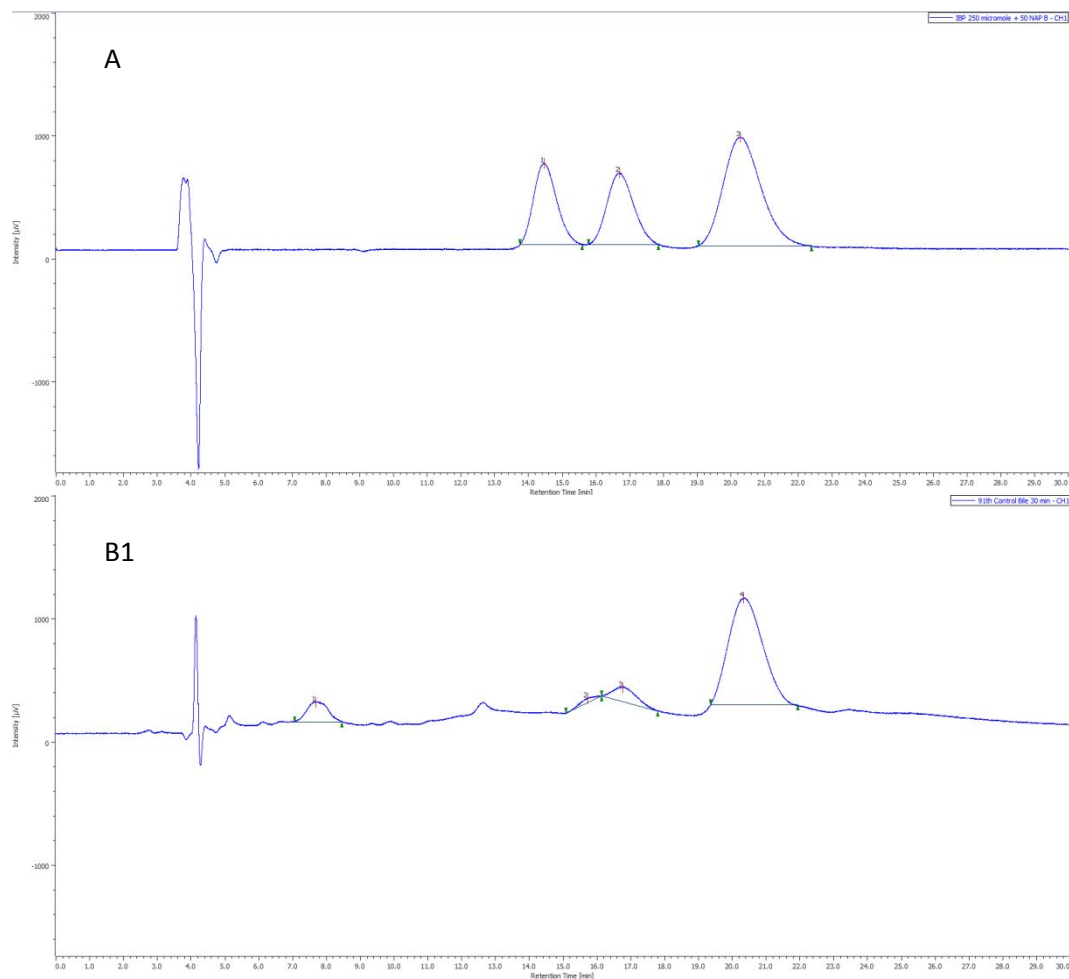


Figure 5S. (A) HPLC-UV chromatogram of 250 μ M of racemic IBP ((*R*)- (**1**) t_R =14.45 min, (*S*)-IBP (**2**) t_R =16.69 min) and NAP (**3**) (t_R =20.26 min) in the mobile phase; HPLC-UV chromatograms of bile extract at (**B1**) 30-minute: unknown peak (**1**) (t_R =7.68 min), unknown peak (**2**) (t_R =15.72 min), (*S*)-IBP (**3**) (t_R =16.75 min), NAP (**4**) (t_R =20.33 min); (**B2**) 60-minute: unknown peak (**1**) (t_R = 7.68 min), unknown peak (**2**) (t_R =15.72 min), (*S*)-IBP (**3**) (t_R = 16.76 min), NAP (**4**) (t_R =23.35 min); and (**B3**) 120-minute: unknown peak (**1**) (t_R =7.69 min), unknown peak (**2**) (t_R =15.72 min), (*S*)-IBP (**3**) (t_R =16.76 min), NAP (**4**) (t_R =20.36 min) of control rats.



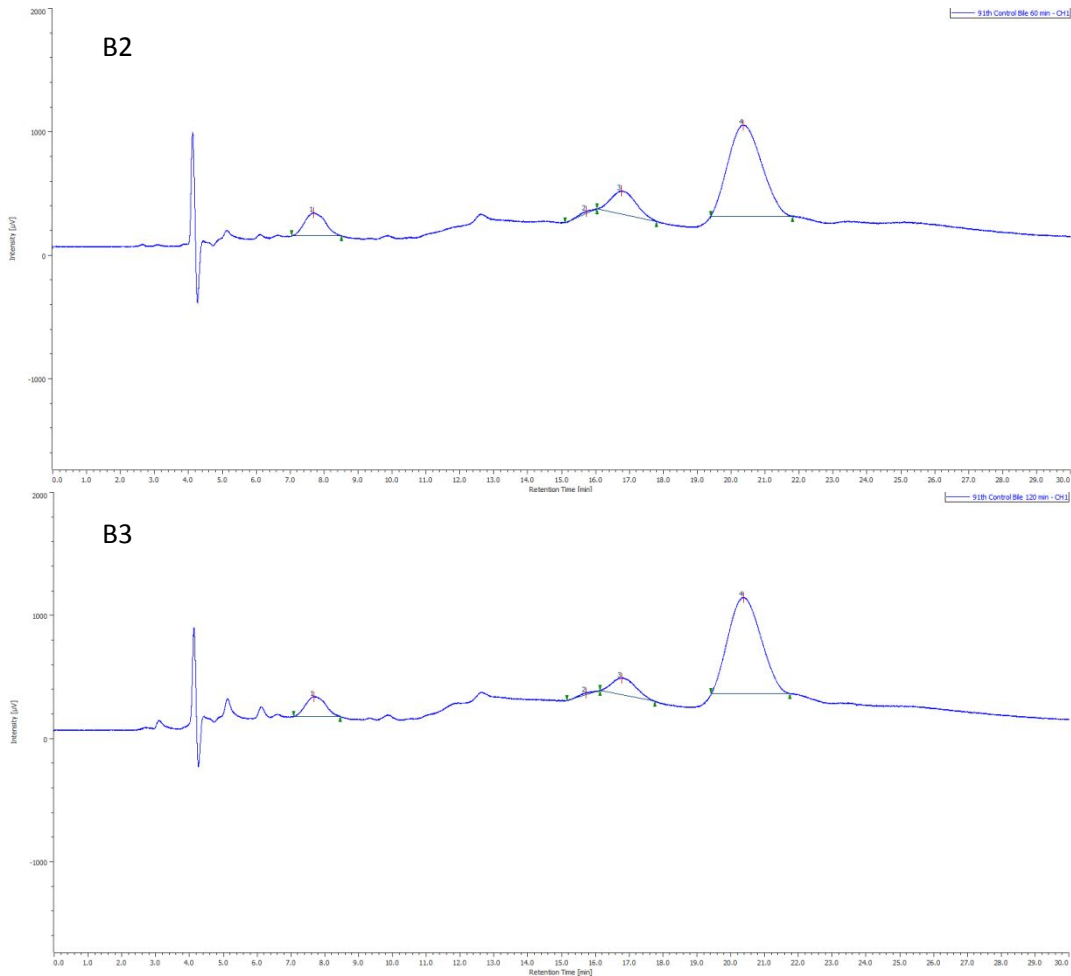
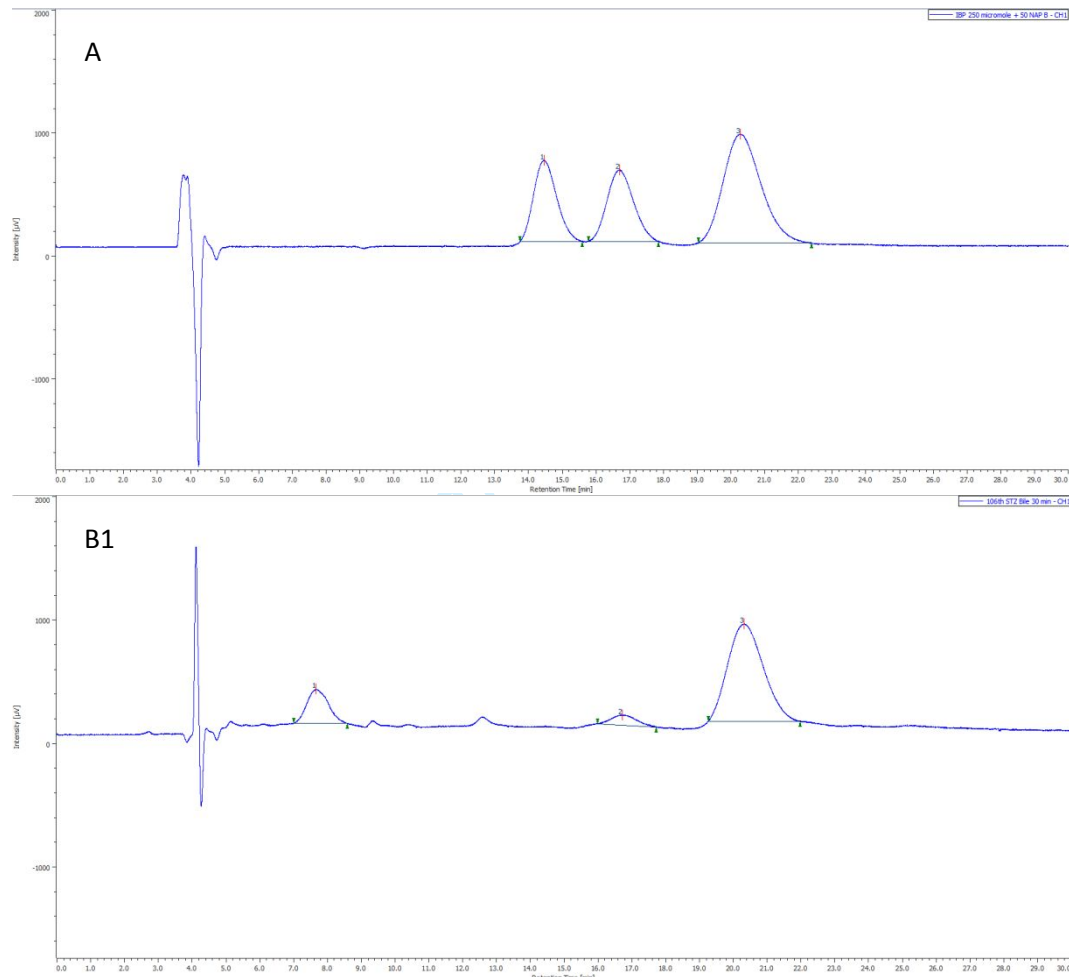


Figure 6S. (A) HPLC-UV chromatogram of 250 mM of racemic IBP ((*R*)- (**1**) $t_R=14.45$ min, (*S*)-IBP (**2**) $t_R=16.69$ min) and NAP (**3**) ($t_R=20.26$ min) in the mobile phase; HPLC-UV chromatograms of excreted bile extract at (**B1**) 30-minute: unknown peak (**1**) ($t_R=7.68$ min), (*S*)-IBP (**2**) ($t_R=16.72$ min), NAP (**3**) ($t_R=20.3$ min); (**B2**) 60-minute: unknown peak (**1**) ($t_R=7.66$ min), (*S*)-IBP (**2**) ($t_R=16.73$ min), NAP (**3**) ($t_R=20.31$ min); and (**B3**) 120-minute: unknown peak (**1**) ($t_R=7.66$ min), (*S*)-IBP (**2**) ($t_R=16.75$ min), NAP (**3**) ($t_R=20.32$ min) of hyperglycemic rats.



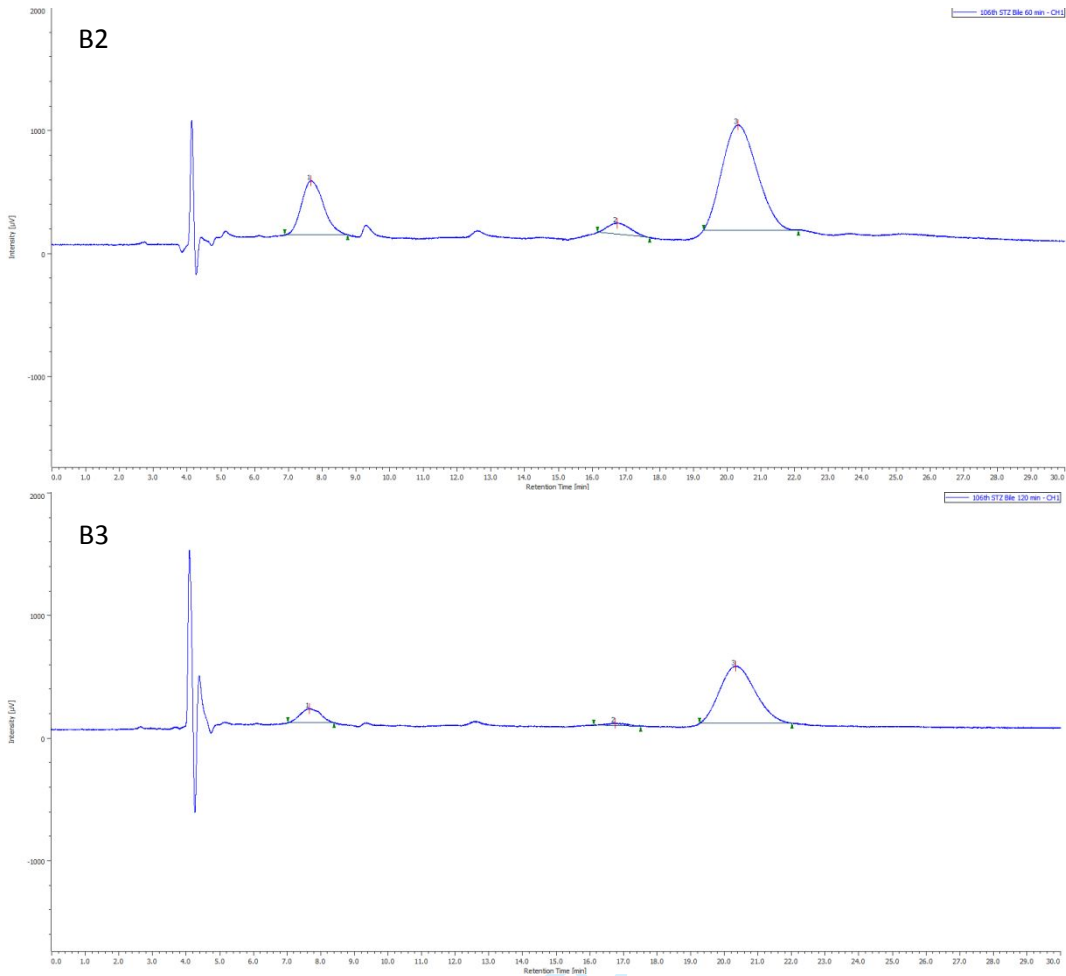


Table 1S. Data for system suitability of methanol solutions of racemic ibuprofen (*rac*-IBP) (100 μ M, 250 μ M) and naproxen sodium (NAP) as internal standard (IS) (50 μ M).

Injections (Standard Solutions)	NAP			rac-IBP				
	C (μ M)	t_R (min)	Area	C (μ M)	t_R (min)	R-Area	t_R (min)	S-Area
1	50	20.24	68666	100	14.48	12019	16.74	12119
2	50	20.22	68779	100	14.47	12081	16.72	12125
3	50	20.29	68783	100	14.50	12034	16.75	12156
4	50	20.30	68542	100	14.52	12034	16.79	12215
5	50	20.31	68632	100	14.53	12065	16.79	12247
Mean		20.27	68680		14.50	12047	16.76	12172
RSD%		0.17	0.13		0.16	0.19	0.17	0.41
Compounds	t_R	RRT	k'	T	NTP	R_s		
NAP	20.27	N/A	19.27	1.23	1567	N/A		
R-IBP	14.50	1.40	13.50	1.24	2057	1.63		
S-IBP	16.76	1.21	15.76	1.16	2009	1.99		
1	50	20.24	68740	250	14.47	32102	16.72	32200
2	50	20.24	68575	250	14.46	32121	16.70	32481
3	50	20.24	68552	250	14.46	32107	16.70	32272
4	50	20.24	68667	250	14.47	32096	16.71	32224
5	50	20.25	68244	250	14.48	31873	16.72	31979
Mean		20.24	68556		14.47	32060	16.71	32231
RSD%		0.03	0.25		0.03	0.29	0.04	0.50
Compounds	t_R	RRT	k'	T	NTP	R_s		
NAP	20.24	N/A	19.24	1.26	1522	N/A		
R-IBP	14.47	1.40	13.47	1.24	2057	1.63		
S-IBP	16.71	1.21	15.71	1.17	2026	1.99		

t_R : retention time, RRT: relative retention time ($RRT = t_{R(NAP)} / t_{R(rac-IBP)}$), k' : capacity factor, T: asymmetry factor, NTP: number of theoretical plates, R_s : resolution.

Table 2S. Data for system repeatability methanol solution of racemic ibuprofen (*rac*-IBP) (100 μ M, 250 μ M) and naproxen sodium (NAP) as internal standard (IS) (50 μ M).

Weighting/Dilution Standard Solution	NAP		rac-IBP		
	C (μ M)	Area	C (μ M)	R-Area	S-Area
1/1	50	68358	250	31427	31471
1/2	50	68736	250	31612	31845
1/3	50	68381	250	31454	32084
2/1	50	68014	250	31765	32110
2/2	50	68568	250	31974	32247
2/3	50	68424	250	32123	32316
Mean		68414		31726	32012
RSD%		0.32		0.81	0.89
1/1	50	68901	100	12396	12362
1/2	50	68867	100	12124	12198
1/3	50	68882	100	12299	12442
2/1	50	68947	100	12284	12450
2/2	50	68993	100	12172	12268
2/3	50	68848	100	12288	12361
Mean		68906		12261	12347
RSD%		0.07		0.73	0.73

Table 3S. Data for system intermediate precision of methanol solution of racemic ibuprofen (rac-IBP) (100 μ M, 250 μ M) and naproxen sodium (NAP) as internal standard (IS) (50 μ M).

Day	Dilution Standard Solution	NAP		rac-IBP		
		C (μ M)	Area	C (μ M)	R-Area	S-Area
1	1	50	68358	250	31427	31471
	2	50	68736	250	31612	31845
	3	50	68381	250	31454	32084
2	1	50	68313	250	31617	31781
	2	50	68687	250	31440	31686
	3	50	68747	250	31325	31546
3	1	50	68884	250	32130	32366
	2	50	68262	250	32055	32349
	3	50	68461	250	32052	32308
Mean			68537		31679	31937
RSD%			0.31		0.93	1.03
1	1	50	68901	100	12396	12362
	2	50	68867	100	12124	12198
	3	50	68882	100	12299	12442
2	1	50	68935	100	12355	12492
	2	50	68227	100	12065	12129
	3	50	68568	100	12207	12291
3	1	50	68905	100	12148	12246
	2	50	68859	100	12178	12315
	3	50	68714	100	12058	12375
Mean			68762		12203	12317
RSD%			0.32		0.94	0.88

Table 4S. Accuracy of NAP, *R*- and *S*-IBP determination in spiked control perfusates and spiked control bile with the same range of standard dilutions of racemic IBP (50 µM, 100 µM, 250 µM) and NAP(50 µM).

NAP			rac-IBP				
C _{spiked perfusate} (µM)	Area	Recovery %	C _{spiked perfusate} (µM)	R-Area	Recovery %	S-Area	Recovery %
50	67646	98.1	50	5299	86.5	5241	85.0
50	67599	98.0	50	5335	87.1	5299	85.9
50	67569	98.0	50	5320	86.8	5227	84.7
50	68004	98.4	100	11355	92.8	11248	90.9
50	67423	97.6	100	11151	91.1	11088	89.6
50	67536	97.7	100	11097	90.7	11006	88.9
50	56635	81.6	250	26897	85.7	26898	85.3
50	56225	81.1	250	26855	85.5	26741	84.8
50	55432	79.9	250	26361	83.9	26326	83.5
Mean		92.3			87.8		86.5
RSD%		8.76			3.23		2.81

C _{spiked bile} (µM)	Area	Recovery %	C _{spiked bile} (µM)	R-Area	Recovery %	S-Area	Recovery %
50	61456	89.1	50	5168	84.3	5164	83.7
50	61475	89.2	50	5127	83.7	5169	83.8
50	61466	89.2	50	5147	84.0	5166	83.8
50	60576	87.7	100	10930	89.3	11049	89.3
50	60411	87.4	100	10916	89.2	11003	88.9
50	60494	87.5	100	10923	89.3	11026	89.1
50	60968	87.9	250	28149	89.6	29544	93.7
50	61118	88.1	250	27995	89.2	28732	91.1
50	61043	88.0	250	28072	89.4	29138	92.4
Mean		88.2			87.6		88.4
RSD%		0.77			2.88		4.09

BBA - Molecular Basis of Disease

Study on oxidative transformations of endogenous lipids, proteins, and amino acids in hyperglycemic rats. Preference of oxidation of non-aromatic sites.

--Manuscript Draft--

Manuscript Number:	
Article Type:	Regular Paper
Keywords:	STZ; Hyperglycaemia; Oxidative stress; Biomarkers; Aromatic hydroxylation
Corresponding Author:	Pal Perjesi, PhD University of Pécs Pécs, Baranya HUNGARY
First Author:	Hawsar Othman Mohamed
Order of Authors:	Hawsar Othman Mohamed
	Attila Almási, PhD
	Szilárd Kun
	István Wittmann, PhD, DSc
	Pal Perjesi, PhD
Abstract:	<p>Background: Hyperglycemia can induce oxidative stress through several mechanisms. Carbohydrates, lipids, proteins, and DNA are the cellular targets of oxidative stress modification. Reactive oxygen species can also generate oxidized drug metabolites, which are not formed in enzyme-catalyzed reactions. The formation of such metabolites can modify the pharmacological action of the parent drug.</p> <p>Methods: Sixteen male Wistar rats were divided into four groups. Group I was the control, and Group II, III, and IV were STZ-treated diabetic animals (n=4 each). At the end of experiments (1, 2, and 4 weeks, respectively), oxidative stress biomarkers including malondialdehyde (MDA), alkyl hydroperoxides, protein carbonyls (prot-DNPH), total cellular thiols (RSH), and tyrosine isomers (o-Tyr + m-Tyr) were determined in the small intestine, liver, and kidney of the experimental animals.</p> <p>Results: The MDA, prot-DNPH, and the o-Tyr + m-Tyr levels followed a similar pattern: the highest values were recorded after two weeks of the STZ treatment. Compensation of the oxidative stress is the least effective in the kidney, where the three biomarkers continuously increased over investigations. The reactions of hydroxyl radicals with aromatic rings were less preferred than those with sensitive amino acid/protein and lipid molecules.</p> <p>Conclusions: The reaction of hydroxyl radicals with the aromatic ring of phenylalanine is less favored than that with sensitive amino acid/protein and lipid molecules. This observation could be one of the reasons they are only limited data on increased non-enzyme catalyzed oxidized/hydroxylated aromatic xenobiotics under hyperglycemic conditions. However, modulation of enzyme and transporter activities is well documented in the literature.</p>
Suggested Reviewers:	Janka Vaskova, PhD Pavol Jozef Stafarik University in Kosice Faculty of Medicine janka.vaskova@upjs.sk Expert on oxidative stress.
	Phiwayinkosi V Dlodla, PhD South African Medical Research Council pdludla@mrc.ac.za Expert on diabetes complications.
	Fatmah A Matough, PhD Universiti Kebangsaan Malaysia Faculty of Health Sciences fatmahmatough@yahoo.com Expert on diabetic complications.
	John B Watkins, PhD Indiana University School of Medicine

	<p>watkins@indiana.edu Expert on diabetic oxidative stress.</p>
--	---

Prof. Dr. M. Paul Murphy
Executive Editor
Biochimica et Biophysica Acta - Molecular Basis of Disease

September 9, 2022

Dear Professor Murphy,

Attached to this letter, please find the manuscript entitled

Hawsar Othman Mohammed, Almási Attila, Balázs Kun, Wittmann István, Perjési Pál

Study on oxidative transformations of endogenous lipids, proteins, and amino acids in hyperglycemic rats. Preference of oxidation of non-aromatic sites.

I am submitting for consideration for publication in your journal, *Biochimica et Biophysica Acta - Molecular Basis of Disease*.

The manuscript describes original research conducted by the authors and is not submitted to any other forum for evaluation for publication.

Thank you very much for your troubles in this matter.

Sincerely yours,

Pál Perjési, Ph.D.
Professor of Pharmaceutical Chemistry
Institute of Pharmaceutical Chemistry
University of Pécs
Hungary

**Study on oxidative transformations of endogenous lipids,
proteins, and amino acids in hyperglycemic rats.
Preference of oxidation of non-aromatic sites.**

Hawsar Othman Mohamed^{1,2}, Attila Almási¹, Szilárd Kun³, István Wittmann³,
Pál Perjési^{1*}

¹Institute of Pharmaceutical Chemistry, Faculty of Pharmacy, University of Pécs, Pécs,
Hungary

²College of Veterinary Medicine, University of Sulaimani, Sulaymaniyah, Kurdistan Region,
Iraq

³Department of Medicine and Nephrological Center, Medical School, University of Pécs,
Pécs, Hungary

*Corresponding author

pal.perjesi@gytk.pte.hu

¹Institute of Pharmaceutical Chemistry, Faculty of Pharmacy, University of Pécs, Pécs,
Hungary

21 Abstract

22 **Background:** Hyperglycemia can induce oxidative stress through several mechanisms.
23 Carbohydrates, lipids, proteins, and DNA are the cellular targets of oxidative stress
24 modification. Reactive oxygen species can also generate oxidized drug metabolites, which are
25 not formed in enzyme-catalyzed reactions. The formation of such metabolites can modify the
26 pharmacological action of the parent drug.

27 **Methods:** Sixteen male Wistar rats were divided into four groups. Group I was the control, and
28 Group II, III, and IV were STZ-treated diabetic animals (n=4 each). At the end of experiments
29 (1, 2, and 4 weeks, respectively), oxidative stress biomarkers including malondialdehyde
30 (MDA), alkyl hydroperoxides, protein carbonyls (prot-DNPH), total cellular thiols (RSH), and
31 tyrosine isomers (*o*-Tyr + *m*-Tyr) were determined in the small intestine, liver, and kidney of
32 the experimental animals.

33 **Results:** The MDA, prot-DNPH, and the *o*-Tyr + *m*-Tyr levels followed a similar pattern: the
34 highest values were recorded after two weeks of the STZ treatment. Compensation of the
35 oxidative stress is the least effective in the kidney, where the three biomarkers continuously
36 increased over investigations. The reactions of hydroxyl radicals with aromatic rings were less
37 preferred than those with sensitive amino acid/protein and lipid molecules.

38 **Conclusions:** The reaction of hydroxyl radicals with the aromatic ring of phenylalanine is less
39 favored than that with sensitive amino acid/protein and lipid molecules. This observation could
40 be one of the reasons they are only limited data on increased non-enzyme catalyzed
41 oxidized/hydroxylated aromatic xenobiotics under hyperglycemic conditions. However,
42 modulation of enzyme and transporter activities is well documented in the literature.

43

44 **Keywords:** STZ, Hyperglycaemia, Oxidative stress, Biomarkers, Aromatic hydroxylation

45

Introduction

Diabetes mellitus is a complex endocrine metabolic disorder that affects a large proportion of the world's population and is on an ever-increasing trend. It is a group of metabolic diseases characterized by hyperglycemia resulting from defects in insulin secretion, insulin action, or both. Characterized by elevated blood glucose levels, diabetes mellitus is divided into multiple categories based on pathogenesis, including type 1 diabetes mellitus (T1DM), type 2 diabetes mellitus (T2DM), gestational diabetes, and other types [1-3].

Hyperglycemia can induce oxidative stress through several mechanisms such as glucose autooxidation, polyol pathway, advanced glycation end products (AGEs) formation, and activation of PKC β 1/2 kinase [4]. All these pathways, in association with hyperglycemia-induced mitochondrial dysfunction (electron and proton leaks) and endoplasmic reticulum (ER) stress, reflect a hyperglycemia-induced process of overproduction of superoxide radical by the mitochondrial electron-transport chain [5]. Accumulation of reactive oxygen species (ROS) promotes cellular damage and contributes to the development and progression of diabetic complications [6, 7]. Carbohydrates, lipids, proteins, and DNA are the targets of oxidative stress modification, and the stable products of ROS-derived macromolecular damage may be used as oxidative stress markers. Oxidative stress biomarkers include malondialdehyde (MDA), 4-hydroxy-2-nonenal (HNE), isoprostanes, protein carbonyls, *m*-nitrotyrosine, alkyl hydroperoxides, protein oxidation products, glycation end products, carbohydrate modifications, and 8-hydroxy-2'-deoxyguanosine (8-OH-dG), an oxidized DNA products [4].

Hyperglycemia can affect the pharmacokinetics and pharmacodynamics of drugs. These changes include reduced gastric emptying time, increased albumin glycation, and altered P-gp expression and CYP activity [8-12]. Furthermore, ROS (\cdot OH, in particular) can generate oxidized drug metabolites, which are not formed in enzyme-catalyzed reactions. These non-enzymatic reactions are essential in cellular metabolism, human health, and aging.[13] The

71 formation of such metabolites can modify the pharmacological action of the parent drug and
72 may also be used as oxidative stress markers [11-13].

73 The streptozotocin (STZ)-diabetic rat is a frequently used experimental model of the
74 chronic complications of human diabetes. STZ is a highly effective and selective cytotoxic
75 agent for pancreatic B cells in intravenous administration. The binding of the drug to its site of
76 action is completed within a short time [3]. Selection of an appropriate dosage of STZ is a
77 critical issue. While a single high-dose injection of STZ can produce type 1 diabetes in adult
78 rats, when injected at the neonatal stage or immediately after birth, it can lead to type 2 diabetes
79 at the adult age [14, 15]. Due to the strain differences, the diabetogenic doses of STZ range
80 from 45 to 70 mg/kg [16]. In our experiment, after the STZ dose of 65 mg/kg, stable diabetes
81 with persistent hyperglycemia (over 20 mM of plasma glucose) was observed during the 4-
82 week study period.

83 Earlier, we reported how intestinal absorption and Phase 2 metabolic transformations
84 of 4-nitrophenol [17], salicylic acid [18], and ibuprofen [19, 20] changed in STZ-treated
85 hyperglycemic rats. Using the same experimental protocol (treatment of experimental rats with
86 STZ (65 mg/kg bw, i.v.) a week before the start of the experiments), we also reported changes
87 in intestinal and hepatic activities of enzymes involved in glucuronide and sulfate metabolites
88 [21].

89 Continuing our studies in the fields, here we report on hyperglycemia's effect on the
90 transformation of some oxidative stress-sensitive endogenous compounds such as cellular
91 lipids, proteins, thiols, and the amino acid tyrosine. The investigated compounds represent four
92 chemically different classes: alkenes, amines, thiols, and substituted aromatic compounds. The
93 latter compound possesses a nucleophilic moiety (aromatic ring) found in our previously
94 investigated xenobiotics [17-20]. The oxidative markers of the selected class of compounds
95 were determined in the small intestine, liver, and kidney samples of experimental rats after 1,

2, and 4 weeks of STZ treatment. The results are compared with those obtained with the previously investigated drugs.

Results

Blood glucose level

Diabetes was induced with a single i.v. dose of 65 mg/kg STZ [6]. Hyperglycemia was confirmed after one week STZ treatment. The average blood glucose level of the control animals was 6.7 ± 1.5 mM, while that of the STZ-treated rats was 23.4 ± 2.8 mM.

Protein content

The protein content (mg/g wet tissue) of the liver, small intestine, and kidney were determined using the calibration curve ($y = 0.2583x + 0.1124$, $r^2 = 0.9997$) obtained by BSA. The results showed that the protein content of each organ was affected by the hyperglycemic conditions (Figure 1). The protein content of the small intestine in all groups is lowered, showing similar reduced values over the four weeks. In the kidney, the values were continuously lowered. The protein content of the liver showed the least reductions, having the two-week STZ-treated samples the lowest values. None of the changes, however, can be assessed statistically (Figure 1).

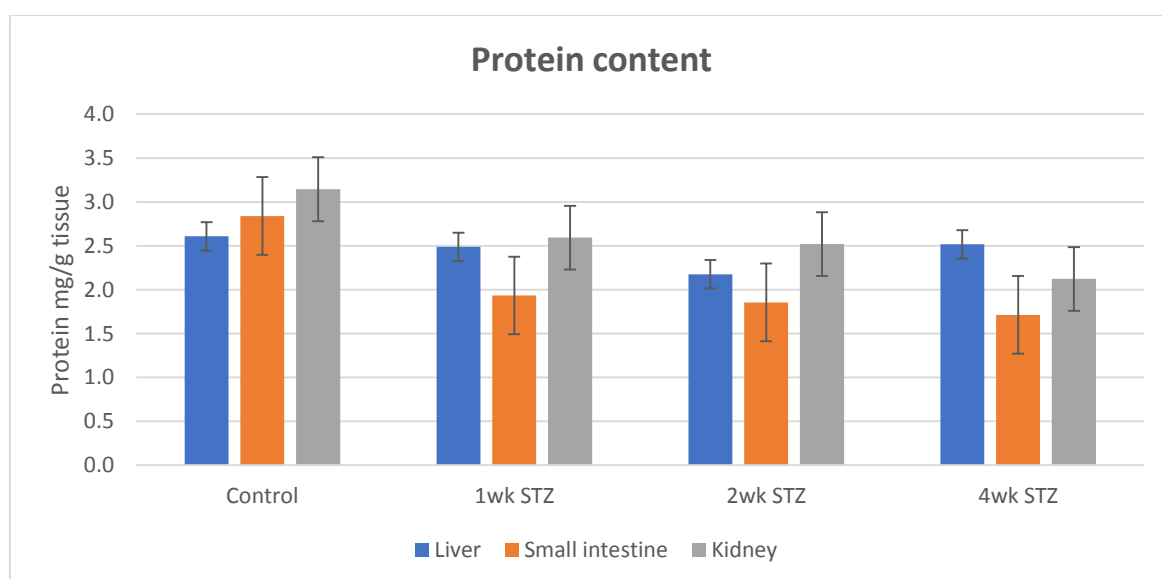


Figure 1. Comparison of the protein contents (mg protein/g wet tissue) in the control, one-week-, two-week-, and four-week-STZ treated rats.

Protein carbonyl (prot-DNPH) content

The carbonyl content of oxidized proteins was determined after derivatization with 2,4-dinitrophenylhydrazine (DNPH). Protein-DNPH content of the STZ- treated samples showed a distinct continuous increase compared to the controls in each tissue homogenate. Each two-week STZ-treated organ level was significantly different from the control. The protein-DNPH level in the four-week STZ-treated liver samples decreased. In the kidney, the protein carbonyl content showed a moderate continuous increase over the four weeks (Figure 2).

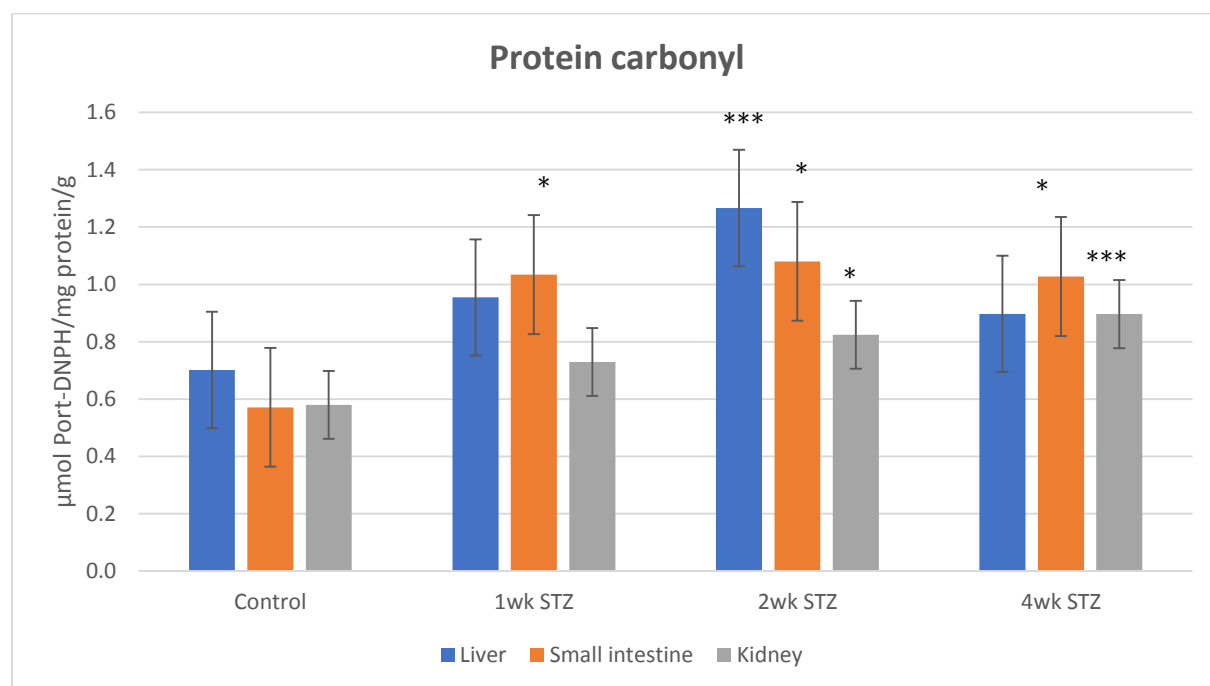


Figure 2. Comparison of the protein carbonyl content (μmol prot-DNPH/mg protein/g tissue) in the control, one week-, two week-, and four week-STZ treated rats. (* $p < 0.05$, ** $p < 0.01$, *** $p < 0.001$).

Determination of diene conjugates

In the liver, the conjugated diene level slightly increased in the hyperglycemic rats at each timepoint. In the small intestine, the conjugated diene level significantly increased at each timepoint. However, the relative increase, specifically in the two-week and four-week hyperglycemic samples, was much higher than in the liver. In the kidney, the diene level was significantly higher in the four-week STZ-treated samples. The one-week and two-week STZ treatment didn't considerably affect the conjugated diene level. The four-week samples, however, showed a statistically higher value than the control (Figure 3).

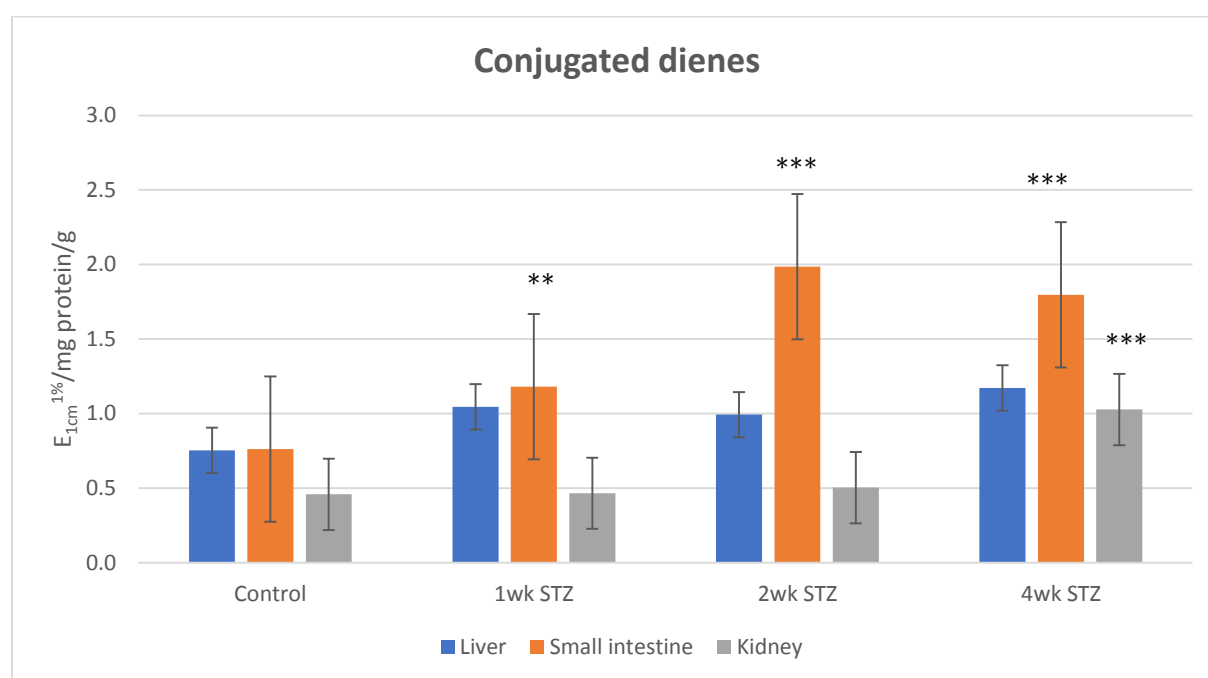


Figure 3. Comparison of the conjugated diene levels ($E_{1cm}^{1\%}/mg \text{ protein/g}$ tissue) in the control, one-week-, two-week-, and four-week-STZ treated rats. (** $p < 0.01$, *** $p < 0.001$).

TBARS determination

MDA is frequently determined as an indicative endogenous metabolite resulting in lipids oxidation by reactive oxygen species [22]. It is a reactive carbonyl compound, readily reacting with nucleophilic sites of proteins and other cellular macromolecules. Accordingly, the MDA test results indicate the steady-state lipid-peroxide levels, which can undergo rearrangements to form MDA under the test conditions. Our results showed a continuous slight increase in the MDA (TBARS) levels in each organ. The TBARS level of the four-week STZ-treated small intestine and kidney samples differed significantly from the control (Figure 4).

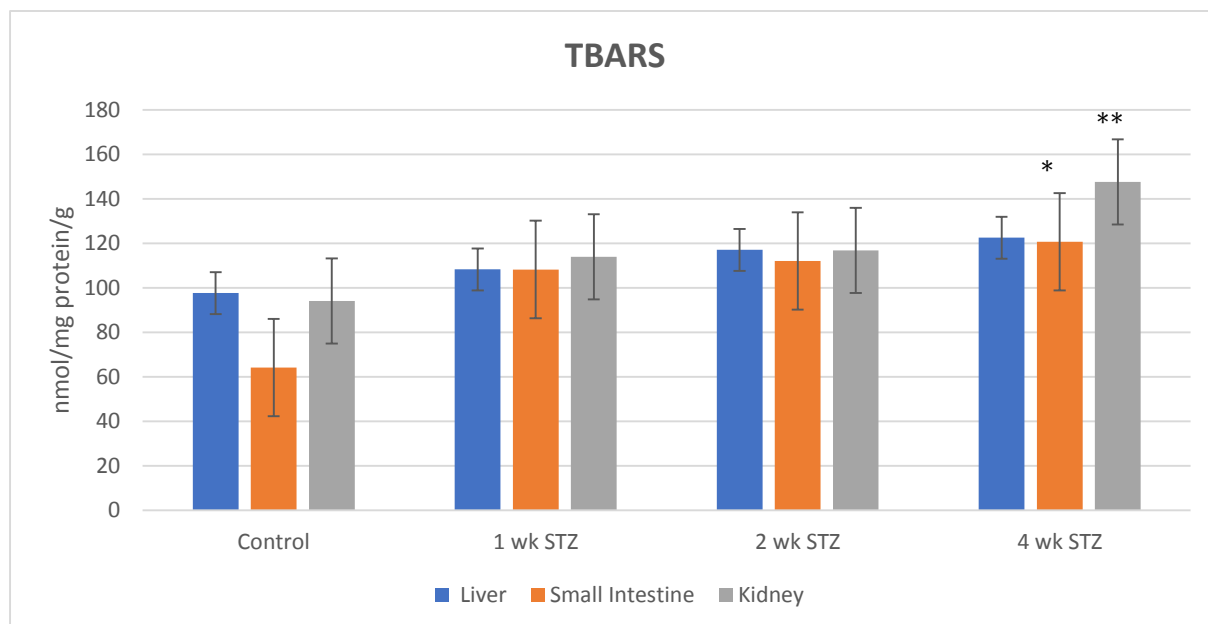


Figure 4. Comparison of the TBARS levels (nmol TBARS /mg protein/g tissue) in control, one-week-, two-week-, and four-week-STZ treated rats. (* $p < 0.05$, ** $p < 0.01$).

Determination of non-protein thiols (NPSH)

STZ-treatment of the experimental animals decreased the liver's non-protein thiol levels at the one-week and four-week timepoints. In contrast, the two-week STZ liver samples had somewhat increased values compared to the control. In the kidney, the thiol content

marginally raised at each timepoint. In the small intestine, the thiol level in the STZ-treated samples increased at each timepoint compared to the control. The lowest values could be measured in the two-week STZ-treated samples (Figure 5).

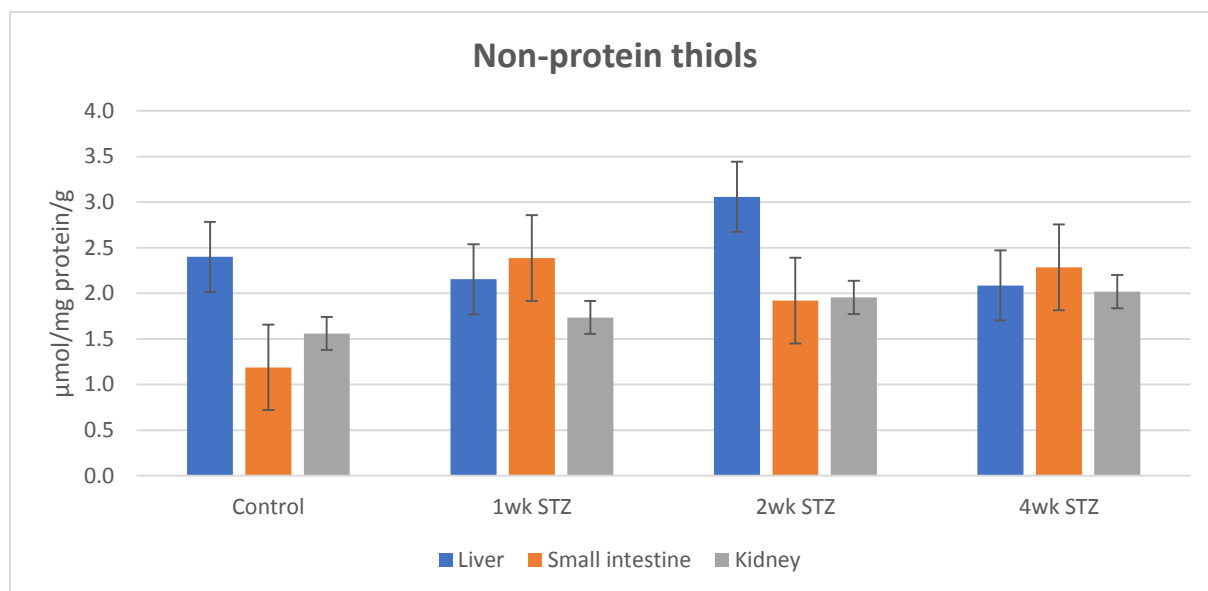


Figure 5. The quantities of non-protein thiols (expressed as $\mu\text{mol GSH/mg protein/g tissue}$) in control, one-week-, two-week-, and four-week-STZ treated rats.

Determination of hydroxylated phenylalanine derivatives

Phenylalanine (Phe) is an essential amino acid that is the physiological precursor of *para*-tyrosine (*p*-Tyr), dihydroxy-phenylalanine (DOPA), catecholamines, melanine, and thyroid hormones [23]. Beyond these enzymatic reactions, Phe, due to the nucleophilic character of its aromatic ring, is a subject of non-enzymatic oxidation processes, i.e., the attack of ROS [24]. In such reactions, all three hydroxylated Phe isomers (*p*-Tyr, *m*-Tyr, and *o*-Tyr) are formed [25]. Under our experimental conditions, the relative amount of the *m*-Tyr, and *o*-Tyr isomers, formed in non-enzyme-catalyzed hydroxylation reactions, increased at the two- and four-week timepoints in each investigated organ (Figure 6).

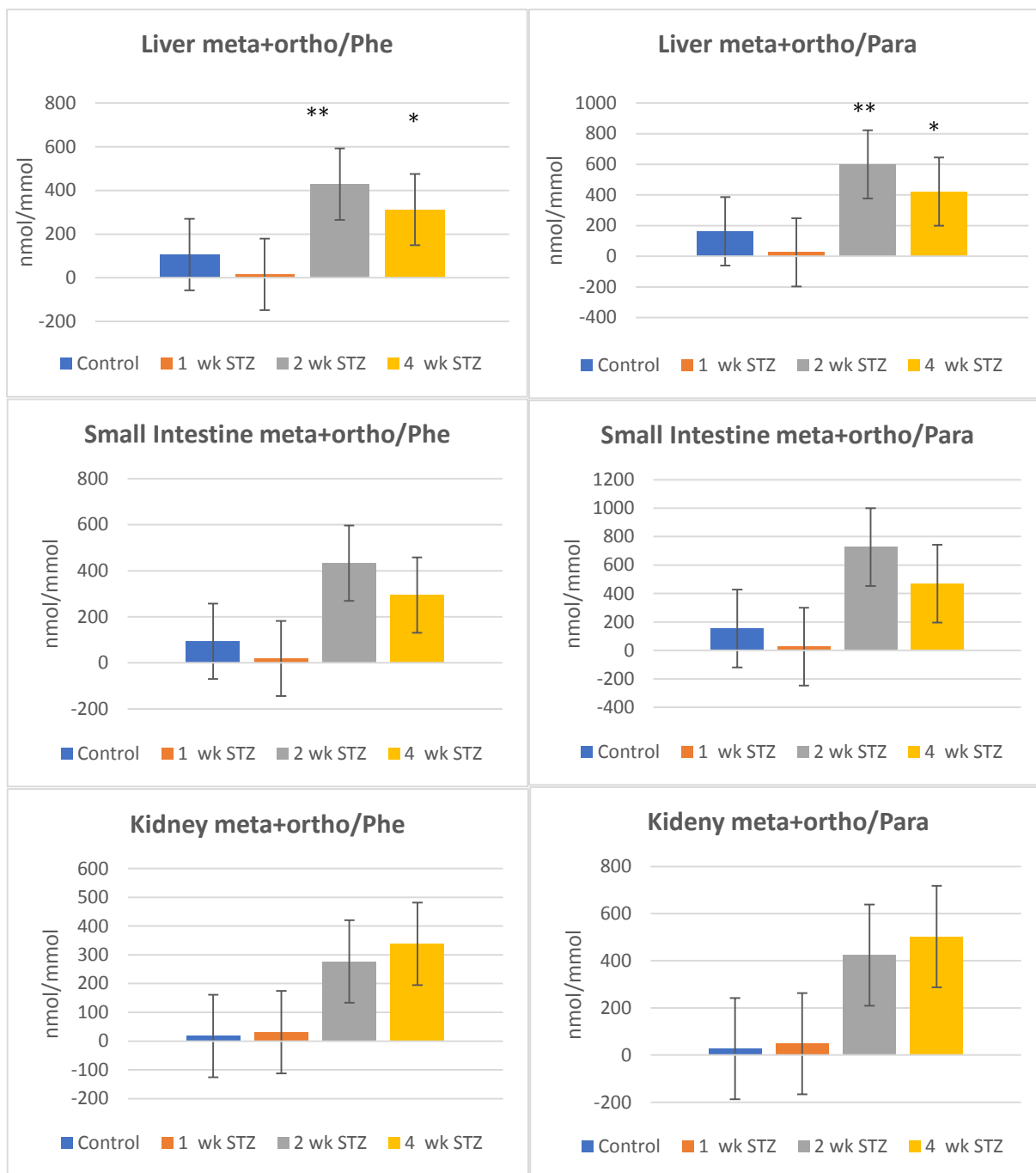


Figure 6. The relative amount of the *m*-Tyr+*o*-Tyr to Phe and *p*-Tyr (nmol/mmol) in control, one-week, two-week, and four-week STZ treated rats. (* $p < 0.05$, ** $p < 0.01$).

Discussion

Several investigators have studied the effect of diabetes on whole-body protein metabolism in humans. These studies demonstrated increased protein breakdown as well as

improved protein synthesis. Net protein catabolism occurs in T1DM patients during insulin deprivation because there is a more significant increment in protein breakdown than protein synthesis [26]. According to these previous observations, the present results showed that the protein content of the small intestine and the kidney were reduced under the hyperglycemic condition. On the contrary, no such degree of reduction in the protein content in the liver was observed (Figure 1). This latter observation can be explained by the major role of the liver in synthesizing proteins.

Proteins are one of the endogenous targets of oxidative stress. Available cysteine residues can easily form disulfide derivatives with the thiol functions of other proteins or glutathione (GSH). GSH can also be oxidized to the respective disulfide (GSSG) in reaction with various endogenous and exogenous oxidizing agents. Lysine and proline residues are the most important precursors of protein carbonylation by the oxidative formation of aldehydic derivatives [27]. The most common method to analyze these latter derivatives is their reaction with 2,4-dinitrophenylhydrazine (DNPH). The resulting phenylhydrazones (prot-DNPHs) can be quantified by spectroscopic, immunological, or mass spectrometric techniques.

UV-Vis determination of carbonyl content of proteins by the DNPH method indicated increased protein oxidation at each timepoint in each organ (Figure 2). The kidney seemed the least sensitive to protein oxidation at each timepoint. Such resistance of proteins can be explained by the high turnover of the antioxidant amino acids, such as lysine, proline, and cysteinyl-glycine [28]. The time dependence of the protein-content-based amount of the DNPH-reactive protein carbonyls showed some characteristic differences: 1. In the liver and the small intestine, the highest amounts could be detected at the two-weeks timepoint. The initial increase slightly dropped by the end of the fourth week. 2. In the kidney, contrary to the other two organs, the level of the oxidized protein content slightly and continuously increased. As mentioned in the Introduction, our previous metabolic studies were performed after one

week of the STZ treatment of the experimental animals [17-21]. The data indicate a substantial increase of the protein oxidation products in the liver (35.7%) and the small intestine (80.7%) at this timepoint (Figure 2).

Peroxidative degradation of membrane lipids is another consequence of oxidative stress. It is initiated by (a) free radical species such as peroxy radicals, hydroxyl radicals, and metal-oxyl radicals derived from the iron-mediated reduction of hydrogen peroxide or (b) non-radical species such as singlet oxygen, ozone, and peroxynitrite generated by the reaction of superoxide with nitric oxide [29]. The most prevalent radical species that can profoundly affect lipids are mainly hydroxyl radicals ($\bullet\text{OH}$). Radical initiators can abstract a hydrogen atom from the allylic position of polyunsaturated fatty acids. As a result, lipid hydroperoxides (LOOHs) - as primary oxidation products - are formed, and simultaneous rearrangement of the neighboring (non-conjugated) double bonds results in a conjugated diene moiety. Conjugated dienes have characteristic UV-absorption around 230 nm [30].

Lipid hydroperoxides, like hydrogen-peroxide, are mild oxidative agents; however, they can be reduced to the respective alcohols [29]. These primary lipid oxidation products can also undergo several decomposition pathways, resulting in - among others - an endogenous malondialdehyde (MDA) level. The endogenous MDA can be involved in enzymatic oxidation, reduction, addition, and condensation with cellular nucleophiles [31-33]. One of the most frequently used methods to measure a tissue sample's lipid-derived total carbonyl content is the thiobarbituric acid (TBA) test. However, most of the MDA measured with the TBA test is formed from the more stable fatty acid hydroperoxides under the strong acid test conditions [34]. Besides MDA, TBA also forms colored adducts with other compounds, including sugars, amino acids, and other aldehydic lipid oxidation products; this leads to the overestimation of MDA by the TBA test [34, 35]. Thus, the results of this test are appropriately reported as thiobarbituric acid-reactive substances (TBARS) rather than MDA [36].

As Figure 3 shows - like the protein oxidation - it was the liver and the small intestine where the highest conjugated diene-level elevations in the STZ-treated animals were observed by the two-week timepoint. The small intestine proved to be the most sensitive organ showing a 55.3%, 160.5%, and 136.8% increase in the conjugated diene level at the one, two, and four-week timepoints, respectively. The highest elevation in the liver and kidney samples could be obtained in the four-week samples (Figure 3).

A comparison of the conjugated diene levels (Figure 3) to that of the respective TBARS levels (Figure 4) showed a relatively lower increase in the TBARS. At the first week timepoint, increased MDA levels could be observed in the liver and the kidney but not in the small intestine. The moderately increased levels can be explained by the effective elimination of the formed lipid hydroperoxides by catalase (in the liver and kidney) and selenium-dependent GSH-peroxidase (GPx2) (in the gastrointestinal system) [37], and the high reactivity of MDA with the endogenous lysine and arginine units [38]. In the later timepoints, however, the oxidative stress caused by the high glucose levels can also contribute to the formation of oxidized lipids, resulting in increased MDA levels [39].

Furthermore, it is reasonable to presume that the continuous food methionine supply (2800 mg/kg) provides enough reducing (thiol) equivalent to convert a part of the conjugated lipid-hydroperoxides to the respective alcohols [40]. These latter derivatives increase the conjugated diene level but can't be converted to MDA. In agreement with this explanation, the intestinal non-protein thiol level increased in the highest ratios in the small intestine over the four-week experiment (Figure 5). Like the conjugated diene level, the highest TBARS level in the kidney could be observed at the four-week timepoint.

Non-protein thiols (NPSH) are one of the most potent cellular antioxidants. Glutathione (GSH) is the most widespread low-molecular-weight antioxidant in the liver and kidney. The NPSH level declined after the one-week STZ treatment in the liver but not in the small intestine

and the kidney. (Figure 5). The reduction of NPSH levels in the liver can be associated with the high glutathione level and glutathione peroxidase (GPx) activity in this organ [41]. Thus, the major portion of the decline in the hepatic NPSH level is due to the GSH-dependent detoxification of the reactive oxygen species (ROS). The initial drop in the NPSH level increased by the end of the second week through a negative feedback mechanism. After this characteristic increase, however, the hepatic GSH level dropped below the control (4th week), probably due to dysregulation of GSH synthesis by the chronic hyperglycemia [42]. A similar decline was not observed either in the small intestine or the kidney. These observations can be explained by the different GSH levels and GPx activity in these two organs. The kidneys are characterized by a lower GSH concentration than the liver and the highest level of cysteine (CYS) among all body tissues [43]. The kidneys' NPSH level depends highly on an adequate supply of glutathione (GSH) to maintain normal function [44]. Thus, the elimination of ROS can not be effectively catalyzed by the GSH/GPx pathway in this organ.

In contrast to the liver, the intestine has in common extremely low GSH peroxidase activity [41]. Thus, this organ has a limited capability to utilize non-protein thiols to protect against oxidative toxicity. Furthermore, the NPSH level was higher than the control over the investigation period. This observation can be explained by the continuous food methionine supply.

Phenylalanine (Phe) is an essential amino acid, which is, among others, converted to *p*-Tyr in an enzyme-catalyzed reaction. The nucleophilic aromatic ring can react with hydroxyl radicals in an addition reaction, and the primary adducts are stabilized as *o*-, *m*-, and *p*-hydroxylated phenylalanines (*o*-Tyr, *m*-Tyr, and *p*-Tyr) [45]. Accordingly, *o*- and *m*-Tyr are specific, stable hydroxyl radical markers [46]. As shown in Figure 6, the *o*-Tyr+*m*-Tyr/*p*-Tyr (or the *o*-Tyr+*m*-Tyr/Phe) ratios slightly decreased at the one-week timepoint of the STZ treatment. Like the prot-DNPH (Figure 2) and the TBARS levels (Figure 4), the ratios

substantially increased in all three organs at the two-week timepoint. A similar tendency of the three parameters could be observed at the four-week timepoint: while the values were somewhat reduced in the liver and the small intestine, they further increased in the kidney. The observations give further experimental evidence of the usefulness of the three parameters to characterize the oxidative state of the investigated organs.

Diabetic patients are at all times at risk of complications. Complications may be macrovascular (coronary heart disease, peripheral vascular disease, and stroke), microvascular (neuropathy, retinopathy, and nephropathy), and both micro- and macrovascular (diabetic foot). It is believed that oxidative stress plays an important role in the development of these vascular complications [47]. Concerning oxidative stress-induced nephropathy, the present data support this theory. The oxidized protein (Figure 2), conjugated dienes (Figure 3), TBARS level (Figure 4), and the *o*-Tyr+*m*-Tyr/*p*-Tyr ratio (Figure 6) steadily increased. On the contrary, the renal GSH didn't show a significant difference over time (Figure 5). Alterations in renal mitochondrial GSH status appear to be associated with chronic hyperglycemia, although the underlying mechanism for these changes has not been established [47]. Earlier, Lash et al. reported significantly higher mitochondrial GSH contents in the kidneys of diabetic rats compared with those of control rats. On the other hand, primary cultures of renal proximal tubular cells from STZ-treated diabetic rats exhibited higher levels of reactive oxygen species and were more sensitive to oxidant-induced injury than cells from control rats [48]. The authors interpreted these findings that the compensatory increases in mitochondrial GSH transport and content are insufficient to counteract the oxidative stress induced by the chronic hyperglycemic state [49, 50].

Since the liver is the main site of enzymatic drug (xenobiotic) metabolism, the observed changes in this organ need special attention. The reduced protein (Figure 1) and NPSH content (Figure 5), the increased protein oxidation (Figure 2), conjugated diene (Figure 3), and TBARS

(Figure 4) levels are in accordance with the oxidative stress developing in this organ by the end of the first week after the STZ treatment. The results are in agreement with our previous experimental findings demonstrating decreased expression of the efflux transporters Mdr1 (P-gp), Mrp2, and Bcrp in the liver of the STZ-treated (hyperglycemic) animals [19].

On the contrary, aromatic (Phe) hydroxylation was reduced at the one-week timepoint. It suggests that the lipids [51] and proteins [52] are more vulnerable to hydroxyl radical attack than the aromatic rings. This might be the reason (at least in part) for the lack of biliary detection of hydroxylated ibuprofen metabolites formed in non-CYP-catalyzed reactions [20].

Conclusions

This study investigated the oxidative transformation of lipids, proteins, non-protein thiols (NPSH), and phenylalanine (Phe) in the liver, small intestine, and kidney in STZ-treated rats at the one-, two-, and four-week timepoints after the STZ-administration. The MDA, prot-DNPH, and the *o*-Tyr+*m*-Tyr levels followed a similar pattern: the highest values were recorded after two weeks of the STZ treatment. The compensation of the oxidative stress is parallel with the change in the NPSH content of the organs. Such compensation is the least effective in the kidney, where the above three parameters continuously increase over the time of investigations. Accordingly, this organ is the most vulnerable to the hyperglycemia-induced oxidative stress.

The results indicate that reactions of hydroxyl radicals (ROS) with the aromatic ring of Phe are less favored than those with sensitive amino acid/protein and lipid molecules. This observation could be one of the reasons they are only limited data on increased non-enzyme catalyzed oxidized/hydroxylated aromatic xenobiotics under the present experimental conditions. However, modulation (mainly depression) of enzyme and transporter activities

(oxidative stress-induced damage) of proteins/lipids) is well documented in the literature [51, 52,44].

Materials and Methods

Chemicals

Copper (II) sulfate pentahydrate ($\text{CuSO}_4 \cdot 5\text{H}_2\text{O}$), sodium sulfate (Na_2SO_4), sodium potassium tartrate tetrahydrate ($\text{KNaC}_4\text{H}_4\text{O}_6 \cdot 4\text{H}_2\text{O}$), potassium iodide (KI), and potassium chloride (KCl) were obtained from Reanal (Budapest, Hungary). Trichloroacetic acid (TCA), sodium hydroxide (NaOH), sodium chloride (NaCl), and ethylenediaminetetraacetic acid disodium ($\text{EDTA} \cdot \text{Na}_2$) were from Molar Chemicals (Budapest, Hungary). Guanidine hydrochloride, glacial acetic acid (CH_3COOH), and thiobarbituric acid (TBA) were purchased from M.P. Biomedicals (Illkirch, France), Scharlau (Barcelona, Spain), and AppliChem (Darmstadt, Germany), respectively. Butylated hydroxytoluene (BHT), Trizma, 5,5'-dithiobis-(2-nitrobenzoic acid) (DTNB), phenylalanine (Phe), *o*-tyrosine (*o*-Tyr), *m*-tyrosine (*m*-Tyr), and *p*-tyrosine (*p*-Tyr) were from Sigma-Aldrich (Budapest, Hungary). Sodium dodecyl sulfate (SDS), methanol (MeOH), ethanol (EtOH), ethyl acetate (EtOAc), dichloromethane, n-hexane, and chloroform (CHCl_3) were obtained from VWR chemicals (Debrecen, Hungary).

Animals and experimental procedure

Male Wistar rats (9-11 weeks old; weighing 250-300 g; TOXI-COOP, Hungary, Budapest) were separated into four groups. Group I was the control, and Group II, III, and IV were induced diabetic animals (n=4 each). They are subdivided into one-week (Group II), two-week (Group III), and four-week (Group IV) diabetic animals. Experimental diabetes was induced by intravenous injection of streptozotocin (STZ) (65 mg/kg bw, i.v.). The experimental animals were provided standard chow (Safe D40, Scientific Diets, Rosenberg, Germany) and water ad libitum. The chow was withdrawn the day before the experiments (at 4 p.m.). Blood

glucose levels were tested on the day of the experiments (at 8 a.m.) to confirm hyperglycemia. The animals were anesthetized with an intraperitoneal injection of urethane (1.2 g/kg bw, i.p.). The abdomen was opened by a midline incision, and the selected organs were collected. The collected samples were stored in a deep freezer (-70 °C) until the analysis.

Sample preparation

Samples were taken from the freezer (-70 °C) and incubated on ice for 5 minutes to become de-frozen and ready. A mass of the organ sample was weighted, then homogenized with the homogenizing buffer pH 7.4, in a proportion (1:3). The buffer was composed of KCl (0.154 M), Trizma (50 mM), and EDTANa₂ (5 mM). The matrix was completed with BHT (50 mg/ml in MeOH). The mixture was homogenized on ice by Witeg® homogenizer (HG-15A) for 90 seconds (50 speed rate). The homogenate was diluted with the buffer to reach the final mass/volume, in a proportion (1:4), sample preparation (homogenate 25%). The prepared samples were dispensed in Eppendorf vials and stored in a deep freezer (-70 °C) until the time of experiments. Before the experiments, the homogenate was removed from the fridge and incubated (37 °C) for 10 minutes in a water bath.

UV-Vis determination of protein content (Biuret protein assay)

To 0.1 ml of organ homogenate (25%) in a 10 mL test tube, 1.0 mL of SDS (8.1 %), 0.9 ml of NaCl (0.9 %), and 8.0 ml of biuret reagent (CuSO₄•5H₂O, KNaC₄H₄O₆•4H₂O, KI, and NaOH in distilled water) were added. The mixture was incubated for 10 minutes at room temperature. Then, 1.0 ml of the sample was measured by UV-spectrophotometer (Jasco® V-750) at 550 nm against the blank. The protein concentration of samples was determined by the equation of calibration curve of bovine serum albumin (BSA) ($y = 0.2583x + 0.1124$, $r^2 = 0.9997$). The calibration curve plot was achieved with different concentrations of BSA in the same procedure of biuret assay designed and performed before sample measurements, as shown in Table 1S [53].

UV-Vis determination of protein carbonyl content (DNPH-protein adducts)

To 0.2 mL of organ homogenate (25%), 1.0 mL of 0.1 M phosphate buffer pH 7.2 and 0.8 mL of distilled water and 2.0 mL of 5mM 2,4-DNPH (in 2 M hydrochloric acid) were added. The mixture was incubated in the dark at room temperature for one hour by vortexing every 15 minutes. Then, 2.0 mL of 50 % trichloroacetic acid was added, and the mixture was kept for another hour under the same condition. After that, the mixture was centrifuged for 15 minutes/5000 rpm. The supernatant was discarded, and the residue was washed with 1.0 mL of EtOH/EtOAc (1:1). The sample was vortexed and centrifuged for 15 minutes (5000 rpm), and the supernatant was discarded. This washing step was repeated three times, and the final residue was dissolved in 1.0 mL of 8 M guanidine hydrochloride. After the sample completely dissolved. 0.1 mL of the solution was diluted with 0.9 mL of 8 M guanidine hydrochloride to be measured using a UV-spectrophotometer (Jasco® V-750). The absorbance was measured at 375 nm against 8 M guanidine hydrochloride [54, 55].

UV-Vis determination of diene conjugates

To 1.0 mL of organ homogenate (25%) in a conical flask with a ground glass joint, 20 mL of chloroform: methanol (2:1 V/v) mixture was added. The mixture was incubated for 20 minutes in a water bath (50 °C) with mechanical shaking. After that, it was washed into a separatory funnel using 10 mL of chloroform: methanol (2:1 v/v) mixture, and 5 mL of distilled water. The mixture was allowed to stand for 20 minutes to allow separation. Then, the bottom phase was filtered into an Erlenmeyer flask and dried over anhydrous sodium sulfate. It was filtered into a weighted round-bottomed flask and evaporated by a rotary evaporator (Heidolph Hei-VAP) at 30°C/100 rpm (20 minutes). After evaporation, the mass of the flask mass was weighed, and the residue was dissolved in MeOH to obtain a 1 mg/mL solution. The absorbance of the obtained solution was measured by UV-spectrophotometer (VWR® U-1600PC) in a

range of 400-200 nm against MeOH. After that, the solution was diluted with MeOH ten times, and the measurement was repeated [56].

UV-Vis determination of malondialdehyde (MDA) (TBARS assay)

To 0.1 ml of organ homogenate (25%), in a well-sealed ground-glass stoppered test tube, 0.2 mL of SDS (8.1 %) and 1.5 ml of CH₃COOH (20 %; pH 3.5) were added. After that, 1.5 ml of thiobarbituric acid (0.8 %) and 0.7 ml of distilled water were pipetted to the mixture. The mixture was incubated in boiling water (95 °C) for one hour to achieve the color reaction (TBARS). The sample was cooled down on ice (5 minutes) and centrifuged (5 minutes, 3000 rpm). 1 mL of the clear supernatant was measured by UV-spectrophotometer (Jasco® V-750) at 532 nm against distilled water [57].

UV-Vis determination of non-protein thiols (NPSH)

To 1.0 ml of organ homogenate (25%), 0.25 mL of BHT (50 mg/ml in methanol) and 0.25 mL of trichloroacetic acid (25 %) were added. The mixture was vortexed and then centrifuged for 5 minutes/5000 rpm. 0.1 mL of the collected supernatant was combined with 2.8 mL of Trizma buffer pH 8.9. The reaction was started after pipetting 0.1 mL of Ellman's reagent (DTNB) (0.01 M in MeOH). The sample was incubated at room temperature for 30 minutes, allowed the maximum reaction, and then measured at 412 nm against the blank. [58, 59].

HPLC determination of tyrosine isomers

Sample preparation

To 50 mg organ sample, 400 µl of 6N hydrochloric acid, 40 µl of 500 mM BHT in methanol, and 4 µl of 400 mM desferrioxamine solution are added. The sample was vortexed for 1 minute and then hydrolyzed at 120 ° C for 18 hours. Then, the sample was allowed to

cool, centrifuged at 3000 rpm for 10 minutes, and filtered through a syringe filter (0.2 μ m) before analysis [60].

HPLC-FLD measurements

HPLC-FLD analyses were performed on a Shimadzu Class 10 HPLC system equipped with an RF-10 AXL fluorescent detector (Shimadzu, Canby, OR, USA). Separation of compounds was performed on a LiChrospher 100 C18 (5 μ m) LiChroCART® 250-4 column at ambient temperature. The mobile phase consisted of 1% (m/v) sodium acetate and 1% (v/v) acetic acid in water (isocratic run). Flow rate: 1.0 ml/min. For Phe: excitation: 258 nm, emission: 305 nm. For Tyr: excitation: 275 nm, emission: 305 nm. Concentrations were determined using external calibration [61].

Statistics

The protein content of homogenate samples was measured by Biuret assay according to the calibration curve of different known concentrations of BSA. TBARS (nmol TBARS/mg protein/g tissue) and GSH (μ mol GSH/mg protein/g tissue) amounts represent the mean \pm S.D. of four animal samples in each group. The value of protein carbonyl content (μ mol/Port-DNPH/mg protein/g tissue) and diene conjugates ($E_{1cm}^{1\%}$ /mg protein/g tissue) are the mean \pm S.D. of animal groups ($n=4$). HPLC-UV integrated peak areas of tyrosine derivatives (nmol/mmol) represent the mean \pm S.D. of animal groups ($n=2$). The difference among groups was analyzed by SPSS one-way Anova. Significant differences from the control value: * $p < 0.05$, ** $p < 0.01$, and *** $p < 0.001$.

Author contributions

Conceptualization (P.P., W.I.), Investigation (H.O.M., A.A., B.K.), Methodology (P.P., W.I., H.O.M., A.A.), Writing – original draft (P.P. and H.O.M.), Writing – review, and editing (P.P., W.I.,

and H.O.M.), Funding acquisition (P.P.). All authors have read and agreed to the published version of the manuscript.

Funding

This study was supported by the European Union and co-financed by the European Social Fund (EFOP-3.6.1.-16-2016-00004).

Data availability

Primary research data are stored in the Institute of Pharmaceutical Chemistry, University of Pécs, Pécs, Hungary.

Ethical approval and consent to participate

The study was designed and conducted according to European legislation (Directive 2010/63/E.U.) [62] and Hungarian Government regulation (40/2013., II. 14.) [63] on the protection of animals used for scientific purposes. The project was approved by the Animal Welfare Committee of the University of Pécs and by the Government Office of Baranya County (license No. BAI35/51-61/2016 and license supplement (supplement No. BAI35/90-5/2019). Consent to participate – NA/Not applicable.

Competing interests

The authors declare that they have no competing interests.

References

- [1] K. C. Mekala and A. G. Bertoni, Chapter 4 - Epidemiology of diabetes mellitus, in: G. Orlando, L. Piemonti, C. Ricordi, R. J. Stratta, and R. W. G. Gruessner, (Eds.), Transplantation, Bioengineering, and Regeneration of the Endocrine Pancreas: Academic Press, 2020, pp. 49-58. Available: <https://www.sciencedirect.com/science/article/pii/B9780128148334000046>
- [2] P. Saeedi, I. Petersohn, P. Salpea, B. Malanda, S. Karuranga, N. Unwin, et al., Global and regional diabetes prevalence estimates for 2019 and projections for 2030 and 2045: Results from the International Diabetes Federation Diabetes Atlas, 9(th) edition, Diabetes. Res. Clin. Pract. 157 (2019) 107843. 10.1016/j.diabres.2019.107843
- [3] C. C. Rerup, Drugs producing diabetes through damage of the insulin secreting cells, Pharmacol. Rev. 22 (1970) 485-518.
- [4] S. Tangvarasittichai, Oxidative stress, insulin resistance, dyslipidemia and type 2 diabetes mellitus, World J. Diabetes. 6 (2015) 456-80. 10.4239/wjd.v6.i3.456
- [5] M. Brownlee, The pathobiology of diabetic complications: a unifying mechanism, Diabetes. 54 (2005) 1615-25. 10.2337/diabetes.54.6.1615
- [6] T. V. Fiorentino, A. Priolella, P. Zuo, and F. Folli, Hyperglycemia-induced oxidative stress and its role in diabetes mellitus related cardiovascular diseases, Curr. Pharm. Des. 19 (2013) 5695-703. 10.2174/1381612811319320005
- [7] E. Wright Jr, J. L. Scism-Bacon, and L. C. Glass, Oxidative stress in type 2 diabetes: the role of fasting and postprandial glycaemia, Int. J. Clin. Pract. 60 (2006) 308-314. 10.1111/j.1368-5031.2006.00825.x
- [8] P. R. Gwilt, R. R. Nahhas, and W. G. Tracewell, The effects of diabetes mellitus on pharmacokinetics and pharmacodynamics in humans, Clin. Pharmacokinet. 20 (1991) 477-90. 10.2165/00003088-199120060-00004

- 495 [9] M. Dostalek, F. Akhlaghi, and M. Puzanovova, Effect of diabetes mellitus on
496 pharmacokinetic and pharmacodynamic properties of drugs, *Clin. Pharmacokinet.* 51 (2012)
497 481-99. 10.2165/11631900-000000000-00000
- 498 [10] M Tran, and F. Elbarby, Influence of diabetes mellitus on pharmacokinetics of drugs.,
499 *MOJBB.* 2 (2016) 3-4. 10.15406/mojbb.2016.02.00016
- 500 [11] Y. Yang and X. Liu, Imbalance of Drug Transporter-CYP450s Interplay by Diabetes
501 and Its Clinical Significance, *Pharmaceutics.* 12 (2020) 348. 10.3390/pharmaceutics12040348
- 502 [12] L. Darakjian, M. Deodhar, J. Turgeon, and V. Michaud, Chronic Inflammatory Status
503 Observed in Patients with Type 2 Diabetes Induces Modulation of Cytochrome P450
504 Expression and Activity, *Int. J. Mol. Sci.* 22 (2021) 4967. 10.3390/ijms22094967
- 505 [13] M. A. Keller, G. Piedrafita, and M. Ralser, The widespread role of non-enzymatic
506 reactions in cellular metabolism, *Curr. Opin. Biotechnol.* 34 (2015) 153-61.
507 10.1016/j.copbio.2014.12.020
- 508 [14] S. Bonner-Weir, D. F. Trent, R. N. Honey, and G. C. Weir, Responses of neonatal rat
509 islets to streptozotocin: limited B-cell regeneration and hyperglycemia, *Diabetes.* 30 (1981)
510 64-9. 10.2337/diab.30.1.64
- 511 [15] J. Fernández-Alvarez, A. Barberà, B. Nadal, S. Barceló-Batllori, S. Piquer, M. Claret,
512 *et al.*, Stable and functional regeneration of pancreatic beta-cell population in nSTZ-rats treated
513 with tungstate, *Diabetologia.* 47 (2004) 470-477. 10.1007/s00125-004-1332-8
- 514 [16] A. Gajdosík, A. Gajdosíková, M. Stefek, J. Navarová, and R. Hozová, Streptozotocin-
515 induced experimental diabetes in male Wistar rats, *Gen. Physiol. Biophys.* 18 (1999) 54-62.
- 516 [17] E. Fischer, A. Almási, S. Bojcsev, T. Fischer, N. P. Kovács, and P. Perjési, Effect of
517 experimental diabetes and insulin replacement on intestinal metabolism and excretion of 4-
518 nitrophenol in rats, *Can. J. Physiol. Pharmacol.* 93 (2015) 459-64. 10.1139/cjpp-2015-0065

- 519 [18] M. Kuzma, E. Nyúl, M. Mayer, E. Fischer, and P. Perjési, HPLC analysis of in vivo
520 intestinal absorption and oxidative metabolism of salicylic acid in the rat, *Biomed. Chromatogr.*
521 30 (2016) 2044-2052. 10.1002/bmc.3783
- 522 [19] N. P. Kovács, A. Almási, K. Garai, M. Kuzma, S. Vancea, E. Fischer, *et al.*,
523 Investigation of intestinal elimination and biliary excretion of ibuprofen in hyperglycemic rats,
524 *Can. J. Physiol. Pharmacol.* 97 (2019) 1080-1089. 10.1139/cjpp-2019-0164
- 525 [20] H. O. Mohammed, A. Almási, S. Molnár, and P. Perjési, The intestinal and biliary
526 metabolites of ibuprofen in the rat with experimental hyperglycemia, *Molecules.* 27 (2022)
527 4000. 10.3390/molecules27134000
- 528 [21] A. Almási, É. dI. L.N. Pinto, N. P. Kovács, T. Fischer, Z. Markovics, E. Fischer, and
529 P. Perjési, Changes in hepatic metabolic enzyme activities and biliary excretion of 4-
530 nitrophenol in streptozotocin induced diabetic rats, *Braz. J. Pharm. Sci.* 54 (2018) e17347.
531 10.1590/s2175-97902018000117347
- 532 [22] A. N. Onyango and N. Baba, New hypotheses on the pathways of formation of
533 malondialdehyde and isofurans, *Free Radic. Biol. Med.* 49 (2010) 1594-600.
534 10.1016/j.freeradbiomed.2010.08.012
- 535 [23] A. B. Lerner, On the metabolism of phenylalanine and tyrosine, *J. Biol. Chem.* 181
536 (1949) 281-294. 10.1016/S0021-9258(18)56648-5
- 537 [24] G. A. Molnár, S. Kun, E. Sélley, M. Kertész, L. Szélig, C. Csontos, *et al.*, Role of
538 tyrosine isomers in acute and chronic diseases leading to oxidative stress - A Review, *Curr.*
539 *Med. Chem.* 23 (2016) 667-85. 10.2174/0929867323666160119094516
- 540 [25] S. Pennathur, J. D. Wagner, C. Leeuwenburgh, K. N. Litwak, and J. W. Heinecke, A
541 hydroxyl radical-like species oxidizes cynomolgus monkey artery wall proteins in early
542 diabetic vascular disease, *J. Clin. Invest.* 107 (2001) 853-60. 10.1172/jci11194

- 543 [26] S. L. Hebert and K. S. Nair, Protein and energy metabolism in type 1 diabetes, Clin.
544 Nutr. 29 (2010) 13-7. 10.1016/j.clnu.2009.09.001
- 545 [27] R. Kehm, T. Baldensperger, J. Raupbach, and A. Höhn, Protein oxidation - Formation
546 mechanisms, detection and relevance as biomarkers in human diseases, Redox. Biol. 42 (2021)
547 101901. 10.1016/j.redox.2021.101901
- 548 [28] G. Garibotto, A. Sofia, S. Saffioti, A. Bonanni, I. Mannucci, and D. Verzola, Amino
549 acid and protein metabolism in the human kidney and in patients with chronic kidney disease,
550 Clin. Nutr. 29 (2010) 424-433. 10.1016/j.clnu.2010.02.005
- 551 [29] A. W. Girotti, Lipid hydroperoxide generation, turnover, and effector action in
552 biological systems, J. Lipid Res. 39 (1998) 1529-42.
- 553 [30] F. P. Corongiu and S. Banni, Detection of conjugated dienes by second derivative
554 ultraviolet spectrophotometry, Methods Enzymol. 233 (1994) 303-10. 10.1016/s0076-
555 6879(94)33033-6
- 556 [31] H. Esterbauer, R. J. Schaur, and H. Zollner, Chemistry and biochemistry of 4-
557 hydroxynonenal, malonaldehyde and related aldehydes, Free Radic. Biol. Med. 11 (1991) 81-
558 128. 10.1016/0891-5849(91)90192-6
- 559 [32] B. C. Shin, J. W. Huggins, and K. L. Carraway, Effects of pH, concentration and aging
560 on the malonaldehyde reaction with proteins, Lipids. 7 (1972) 229-33. 10.1007/bf02533218
- 561 [33] G. M. Siu and H. H. Draper, Metabolism of malonaldehyde in vivo and in vitro, Lipids.
562 17 (1982) 349. 10.1007/BF02535193
- 563 [34] J. M. C. Gutteridge, Free-radical damage to lipids, amino acids, carbohydrates and
564 nucleic acids determined by thiobarbituric acid reactivity, Int. J. Biochem. 14 (1982) 649-653.
565 10.1016/0020-711X(82)90050-7

- 566 [35] D. Tsikas, Assessment of lipid peroxidation by measuring malondialdehyde (MDA)
567 and relatives in biological samples: Analytical and biological challenges, *Anal. Biochem.* 524
568 (2017) 13-30. 10.1016/j.ab.2016.10.021
- 569 [36] D. R. Janero, Malondialdehyde and thiobarbituric acid-reactivity as diagnostic indices
570 of lipid peroxidation and peroxidative tissue injury, *Free Radic. Biol. Med.* 9 (1990) 515-540.
571 10.1016/0891-5849(90)90131-2
- 572 [37] A. Bhattacharyya, R. Chattopadhyay, S. Mitra, and S. E. Crowe, Oxidative stress: an
573 essential factor in the pathogenesis of gastrointestinal mucosal diseases, *Physiol. Rev.* 94
574 (2014) 329-54. 10.1152/physrev.00040.2012
- 575 [38] D. A. Slatter, C. H. Bolton, and A. J. Bailey, The importance of lipid-derived
576 malondialdehyde in diabetes mellitus, *Diabetologia.* 43 (2000) 550-7. 10.1007/s001250051342
- 577 [39] G. Davì, A. Falco, and C. Patrono, Lipid peroxidation in diabetes mellitus, *Antioxid.*
578 *Redox Signal.* 7 (2005) 256-68. 10.1089/ars.2005.7.256
- 579 [40] A. Ayala, M. F. Muñoz, and S. Argüelles, Lipid peroxidation: production, metabolism,
580 and signaling mechanisms of malondialdehyde and 4-hydroxy-2-nonenal, *Oxid. Med. Cell.*
581 *Longev.* 2014 (2014) 360438. 10.1155/2014/360438
- 582 [41] R. A. Lawrence and R. F. Burk, Species, tissue and subcellular distribution of non Se-
583 dependent glutathione peroxidase activity, *J. Nutr.* 108 (1978) 211-215. 10.1093/jn/108.2.211
- 584 [42] S. C. Lu, Glutathione synthesis, *Biochim. Biophys. Acta.* 1830 (2013) 3143-53.
585 10.1016/j.bbagen.2012.09.008
- 586 [43] C. A. Hinchman and N. Ballatori, Glutathione-degrading capacities of liver and kidney
587 in different species, *Biochem. Pharmacol.* 40 (1990) 1131-1135. [https://doi.org/10.1016/0006-](https://doi.org/10.1016/0006-2952(90)90503-D)
588 [2952\(90\)90503-D](https://doi.org/10.1016/0006-2952(90)90503-D)
- 589 [44] L. H. Lash, Role of glutathione transport processes in kidney function, *Toxicol. Appl.*
590 *Pharmacol.* 204 (2005) 329-342. 10.1016/j.taap.2004.10.004

- 591 [45] R. Biondi, Y. Xia, R. Rossi, N. Paolocci, G. Ambrosio, and J. L. Zweier, Detection of
 592 Hydroxyl Radicals by d-Phenylalanine Hydroxylation: A Specific Assay for Hydroxyl Radical
 593 Generation in Biological Systems, *Anal. Biochem.* 290 (2001) 138-145.
 594 10.1006/abio.2000.4958
- 595 [46] G. A. Molnár, Z. Wagner, L. Markó, K. S. T, M. Mohás, B. Kocsis, *et al.*, Urinary
 596 ortho-tyrosine excretion in diabetes mellitus and renal failure: evidence for hydroxyl radical
 597 production, *Kidney Int.* 68 (2005) 2281-7. 10.1111/j.1523-1755.2005.00687.x
- 598 [47] U. Asmat, K. Abad, and K. Ismail, Diabetes mellitus and oxidative stress-A concise
 599 review, *Saudi Pharm. J.* 24 (2016) 547-553. 10.1016/j.jsps.2015.03.013
- 600 [48] L. H. Lash, Renal membrane transport of glutathione in toxicology and disease, *Vet.*
 601 *Pathol.* 48 (2011) 408-19. 10.1177/0300985810375811
- 602 [49] Q. Zhong, S. R. Terlecky, and L. H. Lash, Diabetes increases susceptibility of primary
 603 cultures of rat proximal tubular cells to chemically induced injury, *Toxicol. Appl. Pharmacol.*
 604 241 (2009) 1-13. 10.1016/j.taap.2009.08.007
- 605 [50]
- 606 [51] L. A.-J. Donovan A. McGrowder, Tazhmoye V. Crawford, "Biochemical Evaluation of
 607 Oxidative Stress in Type 1 Diabetes," in *Type 1 Diabetes*, A. Escher, Ed., ed. London, UK:
 608 IntechOpen, 2013, pp. 23-248.
- 609 [52] M. Hecker and A. H. Wagner, Role of protein carbonylation in diabetes, *J. Inherit.*
 610 *Metab. Dis.* 41, (2018) 29-38. 10.1007/s10545-017-0104-9
- 611 [53] A. B. Dawnay, A. D. Hirst, D. E. Perry, and R. E. Chambers, A critical assessment of
 612 current analytical methods for the routine assay of serum total protein and recommendations
 613 for their improvement, *Ann. Clin. Biochem.* 28 (1991) 556-67. 10.1177/000456329102800604

- 614 [54] R. L. Levine, D. Garland, C. N. Oliver, A. Amici, I. Climent, A. G. Lenz, *et al.*,
615 Determination of carbonyl content in oxidatively modified proteins, *Methods Enzymol.* 186
616 (1990) 464-78. 10.1016/0076-6879(90)86141-h
- 617 [55] A. Nakamura and S. Goto, Analysis of protein carbonyls with 2,4-dinitrophenyl
618 hydrazine and its antibodies by immunoblot in two-dimensional gel electrophoresis, *J.*
619 *Biochem.* 119 (1996) 768-74. 10.1093/oxfordjournals.jbchem.a021306
- 620 [56] R. O. Recknagel and A. K. Ghoshal, Quantitative estimation of peroxidative
621 degeneration of rat liver microsomal and mitochondrial lipids after carbon tetrachloride
622 poisoning, *Exp. Mol. Pathol.* 5 (1966) 413-26. 10.1016/0014-4800(66)90023-2
- 623 [57] H. Ohkawa, N. Ohishi, and K. Yagi, Assay for lipid peroxides in animal tissues by
624 thiobarbituric acid reaction, *Anal. Biochem.* 95 (1979) 351-8. 10.1016/0003-2697(79)90738-3
- 625 [58] G. L. Ellman, Tissue sulfhydryl groups, *Arch. Biochem. Biophys.* 82 (1959) 70-7.
626 10.1016/0003-9861(59)90090-6
- 627 [59] J. Sedlak and R. H. Lindsay, Estimation of total, protein-bound, and nonprotein
628 sulfhydryl groups in tissue with Ellman's reagent, *Anal. Biochem.* 25 (1968) 192-205.
629 10.1016/0003-2697(68)90092-4
- 630 [60] E. Mikolás, S. Kun, B. Laczy, G. A. Molnár, E. Sélley, T. Kőszegi, *et al.*, Incorporation
631 of ortho- and meta-tyrosine into cellular proteins leads to erythropoietin-resistance in an
632 erythroid cell line, *Kidney Blood Press Res.* 38 (2013) 217-25. 10.1159/000355770
- 633 [61] J. Mohás-Cseh, G. A. Molnár, M. Pap, B. Laczy, T. Vas, M. Kertész, *et al.*,
634 Incorporation of Oxidized Phenylalanine Derivatives into Insulin Signaling Relevant Proteins
635 May Link Oxidative Stress to Signaling Conditions Underlying Chronic Insulin Resistance,
636 *Biomedicines.* 10 (2022) 975. 10.3390/biomedicines10050975

637 [62] EUROPEAN UNION, DIRECTIVE 2010/63/EU OF THE EUROPEAN
638 PARLIAMENT AND OF THE COUNCIL. <https://eur-lex.europa.eu/eli/dir/2010/63/oj>,
639 (Accessed 22,03,2010)

640 [63] Hungarian Government, A Kormány 40/2013. (II. 14.) Korm. rendelete az
641 állatkísérletekről. <https://www.fao.org/faolex/results/details/en/c/LEX-FAOC124420>,
642 (Accessed 22,03,2010)

643

644

Supplementary Materials

Table 1. Determination of protein content by Biuret assay of different concentrations of the bovine serum albumin (BSA).

No.	BSA volume (mL)	8.1 % SDS (mL)	0.9 % NaCl (mL)	Biuret reagent (mL)	BSA concentration (mg/mL)
1	--	1	1	8	Blank
2	0.1	1	0.9	8	0.3
3	0.2	1	0.8	8	0.6
4	0.3	1	0.7	8	0.9
5	0.4	1	0.6	8	1.2
6	0.5	1	0.5	8	1.5

Figure 1. The calibration curve of the UV-absorbance of different concentrations of the bovine serum albumin (BSA) by Biuret assay.

